

ENERGY, ENVIRONMENT and MATERIAL SCIENCE

**Proceedings of the International Conference on Energy, Environment
and Material Science (EEMAS 2015)**

**Agios Nikolaos, Crete, Greece
October 17-19, 2015**

ENERGY, ENVIRONMENT and MATERIAL SCIENCE

Proceedings of the International Conference on Energy, Environment and Material Science (EEMAS 2015)

**Agios Nikolaos, Crete, Greece
October 17-19, 2015**

Copyright © 2015, by the editors

All the copyright of the present book belongs to the editors. All rights reserved. No part of this publication may be reproduced, stored in a retrieval system, or transmitted in any form or by any means, electronic, mechanical, photocopying, recording, or otherwise, without the prior written permission of the editors.

All papers of the present volume were peer reviewed by no less than two independent reviewers. Acceptance was granted when both reviewers' recommendations were positive.

Series: Energy, Environmental and Structural Engineering Series | 43

ISSN: 2227-4359

ISBN: 978-1-61804-352-8

ENERGY, ENVIRONMENT and MATERIAL SCIENCE

Proceedings of the International Conference on Energy, Environment and Material Science (EEMAS 2015)

**Agios Nikolaos, Crete, Greece
October 17-19, 2015**

Organizing Committee

Editor:

Prof. Aida Bulucea, University of Craiova, Romania

Program Committee:

Prof. Germano Lambert-Torres, Itajuba, MG, Brazil
Prof. Jiri Klima, Technical faculty of CZU in Prague, Czech Republic
Prof. Goricanec Darko, University of Maribor, Maribor, Slovenia
Prof. Ze Santos, Rua A, 119. Conj. Jardim Costa do Sol, Brazil
Prof. Ehab Bayoumi, Chalmers University of Technology, Goteborg, Sweden
Prof. Luis Tavares Rua, Cmte Guyubricht, 119. Conj. Jardim Costa do Sol. Atalaia, Brazil
Prof. Igor Kuzle, Faculty of electrical engineering and computing, Zagreb, Croatia
Prof. Nikolay Djagarov, Technical University of Varna, Bulgaria
Prof. Darko Goricanec, University of Maribor, Maribor, Slovenia
Prof. Maria do Rosario Alves Calado, University of Beira Interior, Portugal
Prof. Gheorghe-Daniel Andreescu, "Politehnica" University of Timisoara, Romania
Prof. Patricia Jota, Av. Amazonas 7675, BH, MG, Brazil
Prof. Frangiskos V. Topalis, National Technical University of Athens, Greece
Prof. Bharat Doshi, John Hopkins University, Maryland, USA
Prof. Gang Yao, University of Illinois at Urbana - Champaign, USA
Prof. Lu Peng, Lusian State University, Baton Rouge, LA, USA
Prof. F. Akgun, Gebze Kocaeli, Turkey
Prof. Y. Baudoin, Royal Military Academy, Brussels, Belgium
Prof. M. Dasenakis, Dept. of Chemistry, University of Athens, Greece.
Prof. G. E. Froudakis, University of Crete, Herakleion, Greece
Prof. R.S.R. Gorla, Cleveland State University, Cleveland, Ohio, USA
Prof. M. Heiermann, Dr., Department of Technology Assessment and Substance Flow, Potsdam, Germany
Prof. C. Helmis, University of Athens, Athens, Greece
Prof. I. Kazachkov, National Technical University of Ukraine (NTUU KPI), Kyiv, Ukraine
Prof. A. M.A. Kazim, UAE University, United Arab Emirates
Prof. G. Kiriakidis, University of Crete, Herakleion, Greece
Prof. A. Kurbatskiy, Novosibirsk State University, Department of Physics, Russia
Prof. P. Lunghi, Dipartimento di Ingegneria Industriale, Universit? degli Studi di Perugia, Italy
Prof. C. Makris, A, Department of Computer Engineering and Informatics., University of Patras, Greece
Prof. S. Ozdogan, Marmara University, Goztepe Campus, Kuyubasi, Kadikoy, Istanbul, Turkey
Prof. P. Pardalos, Department of Industrial and Systems Engineering, University of Florida, USA
Prof. I. Poulios, Dept. of Chemistry, Aristotle University of Thessaloniki, Greece.
Prof. F. Rigas, School of Chemical Engineering, National Technical University of Athens, Greece.
Prof. S. Sohrab, Northwestern University, IL, USA
Prof. A. Stamou, National Technical University of Athens, Greece
Prof. A. I. Zouboulis, Dept. of Chemistry, Aristotle University of Thessaloniki, Greece.
Prof. Zhibing Zhang, University of Birmingham, Birmingham, UK
Prof. Jean-Francois Gohy, Université catholique de Louvain, Belgium
Prof. Waler Caseri, ETH, Zurich, Switzerland
Prof. Jacques Desbrieres, Universite De Pau Et Des Pays De L'Adour, France
Prof. Adrian Schumpe, Technical University of Braunschweig, Germany
Prof. Chris Bowen, University of Bath, Bath, UK
Prof. Jerzy Baldyga, Technical University Warszawska, Poland
Prof. Alirio Rodrigues, University of Porto, Portugal
Prof. Mostafa Barigou, University of Birmingham, Birmingham, UK
Prof. Jaime Wisniak, Ben-Gurion University of the Negev, Beer-Sheva, Israel
Prof. Sohail Murad, University of Illinois at Chicago, USA
Prof. Konstantinos E. Kakosimos, Texas A&M University at Qatar, Doha, Qatar

Prof. Raghunath V. Chaudhari, University of Kansas, USA
Prof. Xijun Hu, The Hong Kong University of Science and Technology, Kowloon, Hong Kong
Prof. Deepak Kunzru, Indian Institute of Technology, Kanpur, India
Prof. Yong Ding, Georgia Institute of Technology, Atlanta, GA, USA
Prof. Yulin Deng, Georgia Institute of Technology, Atlanta, GA, USA
Prof. Paul H. Holloway, Distinguished Prof., University of Florida, Gainesville FL, USA
Prof. Saad Khan, North Carolina State University, Raleigh, North Carolina, USA
Prof. Manijeh Razeghi, Northwestern University, Evanston, IL, USA
Prof. Igor Sevostianov, New Mexico State University, Las Cruces, New Mexico, USA
Prof. Mohindar S. Sehra, West Virginia University, Morgantown, West Virginia, USA
Prof. Tao Liu, Florida State University, Tallahassee, Florida, USA
Prof. Tian Tang, University of Alberta, Edmonton, Alberta, Canada
Prof. Roland Frankenberger, University of Marburg, Marburg, Germany
Prof. Mohamedally Kurmoo, Universite de Strasbourg, Strasbourg, France
Prof. C. C. Sorrell, University of New South Wales, Sydney, NSW, Australia
Prof. Concepcion Lopez, Universitat de Barcelona, Barcelona, Spain
Prof. Alan Dalton, University of Surrey, Guildford, Surrey, UK
Prof. Kourosh Kalantar-Zadeh, RMIT University, Melbourne, Australia
Prof. Constantinos Tsitsilianis, University of Patras, Patras, Greece
Prof. Tetsu Yonezawa, Hokkaido University, Kita Ward, Sapporo, Hokkaido Prefecture, Japan
Prof. Daolun Chen, Ryerson University, Toronto, Ontario, Canada
Prof. Mohamed M. Chehimi, Universite Paris Diderot, Paris, France
Prof. Vincenzo Fiorentini, Universita degli studi di Cagliari, Cagliari, Italy
Prof. Tamas Ungar, Eotvos Lorand University (ELTE), Budapest, Hungary
Prof. Anthony W. Coleman, Universite Claude Bernard Lyon 1, Lyon, France
Prof. Albert Chin, IEEE Fellow, OSA Fellow, National Chiao Tung University, Hsinchu, Taiwan
Prof. Artur Cavaco-Paulo, Universidade do Minho, Braga, Portugal
Prof. Yoshihiro Tomita, Kobe University, Kobe, Japan
Prof. Jian Wang, Los Alamos National Laboratory, Los Alamos, NM, USA
Prof. Byung K. Kim, Pusan National University, Busan, South Korea
Prof. John T. Sheridan, University College Dublin, Belfield, Dublin, Ireland
Prof. Chi-Wai Chow, National Chiao Tung University, Hsinchu, Taiwan
Prof. Christian M. Julien, Universite Paris-6, Paris, France
Prof. Chun-Hway Hsueh, National Taiwan University, Taipei, Taiwan
Prof. Hyung-Ho Park, Yonsei University, Seodaemun-gu, Seoul, Korea
Prof. Victor M. Castano, Universidad Nacional Autonoma de Mexico, Mexioc City, Mexico
Prof. Peter Chang, University of Saskatchewan, Saskatoon, Saskatchewan, Canada
Prof. Dean-Mo Liu, National Chiao Tung University, HsinChu, Taiwan
Prof. Rui Vilar, Instituto Superior Tecnico, Lisboa, Portugal
Prof. Hugh J. Byrne, Dublin Institute of Technology, Dublin, Ireland
Prof. Won-Chun Oh, Hanseo University, Seosan-si, Chungcheongnam-do, South Korea
Prof. Yuanhua Lin, Tsinghua University, Haidian, Beijing, China
Prof. S.C. Tjong, City University of Hong Kong, Sham Shui Po District, New Kowloon, Hong Kong
Prof. Huan-Tsung Chang, National Taiwan University, Taipei City, Taiwan
Prof. Jing Zhang, Donghua University, Shanghai, China
Prof. Veronica Cortes de Zea Bermudez, Universidade de Tras-os-Montes e Alto Douro, Vila Real, Portugal
Prof. Jun Zhang, Inner Mongolia University, Hohhot, Inner Mongolia, China
Prof. Israel Felner, Hebrew University of Jerusalem, Jerusalem, Israel
Prof. Sukhvinder Badwal, CSIRO Energy Technology, Australia
Prof. Te-Hua Fang, National Kaohsiung University of Applied Sciences (KUAS), Kaohsiung, Taiwan
Prof. Belkheir Hammouti, Mohammed Premier University, Oujda, Morocco
Prof. Mohd Sapuan Salit, Universiti Putra Malaysia, Selangor, Malaysia
Prof. Kwansoo Chung, Seoul National University, Seoul, South Korea
Prof. Zhongfang Chen, University of Puerto Rico, San Juan, Puerto Rico

Prof. Soon-Ku Hong, Chungnam National University, Daejeon, South Korea
Prof. Hannes Jonsson, University of Iceland, Reykjavik, Iceland
Prof. Culea Eugen, Technical University of Cluj-Napoca, Cluj-Napoca, Romania
Prof. Vesselin Dimitrov, University of Chemical Technology and Metallurgy, Sofia, Bulgaria
Prof. Shadpour Mallakpour, Isfahan University of Technology, Isfahan, Iran
Dr. Stergios Pispas, National Hellenic Research Foundation (NHRF), Athens, Greece
Dr. Anna Lukowiak, Polish Academy of Science, Wroclaw, Poland

Additional Reviewers

Abelha Antonio	Universidade do Minho, Portugal
Angel F. Tenorio	Universidad Pablo de Olavide, Spain
Miguel Carriegos	Universidad de Leon, Spain
Alejandro Fuentes-Penna	Universidad Autónoma del Estado de Hidalgo, Mexico
Bazil Taha Ahmed	Universidad Autonoma de Madrid, Spain
M. Javed Khan	Tuskegee University, AL, USA
Moran Wang	Tsinghua University, China
Kazuhiko Natori	Toho University, Japan
Zhong-Jie Han	Tianjin University, China
Genqi Xu	Tianjin University, China
James Vance	The University of Virginia's College at Wise, VA, USA
Jose Flores	The University of South Dakota, SD, USA
Valeri Mladenov	Technical University of Sofia, Bulgaria
Minhui Yan	Shanghai Maritime University, China
Francesco Zirilli	Sapienza Universita di Roma, Italy
Tetsuya Shimamura	Saitama University, Japan
Andrey Dmitriev	Russian Academy of Sciences, Russia
Dmitrijs Serduks	Riga Technical University, Latvia
George Barreto	Pontificia Universidad Javeriana, Colombia
Francesco Rotondo	Polytechnic of Bari University, Italy
Masaji Tanaka	Okayama University of Science, Japan
Imre Rudas	Obuda University, Budapest, Hungary
Ole Christian Boe	Norwegian Military Academy, Norway
Stavros Ponis	National Technical University of Athens, Greece
Frederic Kuznik	National Institute of Applied Sciences, Lyon, France
Jon Burley	Michigan State University, MI, USA
Eleazar Jimenez Serrano	Kyushu University, Japan
Hessam Ghasemnejad	Kingston University London, UK
Konstantin Volkov	Kingston University London, UK
Takuya Yamano	Kanagawa University, Japan
João Bastos	Instituto Superior de Engenharia do Porto, Portugal
José Carlos Metrônho	Instituto Politecnico de Castelo Branco, Portugal
Philippe Dondon	Institut polytechnique de Bordeaux, France
Xiang Bai	Huazhong University of Science and Technology, China
Tetsuya Yoshida	Hokkaido University, Japan
Shinji Osada	Gifu University School of Medicine, Japan
Kei Eguchi	Fukuoka Institute of Technology, Japan
Yamagishi Hiromitsu	Ehime University, Japan
Santoso Wibowo	CQ University, Australia
Sorinel Oprisan	College of Charleston, CA, USA
Deolinda Rasteiro	Coimbra Institute of Engineering, Portugal
Matthias Buyle	Artesis Hogeschool Antwerpen, Belgium

Table of Contents

Waste Analysis and Categorization in the Construct of Hotels Supply Chain	11
<i>Raid Al-Aomar, Matloub Hussain</i>	
Particularities of Power Transformer Reuse with Respect to Re-Stamp Process Based on Life Cycle Assessment Tool	16
<i>Niculae N. Boteanu, Florin Ravigan, Mihai Iacob</i>	
Glass – Structural Material of Buildings	23
<i>Marcela Karmazínová, Jindrich Melcher</i>	
Identifying the Transfer Function Specific to Environmental Contamination with Flue Gas Toxics	34
<i>Corina C. Brîndușa, Eliza Gofită, Nikos E. Mastorakis, Carmen A. Bulucea, Niculae Boteanu, Andreea C. Jeles, Mihnea Glodeanu, Cornelia A. Bulucea</i>	
Optimization of Bait Sprays Against <i>Dacus Oleae</i> Using Embedded Systems, GIS and Web-Based Applications	42
<i>George N. Fouskitakis, Lefteris D. Doitsidis, Iraklis I. Rigakis, Kyriaki N. Varikou, Ioannis V. Sarantopoulos, Androniki K. Papafilippaki, Kyriaki G. Maniadaki, Athanasia E. Mpirouraki, Emmanuel N. Antonidakis</i>	
Monospecific Dominance in a Alluvial Mixed Ombrophylous Forest in Southern Brazil	48
<i>J. Carvalho, F. Galvão, R. Rios, S. J. E. Velazco</i>	
New Technology of Renewable Energy Generation	54
<i>S. Tounsi</i>	
Effects of Gamma Radiation on Some Hematological Parameters in Female Rats	61
<i>Ali Abid Abojassim, Haider Salih Jaffat, Adhraa Baqir Hassan</i>	
Risk of Acid Attack on Plants: A Review	66
<i>S. Behera, B. Mallick, T. N. Tiwari, P. C. Mishra</i>	
In-Vitro Evaluation of Cytotoxicity, Antiviral and Virostatic Activity of PMF Derived from Camel Urine	72
<i>Noor S. O., AlAttas S. G., Khorshid F. K., Elsourojy Y. A., Tawfik N.</i>	
Safety Profile of PMF a Fraction Derived from Camel Urine on Mice (Acute Study)	77
<i>Samar O. Rabah, Faten A. Khorshid, Huda Aboarik, Nahid H. Hajrah, Jamal S. Sabir, Roop S. Bora</i>	
Magnetic Effects in the Thermodynamics of the Process of Thinking	81
<i>Aibassov Yerkin Zhakenovich, Savizky Ruben, Yemelyanova Valentina, Shakieva Tatyana, Tussupbaev Nessipbay, Bulenbayev Maxat, Blagikh Evgeniy</i>	

Organic-Inorganic Ion-Exchangers Containing Nanoparticles of Zirconium Hydrophosphate for Electrodeionization Processes	85
<i>Yu. S. Dzyazko, L. N. Ponomaryova, Yu. M. Volkovich, V. E. Sosenkin, V. N. Belyakov</i>	
Effect of Iron (Fe³⁺) and Magnesium (Mg²⁺) During Biodegradation of Organic Matter by Clostridium Butyricum in the Leachate	100
<i>M. Redzwan Tamat, M. Firdaus Othman, Y. Syafikah Razali, N. A. Serri, H. Azan Tajarudin</i>	
The Oxidation Behavior of Titanium Aluminide at 850°C	106
<i>Alexandra Banu, Elena Maria Anghel, Marcu Maria, Georgescu Luminita</i>	
Oxygen Isotopic Comparisons of the Microcrystalline Silica; In the Case of Different Chrysoprases in Turkey	110
<i>Murat Hatipoğlu, Nurdane İlbeyle</i>	
Authors Index	124

Waste Analysis and Categorization in the Construct of Hotels Supply Chain

Raid Al-Aomar, Matloub Hussain

Abstract—This paper aims at analyzing and categorizing the wastes across the supply chain of the hotel industry. Literature search showed a need for empirical studies that explore the construct of hotels supply chains, analyze wastes across the supply chain construct, and address sustainability practices. The paper provides a structured approach that can be used to assist the analysis and categorization of different types of wastes across the supply chain of hotels and support future research. To this end, the study first develops a SIPOC-based construct of a hotel supply chain and identifies the types of waste at various construct elements. Second, the study categorizes hotel supply chain wastes using lean principles and provides guidelines for waste reduction using lean techniques and green practices. The emphasis is on reducing the identified types of wastes in a hotel supply chain to increases its operational and economic effectiveness and improves the overall service quality. This also contributes to the effort of incorporating sustainability in the supply chains of hotels and services in general. The study is conducted in selected hotels in Abu Dhabi (AD) area in the UAE.

Keywords— Hotel Industry, Lean Thinking, Supply Chain Sustainability, Waste Analysis.

I. INTRODUCTION

Sustainability has been of great interest in the last decade for academia and industry due to pressures from various stakeholders to embrace a commitment to sustainability practices. In sustainable organizations, the environmental and social criteria need to be fulfilled by operations managers, while maintaining competitiveness and meeting customer needs and related economic criteria [1]. This implies that organizations have to satisfy multiple and conflicting objectives such as maximizing profits while reducing operating costs, minimizing the environmental impacts and maximizing the social well-being [2, 3].

A supply chain is often viewed as a network of critical links that connects organizations (stakeholders) together and links each organization's inputs to its outputs. As defined by Bowersox and Closs [4], the supply chain refers to all those

This work was supported by the Office of Research and Sponsored Programs (ORSP) at Abu Dhabi University (ADU) through an internal research incentive fund.

Raid Al-Aomar is with the College of Engineering at Abu Dhabi University, UAE (phone: +971-2-501-5763; fax: +971-2-586-0182; e-mail: raid.alaomar@adu.ac.ae).

Matloub Hussain is with the College of Business and Business Administration at Abu Dhabi University, UAE (phone: +971-2-501-5869; fax: +971-2-586-0182; e-mail: matloub.hussain@adu.ac.ae).

activities associated with the transformation and flow of goods and services, including money and information flows, from the sources of materials to end users. For example, a hotel supply chain is a network of organizations (suppliers, logistics partners, and stakeholders) engaged in delivering different hotel services to customers. Such network functions through the flow of information (e.g., reservations), monetary transactions (e.g., payments and charges), and physical items (e.g., food and drinks). Further details of supply chain components and functions can be found in [5]. Figure 1 depicts the main components of a service supply chain.

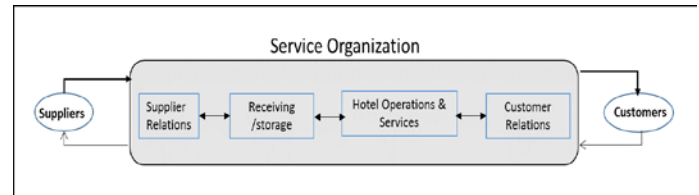


Fig. 1 the main components of a service supply chain

The term of “reverse logistics” is also used to indicate the flow of material backward from customer to sources through recycling, repair, rework, reuse, refurbishment, and so on. Such flow is also gaining ground in hotel industry especially in terms of recycling and reuse. Reverse logistics is considered a strategy for developing sustainable supply chains.

Supply chain sustainability has attracted a growing attention from researchers and practitioners and in various sectors of the economy across the world. That is mainly due to the growing cost of supply chain operations, the increase in stricter environmental regulation and legislations, and the growing competition based on cutting costs and reducing wastes. There is also an agreement among researchers that the concept and techniques of sustainability in services in general are still in the development compared to those in the manufacturing companies.

Sustainable supply chain aims to deliver quality products and services across the supply chain while increasing effectiveness, reducing waste and costs, and being environmentally responsible [6]. The typical challenge that faces organizations in this regard is how to be productive and profitable while being sustainable.

However, few researchers have actually analyzed the wastes of the hotels supply chains and the application of lean techniques and green practices for waste reduction. For example, Vlachos and Bogdanovic [7] presented a survey-

based study on the lean thinking in European hotel industry. Green practices in hotel industry are relatively more common across the supply chain. An approach known as “triple bottom line” is commonly used to assess supply chain sustainability based on social, environmental, and economic performance [8].

Thus, there is a need for the research on hotels supply chain to analyze and categorize wastes and to link the identified wastes to lean techniques and green practices. Most existing research is mainly focused on assessing and modeling the environmental and economic impacts of the hotel supply chains and prescribing action plans and polices to reduce such impact. This paper presents an exploratory study of hotels supply chain construct and wastes. The study is conducted in selected hotel in Abu Dhabi area in the UAE.

II. STUDY FRAMEWORK

The hotel supply chain is a typical example of service supply chain that is amenable to sustainability practices. Different aspects of hotel supply chains have been explored in body of literature. However, the complete hotel supply chains have not been exclusively investigated yet [9, 10]. Thus, this research will first focus on identifying the construct of the hotel industry supply chain, analyzing pertinent wastes across the supply chain, identifying existing lean and green practices, then assessing the extent of adopting lean and green techniques. As shown in Figure 2, the key elements of the research framework include:

- Supply chain construct
- Waste analysis
- Lean practices (sustainability focus)
- Green practices (sustainability focus)

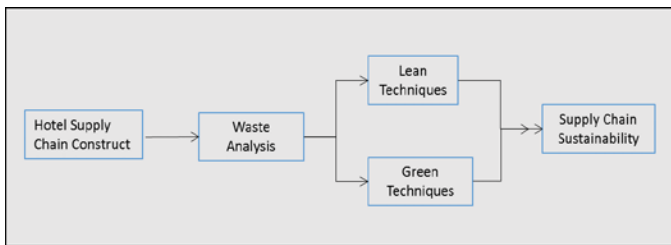


Fig. 2 study framework for hotel supply chain sustainability

A. Construct of Hotel Supply Chain

Before incorporating lean and green practices into the hotel supply chain, it is crucial to understand the construct of the hotel procurement system as well as key hotel operations [11]. As shown in Figure 1, as a service industry, the hotel supply chain is made of the typical elements of Supplier Relationship Management (SRM), logistics, storage, organizational processes and service operations, and of Customer Relationship Management (CRM). These elements which vary from one hotel to another are developed based on the requirements of key hotel services such as:

- Lodging and accommodation
- Restaurants and food services

- Hotel amenities and guest services
- Meetings, events, and conferences

These services require tangible inputs from suppliers and different service providers such as culinary material and other in-bound logistics to ensure efficient delivery of daily hospitality services [12]. Other services in the hotel such as reservation, reception, check-in, check-out, and customer service may not need tangible material as inputs but they need internal and external support and inputs from partners and suppliers such as information, technical support, payment system, security, and so on. Almost all hotel services can be oriented around the hotel guest. As an output, hotel provide services such as catering, events management, and accommodation.

The Supplier-Input-Process-Output-Customer (SIPOC) chart is used in this research to provide the hotel supplies and operations manager with a platform to list the relevant information regarding the hotel supply chain construct, wastes, and the currently used lean and green practices. Figure 3 shows a template of the used SIPOC chart.

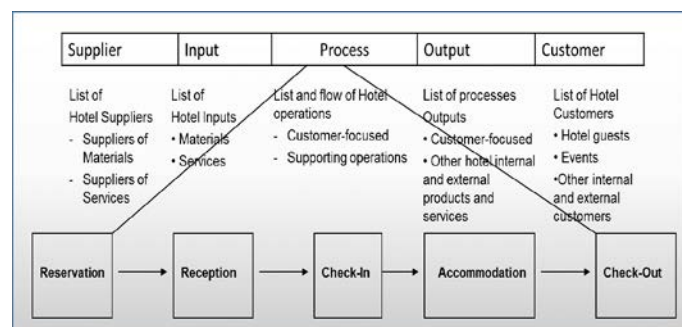


Fig. 3 SIPOC chart of the hotel supply chain construct

B. Waste Analysis

Wastes management is a key business function in most hotels at different star level. This is mainly due to the increased amount of tangible and intangible wastes that are created as a result of hotel services such as accommodation, dining, laundry, and hosted events. This includes food, materials, papers, and so on. The list of wastes in a hotel can also include wastes related to key resources such as water, electricity and energy, and pollution. The list becomes overwhelming when you add to it intangible wastes such as delays, cancellations, complains, errors, and over capacity. As these wastes affect the direct and indirect operational cost, hotels management typically value and support the deployment lean and green techniques that are expected to lead to the reduction or even elimination of different types of wastes. Thus, it is important for any hotel supply chain sustainability framework to analyze the different types of wastes in hotel procurement system and operations and at different stages of the hotel supply chain.

C. Lean Techniques

Lean thinking which was started to reduce or eliminate

production wastes in Toyota has recently developed into a management philosophy that focuses on increasing the effectiveness of the organization. Womack *et al.* [13] describe waste as any activity which uses resources, but creates no value. This includes over production, excess processing, inventory, rework, motion, transport and material handling, defects, failures, setup and underutilizing skills and resources.

The lean supply chain is an approach that is focused on streamlining the flow of goods and information across the supply chain and reducing the supply chain cost by eliminating non-value-added activities through the adoption of lean techniques. To this end, lean principles and tools are applied to the supply chain elements and functions (supplier selection, purchases, shipping, order management, warehousing, manufacturing/processing, transportation, distribution, etc.) to transform it into a value chain. Examples include Kaizen, error-proofing (poke-yoke), flow analysis, line balancing, inventory control, quality-at-the-source, JIT, 5S, etc.

D. Green Practices

The main objective of green SCM is to extend the traditional supply chain to deal with the effects of products and processes. Extended supply chain models often include recycling and remanufacturing operations along with measures to reduce emissions and conserve energy. As an outcome, green SCM can reduce waste, minimize pollution, save energy, conserve natural resources, and reduce carbon emissions. Details on adding the “Green” component to the supply chain management can be found in [14].

In the hotel industry, the application of green technology is expanding as a result of strict regulations and the growing customer awareness of environmental concerns. It is therefore important for a hotel sustainability framework to include specific green practices that can be deployed and lead to conservation of resources, reduction of energy and emissions, and efficient recycling. Examples include environmental standards, safety standards, pollution reduction, recycling, reuse, take-back, energy efficiency, water conservation, green technology, green suppliers, clean transport, hazardous material treatment, etc.

III. STUDY RESULTS

The study has adopted a survey-based industry research to collect empirical data from the hotel industry in Abu Dhabi (AD) of the UAE. It is an exploratory study of the construct and waste types in the hotel supply chain along with an analysis of and categorization of wastes. To this end, a survey is designed and distributed to about thirty 3, 4, and 5 stars hotels in AD area. The survey has collected basic hotel information and identified the types of waste currently exist in the hotel supply chain. The results of the survey were studied and analyzed to answer the following two research questions:

- RQ1: What is the construct of the supply chain of hotels?
- RQ2: What types of waste exist in the supply chain of hotels?

The study results were obtained from the surveys collected

from 30 hotel in AD area. The survey has targeted only the 3, 4, 5-star rated hotels in the Emirate of AD in the UAE. A total of 50 surveys were distributed and 30 were qualified. Key descriptive summary is as follows:

- The rating of the surveyed hotels is as follows; 20 five star, 8 four starts, and 2 three stars. The reason for focusing on 5-star hotels and is getting better response is due to the fact that they have well-established systems and standards (including green and environmental) and more focus of effectiveness (lean practices).
- Hotel size is assessed in terms of hotel employee and rooms for guest accommodation. Number of employee ranges from 45 to 1500. The rooms’ number ranges from 95 to 823.
- The level of management is distributed between mid and top level (18 mid-level and 12 top-level). This indicates the interest and the organization seriousness when it comes to such practices.

A. Answers to Research Questions

To answer the first research question, a SIPOC chart is developed to present the construct of AD hotels supply chains based on the collected information from the surveyed hotels. The chart lists hotel suppliers, inputs supplied and used by hotel’s main processes, the products and services of these processes, and their customers. Each column in the chart lists the items indicated by each surveyed hotel. For example, the Suppliers column list almost all types of suppliers who provide the hotels with products, parts, food, drinks, materials, and services (IT, security, landscaping, entertainment, repair, etc.). The chart provides a comprehensive view of the hotel supply chain construct.

The main hotel processes and operations represent the core of the construct. These processes takes key inputs and produce key outputs in terms of products and services to guests and hotel internal and external customers. Table 1 provides a summary of main hotel processes along with their inputs and outputs. Suppliers list is not included for confidentiality and customers are limited to hotel guests.

Typically such construct operates through a logistic system that flows material, information, and money across the supply chain. The logistic system includes procurement, transportation, material handling, warehousing, and distribution. Such system is managed through an integrated database and network or an Enterprise Resource Planning (ERP) system.

To answer this question, a SIPOC chart is developed to categorize and summarize the hotel wastes based on the developed construct. As shown in Table 2, the chart lists wastes created by suppliers and customers and observed in the inputs used by hotel processes, within the processes, and their produced outputs. Suppliers produce wastes as well as customers. SRM and CRM can work with both ends of the supply chain on waste reduction.

Table 1 summarized I-P-O construct of the hotel supply chain

Inputs/supplies	Main Processes	Outputs/services
Online bookings Phone reservations Booking website Reservation software	Reservation and booking	Confirmed reservations Events schedule Facilities planning
Guests arrivals Stationary and Office equipment Newspapers and magazines Printing and promotional items	Reception	Check-In Room assignment Payment Check-out Concierge service
Room furniture Entertainment system Linens, towels, bedsheets, robes, etc. Tea, Coffee and Coffee Machines Room amenities Bathroom amenities Room accessories and room decoration Tissues and disposable cleaning papers Promotional items	Room accommodation	Guest comfortable stay Room services
Food and drinks Fruits and vegetables Cooking materials Cooking equipment Cookware and glassware Kitchen furniture Energy and electricity Hardware supplies Cleaning materials Grocery Items (Cereals, Pulses, Spices, canned vegetables, jams, etc.)	Restaurants culinary and cooking	Meals Buffets Rooms catering External catering Room services Events catering Others food services
Maintenance repair and operating supplies. Plumbing and sensor water taps, electrical and lighting fittings, lambs, etc. HVAC system and equipment Security equipment and software Lifts and escalators	Maintenance	Available water and electricity Functional lightening system Functional HVAC system Functional plumbing system Functional security system Functional lifts and escalators

Awareness plans to customers, visitors, and guests and sourcing decisions to select eco-friendly and reliable suppliers (e.g., green suppliers) are initiatives that can achieve such objectives. However, the I-P-O waste reduction is within the control of the hotel management system. That is where most of the effort of engineering and operational excellence should be directed.

Table 2 SIPOC summary of hotel supply chain wastes

Suppliers	Inputs	Processes	Outputs	Customers
Delivery delay Wrong delivery Transportation delay Wrong material Broken items Wrong mix Shortage	Packaging materials wrongly received Item Defects Excessive inventory Improper storage Damaged material Wrong resource allocation	Garbage waste Used Oil Paper/cardboard/plastics/ Organic waste Raw food Unclear communication Defects: pipes, lambs, hardware Over-processing Under-utilization Waiting, idle time Excessive multitasking	Cooked food waste Amenities waste Delay in guest services Wrong invoicing Misinformation Over Production of food Delay	Wrong reservations Late arrivals Cancelations No shows Late changes Caus Food leftovers Wrong orders Excessive use of water Excessive use of AC Keeping lights on Damaging room furniture and accessories Leaving and spreading dirt Delay in check-out

As seen in Table 2, the wastes across the supply chain can be categorized as tangible (material, item shortage, bad food, defects, etc.) and intangible (delays, errors, bad scheduling, etc.). Hotel supply chain wastes can be also related to the seven wastes or non-value-added (NVA) of lean philosophy.

Table 3 categorizes of the identified wastes in the hotel supply chain into the seven common types of waste according to lean principles and thinking.

Table 3 lean-based categorization of wastes in hotels supply chain

Lean Waste	Waste examples in hotel supply chain
Defects	Broken items, spoiled or expired food and milk, invoicing errors, reservation errors, scheduling conflicts, wrong material, damaged materials, damaged amenities, rejects, return, rework, repair, nonconforming items, parts, devices, and equipment, etc.
Delay/waiting	Late delivery, late shipment, late arrival, services delay, check-in/out delay, customer waiting time, work idle time, unclear communication, resources underutilization, etc.
Overproduction	More than needed supplies, excessive food cooking and catering, garbage, water waste, energy waste, etc.
Overprocessing	Exceeding standards, using expensive equipment, complex operations, complex services, overqualified resources, wrong resource allocation, excessive multitasking
Inventory	Keeping large amount of raw food and drinks, improper storage, excessive storage of cleaning materials, spare parts, tools, equipment, etc.
Transportation	Long distance supplies and shipments, less than full trucks, returns, excessive material handling, back and forth movements, etc.
Motion	Failure to follow standard operating procedures, lack of labor training and skills, excessive worker motion in cooking, housekeeping, and other hotel services and operations.

The role of lean and green techniques will be focused on eliminating/reducing these types of wastes. Such classification can be used by hotel management to select the most effective lean and green techniques that result in the most reduction of wastes across the supply chain. That explains the need for lean and green techniques in the next research question.

Some hotels have developed plans for classifying and recycling different types of hotel wastes. These wastes are assumed to remain after implementing lean and green practices. Table 4 presents an example of wastes classification. Some wastes are treated by private recycling contractors, some are treated internally in the hotel, and some are sent for disposal.

Table 4 example of plan for hotel classification of wastes

Waste Type	Source	Recyclable	Hazardous	Treatment/Disposal plan
Cardboard/ papers	Rooms offices	Yes	No	ABC company
Food	restaurants	No	No	Disposal
Cans	Restaurants, Rooms, Offices	Yes	No	ABC company
Metals	Rooms, Offices	Yes	No	ABC company
Oils	Restaurants	No	Yes	Disposal
Glass	Restaurants, Rooms	Yes	Yes	ABC Company
Used water	All	Yes	No	Hotel facility
General waste	All	No	No	Disposal

IV. DISCUSSION AND CONCLUSION

The study has explored the hotel supply chain construct and identified, categorized, and analyzed the wastes across the supply chain of hotel industry. Results provided guidelines for assessing and analyzing sustainability practices in hotels supply chains. In general, the study found that the sustainability concept in terms of lean and green practices is relatively new to the hotel industry in AD. Many surveyed

hotels view sustainability as adhering to environmental standards an audits rather than technical lean and green practices. Results showed that 5-star hotels have relatively better sustainability practices across the supply chain in terms of well-established systems and standards (including green and environmental) with more focus of the chain effectiveness (lean practices).

The SIPOC chart is found to be a good platform for analyzing the construct of hotels supply chain based on the collected information from the surveyed hotels. The chart lists hotel suppliers, the inputs supplied and used by hotel's main processes, the products and services of these processes, and their customers. The construct showed the size and diversity in some cases the complexity of hotels supply chains when analyzed with a comprehensive view from sources of inputs to the flow of services and operations towards hotel customers and guests. The main hotel processes and operations represent the core of the developed construct. These processes takes key hotel inputs and produce key outputs in terms of products and services to guests and hotel internal and external customers. Typically such construct operates through a logistic system (procurement process) that flows material, information, and money across the supply chain.

A SIPOC chart is also developed to categorize and summarize the hotel wastes based on the developed construct. The chart listed wastes created by suppliers and customers and those observed in the inputs used by hotel processes, within the processes, and their produced outputs. The wastes across the hotel supply chain were then categorized as tangible (material, item shortage, bad food, defects, etc.) and intangible (delays, errors, bad scheduling, etc.). Wastes were also related to the seven types of wastes or non-value-added (NVA) of lean philosophy.

Such categorization can help the hotel management in identifying and directing effective green practices and lean techniques to reduce the identified types of wastes. For example, recycling and reuse green practices can target tangible wastes and JIT and Kaizen techniques can target the intangible delays and errors. Similarly, each type of lean waste can be targeted by specific lean technique (e.g., defects by quality at the source, overproduction by pull JIT system, excessive inventory by inventory control systems, and so on).

The study recommended that SRM and CRM fronts of the hotel can work with both ends of the supply chain on waste reduction through awareness plans to customers, visitors, and guests and proper sourcing decisions to select eco-friendly and reliable suppliers. However, the hotel sustainability practices should be focused on the I-P-O waste reduction (i.e., with the hotel forward flow and reverse logistics). That is where most of the effort of engineering and operational excellence should be directed.

ACKNOWLEDGMENT

The researchers would like to thank the ORSP office, the students who helped in collecting research data, and the hotel industry in the Emirate of Abu Dhabi of the UAE.

REFERENCES

- [1] P. Cerin, and L. Karlson, "Business incentives for sustainability: a property rights approach," *Ecological Economics*, 40, pp. 13-22, 2002.
- [2] P. Taticchi, F. Tonelli, and R. Pasqualino, "Performance measurement of sustainable supply chains: A literature review," *International Journal of Productivity & Performance Management*, 62, pp. 782-804, 2013.
- [3] C. Colicchia, G. Marchet, M. Melacini, and S. Perotti, "Building environmental sustainability: empirical evidence from Logistics Service Providers," *Journal of Cleaner Production*, 59, pp. 197-209, 2013.
- [4] D.J. Bowersox, D.J. Closs, and M.B. Cooper, *Supply chain logistics management*. McGraw-Hill, New York, 2002.
- [5] C.B. Bozarth and R.B. Handfield, *Introduction to operations and supply chain management*, 3e. Prentice Hall, New York, 2013.
- [6] K. Sengupta, D.R. Heiser, and L.S Cook, "Manufacturing and service supply chain performance: a comparative Analysis," *Journal of Supply Chain Management*, 42 (4), pp. 4-15, 2006.
- [7] I. Vlachos and A. Bogdanovic, "Lean thinking in the European hotel industry," *Tourism Management*, 36, pp. 354-363, 2013.
- [8] C. R. Carter and D. S. Rogers, "A framework of sustainable chain management: moving toward new theory," *International Journal of Physical Distribution & Logistics Management*, Vol. 38 Iss.: 5, pp.360 – 387, 2008.
- [9] H. Tsai, N.K.F. Tsang, and S.K.Y. Cheng, "Hotel employees' perceptions on corporate social responsibility: The case of Hong Kong," *International Journal of Hospitality Management*, 31, pp. 1143–1154, 2012.
- [10] X. Xu and D. Gursoy, "A Conceptual Framework of Sustainable Hospitality Supply Chain Management," *Journal of Hospitality Marketing & Management*, 24, pp. 229–259, 2015.
- [11] W. Atkinson, "Hotel chains awaken to the value of the supply chain," *Purchasing*, 135 (1), pp. 19-20, 2006.
- [12] K.A. Fantasy, V. Kumar, and U. Kumar, "Supply management practices and performance in the Canadian hospitality industry," *International Journal of Hospitality Management*, 29 (4), pp. 685–693, 2010.
- [13] J.P. Womack, D.T. Jones, and D. Roos, *The machine that changed the world: the story of lean production--Toyota's secret weapon in the global car wars that is revolutionizing world industry*, Free Press, 2007.
- [14] S.G. Azevedo, H. Carvalho, and V.C. Machado, "The influence of green practices on supply chain performance: A case study approach," *Transportation Research Part E: Logistics and Transportation Review*, 47(6), pp. 850-871, 2011.

Particularities of power transformer reuse with respect to re-stamp process based on life cycle assessment tool

Niculae N. Boteanu, Florin Ravigan and Mihai Iacob

Abstract—This paper aims to demonstrate some sustainability aspects of power transformers, regarding the life cycle assessment with respect to transformer reuse phase through the re-stamping process. The study enhances the way of thinking that technical activities cannot be separated from the environmental impact of anthropogenic actions since within the present industrial world no biological ecosystem is free of human influence. This study is focused in assessing some sustainability aspects of power transformers, regarding the life cycle assessment, as well as the environmental impact. Power transformer, as main equipment used in the electrical transmission and distribution systems, have been analyzed in terms of efficiency and sustainability parameters, under the legislation and standards in use, in order to reintroduce the product in operation and to continue its life cycle.

Keywords—Electric power transformer, life cycle assessment, re-stamp process

I. INTRODUCTION

POWER transformers, as main equipment used in the electrical transmission and distribution systems, must be analyzed in terms of efficiency and sustainability parameters, under the legislation and standards in use. As a consequence, a holistic approach of technical, environmental and economic aspects could be highlighted [1].

We note that power transformers are electric equipment that entail significant expenditures and long times related to procurement and manufacturing processes [2-5]. Although the costs and prices vary by manufacturer and by size, a large power transformer cost can reach millions of Euros or dollars. One could also note that the a large power transformer weight is varying between 100 and 400 tones, entailing a big amount

Niculae Boteanu is with the University of Craiova, Faculty of Electrical Engineering, Romania,; e-mail: nboteanu@em.ucv.ro.

Florin Ravigan is with the University of Craiova, Faculty of Electrical Engineering, Romania,; e-mail: florin.ravigan@ie.ucv.ro.

Mihai Iacob is with the Elecmond Electric, Craiova, Romania,; e-mail: cezar@elecmond.ro.

of raw materials. It must be also noticed that procurement and manufacturing of power transformers represent a complex process that requires qualified manufacturers, the purchase of raw materials, a competitive bidding process, as well as special modalities of transformer transportation for the use phase in a certain electric network (because of the size and weight of a large power transformer).

In the manufacturing process of a power transformer there are necessary two important raw materials, namely copper and electrical steel, that account for over 50 percent of the total cost of the power transformer. We might recall that electrical steel is used for the core of a power transformer, and its characteristics are crucial to the efficiency and performance of the equipment, while copper is used for the transformer windings.

From the view point of natural raw depletion and environmental stewardship [6], the production and operation stages of a power transformer life must be correlated to the stage of transformer reuse [2-5]. Over the last few decades, international legislation have required environmental impact assessment be carried out for all phases of transformer life [6-9], according to Life Cycle Assessment tool, which includes the production phase, use phase, re-use phase and end-of-life phase. Modeling of all these transformer life stages might offer solutions for further improvement potential, focusing on technologies that reduce the electricity losses during the use phase, and on alternative materials for reducing human health and environmental impacts [7-8]. That means that the ability to adapt to changing conditions and prepare for should be based on the strong conviction that within the present industrial world the overall objective must be to enhance thinking that anthropogenic activities should be viewed in concert with the entire system on Earth [6-9].

This paper deals with some sustainability aspects of power transformers, regarding the life cycle assessment with respect to transformer reuse phase through the re-stamping process.

II. SUSTAINABLE OPERATION OF POWER TRANSFORMERS

Life Cycle Assessment (LCA) is the most appropriate managerial instrument that offers a framework integrated to Cleaner Production and Industrial Ecology for analyzing a

system, a product or an equipment from the extraction phase through the operation stage until the end of the product [7-12]. In an illustrative assertion, the full Life Cycle Assessment (LCA) is denoted as Cradle-to-grave, meaning from resource extraction - cradle to use phase and disposal phase grave, or in a new form as Cradle-to-craddle, in order to emphasize that anthropogenic activities should not be generated any waste, and the end of life of a product should mean the beginning of life of a new product [9-14].

Over the last few decades, international legislation have required environmental impact assessment be carried out for all phases of transformer life [7-15], according to Life Cycle Assessment tool, which includes the production phase, use phase, re-use phase and end-of-life phase.

The operation principle of a three phase transformer follows. Varying currents flowing in the primary winding (due to the varying phase voltages u_A , u_B and u_C) create a varying magnetic flux in the transformer core, and thus a varying magnetic field through the secondary winding [8,16-17]. This varying magnetic field induces a varying electromotive force in the secondary winding. If a three-phase electric load is connected to the secondary winding, electrical energy is transferred from the primary circuit through the transformer to the load.

For a three-phase transformer, electrically and magnetically symmetric, one could obtain the equations corresponding to the mathematical pattern [8,16], written with phase quantities space phasors in fixed coordinates, according to the following system:

$$\begin{aligned} \underline{u}_1 &= R_1 \cdot \underline{i}_1 + \frac{d \Psi}{dt} \\ -\underline{u}_2 &= R_2 \cdot \underline{i}_2 + \frac{d \Psi}{dt} \\ \underline{\Psi}_1 &= L_{\sigma 1} \cdot \underline{i}_1 + \underline{\Psi}_{u1} \\ \underline{\Psi}_2 &= L_{\sigma 2} \cdot \underline{i}_2 + \underline{\Psi}_{u2} \\ \underline{i}_1 + \underline{i}_2 &= \underline{i}_{1\mu} \\ \underline{i}_2 &= \frac{w_2}{w_1} \cdot \underline{i}_1 \\ \underline{u}_2 &= (-\underline{u}_2) \cdot (-\frac{w_2}{w_1}) \end{aligned} \quad (1)$$

where:

- \underline{u}_1 is primary voltage space phasor;
- \underline{i}_1 = primary current; space phasor
- \underline{u}_2 = secondary voltage space phasor;
- \underline{i}_2 = secondary current space phasor;
- $\underline{\Psi}_1$ = primary magnetic flux space phasor;
- $\underline{\Psi}_2$ = secondary magnetic flux space phasor;

$\underline{\Psi}_{u1}$ = main (useful) magnetic flux space phasor;

$\underline{i}_{1\mu}$ = magnetizing current space phasor;

R_1 = primary phase resistance;

R_2 = secondary phase resistance;

$L_{1\sigma}$ = primary leakage inductance; and

$L_{2\sigma}$ = secondary leakage inductance.

It might be emphasized that these equations must be completed with the magnetization curve of the ferromagnetic core of the electric transformer, since this characteristic contains information about the saturation degree of the magnetic useful flux. Depending on the magnetization curve shape, namely a linear or non-linear dependence between the magnetic flux and the magnetizing current it results a linear or non-linear mathematical model, respectively.

Modelling of power transformer might offer solutions for further improvement potential, focusing on technologies that reduce the electricity losses during the use phase, and on alternative material reducing human health and environmental impacts [2-4,7-8,12,16]. Hence, improved technical options of transformers considered as Best Available Technologies (BAT) or Best Not yet Available Technologies (BNAT) take into consideration [2-3,7]:

- applying improved cold grain oriented (CGO) steel, with improved cutting technology, and decreased lamination thickness;
- optimization of copper or aluminum windings;
- optimization of core design policies and measures fostering energy efficiency;
- change from CGO steel technologies, with a crystalline atomic structure, to transformers with amorphous cores, which have a non-crystalline anisotropic atomic structure;
- utilization of superconducting technology;
- using of smart grid technology to switch off a by-pass transformers off peak load.

The legislation and standards in use widely accept that the most important efficiency parameters are the load and no-load losses, which are responsible for the electricity waste during the use phase [7,13-15,17]. These parameters are covered by different European and international standards and regulations.

III. LIFE REUSE PHASE OF POWER TRANSFORMERS THROUGH RE-STAMP PROCESS

According to the principles and strategies of industrial ecology and cleaner production, the Life Cycle Assessment (LCA) became the most important tool in the management of each industrial organization [9,12]. Within the framework of cleaner production one of the main technico-ecological request correlated to economics is related to the technological consumption reduction, since this is the component with the biggest share in the operational costs.

Taking into consideration that nowadays in the Romanian Electrical System exist numerous power transformers that have

been manufactured many decades ago, which theoretically exceeded the normal life cycle, one could raise the issue of new solutions for adapting these existing transformers' use in the conditions of a diminished industry, aiming an optimization of power transformers loading.

Most often, in the case of under-loaded transformers, the reference is expressed by the no-load losses. From this perspective, one might note that for such a location it is indicated the use of an electric transformer with the rated power as low as possible, in order to imply the smallest no-load losses.

It is important to highlight that with respect to the power transformer losses, the decisions should be taken following a comparison among the transformer losses curves in direct correlation with a prognosis on the load curve. It means that to purchase a new power transformer the beneficiary should be concerned not only on the load characteristic, the no-load and load losses, but also on the transformer price.

In the past the transformer manufacture have been based sometimes on the concept of avoidance of copper and aluminum consumption waste, that led to transformers characterized by the life use stage with big non-load and short-circuit losses. One could note that the no-load losses (P_0) are permanent and lead to increased electrical energy expenditures of the industrial companies that exploit the power transformers.

In line with the previous idea concerning the no-load energy waste, it must be recalled that very often these power transformers are of a larger rated power than necessary for certain industrial companies. As a consequence of the

than another one of same rated power, since the cooling system is better.

As example, one could note that: from transformers of 63

S[kVA]	63	100	250	400	630	1600
P ₀ [W]	300	350	680	940	1250	2700
P _k [W]	1500	2300	4400	6000	8200	18000

Table 1 Classic transformers with normal losses

kVA might be obtained transformers of 50 kVA; from transformers of 100 kVA are obtained transformers of 75 kVA; from transformers of 160 kVA can be obtained transformers of 125 kVA; from transformers of 250 kVA are obtained transformers of 200 kVA; from transformers of 400 kVA are obtained transformers of 315 kVA; from transformers of 630 kVA are obtained transformers of 500 kVA; from transformers of 1000 kVA are obtained transformers of 800 kVA; from transformers of 1600 kVA are obtained transformers of 1200 kVA. For a classic transformer of 400 kVA re-stamped into a transformer of de 315 kVA this operation leads to no-load losses P_0 smaller than those of a transformer of 250 kVA (namely, 625 W to 650 W), while the short-circuit losses P_k are in the range of same losses in a new transformer manufactured with reduced losses of same rated power (namely, 4200 W) according to the tables 1,2,3.

It must be emphasized that there are also possible other power changes, aiming to better performances than those presented previously. Moreover, one could also change the

S[kVA]	40	63	100	125	160	200	250	315	400	630	800	1000	1600
P ₀ [W]	185	250	320	380	460	580	650	680	930	1300	1350	1700	2300
P _k [W]	985	1350	1750	2100	2350	2800	3250	4200	4600	6500	8600	10500	14960

Table 2 Low losses transformers

economic activity resizing in Romania, the necessary of installed power of these industrial companies decreased.

In the context of alignment of electrical energy prices to the European level, the need to reduce the electricity consumption is vital in order to maintain or even increase the competitiveness of economical companies of Romania. Nowadays the solution applied in order to reduce the installed power consists in changing the existent electric transformer to a transformer of lower rated power.

Following the observation that a power transformer is a static electromagnetic equipment, without components in move, it is ascertained that a power transformer could have a long and sustainable operation life. Based on this premise will be a question of opportunity to realize the decrease of no-load losses (P_0) and of the windings 'losses (P_k) without being necessary to purchase a new transformer. This way the transformer efficiency might be improved through the re-stamp process. This technological operation consists in the transformer rewinding corresponding to a smaller apparent power, having as a benefit the decrease of electric losses in the power transformer. In these operation conditions the power transformer might be overloaded if necessary for a longer while

transformation ratio of a power transformer, depending on the need of the beneficiary.

As example, it is presented the re-stamp operation for a

S[kVA]	50	75	200	315	500	1200
P ₀ [W]	150	200	580	625	910	1600
P _k [W]	1000	1350	2800	4200	6000	14500

Table3 Transformers re-stamp

transformer from 6/0.4 kV to 20/0.4 kV. In order to perform the re-stamp operation there are necessary the technological operations of removal of the active part; removal of accessories on the active part; MV and LV bushings comutator of plots; MV and LV connections of oil level conservative, etc.; removing the coil from the columns of the magnetic core; cleaning and technical inspection for core supportive scaffolding for the core, of the tiles and pressing rings and tie bar bolts etc. All these are labeled to identify and possible replacements substandard. It will carry out cleaning, sanding until metallic luster, priming and painting of metal constructions of transformer (pan, cover, conservative, supportive scaffolding for the core). The tank tightness shall be verified in order to eliminate oil leaks. Technological will

continue execution of spare parts, and brake pressing supporting connections; proper execution of the new power transformer coils; mounting the coils on the column of the magnetic core; execution of connections and mounting wafer switch on the MV; execution for secondary connections (LV); drying the active part is made in special installations and high vacuum environment; filling with transformer oil; transformer accessories mounting (bushings, oil level, etc.).

After re-stamping tests and measurements are performed according SREN 60076 2003 PE 116/1994 and include: Checkout of transformation ratio. Ascertainment of the connection group. Determination of the ohmic resistance of the windings. Measurement of the insulation resistance of the windings to the ground and determination of the absorption coefficient. Verification of the dielectric strength of the oil. No-load test with the measurement of no-load losses. Short-circuit test, with the measurement of the load losses and short-circuit voltage. The test with applied voltage to verify the windings insulation to the ground. The test with induced voltage to verify the insulation between the winding turns. Leak testing using nitrogen pressure. Finishing and certification of transformer.

Given the technological progress, the Regulation. 548/2014 on the implementation of Directive 2009/125 / EC of the European Parliament and of the Council as regards small, medium and large power transformers [18] recommended that the verification and operations to assess at least: the ability to determine the minimum values on maximum efficiency index for all transformers; the ability to separate itself transformer losses from other losses associated with other components which function as voltage regulation, when appropriate; opportunity to establish minimum performance requirements for single-phase power transformers as well as for small power transformers; appropriateness, in time, the concessions granted transformers installed on poles and special combinations of winding voltages for medium power transformers; the ability to reduce the environmental impact, other than energy consumption in the use phase.

IV. CASE STUDY. EXPERIMENTAL RESULTS OF POWER TRANSFORMER FOR LIFE REUSE PHASE

In order to be reused, a failed transformer must be repaired and then submitted to specific tests. In this section there are presented the results of a transformer and an autotransformer testing according to IEC standards and EU legislation [17-18].

The most important efficiency parameters of transformers are no-load and load losses, which are responsible for the electricity losses during the use phase. These parameters are covered by different standards depending on the transformer type, the main being the IEC 60076-1, that is the general generic standard for power transformers with European equivalent EN 60076-1.

I. Hence, for the transformer that had failed during the use phase in the Romanian Energetic System, after repairing it, the compulsory tests for the transformer reuse were performed.

The transformer with the terminals' connection Y0d – 11, rated power $P_N=250\text{MVA}$, rated voltage $UN=110/22\text{kV}$, Highest

voltage for equipment $U=123\text{kV}$ and rated current $I_N=131,2/656\text{A}$ had been submitted to tests in order to be reuse within the Romanian Electric System after the repair process.

First step consisted in verifying the terminals' connection Y0d – 11 and the transformation ratios, as below in Table 4.

Tested terminal	Earthed terminals	
	Direct	Trough resistors [Ω]
A	B, C, a, b, c	N (1)
N	a, b, c	A, B, C (1)
a	N, A, B, C	b, c (1)

Table 4

Further there were performed the tests according to IEC standards.

II. Further in this paper there will presented the full and chopped lightning impulses of transformer tests from manufacturers that were investigated by method of graphically recording according to IEC 60060-1/1989, IEC 61083-2/1996 and IEC 60076-3/2000. In this case study the tested product was a three- phase transformer ONAF 250 MVA; 110/22 / 30 kV; Connection Y0d – 11

The technical characteristics established by manufacturer are:

- Rated power: OFAF 280 for HV / 280 for MV / 60 MVA for LV
- Rated voltage: 110 kV for HV; 22 kV for LV
- Rated normal current: 131.2A for HV; 656 A for LV
- Rated frequency: 50 Hz.

The reference standard is IEC 60076 – 3/ 2000, and the tests performed were for 1.2 / 50 μs full wave lightning impulse test.

Tested terminal	Full wave (kV)	Cut wave (kV)	Wave- shape	
			Full wave (μs)	Cut wave (μs)
A, B, C	450	450	0,84÷1,56 / 40÷60	1.2 / 2 ÷ 6
N	290	-	0,84÷13 / 40÷60	-
a, b, c	125	125	0,84÷1,56 / 40÷60	1.2 / 2 ÷ 6

Table 5

One could note that for the lightning impulse test for full wave 1.2 / 50 μs the atmospheric conditions were: $p = 1000 \text{ mbar}$; $t = 13^\circ\text{C}$; $hr = 66\%$. the test standard: IEC 60076 – 3 / 2003, clause 13 and 14, and the rated lightning impulse withstand voltages as below in Table 6.

Tested terminal	Parameters of impulse generator			
	Stages number	C_s [μF]	R_s [Ω]	R_p [Ω]
A, B, C	4 x 1	0,144	253,8	590
N	2 x 1	0,288	288	153,3
a, b, c	1 x 4	2,304	47	46

Table 6

The parameters of the impulse generator 4.2 MV no.5 – 1197 and of the used voltage divider were the following.

As an Addenda one could note that C_s is the equivalent capacity of impulse generator; R_s is equivalent serial

resistance of impulse generator; and R_p is equivalent parallel resistance of impulse generator

The terminal connections of the tested autotransformer were as below, with the notes that: during the test, core, frame, tank and terminals of current transformers were connected to earth; during the tests the tap changer was on following position: N, A, a, b, c – 1; B – 10; C – 19.

In Fig. 1 it is represented the Scheme winding neutral HV test, while Fig.2 encompasses the HV winding neutral terminal testing circuit and in Fig. 3 is depicted the Test Scheme of the LV winding line terminals.

As a Legend for the above figures one could note that: C_s is equivalent capacitance of impulse generator; C_1 is HV

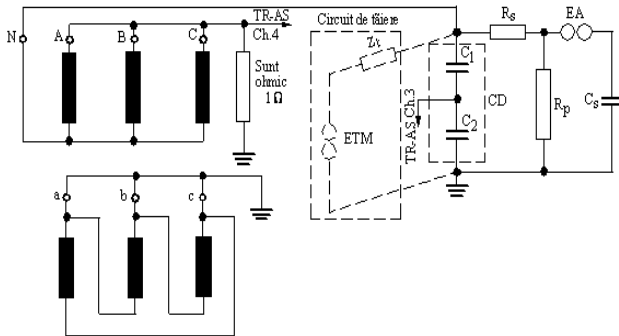


Fig.1 Test scheme of HV winding neutral

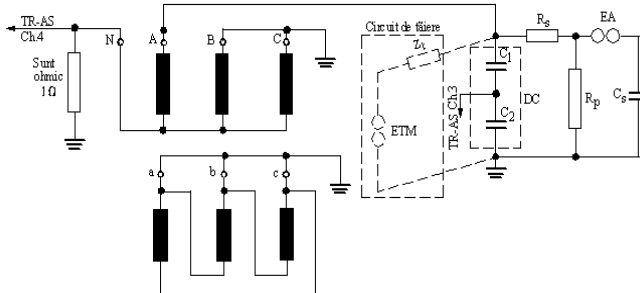


Fig.2 Test scheme of the HV winding line terminals HV

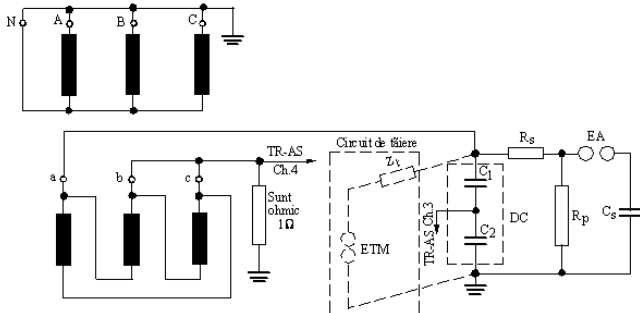


Fig.3 Test scheme of the LV winding line terminals LV

capacitance of divider; C_2 is LV capacitance of divider; R_s represents the equivalent serial resistance of impulse generator; R_p is the equivalent parallel resistance of impulse generator; DC/CD is capacitive divider; EA is the sphere-gap; ETM is the multiple chopping-gap; Z_c is the chopping circuit impedance.

In Figs. 4-6 there are presented the corresponding oscillograms.

One could note that:

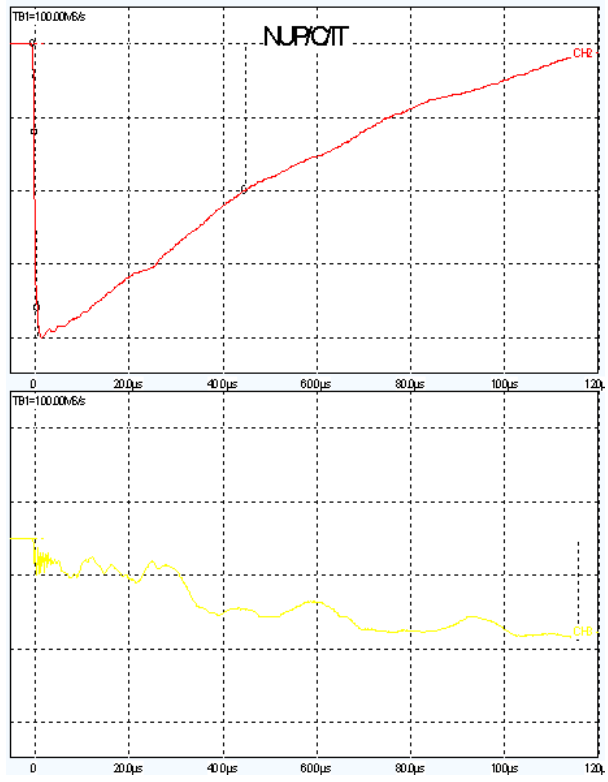


Fig.4 Regarding the CH₂- NUP/C/HV for
 $U_p=227\text{kV}$, $T_1=1,14\mu\text{s}$, $T_2=45,4\mu\text{s}$, CH₃ for $I_p=1254\text{A}$ and CH₃

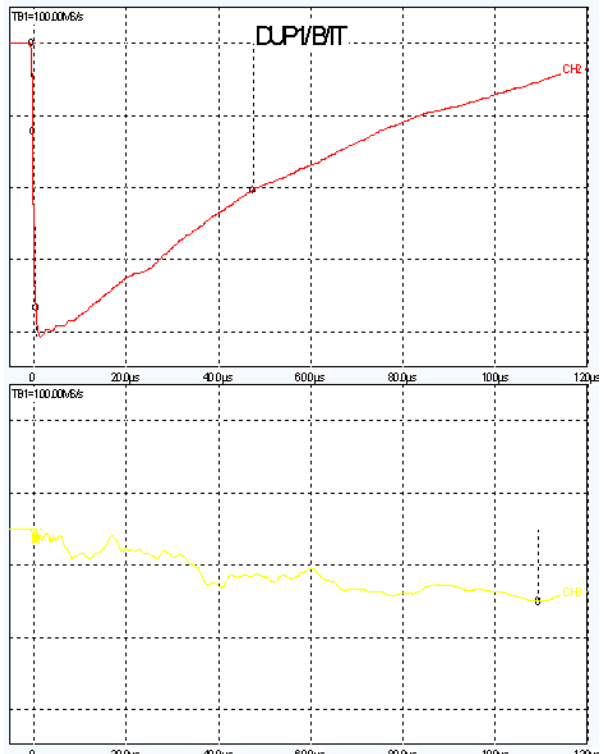


Fig.4 Regarding the CH₂- DUP/B/HV, eval. LI, for $U_p=451,6\text{kV}$,
 $T_1=1,15\mu\text{s}$, $T_2=48,2\mu\text{s}$, and CH₃, eval. P_k for $I_p=160,2\text{A}$

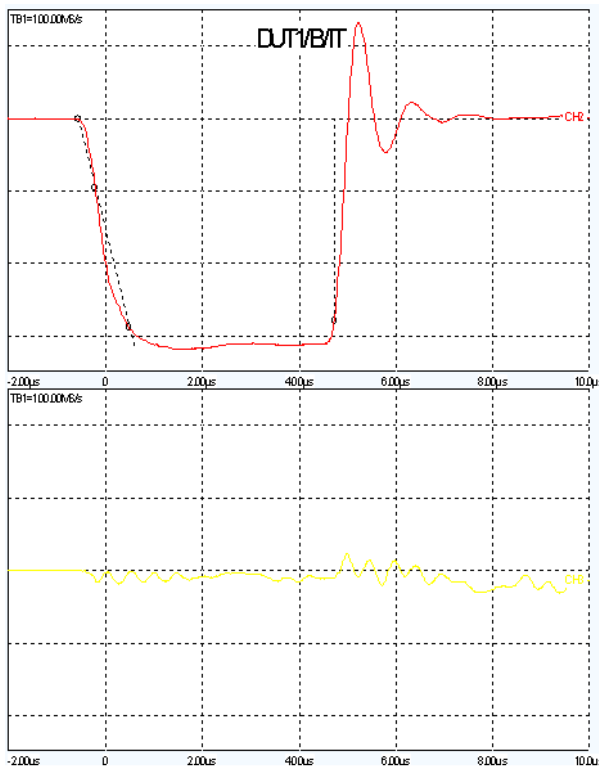


Fig.5 Regarding the CH₂- DUT1/B/HV, eval. LI, for U_p=453,9kV, T₁=1,16μs, T_c=5,29μs, and CH₃, eval. P_k for

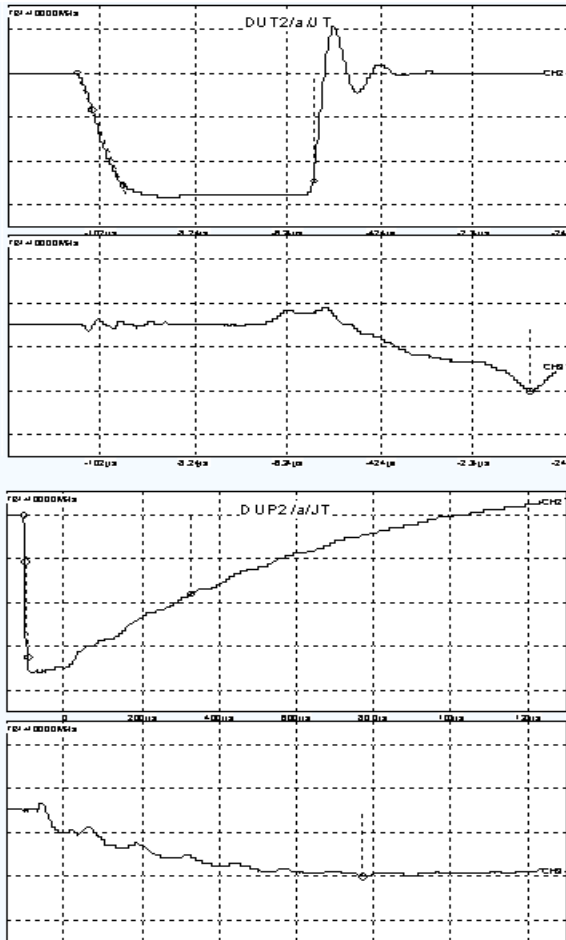


Fig.6 Regarding the CH₂ – DUT2/LV, for U_p=123,5kV, T₁=1,1μs, T_c=5,8μs, and CH₃ for I_p=208,2A; DUP2/LV for U_p=125,2kV, T₁=1,02μs, T₂=42,4μs, and CH₃ for I_p=500,2A

tail time; T_c – chopping time – parameters of testing impulse wave; I_p – current peak value measured on the tested phase.

2. Wave forms of voltage impulse during the tests were inside of the limits prescribed by the test norms.

As a test conclusion one could emphasize that the product passed the test.

V. CONCLUSION

This study was thought and conducted according to the recommendations and requirements given in the IEC standards, the ISO 14040 series of LCA standards.

This paper demonstrated some sustainability aspects of power transformers, regarding the life cycle assessment with respect to transformer reuse phase through the re-stamping process.

A main purpose of the paper was to point out that a holistic approach to technical, environmental and economic aspects must be highlighted. No missing test standards or measurement procedures on energy use and other environmental parameters have been identified for power transformers.

REFERENCES

- [1] J. Ray, "The environmental impacts of electrical transformers", *The Electricity Forum. Electrical Transformers Explained*, Available at: http://www.ehow.co.uk/info_8388486_environmental-impacts-electrical-transformers.html, Accessed on 10 July 2014.
- [2] NIEHS Working Group Report of National Institute of Environmental Health Sciences of US National Institutes of Health, "Assessment of Health Effects from Exposure to Power-Line Frequency Electric and magnetic Fields", Brooklyn Park, Minnesota 16-24 June, 1998, available at: http://www.niehs.nih.gov/health/assets/docs_a_e/emf1.pdf, Accessed on 29 July 2014.
- [3] VITO&BIOIS, Report on Distribution and Power Transformers, Contract N°. S12.515810 call ENTR/2008/039, "Sustainable Industrial Policy – Building on the Ecodesign Directive – Energy-Using Product Group Analysis/1", September 2010, Available at: http://www.ebpg.bam.de/de/ebpg_medien/entr2/402_studyd_10-10_part1-7.pdf, Accessed on 10 July 2014.
- [4] Office of Electricity Delivery and Energy Reliability under the direction of Patricia Hoffman, Assistant Secretary, and William Bryan, Deputy Assistant Secretary. "Infrastructure Security and Energy Restoration", Report of U.S. Department of Energy on LARGE POWER TRANSFORMERS AND THE U.S.ELECTRIC GRID. DOE / OE / ISER , June 2012, Available at http://energy.gov/sites/prod/files/Large%20Power%20Transformer%20Study%20-%20June%202012_0.pdf, Accessed on 30 July 2015
- [5] F.X. Zgainski, B. Caillault, V.L. Renouard. Validation of power plant transformers re-energization schemes in case of black-out by comparison between studies and field tests measurements. The International Conference on Power Systems Transients (IPST'07) in Lyon, France on June 4-7, 2007, Available at http://ipstconf.org/papers/Proc_IPST2007/07IPST115.pdf, Accessed on 10 July 2015
- [6] United Nations, *The future we want*, United nations Conference on Sustainable Development, Rio de Janeiro, Brazil, 20-22 June 2012,

- Available at: http://www.unep.fr/scp/pdf/Rio_The_Future_We_Want.pdf
Accessed on 10 June, 2015
- [7] C.A.Bulucea, D.A. Nicola, N.E. Mastorakis, P. Dondon, C.A. Bulucea, D.C. Cismaru, "Fostering the Sustainability of Power Transformers", Recent Researches in Environmental & Geological Sciences, Proceedings of 7th WSEAS International Conference on Energy and Environment (EE'12), Kos Island, Greece, July 14-17, 2012, pp.72-81.
- [8] C.A. Bulucea, D.A. Nicola, M.A. Rosen, N.E. Mastorakis, C.A. Bulucea, "Modelling Examples of Sustainable Electric Power Equipment", Recent Advances in Environmental and Earth Sciences and Economics, Proceedings of the 2015 International Conference on Energy, Environment, Development and Economics (EEDE 2015) Proceedings of the 2015 International Conference on Geology and Seismology (GESE 2015) Proceedings of the 2015 International Conference on Maritime and Naval Science and Engineering (MANASE 2015) Proceedings of the 2015 International Conference on Water Resources, Hydraulics & Hydrology (WHH 2015), Series: Energy, Environmental and Structural Engineering Series | 38, Zakynthos Island, Greece July 16-20, 2015, pp.108-115.
- [9] LCA study of current transformers", DANTEs project co-funded by the EU Life-Environment Program, Available at: <http://www.dantes.info/Publications/Publication-doc/DANTEs%20ABB%20LCA%20study%20of%20instrument%20transformers.pdf>, Accessed on 19 July 2014.
- [10] T.E. Graedel, "On the Concept of Industrial Ecology", *Annual Review of Energy and the Environment*, Vol. 21, November 1996, 69-98.
- [11] B.R. Allenby, *Industrial Ecology: Policy Framework and Implementation*. Prentice-Hall, New Jersey, 1999.
- [12] N.Boteanu, F.Ravigan,"Some aspect of assessment of environmental and human health effects of power transformer life cycle", ISBN 978-1-61804-255-2, Proceedings of the 2nd International conference on Environment, Energy, Ecosystems and Development EEEAD2014, Athens, Greece, November 28-30, 2014, pp.39-45.
- [13] Electromagnetic Compatibility – the EMC Directive 89/336/EEC, 1992, Available at: http://ec.europa.eu/enterprise/policies/european-standards/harmonised-standards/electromagnetic-compatibility/index_en.htm, Accessed on 1st September 2014
- [14] Guide to the implementation of directives based on the New Approach and the Global Approach, European Commission, 2000, Available at: http://ec.europa.eu/enterprise/policies/single-market-goods/files/blue-guide/guidepublic_en.pdf , Accessed on 14 June 2014.
- [15] Directive 2004/40/EC of the European Parliament and of the Council – electromagnetic fields and waves, of 29 April 2004 on the minimum health and safety requirements regarding the exposure of the workers to risks arising from electromagnetic fields and waves.
- [16] D.A. Nicola, C.A. Bulucea, *Electrotechnics, Electrical Equipment and Machines*, Vol. II "Electrical Equipment", Publishing House SITECH Craiova, 2005.
- [17] IEC 60076-1 (2000) series on Power Transformers, Available at: <http://webstore.iec.ch/>, <http://www.saiglobal.com/pdftemp/previews/osh/as/as60000/60000/60076.1-2005.pdf> , Accessed on 25 August 2014.
- [18] Commission Regulation (EU) No 548/2014 for small, medium and large power transformers, Available at http://www.tuv.com/en/usa/about_us/regulations_and_standard_updates/latest_regulations_us/latest_regression_content_us_220106.html , Accessed on 15 July 2015.

Glass – structural material of buildings

Marcela Karmazínová and Jindrich Melcher

Abstract—In the period of several last decades, glass is used not only as a transparent filling of building openings, but also as the statically and dynamically loaded civil engineering structural component. Structural glass is brittle material without elastic or elasto-plastic behaviour, so the missing pliability of the material cannot help to decrease the influence of the local stresses concentration. Also the deformations of the slab structures can significantly exceed the slab thickness, so it is necessary to apply the theory of the large deflections, i.e. geometrically nonlinear theory of the 2nd order of thin slabs. Thus, the design of load-carrying structures made of structural glass requires diametrically different approaches than in the case of conventional building materials. The paper presents some examples of the arrangement of load-carrying structural systems and inclusion of the glass components into the buildings, structural details and used basic materials. Significant parts of the verification of the reliability of structural glass systems are experiments and loading tests realized for the real load and boundary conditions and for the real composition of used materials corresponding to the verified structure. In the paper, basic typical failure modes of the components made of float glass and laminated float or tempered glass with intermediate foil. Also the examples of realized buildings using load-carrying components of structural glass are mentioned, respectively also their damage and crash.

Keywords—Structural glass, float glass, tempered glass, material property, building, civil engineering, failure.

I. INTRODUCTION

THE basic classic materials of building load-carrying structures (masonry, concrete, steel, timber) are more significantly complemented (in the last period) by structural glass, which is not only traditional filling of smaller window openings, where their dimensions (thickness) arising from the long term practical experience has not been usually verified by the static assessment. Emerging trends in the architectonic creation of the buildings requiring large glazed areas of civil structures, but – on the other hand – also the possibilities of their realization related to the development of the production technology of the large scaled glass components, bring new

This work was supported by the Ministry of Education, Youth and Sports of the Czech Republic under the research projects LO1408 “AdMaS UP – Advanced Materials, Structures and Technologies”, within the “National Sustainability Programme I”.

Marcela Karmazínová, Professor of Civil Engineering, is the head of the Department of Metal and Timber Structure of the Faculty of Civil Engineering at the Brno University of Technology, Veveří St. 331/95, 602 00 Brno, Czech Republic (corresponding author to provide phone: +420 541 147 310; fax: +420 549 245 212; e-mail: karmazinova.m@fce.vutbr.cz).

Jindrich Melcher, Professor of Civil Engineering, is the head of the Pooled Testing Room for Load-Carrying Structures of the Department of Metal and Timber Structure, Faculty of Civil Engineering, Brno University of Technology (e-mail: melcher.j@fce.vutbr.cz).

challenges for the industry of the glass production, as well as for structural engineers.

Similarly as traditionally in the case of load-carrying civil structures, glass requires – in dependence on the support type, load intensity and material properties – the verification of the reliability, durability and effectiveness, as it is, in civil engineering practice, necessary in the case of other structural materials.

For the reasons mentioned above, the attention is paid to the research, realization and development of methods for the design and resistance of the load-carrying structures made of structural glass, over the world. For further development of the usage of load-carrying structural glass in civil engineering structures, it is important to develop the new technologies and procedures of the glass production, which are ensured by many significant producers of the diverse assortment of glass components, as well as respective supply companies.

II. MATERIALS AND COMPOSITION OF STRUCTURAL GLASS ELEMENTS

A. Annealed Glass, Float Glass

The basic type of building glass, which can be modified and treated by tempering, staining, sandblasting and cutting, is clear float glass. The input raw material for its production is silica in the form of sand, soda in the form of carbonate and sulphate, and limestone as a stabilizer. Flat clear glass is an input raw material for the wide range of the usage of glass in building structures (interiors and claddings of buildings). The basic overview of the heat-strength treatments of float glass with appropriate technical terminology is shown in Fig. 1.

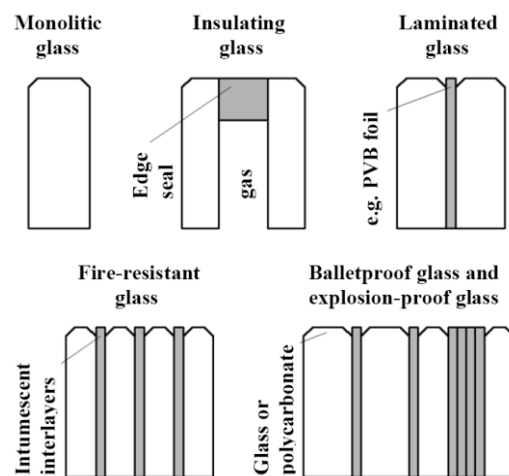


Fig. 1 composition and terminology of structural glass components

B. Fully Tempered Glass, Toughened Glass

The increasing of the mechanical resistance of float glass can be reached using the technology of heat-toughening (tempering) that means glass is heated to the specific temperature (about 650 °C) and subsequently it is cooled by the sharp airflow. Due to the cooling, inside the structure of heat-strengthened glass the tensile stress occurs, while on the surface the compression stress occurs.

Thus, the physical properties from the viewpoint of the strength are significantly changed. In the case of breaking, glass will break into small pieces, so the risks of personal injury and property damage are minimized. The new distribution of the stress in toughened glass affects the essential change of glass properties.

Fully-tempered glass will obtain the resistance to the strike, and further, the flexural strength and thermal resistance up to 200 °C will be increased. Thanks to these properties, this glass is classified as safety glass. Glass must be finally machined (drilling holes, grinding edges, etc.) before tempering, because its further machining after toughening is not already possible.

The usage of heat-toughened glass requires significant attention from the viewpoint of the elimination of safety risks associated with keeping technological limits of dimensions and shape of the component, initial deformations and failures, details of bearing on the support structure, and so on. The special problem can also be spontaneous explosion of heat-toughened glass.

The problems mentioned above are in detail discussed, for example, in the sources [4] and [5], which define the basic causes of the failures of glass:

- the breakage of glass due to the temperature shock;
- the failure of glass due to the assembly mistake;
- the failure of glass caused by the poor machining;
- the condensation in the interspace of insulating double glass or triple glass;
- the spontaneous explosion of heat-toughened glass.

In the cases, when the risk of the spontaneous breakage of glass with nickel sulphide (NiS) inclusions is inadmissible, it is recommended to use so-called "heat-soak" test of already heat-treated glass panes. So it is practically avoided the usage of glass, which can crack without previous warning due to anomalies caused in the tempering process.

C. Heat Strengthened Glass, Partly Toughened Glass

The next type of heat-strengthened glass is semi-hardened partly toughened glass. Its mechanical properties of soda-lime-silica glass do not change during the progressive heating at least up to 200 °C and they are not influenced by the temperatures below freezing.

In the production process, glass is subjected to the special heat treatment, which is different from usual heat toughening. The temperature of glass heating and the time of the whole treatment process are different. Then, the result is glass with increased mechanical resistance (compared with float glass), and in the case of breakage, the pane is broken to the larger pieces. The resistance to the heat stress is also higher. The

advantage is, that this type of glass has no nickel sulphide inclusions (NiS) and resists to the temperature difference of up 100 °C.

D. Laminated Safety Glass

Laminated safety glass is composed of two or more panes of tempered or heat-strengthened glass with the usage of intermediate foil inserted in autoclave at the temperature of about 140 °C and the pressure of 0.8 MPa. Most often used intermediate foils are polyvinyl butyral (PVB) or ethylene vinyl acetate (EVA) foils. The thickness of the foil is, according to the type, 0.38 mm or 0.76 mm.

In the case of breakage, safety glass remains glued to the foil and the personal injury and property damage are avoided. In the cases, when one of glass is not damaged, the wholeness of glass pane is maintained.

Safety glass has the application there, where it is required avoiding injury, to protect against burglary and firearms and noise protection. The combination of laminated heat-toughened glass is also used for walkable glass slabs.

Safety laminated glass with acoustic effect uses PVB foil and reaches improved characteristics for avoiding the noise spreading. The properties of this glass depend on the specific composition and combination of the glass panes and foils. The maximal value of the sound attenuation is 45 dB.

III. PRINCIPLES OF DESIGN OF STRUCTURAL GLASS COMPONENTS

The default illustrative comparison of the static behaviour of glass, steel and concrete is evident from stress-strain diagrams for these materials drawn in Fig. 2. The course of those diagrams indicates the response of the relevant material to the load.

It is evident, that structural glass is ideal elastic brittle material without elastic-plastic or plastic behaviour, and thus, pliability (ductility) of the material cannot decrease the influence of the concentration of local stresses in the case of intensive loading.

From the viewpoint of the design of structural details and connections, it is necessary to eliminate the direct contact of glass and supporting steel structure, for example using plastic washers, inserts, eventually sealants or backed silicone profiles, which allow to exclude failures arising from the rigidity of locally loaded glass component.

In addition, the deflection of slab structures – particularly in the case of one-layer panes – can significantly exceed the slab thickness, so for the static analysis it is necessary to utilize the theory of the large deflections, i.e. geometrically nonlinear 2nd order theory of thin slabs, instead of the classic Kirhoff's theory of thick slabs. In this case, the flexural effects are supplemented by the membrane components of the load in the slab plane.

The principles of the design of the load-carrying structures with the application of structural glass require markedly different approaches than in the case conventional building materials.

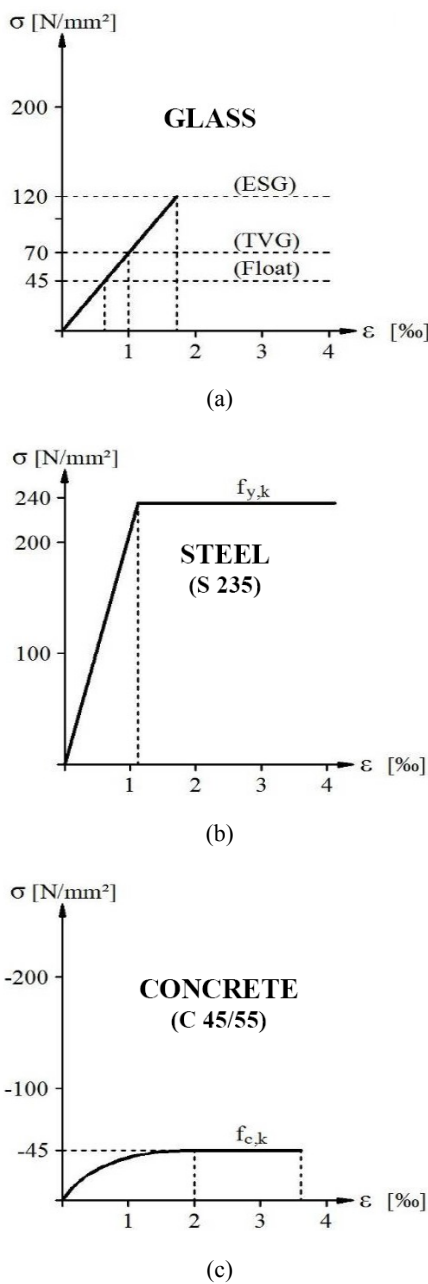


Fig. 2 characteristic stress-strain diagrams of (a) glass, (b) steel, and (c) concrete

Basic material, mechanical and physical characteristics of soda-lime-silica glass are mentioned in Table 1.

Table 1 characteristic values of soda-lime-silica glass

Quantity	Symbol	Value and unit
Density (specific weight)	ρ	2 500 kg·m ⁻³
Young's modulus of elasticity	E	70 000 N·mm ⁻²
Shear modulus of elasticity	G	30 000 N·mm ⁻²
Poisson's coefficient	μ	0.23
Coefficient of thermal expansion	α	$9 \cdot 10^{-6}$ K ⁻¹

The philosophy, methodology and procedures of the design of load-carrying structures for the basic materials (concrete, masonry, steel, timber, steel-concrete) are in detail elaborated and introduced in the unified European Standards (Eurocodes).

In general, for structural glass, all the principles defined in EN 1990 – Eurocode: Basis of Structural Design and EN 1991 – Eurocode 1: Loading Actions, where the principles for the loads by snow, wind, dead load, live load, etc. are mentioned, are valid.

Normative uniform European document allowing the static design of load-carrying systems with the usage of structural glass is however in the stage of the proposal and it is not definitively approved. Therefore, in this paper, informative data only, following the concept of selected procedures for the design of building structures with the usage of structural glass are mentioned, in the meaning of prepared normative documents arising from the methodology of limit states.

A. Strengths of Structural Glass

The basic characteristic strength of float glass f_{kg} , as a basic material property, can be given as the value of

$$f_{kg} = 40 \text{ N/mm}^2. \quad (1)$$

The characteristic strength f_k of the component made of structural glass can be determined according to the formula

$$f_{Rk} = k_{mod} \cdot k_{sp} \cdot f_{kg}, \quad (2)$$

where k_{mod} is the factor of the type and duration of the load, which reaches the values in the range from 0.29 to 1.00;

k_{sp} is the factor of the type of the surface of glass component, which reaches the values in the range from 0.32 to 0.55.

The basic characteristic strength of heat-strengthened glass can be given as the value of

$$f_{kg} = 70 \text{ N/mm}^2. \quad (3)$$

The basic characteristic strength of heat-toughened glass can be given as the value of

$$f_{kg} = 120 \text{ N/mm}^2. \quad (4)$$

The characteristic strength of the components made of structural heat-treated glass can be in principal determined according to the same formula as for float glass, i.e. formula (2), where, similarly as in the case of float glass, k_{mod} is the factor of the type and duration of the load and k_{sp} is the factor of the type of the surface of glass component.

B. Resistance of Structural Glass Load-Carrying Systems

The verification of the resistance of load-carrying system with the usage of structural glass for the ultimate limit state

can be performed according to the design reliability condition:

$$E_d \leq R_d, \quad (5)$$

where E_d is the design value of the load effect;

R_d is the design value of the resistance of the structural component or system.

The design strength f_{Rd} of the structural glass component can be determined according to the formula:

$$f_{Rd} = f_{Rk} / \gamma_M, \quad (6)$$

where the value of the reliability safety factor γ_M is recommended to take as

$$\gamma_M = 1.2. \quad (7)$$

From the viewpoint of the serviceability limit state, the permissible values of the deflections δ_{lim} are given as (up to)

$$\delta_{lim} = L / 100, \quad (8)$$

where L is the span of the component between supported edges.

All the indicated design factors, material characteristics and reliability coefficients will be more in detail defined after the approval of the prepared European document EN 13474 Glass in Civil Engineering.

In conclusion of this paragraph, it should be noted, that it is not recommended to use and design the thickness of one layer of load-carrying structural glass less than 3 mm and greater than 25 mm.

IV. SELECTED EXAMPLES OF REALIZATIONS AND STUDIES

The development of the use of the building load-carrying systems with the application of structural glass is further indicated by the selection of illustrative examples of buildings and project studies realized over the world, but also in the Czech Republic.



Fig. 3 stairs in Audio-Video Shopping Center, New York

The glass stair, suitably integrated to the interior of the Audio-Video Centre in San Francisco, is shown in Fig. 3 (photo J. Melcher). Glass does not prevent the vista to the internal space of the building. The stair grades, as well as the vertical supporting structure stiffened by supporting transverse ribs, are designed and made of glass. Transverse stiffening ribs are necessary, with respect to the insurance of the resistance of the high slender wall subjected to the vertical compression load.



Fig. 4 Juilliard School in Lincoln Center, New York

The structures in the areas of Lincoln Centre in New York stiffened by twisted rope are illustrated in Fig. 4. Partition peripheral or external walls or, eventually, railing fillings without significant effects of the basic loadings (vertical load, wind, and so on) shall be assessed according to the technical document ČSN EN 12600 Glass in Civil Engineering – Shuttle Test – Method of Impact Test (ČNI Prague, 2003) and ČSN 74 3305 Protective railings (ČNI Prague, 2008).

High glazed peripheral building walls – with respect to the significant effects of the wind load (compression or sucking) – shall be necessarily stiffened by the steel load-carrying structure, which create the support system of peripheral glass cladding.



Fig. 5 (a) wall in Waterloo Station, London; (b) hall of International Forum, Tokyo

In Fig. 5 (a) (photo J. Melcher), the structure of the glazed wall in the area of Waterloo Station in London, with the steel support structure, which is created by the truss system with ties and struts placed both outside and inside the building, is shown. In Fig. 5 (b) (photo J. Melcher), the structure of the glazed wall of so-called Glass Hall in the areas of the International Forum in Tokyo, with steel support structure, created by the truss system with ties and struts placed inside the building, is shown.

From the shots mentioned the arrangement of the relevant structural system is evident, and mentioned examples indicate large diversity of the composition and structural design of load-carrying systems with the usage of structural glass.

The illustration of the successful usage of structural glass in the Czech Republic is the oblique façade of the store Sykora Home Prague [6] in Fig. 6. The wall of the façade is along the top line inclined from the vertical plane. The laminated glass panels are through the targets anchored to the steel load-carrying structure created by lattice crosspieces, which are supported by steel columns inclined in parallel with the façade. The lattice tube crosspieces are supported by the system of rectifiable parallel ties DETAN.



Fig. 6 structure of oblique façade of Sykora Home building, Prague

The example of the usage of structural glass for the roofing of the platform of bus station near the railway station Ostrava – Svinov is shown in Fig. 7. The work has been ensured by the company METALPROGRES Inc. Těčice, and on the base of this, the experimental programme [7], [9] of the verification of load-carrying capacity and deformations of the panels made of structural glass corresponding the real composition and supporting of test specimens, has been realized. Relevant loading tests are more in detail mentioned below in the chapter 5.

The roofing component made of two-layer tempered glass with intermediate foil showed the possibility of the fall of glass slab to the covered space in the case of the failure around metal targets. With regards to otherwise favourable deformation and strength characteristics of proposed

composition of roofing panel, it can be effective, to eliminate this problem by supplementary technical modification, which will exclude the fall of the failed specimens. The proposed modification lies in the inserting protective rope (see Fig. 7) under glass slab. The rope is anchored to the shackles in the axis of the bolts of circle connecting plates, and it is lead diagonally and further along the line connecting four support nodes of glass slab. The utilized steel rope had the diameter of 5 mm; in general it is enough to design the rope according to the corresponding self weight and the number of the hangings. The failed pane composed of laminated tempered glass is detained by the protective rope, it remains undivided thanks to the stiffening effect of the foil and in addition, it is capable of transport and manipulation when replacing.



Fig. 7 roofing of platform of bus station, Ostrava - Svinov

In the period of the last years, the usage of the large-scale glazed façades of buildings has been significantly spread. Their necessary stiffening, in relation to the adverse effects of compression and sucking of the wind, is ensured by the transverse glass ribs, so-called fins, which are inserted, in parallel in the certain distances, into the façade system.

Various possibilities of the composition of the glass walls of the mentioned type are documented by the examples of the realizations over the world, but also in the Czech Republic.

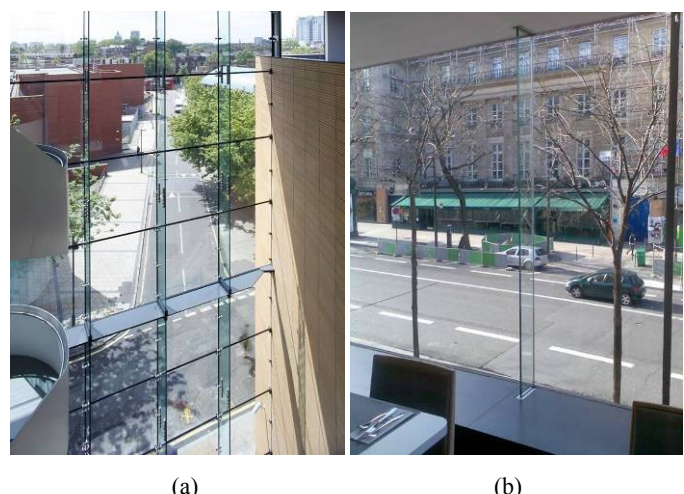


Fig. 8 (a) South Bank University, London; (b) Holiday Inn, Paris

Fig. 8 (a) shows the shot of the structural glass wall stiffened by transverse glass ribs in the building of London South Bank University. Another example of the similar solution of the restaurant glass wall in Holiday Inn Hotel in Paris is shown in Fig. 8 (b) (photo J. Melcher). Further, the solution realized in Burj Al Arab Hotel in Dubai is illustrated in Fig. 9, and finally, the glass wall in the building of Harbour Grand Kowloon Hotel in Hong Kong is in Fig. 10 (photo J. Melcher).



Fig. 9 Burj Al Arab Hotel, Dubai



Fig. 10 Harbour Grand Kowloon Hotel, Hong Kong

From the structures of the similar type realized in the Czech Republic, it is documented the glass façade stiffened by transverse ribs, which lines the stairs tower of the new building of the Faculty of Civil Engineering of Technical University of Ostrava, as indicated in Fig. 11 (photo J. Melcher). This work was tasked by the company TOLZA, Ltd., Brno. The tests of the connection of the transverse rib to the façade of the type of “metal plate – glass” with the usage of two-component silicon sealant, have been performed, as illustrated in Fig. 12.

The specimens with surface treated by powder-coated Al-profile, with coating represented by polyester thermoset powder of PE GREY RAL7015 GLOSS, or eventually, powder coating of Interpol D1036 Lesk 85, showed the

satisfactory adhesion of sealant to metal and glass, and the failure always occurred on the shear area going through silicon part of the specimen – for more see e.g. [8].



Fig. 11 structural glass façade stiffened by transverse ribs – Faculty of Civil Engineering, Technical University of Ostrava

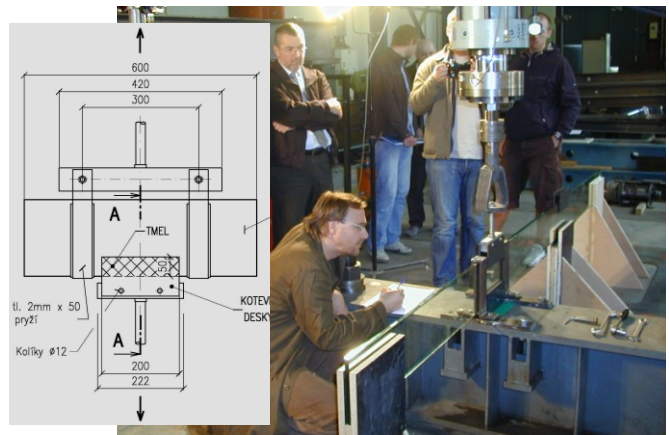


Fig. 12 tests of sealant for glass façade for Faculty of Civil Engineering, Technical University of Ostrava

The special structural group with the usage of exposed load-carrying glass components are large aquariums in the areas of ZOOs or social centres.



Fig. 13 aquarium on area of exposition of ZOO Park

The example of the aquarium in the interior of the building of ZOO Park is shown in Fig. 13. Probably due to the imperfect structural solution of the spot support of the load-carrying structure near the edge of the glass wall, the aquarium has been failed when filling by water, as evident from Fig. 14 (photo J. Melcher). The vertical wall of the aquarium composed of laminated glass with the thickness of $3 \times 8 = 24$ mm with inserted intermediate PVB foil had the width of 4 800 mm and the height of 2 800 mm. It was divided by vertical gaps, at the thirds of the length filled by silicon sealant. The illustrative utilization of ANSYS software (J. Kala) for the elaboration of the expertise of the crash is briefly shown in Fig. 15.



Fig. 14 damage of aquarium after filling by water

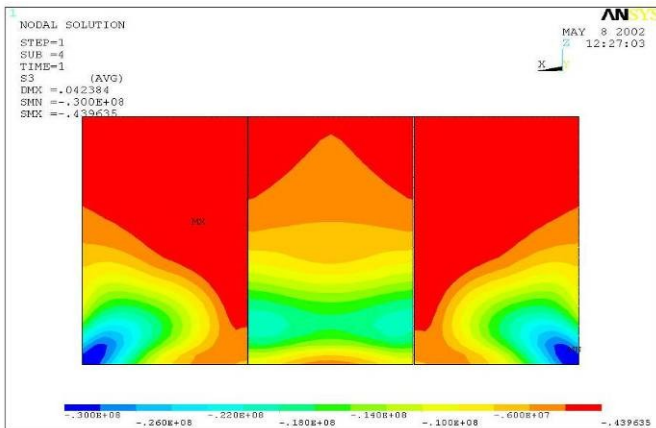


Fig. 15 illustrative utilization of ANSYS software for elaboration of static assessment

In this connection it is also interesting to mention the transparent wall of the greatest world aquarium in the shopping centre Dubai Mall in Dubai illustrated in Fig. 16.

The transparent front wall has the width of 32.88 m, the height of 8.3 m and the thickness of 750 mm. The weight of the wall is 245 614 kg. Technically it is not the material corresponding building glass, although it is sometimes marked as acrylic glass. Chemically it is the transparent thermoplastic PMMA (polymethylmethacrylate), often used as an alternative

to glass, characterized by the small weight and the high resistance to the fragmentation failure. Its widening in the practice has been introduced after 1933 year under the trademark Plexiglass, later ACRYLITE®, Lucite and Perspex.



Fig. 16 aquarium in shopping centre Dubai Mall

V. VERIFICATION EXPERIMENTS AND STRUCTURAL GLASS COMPONENTS TESTING

The authors' workplace, i.e. the Department of Metal and Timber Structures of the Faculty of Civil Engineering at Brno University of Technology (BUT), pays long term attention to the verification of the resistance and analysis of the actual behaviour of load-carrying structural components and systems composed of steel, timber, steel-concrete, glass-fibre-concrete, glass, combined structures and also composites, eventually other materials, with considering the influence of their imperfections (geometrical, structural and constructional) – see e.g. [9], [7] and [10] to [20].

This tradition, which is continuously following, has been already introduced under the action of Professor Ferdinand Lederer on the authors' workplace, together with the accent to the questions of the theory, calculation methods and static and structural design of the load-carrying components and systems made of these materials.

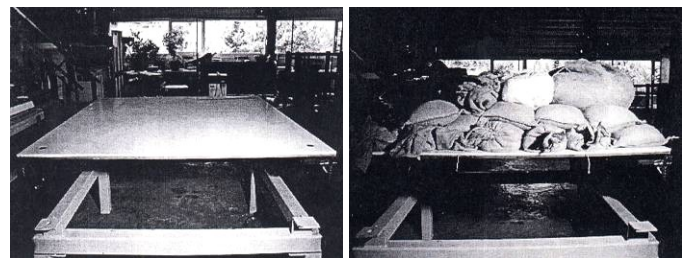


Fig. 17 traditional method of uniform loading of planar components

Within the loading of the structural glass load-carrying components, the primary problem is the realization of the full uniform load simulating compression or sucking of the wind, eventually snow load. The loading process should allow

monitoring and recording the deflections, and also damage of tested specimens in the progress of increasing or decreasing the load.

It is evident, that the traditional method of the loading of the planar structural components by full uniform load using weighed ballast gradually loaded at the tested specimen, used sometimes even at the front foreign research or university workplaces (see Fig. 17), is imperfect and unsuitable method for the verification of the actual behaviour of the glass panes.

In the testing room of the Department of Metal and Timber Structures of the Faculty of Civil Engineering at BUT, the new efficient so-called vacuum test method allowing the uniform loading of the planar structural components, has been developed after 1980 year. Fig. 18 shows one of the first experiments of the type mentioned, used for the verification test of the resistance of glass fill of the railing of the bridge of Vysocina at Velké Meziříčí (given by the task of A. Pechal), to the uniform load corresponding the effects of compression or sucking of the wind.



Fig. 18 loading test of railing fill – bridge of Vysocina

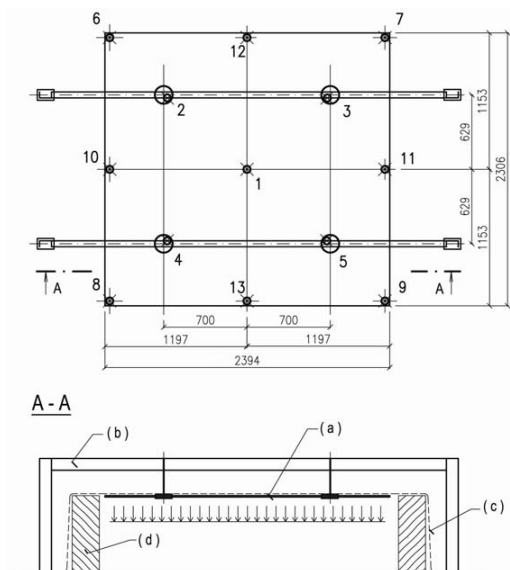


Fig. 19 scheme of arrangement of vacuum loading test of structural glass planar component

The basic scheme of the arrangement of the vacuuming in the loading test of the structural glass component is shown in Fig. 19. The component tested (a) is supported as corresponds with the real structure, for example line supports or single

support nodes or targets (c), anchored to the helping frames, similarly as in the real load-carrying system. The slab specimen supported as mentioned, is installed to the separate testing box (d) represented by the rigid peripheral timber frame, and the tested specimen together with the box are covered by the transparent plastic foil (e) glued to the stiffened floor of the testing room. The floor must be stiffened, with regards to the significant effect of sucking in the closed testing box.

From the space closed under the transparent foil the air is sucked, and then, the tested specimen is ideally uniformly loaded by the effect of the atmospheric overpressure. The overpressure is measured by the electrical sensor with the digital pressure gauge, and in parallel, for checking, it is verified using the liquid barometer. The regime of the uniform loading and reloading may be simply regulated and the load intensity is determined measuring the overpressure between the external environment and the space closed by foil. The illustrative shot of the real test of vacuum loading of structural glass is in Fig. 20.



Fig. 20 illustration of arrangement of real test of structural glass



Fig. 21 failure of single-layer float glass – test specimen T1



Fig. 22 failure of single-layer float glass – test specimen T1

Experiments verifying the actual behaviour of the glass components allow analysing the deformations (deflections) and the ultimate load-carrying capacity, as well as the failure mechanism in dependence on various material and structural composition of the glass component.



Fig. 23 failure of laminated float glass – test specimens T3, T4



Fig. 24 typical failure around local target support – specimens T3, T4



Fig. 25 failure of laminated tempered glass – test specimens T5, T6

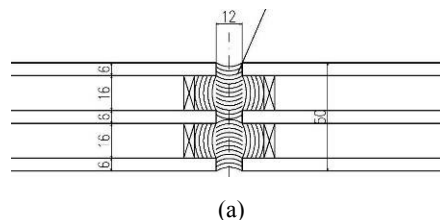


Fig. 26 influence of safety rope on failure of specimens T5, T6

Characteristic examples of the failure of the glass specimens tested within the research programme [7], [9] are, for the illustration, indicated in figures below. Failure of the test specimen made of single-layer tempered glass (T1) is characterized by breaking up to small fragments – see Fig. 21.

The test specimen made of laminated double-layer tempered glass (T2) has been failed by tearing from the supporting targets and by the subsequent falling of the whole specimen – see Fig. 22. The essentially different failure mechanisms of the test specimens made of laminated float glass (T3, T4) and laminated tempered glass with intermediate foil (T5, T6) are evident from the shots in Figs. 23 and 24, in comparison with Figs. 25 and 26.

On the base of tests realized on the authors' workplace, the failure mechanism of the component made of structural glass of different composition arrangement is indicated further. It is the wall component made of insulating triple-layer glass in the arrangement according to Fig. 27 (a). The tests have been realized for the company GLASS EXPERTS, Ltd., Žlutice.



(a)



(b)

Fig. 27 loading test of pane made of insulating triple-layer glass: (a) composition of glass component; (b) failure of glass component

On the base of the tests realized on the authors' workplace, the failure mechanism of the component made of structural glass of different composition arrangement is indicated further. It is the wall component made of insulating triple-layer glass in the arrangement according to Fig. 27 (a). The tests have been realized for the company GLASS EXPERTS, Ltd., Žlutice.

The test specimen is the wall component made of structural float glass created by 3 parallel elements with the thickness of 3×6 mm, the width of 700 mm and the length of 2 470 mm, which are connected by structural silicon on the longitudinal sides. The glass part of the test specimen is on the perimeter mounted in the steel frame, the basic part of which is represented by the square hollow thin-walled cross-section with the dimensions of $60 \times 60 \times 4$ mm.

The failure occurs suddenly, at the initiation of the fracture of glass due to the deformation in the area of the anchorage of glass panes into the rigid peripheral steel frame. The character of the failure corresponds to the unfavourable arrangement of used float glass, as illustrated in Fig. 27 (b).

VI. EXPERIMENTAL VERIFICATION OF STIFFNESS PARAMETERS OF STRUCTURAL GLASS

Within the loading tests of the structural glass panes intended for the roofing bus station platform (see above), the verification of stiffness parameters of glass has also been performed, to verify the actual values of Young's modulus of elasticity and, in the case of laminated double-layer glass, the actual values of the flexural stiffness and from these arising the actual values of the second moments of area influenced by the non-stiff connection between glass layers given by the intermediate foil.

According to the producer of glass plated structural components mentioned above, the value of Young's modulus of elasticity of glass has been recommended as $E = 70 \text{ GPa}$, but this is only generally considered value, which has not been verified by the producer. Therefore before the loading tests, the experimental verification of the Young's modulus has been performed at first. In this connection, as the second one, it was to verify the flexural stiffness of the test specimens with regards to their composition (laminated glass with the intermediate foil) and the production technology of glass.

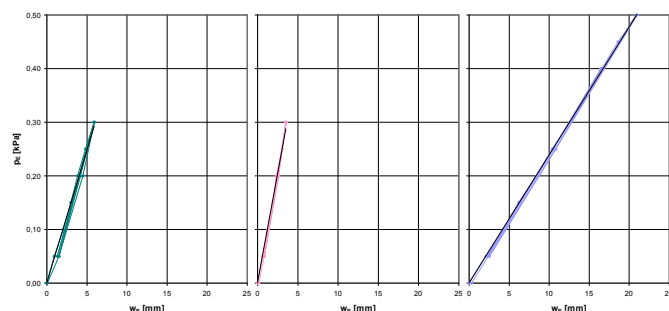


Fig. 28 relationships “ $p_E - w_E$ ” obtained directly from tests

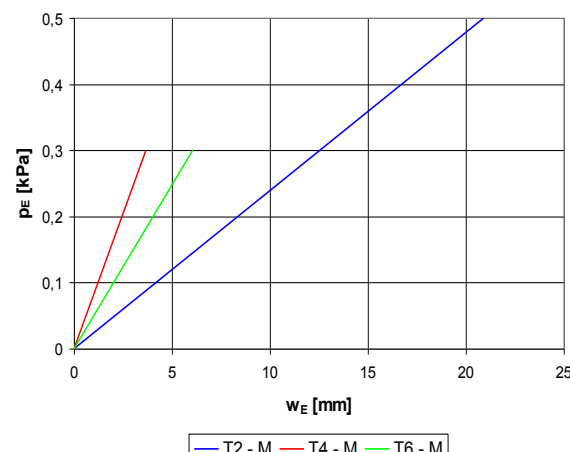


Fig. 29 relationships for stiffness derivation

For this reason, the test specimens have been supported on the shorter opposite sides of the plate, as the simply supported structural members. The theoretical span of the member was 2 294 mm. The specimens have been subjected to the uniform loading up to the load value about of 10 % of the predicted load-carrying capacity. The specimens have been repeatedly loaded and unloaded and the relationships of “load – deflection” (“ $p_E - w_E$ ”) have been monitored. The “ $p_E - w_E$ ” relationships obtained from the tests for all test specimens are illustrated in Fig. 28. Using the regression analysis, the linear relationships have been derived (see Fig. 29). From them, Young's modulus of elasticity, the flexural stiffness, and the effective second moment of area can be determined (Table 2).

Table 2 stiffness parameters (per width of 1 m)

Specimen	T1, T2	T5, T6	T3, T4
$E I_{eff} [\text{Nmm}^{-2}]$	$8.654 \cdot 10^9$	$18.029 \cdot 10^9$	$29.568 \cdot 10^9$
$I = 1/12 b t^3 [\text{mm}^4]$ ^{x)}	$144 \cdot 10^3$	$341 \cdot 10^3$	$667 \cdot 10^3$
$k (I_{eff} = k I)$	1.0	0.879	0.879
$E [\text{GPa}]$	60.1	60.1	50.5

^{x)} t is total thickness of layered glass (12 mm, 2x8 mm, 2x10 mm)

Using the relationship between the load p_E and corresponding deflection w_E in the mid-span, the effective flexural stiffness $E I_{eff,1}$ can be derived, if E is the modulus of elasticity and $I_{eff,1}$ is the effective second moment of area. For single-layer tempered glass (test specimens T1, T2), the effective second moment of area is in the form of $I_{eff,1} = I = 1/12 (b \cdot t^3)$, thus $k = I_{eff} / I = 1$, and from where the modulus of elasticity E of tempered glass can be derived directly. Using this value of the elasticity modulus for tempered layered glass (tempered glass of the same mechanical properties) with intermediate foil (test specimens T5, T6), and using the stiffness $E I_{eff}$, the effective second moment of area of double-layer glass can be derived as $I_{eff} = k I$, where the coefficient k expresses the reduction of the second moment of area I considered for the solid cross-section with the thickness of t , due to the influence of the pliability of the foil connection. Assuming, that also for laminated non-tempered glass (test specimens T3, T4) the influence of the foil on the effective second moment of area may be expressed by the same coefficient of the pliability k , then the (at least tentative) value of the elasticity modulus of non-tempered glass can be derived.

VII. CONCLUSIONS

Structural glass is already the important part of the wide spectrum of the materials of load-carrying structures of civil engineering buildings over the world and also in the Czech Republic. Nevertheless, the typical examples mentioned above cannot systematically illustrate all the possibilities of the structural composition and structural detailing from the

viewpoint of the usage of glass in civil engineering structures, but they can indicate the modern trends of the architectonic creation of the buildings requiring the large glazed areas of civil engineering structures and also the possibilities of their realization in the connection with the development of the production technology of the large scale glass components and with the new challenges for the industry of the glass production, as well as for the structural engineers.

The paper was focused on the significant field of the design and realization of buildings with the application of structural glass including the verification of the dimensions of the glass components in relation to the material, load intensity and boundary conditions on the one hand, and the verification of the theoretical assumptions and design methods through the experiments and loading tests taking into account the influence of the initial imperfections of the real load-carrying system on the other hand.

The general philosophy and methodology of the static and structural design of buildings using structural glass arises from the similar general principles, as in the case of other materials of load-carrying structures. However, glass has many fundamentally different properties that can influence its behaviour in the structure (thermal shock, failures of glass caused by the material inhomogeneity due to the inclusions, spontaneous explosion, material brittleness without elasto-plastic or plastic behaviour and without the possibility to decrease the influence of the concentrations of local stresses, necessity of the utilization of geometrically non-linear 2nd order theory of thin slabs, etc.). This paper thus also tried at least briefly to warn to some problems mentioned above, requiring more detailed consideration and cognition.

ACKNOWLEDGEMENT

The paper has been elaborated within the research project No. LO1408 "AdMaS UP – Advanced Materials, Structures and Technologies" supported by the Ministry of Education, Youth and Sport of the Czech Republic, within the framework of the National Sustainability Programme I.

REFERENCES

- [1] Š. Popovič, *Production and processing of flat glass* (Výroba a zpracování plochého skla – original in Czech language), Grada Publishing a.s. Praha, 2009. ISBN 978-80-247-3154-4.
- [2] M. Haldmann, A. Luible, M. Overend, *Structural Use of Glass*, Zurich: ETH Zurich, 2008, 215 pp. ISBN 3-85748-119-2.
- [3] A. Goris, *Bautabellen für ingenieure: mit Berechnungshinweisen und Beispielen*, Köln, Wolters Kluwer Deutschland GmbH, 2008, 555 pp. ISBN 978-3-8041-5236-6.
- [4] M. Sázovský, "How to avoid the most common failures of structural glass – I. Part" ("Jak předcházet nejčastějším poruchám stavebního skla – I. díl" – original in Czech language), *Stavebnictví*, Vol.10, 2010, pp. 45-48. ISSN 1802-2030.
- [5] M. Sázovský, "How to avoid the most common failures of structural glass – II. Part" ("Jak předcházet nejčastějším poruchám stavebního skla – II. díl" – original in Czech language), *Stavebnictví*, Vol.01, 2011, pp. 52-55. ISSN 1802-2030.
- [6] F. Stejskal, "Steel structure of store building of Sykora Home, Praha – Vysočany" ("Ocelová konstrukce stavby obchodního domu Sykora Home v Praze Vysočanech" – original in Czech Language), *Stavebnictví*, Vol. 03, 2010, p. 9. ISSN 1802-2030.
- [7] J. Melcher and M. Karmazínová, "The experimental verification of actual behaviour of the glass roofing structure under uniform loading", In *Proceedings of the 4th European Conference on Steel and Composite Structures "EUROSTEEL 2005"*, Druck und Verlagshaus Mainz, GmbH Aachen, Maastricht, 2005, Vol. B, pp. 2.4-1 – 2.4-8. ISBN 3-86130-812-6.
- [8] J. Melcher and M. Karmazínová, "Strength and deformational characteristics of structural sealant in load-carrying connections of structural glass components" ("Pevnostní a pětvárné charakteristiky strukturálního tmelu v nosných spojích dílců z konstrukčního skla" – original in Czech language), In *Proceedings of the International Conference "70 years of Civil Engineering Faculty of Technical University in Bratislava"*, STU: Bratislava, 2008, 6 pp. ISBN 978-80-227-2979-6.
- [9] J. Melcher and M. Karmazínová, "The design and experimental verification of actual behaviour of the structural glass in roofing and facade systems", In *Proceedings of the 3rd International Conference on Structural Engineering, Mechanics and Computation "SEMC 2010"* held in Cape Town, Millpress: Rotterdam, 2007, pp. 657-658. ISBN 978-90-5966-054-0.
- [10] J. Melcher, "Behaviour of Thin-Walled Corrugated Sheets and Restrained Beams", In *Proceedings of the IABSE Colloquium Stockholm 1986 Thin-Walled Metal Structures in Buildings*, IABSE, ETH – Hönggerberg, Zürich, 1986, pp. 199-206.
- [11] J. Melcher, "Full-Scale Testing of Steel and Timber Structures", In *Proceedings of International Seminar "Structural Assessment" – The role of large and full-scale testing* (K. S. Virdi and others, Ed.), E&FN SPON: London, 1997, pp. 301–308. ISBN 0 419 22490 4.
- [12] J. Melcher and M. Karmazínová, "Glass and metal – modern materials of civil engineering buildings" ("Sklo a kov – soudobé materiály občanských staveb" – original in Czech language), In *Proceedings of the National Conference Steel Structures*, Hustopeče 2001, Czech Society for Steel Structures.
- [13] J. Melcher and M. Karmazínová, "On problems of the design of load-carrying systems made of structural glass" ("K problémům dimenzování nosných systémů z konstrukčního skla" – original in Czech language), In *Proceedings of VIII. Conference Ecology and New Building Materials and Products*, Telč, VUSTAH: Brno, 2004.
- [14] J. Melcher and M. Karmazínová, "Structural glass in systems of buildings roofing" ("Konstrukční sklo v systémech zastřešení budov" – original in Czech language), In *Proceedings of the 2nd International Conference Buildings Roofing*, BUT – Faculty of Civil Engineering: Brno, 2004, pp. 13-18. ISBN 80-214-2588-1.
- [15] J. Melcher and M. Karmazínová, "On problem of the design of structural glass", In *Proceedings of the International Conference VSU 2005*, Sofia, 2005, Vol. II, pp. 233-238. ISBN 954-331-003-3.
- [16] J. Melcher and M. Karmazínová, "On problems of the design of load-carrying structures made of structural glass" ("K problémům dimenzování nosných konstrukcí z konstrukčního skla" – original in Czech language), *Konstrukce, Konstrukce Media, s.r.o.*: Ostrava, 2005, Vol. 4, No. 4, pp. 21-24. ISSN 1213-8762.
- [17] M. Karmazínová and J. Melcher, "Structural glass in metal load-carrying systems of building constructions", In *Proceedings of the 2nd International Conference on Advances in Civil Engineering and Building Materials CEBM 2012*, CRC Press, Taylor & Francis Group / Balkema: Hong Kong, 2012, pp. 591-596. ISBN 978-0-415-64342-9.
- [18] O. Pešek and J. Melcher, "Influence of shear forces on deformation of structural glass beam", In *Proceedings of the 3rd European Conference of Civil Engineering (ECCIE'12)* held in Paris, NAUN & WSEAS Press: 2012, pp. 240-245. ISSN 2227-4588, ISBN 978-1-61804-137-1.
- [19] O. Pešek, J. Melcher and M. Pilgr, "Numerical analysis of hybrid steel-glass beam", In *Proceedings of the 3rd European Conference of Civil Engineering (ECCIE'12)* held in Paris, NAUN & WSEAS Press: 2012, pp. 234-239. ISSN 2227-4588, ISBN 978-1-61804-137-1.
- [20] J. Melcher and M. Karmazínová, "Problems of behaviour and analysis of glass structural members with respect to their application in construction", In *Proceedings of the Seventh International Structural Engineering and Construction Conference "ISEC-7"* held in Honolulu "New Developments in Structural Engineering and Constructions", Research Publishing Services: Singapore, 2013, Vol. I, pp. 111-116, doi: 10.3850/978-981-07-5354-2_St-43-111. ISBN-13: 978-981-07-5355-9, ISBN-10: 981-07-5355-1.

Identifying the transfer function specific to environmental contamination with flue gas toxics

Corina C.Brîndușa, Eliza Gofită, Nikos E. Mastorakis, Carmen A. Bulucea,
Niculae Boteanu, Andreea C. Jeles, Mihnea Glodeanu, and Cornelia A.Bulucea

Abstract— Flue gas toxics in an electrical generating station, such as carbon oxide (CO), carbom dioxide (CO₂), sulfur dioxide (SO₂), nitrogen oxides (NO_x), and particulate matter (PM), can cause poisoning by environmental contamination. These persistent pollutants from the flue gas in a coal-fired power plant represent environmental xenobiotics and are presented in this study. Construction of mathematical models that reflect the data of type: Index of Atmospheric Purity IPA / areas studied; IPA / presence of the species (%) IPA / fertility species are important for a geographic area. Identification of a mathematical model to process data of type: *ipa / f*, (fertility species) is enabling the extraction of relevant conclusions on a polluter / geographical area. Analysis of specific variables of type *ipa (%) / f (%)* can be based on a mathematical model. Identifying the mathematical model (transfer function) is indirect through analogy electronic structures complex quadripole *RC + OA*. Mathematic residue analysis allows validation of the model (transfer function). A mathematical model of transfer function type allows the numerical simulation of the expression of output quantity by using a specialized soft. This study aims to emphasize the need for joint efforts of scholars in medicine, environmental and electrical engineering for enhancing knowledge of the environmental and human health impacts of anthropogenic actions, mostly industrial practices.

Keywords— RC quadripole, mathematical model, environmental contamination, toxics, transfer function.

Corina C. Brîndusa is with the Faculty of Medicine, University of Medicine and Pharmacy Craiova, Romania, e-mail: corinaa_b@yahoo.com.

Eliza Gofită is with the Faculty of Pharmacy, University of Medicine and Pharmacy Craiova, Romania, e-mail: elisagofita@yahoo.com.

Nikos E. Mastorakis is with the Technical University of Sofia, Industrial Engineering Department, Sofia, Bulgaria & Military Institutions of University Education (ASEI), Hellenic Naval Academy, Piraeus 18539, Greece , e-mail: mastorakis4567@gmail.com

Carmen A. Bulucea is with the Faculty of Medicine, University of Medicine and Pharmacy Craiova, Romania, e-mail: carmen.bulucea@gmail.com.

Niculae Boteanu is with the Faculty of Electrical Engineering, University of Craiova, Romania, e-mail: boteanu.niculae@gmail.com.

Andreea.C. Jeles is with the Technical College of Arts and Crafts “C Brancusi” Craiova, Romania, e-mail: andreee_83@yahoo.com.

Mihnea Glodeanu is with the Faculty of Agriculture, University of Craiova, Romania, e-mail: mihneaglodeanu@yahoo.com

Cornelia A. Bulucea is with the Faculty of Electrical Engineering, University of Craiova, Romania, e-mail: abulucea@gmail.com.

I. INTRODUCTION

Industrial pollution of the atmosphere is a direct consequence of anthropogenic activity. Atmospheric pollution has a direct impact on the biosphere. Because pollutants in the atmosphere rapidly disperse the implementation of their treatment is difficult in practice. Still, one could highlight that air pollution is generally affecting the human health, and flora and fauna, as well as humans' life environment [1]-[7].

Within the present industrial metabolism it is increasingly accepted globally that electric and thermal energy generation, as a main consumer of fossil fuels in general and coal in particular, is causing human health and environmental problems because of emissions [3]-[9]. The pollutants in the air from combustion processes of solid fuels are part of toxic substances. Examples of substances that can cause poisoning by environmental contamination are: carbon oxide (CO), carbom dioxide (CO₂), sulfur dioxide (SO₂), nitrogen oxides (NO_x), and particulate matter (PM). These substances appearing into the atmosphere from combustion processes are affecting the natural environment, encompassing flora, fauna and humans' life.

Air pollution generated by *artificial sources* can be produced by human activity [1]-[3]. In this sense an important case is the *column of point sources of gas* released into the atmosphere through a free routing system usually chimneys. An example of industrial pollutants is the thermal power plant units which constitute *continuing sources*: continuous operation / constant emission / long time (* 1 year).

As a major source of sulfur oxides, coal-fired electrical generating stations represent a large contributor to acid precipitation. Coal-fired industrial operations are also a significant source of nitrogen oxides, with an impact comparable to that of transportation [1]-[9]. Hence, the combustion of coal strongly contributes to acid precipitation and climate change due to global warming [1]-[9]. Furthermore, the health of humans and other life forms is impacted of burning coal in electrical generating stations, and is a serious concern [1]-[15].

Over the last several decades, the term xenobiotic which is coined in the field of immunotoxicology, has become increasingly accepted as relating to environmental impact [9]-[13]. Environmental xenobiotics are defined as substances foreign to a biological system, which did not exist in nature before their synthesis by humans. Environmental xenobiotics

are becoming problematic in medicine and environmental systems, since they are relatively new substances and difficult to categorize and to assess their effects on human health and the environment [9]-[13].

As previously stated, coal-fired electrical generating stations emit particulate matter, SO_2 , NO_x as well as gases that undergo chemical reactions to form fine particles in atmosphere [4]-[9],[14]. These reactive chemicals (particulate matter, sulfur dioxide and nitrogen oxides) represent environmental xenobiotics, which spread over hundreds to thousands of kilometers downwind of power plants. In addition to the environmental harm caused by greenhouse gases and other emissions, the air emissions of coal-fired power stations encompass a certain amount of toxic xenobiotics that result in significant numbers of human deaths and diseases [4]-[5],[9]-[14].

The harmful effects of environmental xenobiotics on humans and ecosystems are often unpredictable [9]-[13]. Through exposure to these environmental xenobiotics, people are submitted to irritating the skin and mucous membranes [3]. Some studies have shown that people can also experience heart disease, respiratory illness and lung cancer, as well as such other health problems as adverse reproductive outcomes, infant death, chronic bronchitis, asthma, and other lung diseases [9]-[13]. The immune system as a whole can be the target for xenobiotic induced toxicity, since environmental xenobiotics have the capacity to suppress the body's defence against reactive chemicals and pathogenic microorganisms. This suppression can cause increased susceptibility to cancer or autoimmune diseases. Moreover, environmental xenobiotics may be associated with endocrine alterations in people and wildlife. As a consequence, the pollutant load from environmental xenobiotics represented by the air emissions (particulate matter, sulfur dioxide and nitrogen oxides) during the operation of coal-fired power plants concern researchers in medical and environmental fields.

Over time, practical technical difficulties have been observed in removing the impurities from the solid fuel prior to combustion, because of the chemical composition and structure of coal [9]-[15]. Advanced technologies are continually being developed, with the aim of either (1) reducing power station emissions by implementing desulphurization technology, coal washing, and flue gas scrubbers and electrostatic precipitators that treat exhaust gases, or (2) applying carbon capture and storage to emissions from coal power stations. Even so, the environmental and human health impacts caused by the toxic emission of coal-fired power plants are often unpredictable and dangerous.

Flue gas monitoring during the operation of a thermoelectric coal-fired power plant is an essential step in assessing the environmental and human health impact of flue gas toxics and will be presented in the next section.

II. CASE STUDY. MONITORING OF FLUE GAS COMPONENTS IN TURCENI THERMOELECTRIC POWER PLANT

A. Assessment of Flue Gas Components

The environmental pollutants belonging to flue gas toxics, as sulfur dioxide SO_2 , nitrogen oxides NO_x , particulate matter PM, and carbon dioxide CO_2 have been analyzed in this case study performed to Turceni power plant of Romania.

Thermoelectric power generation in a coal-fired plant consists in the conversion of thermal energy into electrical energy. The source consists in a coal-fossil fuel to heat a liquid to produce a high pressure gas (usually water is heated to produce steam) which then is expanded over a turbine that runs an electric generator. The driving force for this process is the phase change of the gas to a liquid following the turbine, and this is where the requirement for cooling water arises. A vacuum is created in the condensation process which draws the gas over the turbine, since this low pressure is critical to the thermodynamic efficiency of the process. Mainly, the water requirement in coal-fired power plants is as cooling water for condensing the steam. The steam condensation typically occurs in a shell-and-tube heat exchanger that is known as a condenser. The operating parameters of the cooling system are critical to the overall power generation yield.

At power plants, the combustion gas, which is called flue gas, is exhausted to the outside air through the chimney. Flue gas is usually composed of carbon dioxide, water vapor, as well as sulfur oxides, nitrogen oxides, particulate matter and carbon monoxide [1]-[2], [4]-[9].

It must be noted that because the combustion flue gases inside the chimney are much hotter than the environmental air, and consequently less dense than the outside air, at the bottom of the vertical column of hot flue gas the pressure is lower than at the bottom of a corresponding column of outside air. That means the driving force moving the combustion air into the combustion zone, as well as flowing the flue gas up and out of the chimney is represented by that higher pressure outside the chimney [1]-[2], [4]-[9].

There are a series of end-of-pipe technologies for treating and removing pollutants from the flue gases produced by burning coal in the electrical generating stations. Still, aiming to the sustainable framework of Cleaner Production, these emerging technologies for the treatment and removal of pollutants from the combustion gases should be accompanied worldwide by responsible monitoring of the environmental pollutants.

Flue gases monitoring during the operation of a coal-fired power plant is an essential step in assessing the environmental and human health impact of pollutants.

This case study had been performed in Turceni electrical generating station on the thermoelectric units of 330 MW.

The coal-fired flue gas toxics has four main components: sulfur dioxide SO_2 , carbon dioxide CO_2 , particulate matter PM, nitrogen oxides NO_x .

This paper presents the assessment of the pollutant emissions as a source of environmental xenobiotics, from the Turceni power plant based on the Strategy and Economic Development Division (SEDD) methodology, which is described in the Romanian Electrical Department as calculation method PE-1001 [15]. The methodology is based on the models that depict the emission factors for fuel combustion processes [4]-[5],[9],[15] and has been applied since 1994. For distinct pollutants, the emission factors are determined experimentally [9].

By definition, the emission factor represents the pollutant amount evacuated in atmosphere per heat quantity unit produced by fuel combustion in the boiler [1]-[2],[4]-[9],[15]. For distinct pollutants the emission factors are determined experimentally. They are depending on fuel characteristics, constructive type of the combustion installation, as well on fuel calorific power. Emission factors can be corrected in accordance with the fuel composition and the applied combustion technology. Fuel amount and according calorific power are determined by fuel lot.

One could also notice that in case of several fuel types utilization, the total amount of a certain pollutant is determined by summing the emissions corresponding to each of them.

The flow rate of the pollutant evacuated into the atmosphere (the emission) is determined [4]-[5], [9], [15] as:

$$E_{pol} = B \cdot H_{ic} \cdot e_{pol} [\text{kg} / \text{h}] \quad (1)$$

where: E_{pol} [kg/h] is the flow rate of pollutant evacuated into atmosphere; B [kg/h] is the fuel flow rate; H_{ic} [kJ/kg] is the inferior calorific power of fuel, and e_{pol} [kg/kJ] is the emission factor.

The mass concentration of the pollutant evacuated by combustion is determined as:

$$C_{mPol} = E_{pol} \cdot 10^6 / D_{Gaze} [\text{mg} / m_N^3] \quad (2)$$

where: E_{pol} [kg/h] is the mass flow rate of pollutant evacuated into atmosphere, and D_{Gaze} [m_N^3 / h] is the volume flow rate of combustion gases.

For the coal-fired flue gas toxics in this study there are presented models of the pollutant components SO_2 , NO_x , PM (ash and dust), CO_2 .

The emission factor for sulfur dioxide is:

$$e_{SO_2} = \frac{M_{SO_2} \cdot S}{M_s \cdot 100} \cdot (1 - r) [\text{kg}/\text{kJ}] \quad (3)$$

where: e_{SO_2} [kg/kJ] is the emission factor for SO_2 ; M_{SO_2} [kg/kmol] is the molecular mass of SO_2 ; M_s [kg/kmol] is the molecular mass of sulfur; S [%] represents the sulfur amount into the fuel; H_{ic} [kJ/kg] is the inferior calorific power of the fuel, and r is the retention degree of sulfur in slag and ash ($r = 0.2$ for lignite coal fuel).

For the model of nitrogen oxides the calculation of NO_x emission is based on the emission factors that are indicated on Table 1, applying then an oxygen correction for a 100% load of the boiler.

Table 1

Fuel	$e_{NO_x}^{100}$					
	Thermal power of boiler [MWt]					
	50 - 100		100 - 300		>300	
	kg/kJ	g/GJ	kg/kJ	g/GJ	kg/kJ	g/GJ
Lignite	$2 \cdot 10^{-1}$	200	$2,2 \cdot 10^{-1}$	220	$2,6 \cdot 10^{-1}$	260
Coal	$3,8 \cdot 10^{-1}$	380	$4,2 \cdot 10^{-1}$	420	$4,5 \cdot 10^{-1}$	450
Oil	$1,9 \cdot 10^{-1}$	190	$2,1 \cdot 10^{-1}$	210	$2,8 \cdot 10^{-1}$	280
Natural gas	$1,3 \cdot 10^{-1}$	130	$1,5 \cdot 10^{-1}$	150	$1,7 \cdot 10^{-1}$	170

For the emission calculation at partial loads (>50%) the following correction it is applied:

$$e_{NO_x}^x = e_{NO_x}^{100} [a + (1 - a) \frac{L - 50}{50}] [\text{kg}/\text{kJ}] \quad (4)$$

where: $e_{NO_x}^x$ [kg/kJ] is the emission factor at load x; $e_{NO_x}^{100}$ [kg/kJ] is the emission factor at load 100%; L [%] is the boiler load, and a is the fuel type coefficient (a = 0.5 for coal fuel).

Calculation of emission factor specific to particulate matter PM (ash and dust) pollutant is determined as follows:

$$e_{Pub} = \frac{(1 - x/100)(1 - y/100) * A/100}{H_{ic}} [\text{kg}/\text{kJ}] \quad (5)$$

where: e_{Pub} [kg/kJ] is the emission factor for ash; A [%] is the ash content in the coal; x [%] is the retention degree of ash in the focus; y [%] is the yield of the installation for dust retention; H_{ic} [kJ/kg] is the inferior calorific power of fuel.

Table 2

Parameter	MU	Lignite	Coal	Coal (import)
A – ash content in coal	[%]	40	30	20
x – retention degree of ash in focus	[%]		15	
y – efficiency of dust retention installation (electrostatic precipitator)	[%]		94 – 99 depending on time interval after each shaking	

Emission factors for CO_2 , according to European Union regulation, are depicted in Table 3.

Table 3

Fuel	e_{CO_2}	
	kg/kJ	g/GJ
Coal (lignite)	$98 \cdot 10^{-6}$	98000
Oil	$72 \cdot 10^{-6}$	72000
Natural gas	$50 \cdot 10^{-6}$	50000

Calculation of emission factor specific to pollutant CO_2 is determined as:

$$e_{CO_2} = \frac{M_{CO_2} \cdot C}{M_C \cdot 100} \cdot \frac{100}{H_{ic}} [\text{kg}/\text{kJ}] \quad (6)$$

where: e_{CO_2} [kg/kJ] is the emission factor for CO_2 ; M_{CO_2} [kg/kmol] is the molecular mass of carbon; C [%] is the carbon content in the fuel; H_{ic} [kJ/kg] is the inferior calorific power of the fuel.

The SEDD methodology had been applied in Turceni electrical generation station taking into consideration three distinct situations [9]:

(1) Operation of Turceni power plant at 33.33% capacity of installed power (660 MW), that is corresponding to 2 thermoelectric units ($n=2$) of 330 MW in operation for an hour on basis of lignite-fired [10,15,16]; in this case, 1 chimney for flue gas is evacuating the pollutants from the two thermoelectric units mentioned as above;

(2) Operation of Turceni power plant at 66.66% capacity of installed power (1320 MW), that is corresponding to 4 thermoelectric units ($n=4$) of 330 MW in operation for an hour on basis of lignite-fired; in this case, 2 chimneys for flue gas are evacuating the pollutants from the 4 thermoelectric units mentioned as above;

(3) Operation of Turceni power plant at full capacity of installed power (1980 MW), that is corresponding to 6 thermoelectric units ($n=6$) of 330 MW in operation for an hour on basis of lignite-fired; in this case, 3 chimneys for flue gas are evacuating the pollutants from the 6 thermoelectric units mentioned as above.

Mathematical models of the methodology SEDD has been used for depicting the emission factors specific to fuel combustion in the thermoelectric units of Turceni power plant. The following operation conditions have been assumed in this case study [4],[9]:

- a) fuel type is lignite coal with the inferior calorific power $H_{il}=6280\text{ kJ/kg}$, sulfur content $S=0.8\%$, carbon content $C=20\%$, ash content $A=25.5\%$, total wet $W=45\%$;
- b) flow rate of consumed coal per a thermoelectric units of 330MW is determined on basis of the medium flow rate of coal pulverized by the 5 coal mills $5*92.6\text{ t/h}$, and accordingly the lignite flow rate that is taken into consideration is $B_L=5*92.6\text{ t/h}=463\text{ t/h}=463*10^3\text{ kg/h}$;
- c) oil as fuel support has the inferior calorific power $H_{ip} = 39770\text{ kJ/kg}$, sulfur content $S=3\%$, carbon content $C=76\%$;
- d) the flow rate of consumed oil per a thermoelectric unit of 330 MW is $B_p=10*10^3\text{ kg/h}$;

Taking into consideration the SEDD methodology there were determined the emission factor, the flow rate and the mass concentration for the flue-gas pollutants: SO_2 , CO_2 , PM and NO_x , both by lignite combustion and by oil combustion [4]-[5], [9].

B. Experimental Evaluation of Flue Gas Components on Thermoelectric Units of Turceni PowerPlant

The testing validation of SEDD methodology for the thermal units of Turceni Electrical generating station had been carried out, in order to obtain a reliable comparison of the results [4],[9].

In line with this idea we have proposed an experimental validation of the mathematical model evaluation of flue gas emission by recordings achieved on Calcination Evaluation Stand together with Chemical Laboratory – Coal Section within Turceni electrical generating station (see Fig.1).



Fig.1.1. Planetary ball mill



Fig.1.2 Calcination furnace



Fig.1.3 Drying oven



Fig.1.4 Calorimetric bomb

The recorded data have been processed using a AMD multiprocessor computer system that allowed the StatSoft STATISTICA - Version 7.0 software running, for date acquisition and processing. This way the concentrations of flue gases leaving the chimney. One could note that the lignite coal fuel taken into the case study has: the inferior calorific power $H_{il}=6280\text{ kJ/kg}$; the sulfur content $S=0.8\%$, the carbon content $C=20\%$, the ash content $A=22.5\%$, and the total wet $W=45\%$.

The resulting data regarding emission factor and pollutant concentration for the flue gases pollutant components: sulfur dioxide SO_2 , carbon dioxide CO_2 , particulate matter PM and nitrogen oxides NO_x have been determined [4]-[5], [9].

The analysis is carried out on basis of three samples extraction, and according to the data depicted as above, for each pollutant component of the flue gas caused by burning of lignite coal fuel the following average values have been obtained:

- a) for sulfur dioxide SO_2 : the emission factor. $e_{L\text{SO}_2} = 2.06*10^6 \text{ kg/kJ}$; the pollutant concentration $C_{m\text{SO}_2} = 3878 \text{ mg/m}^3$; the average error $\varepsilon_{msd} \leq 1\%$; the maximum error $\varepsilon_{max} \leq 3\%$.
- b) for carbon dioxide CO_2 : the emission factor.: $e_{L\text{CO}_2} = 118*10^{-6} \text{ kg/kJ}$; the pollutant concentration $C_{m\text{CO}_2} = 36744 \text{ mg/m}^3$; the average error : $\varepsilon_{msd} \leq 1\%$; the maximum error $\varepsilon_{max} \leq 3\%$.

c) for particulate matter PM: the emission factor $e_{LPulb} = 0.35 \times 10^{-6}$ kg/kJ; the pollutant concentration $C_{mPulb} = 598$ mg/m³_N; the average error $\varepsilon_{msd} \leq 1.5\%$; the maximum error $\varepsilon_{max} \leq 4\%$.

d) for nitrogen oxides NO_x: the emission factor $e_{LNO_x} = 2.47 \times 10^{-7}$ kg/kJ; the pollutant concentration $C_{mNO_x} = 487$ mg/m³_N; the average error $\varepsilon_{msd} \leq 1.5\%$; the maximum error $\varepsilon_{max} \leq 3\%$.

It must be noted that the errors between the calculated and experimental results are within the range accepted by environmental regulations, supporting the reliability of SEDD methodology.

As discussion at this point one could note that flue gases monitoring during the operation of a coal-fired electrical generating station is an essential step in assessing the environmental and human health impact of pollutants caused by industrial activities [4]-[5],[9]. Procedures should impose worldwide the estimation of yearly emissions of primary particulate matter, sulfur oxides and nitrogen oxides on the total megawatt-hours generated by each power plant. Since the emissions from coal-fired power plants are dispersed over a large area, further should impose the population living around every power plant be included in specific databases and a mapping program, aiming that it could be medically useful.

III. MATHEMATICAL METHOD OF TRANSFER FUNCTION TO IDENTIFY THE FLUE GAS TOXICS

In this case study, given that Turceni thermoelectric power plant comprises six thermal units of 330 MW, it results a total installed power of 1980 MW which means a significant impact of the punctual pollution that induces heavy effects on the biosphere [4]-[5].

A chimney of a thermal power unit generates a cloud of burning powder that disperses on relatively large surfaces. There are studies addressing the effect of excessive generated pollution specific to Jiu Valley area, which is a cluster of relatively medium-sized urban settlements [1]-[2],[5]-[9]. Unfortunately such an industrial area is favoring negative effect of pollution caused by CO, SO₂, NO_x, powders as result of combustion of coal in thermoelectric power units belonging to the Paroșeni power plant.

The direct effect of pollution is given by the frequency and abundance of local plant species that are found in these geographical areas dominated by polluters with particularly large installed capacity. A study of Al Ionescu et al. [16] had sought an unitary image of environmental pollution by studying flora developed around such continuous power sources. In this regard they used the Atmospheric Purity Index, IPA, formulated in studies of Slover [17] and Lebane [18]. Its analytical formula takes into account the number of species, n , the abundance of each species, f , the specific environmental

cortege, Q , ($IPA = \frac{1}{10} \sum_{i=1}^n Q_i \cdot f_i$). This is a mathematical

model that allows drawing conclusions on the environment /

flora in a geographic area. Such a mathematical model contains a high level of generality because of the nature / number of inputs.

Construction of mathematical models that reflect the data type: IPA / areas studied; IPA / presence of the species (%); IPA / fertility species are important for a geographic area.

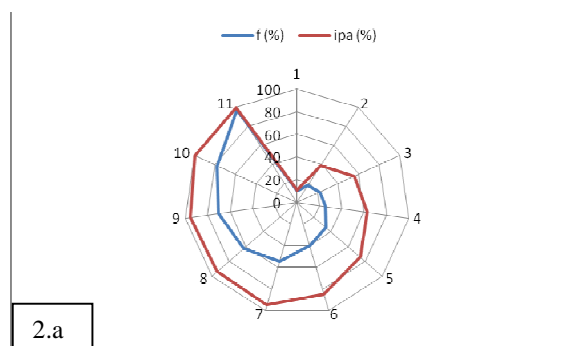
We sought to identify a mathematical model reflecting the data type: IPA / F, fertility species. We believe that these data reflect the factual position well an industrial polluter in the local geographic area.

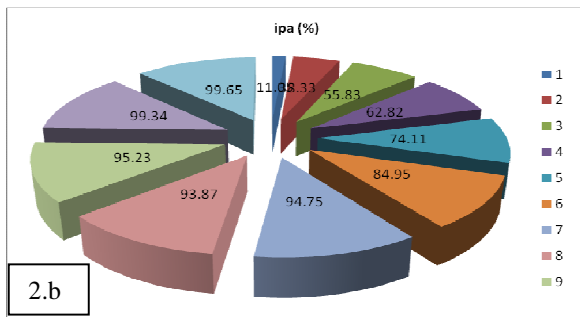
There are geographical areas where we have excessive pollution, significantly above the generally accepted technical parameters. Jiu Valley is dominated by polluter SE Paroșeni thermoelectric power plant, through thermal power units on coal of pit coal type. Although pit coal is the burning fuel we believe that the data for the system inputs are covering also the thermal power units based on lignite coal type. This observation is suitable since the quantity of lignite burned in a thermal power unit of SE Turceni power plant is far greater than the quantity of coal burned in a thermal power unit of SE Paroșeni power station (with same installed power). The explanation is given by the superior calorific value of the pit coal compared to that of the lignite. So we can say that a thermal power unit of SE Turceni is more polluting than a thermal unit of SE Paroșeni because of the quantity of CO, SO₂, NO_x, powders released into the atmosphere [1], [5]-[8].

As stated before, the direct effect of this type of air pollution is reflected by Atmospheric Purity Index, IPA. For our study are relevant the input data into a system of type: fertility species F(%) / IPA. Pollution caused by CO, SO₂, NO_x, powders, particular matter was investigated in the study of Al. Ionescu et al. [16] for many mono-industrial areas of Romania. Species of plants envisaged by it is *marchantia polymorpha* (we have a specific input correlation between the quantities F and IPA (F reflected by IPA).

In heavily polluted areas (including geographic area affected by SE Turceni power plant) we have a restriction of plant diversity, as well as their decreased fertility. An indirect approach to toxicology problems related to toxic substances, type CO, SO₂, NO_x, particulate matter, is that which is indicated in determination of the relation between *ipa* and *f*.

In our research is appropriate to use relative values of inputs into the system: *ipa* (%); *f* (%) on the basis of their extreme limits. This furthers relevant findings in our research. In Fig.2 a), b) are presented the evolution of the *ipa* (%/f(%)).



Fig. 2. Evolution of the *ipa* (%) / *fertility species f* (%).

*Source: Adapted from A. Ionescu. [6].

Construction of the mathematical model for analyzing the dependence *ipa* (%) / *f* (%) it is indirectly carried out by analogy with electrical structures passive of electric quadripole type. We started from several published studies that built such a mathematical model [19]-[21].

We relied on indirect identification of the transfer function by making a complex electronic structure. This structure is composed mainly of the quadripole resistor-capacitor *RC*, repeater signal A_1 , the amplifier / inverter signal A_2, A_3 .

Based on the electronic structure of complex (based on the quadripole *RC*), represented in Fig. 3 (composed mainly of quadripole *RC*, repeater signal A_1 , amplifier / signal inverter A_2, A_3), we can build a mathematical model through the operational calculation [22].

We have the relationships:

$$u_1(t) = Ri + \frac{1}{C} \int idt \quad (7)$$

$$u_C(t) = \frac{1}{C} \int idt \quad (8)$$

$$u_2(t) = K_1 K_2 u_C(t) + K_1 K_2 K_3 U_1 \quad (9)$$

The transfer function at the step input, $\frac{1}{s}$, is:

$$H_{21}(s) = K_1 \cdot K_2 \cdot \frac{1}{s(1 + \tau \cdot s)} \quad (10)$$

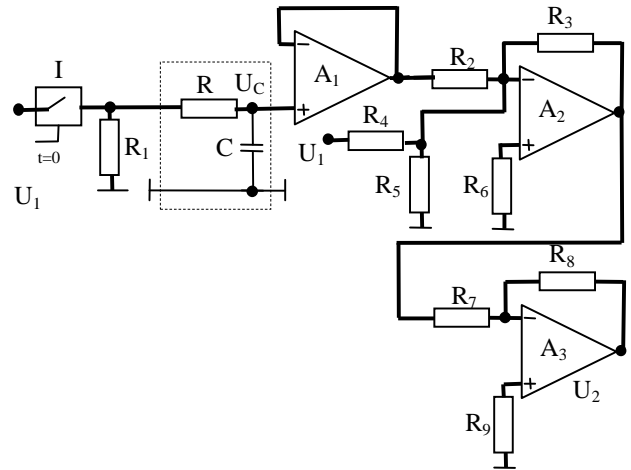
where:

$$\tau = RC \quad (11)$$

$$K_1 = \frac{R_3}{R_2} \quad (12)$$

$$K_2 = \frac{R_8}{R_7} \quad (13)$$

$$K_3 = \frac{R_5}{R_4 + R_5} \quad (14)$$

Fig. 3. Electronic Structure: *RC* + *OA*

Observations: - the resistances R_6, R_9 –are indefinite; - A_1, A_2, A_3 - precision OA with the input jFET ; - the scheme does not apply to direct measurements.

One could note that we took into consideration that A_2 and A_3 are affected by signals on the inverting input. So, if we would measure the voltage level after A_2 we would find out a negative level, (to the ground). This is the reason we introduced the inverter A_3 which allows obtaining a positive level at the output, (namely, U_2)

The resistances R_6, R_9 are undefined, meaning that they are not important as dimensioning values in this electronic configuration. Rather we have introduced them in the electric circuit in order to emphasize that they could solve several disadvantages, such as achievement of a floating potential of the non-inverting inputs of the operational amplifiers A_2 and A_3 , (R_6 and R_9).

In applying at the input of the quadripole *RC* ($t = 0$) an electrical signal of value U_1 , at the structure output it will result an electrical signal that tends to the value U_2 , after an interval of time (a multiple of the *RC* quadripole constant, $\tau = RC$).

Considering the type of the followed process, we have chosen a constant with a relatively high, $\tau = 18$. We hold for the input signal, of step type, the value $U_1 = 1V$.

We complete Table 4:

- row (3) with values calculated (forecast), based on the model $[L^{-1} H_{21}(s)]_{t=0}^{t=3\tau}$;

- row (2) with process values (observed), according to Fig. 2.a,b;

- row (4) contains residues (these values representing value of the prediction error calculated as the difference between the observed values and the predicted values, see Fig. 4).

Table 4. Calculation of residues ipa (%) / f (%).

Sample No.	1	2	3	4	5	6
Process value	11. 05	38. 33	55. 83	62. 82	74. 11	84. 95
Calculated value	12. 47	40. 67	53. 79	60. 89	76. 28	83
Residues value	-1. 42	-2. 34	2. 04	1. 93	-2. 17	1. 95
Sample No.	7	8	9	10	11	
Process value	94. 75	93. 87	95. 23	99. 34	99. 65	
Calculated value	92. 61	95. 13	96. 79	97. 88	99. 3	
Residues value	2. 14	-1. 26	-1. 56	1. 46	0. 35	

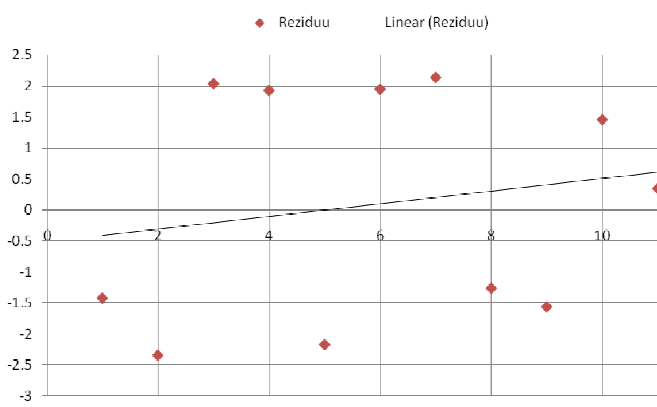


Fig. 4. Residues diagram

IV. DISCUSSION AND CONCLUSIONS

Chronic poisoning occurs after repeated absorption of small doses of toxic substances. The toxic action is caused either by the accumulation of the substances in the body, in various organs or tissues, or by the summation of the effects of lesions over time with the occurrence of pathological conditions [3]. One of the most common causes of chronic poisoning is contamination of the natural environment [23].

Flue gas monitoring during the operation of a thermoelectric coal-fired power plant is an essential step in assessing the environmental and human health impact of pollutants caused by industrial activities.

Environmental xenobiotics from the flue gas of the coal-fired electrical generation stations became problematic in medicine and environmental systems since, in addition to the environmental harm caused by greenhouse gases and other emissions, the flue gases toxics result in significant perturbations of the immune system of humans and other life forms [9].

Procedures should impose worldwide the estimation of yearly emissions of primary particulate matter, sulfur oxides and nitrogen oxides on the total megawatt-hours generated by each power plant. Since the emissions from coal-fired power

plants are dispersed over a large area, legislation should impose further that the population living around every power plant be included in specific databases and a mapping program, aiming that it could be medically useful [4]-[5], [9].

Developing a complex mathematical model of correspondence $ipa(%) / f(%)$ allows numerical simulation [16], [22] per PC on a specialized utility.

It is possible to develop mathematical models for analyzing the dependence $ipa(%) / f(%)$ based on a so-called indirect process of building a mathematical model. We consider that the construction of the mathematical model in the form of the transfer function may be obtained by analogy with the electronic structure of the type RC quadripole.

It is important that the construction of such a model to have a mathematical model validation stage. Residue analysis allows to validate the mathematical model $ipa(%) / f(%)$, based on the mathematical model built on a complex electronic structures: quadripole $RC + OA$.

The transfer function is a mathematical model in operation. Based on the analysis of residues we can accept that such a mathematical model $H_{21}(s) = H_{ipa/f}(s)$, applies to the environmental pollution by toxics of type CO, SO₂, NO_x, particular matter.

Compliance with Sustainable Development imposes on each existing coal-fired electrical generating station to be installed and activated both modern pollution control technology and depollution equipment as well. This way one could assume that the end-of-pipe treatments would reduce the environmental and human health impacts and will slow the process of degradation of life on Earth. We must believe that investing in cleaner production to prevent pollution and reduce coal-resource consumption should be a responsible approach, more effective than continuing to apply the end-of-pipe solutions in the coal-fired electrical generating stations.

This findings of this work aims to emphasize the power of science and the need for joint efforts of scholars in medicine, environmental and electrical engineering for enhancing knowledge of the environmental and human health impacts of anthropogenic actions, mostly industrial practices.

REFERENCES

- [1] M. Istrate, M. Gusa, *Impactul producerii, transportului si distributiei energiei electrice asupra mediului* (Environmental Impact of Electric Energy Generation and Transportation), AGIR Publishing House, Bucharest, 2000.
- [2] U.C. Mishra, "Environmental impact of coal industry and thermal power plants in India", *Journal of Environmental Radioactivity*, 2004, 72(1-2): 35-40.
- [3] I.E. Gofita, "Toxicologia", Editura Medicală Universitară, Craiova, 2011.
- [4] C.A. Bulucea, A.C. Jeles, N.E. Mastorakis, C.A. Bulucea, C.C. Brindusa, "A case study on monitoring environmental impact of flue gases to a coal-fired electrical generating station", *Models and Methods in Applied Sciences: Proc. IAASAT Int. Conf. on Environment, Economics, Energy, Devices, Systems, Communications, Computers, Mathematics*, University Center Drobeta Turnu Severin, Romania, October 27-29, 2011: 90-99.
- [5] C.A. Bulucea, N.E. Mastorakis, M.A. Rosen, C.C. Brîndușa, C.A. Bulucea, A.C. Jeles, "Enhancing Understanding of the Environmental Xenobiotics in Coal-Fired Flue Gas", *Recent Researches in Environment and Biomedicine, Proceedings of the 6th International*

- Conferences on Energy and Development Environment- Biomedicine (EDEB'12), Vouliagmeni, Greece, March 7-9, 2012, pp.58-67*
- [6] D. Fodor, D. Baican, *Impactul industriei minere asupra mediului*, Editura INFOMIN, Deva, 2001.
 - [7] C. RădulescuR. Sârbu, "Impactul activității de procesare a căburilor din Valea Jiului asupra mediului", *Buletinul AGIR*, nr. 3, 2006.
 - [8] S. Penney, J. Bell, J. Balbus, "Estimating the health impacts of coal-fired power plants receiving international financing", Report of Environmental Defence Fund, Washington, DC, 2009.
 - [9] C.A.Bulucea, M.A. Rosen, N.E. Mastorakis, C.A. Bulucea, C.C. Brindusa, A.C. Jeles, "Addressing the Impact of Environmental Xenobiotics in Coal-Fired Flue Gas", *Sustainability* 2015, 7, 2678-2694.
 - [10] A.J. Cohen, H.R. Anderson, B. Ostro, K.D. Pandey, M. Krzyzanowski, N. Kunzli, K. Gutschmidt, A. Pope, I. Romieu, J.M. Samet, K. Smith, "The global burden of disease due to outdoor air pollution", *Journal of Toxicology and Environmental Health*, Part A, 2005, 68: 1301-1307.
 - [11] P.S. Nagarkatti, M. Nagarkatti, "Immunotoxicology: Modulation of the immune system by xenobiotics", *Defence Science Journal*, 1987, 37(2): 235-244.
 - [12] L.D. Koller, "Immunotoxicology today", *Toxicologic Pathology*, 1987, 15(3): 346-351.
 - [13] B.J. Danzo, "Environmental xenobiotics may disrupt normal endocrine function by interfering with the binding of physiological ligands to steroid receptors and binding proteins", *Environmental Health Perspectives*, 1997, 105(3): 294-301.
 - [14] E. Hnatiuc, *Procedes électriques de mesure et de traitement des polluants* (Electrical Methods for Measurement and Treatment of Pollutants), Editions TEC&DOC, Lavoisier Publishing House, Paris, 2002.
 - [15] Strategy and Economic Development Division within Romanian Electrical Department , Metodologie de evaluare operativă a emisiilor de SO₂, NO_x, pulberi (cenusă zburătoare) și CO₂ din centrale termice și termoelectrice (Methodology for operative evaluation of emissions of SO₂, NO_x, particulate matter (fly ash) and CO₂ in the thermal and electric power stations), Romanian Autonomous Electricity RENEL, Bucharest, 1994.
 - [16] A. Ionescu, Gh. Serbanescu, Gh. Mohan, *Elemente din simptomatologia poluării la plante*, Editura Academiei Române, 1973.
 - [17] J.R. De Sloover, "Pollution atmosphérique et tolerance spécifique chez les lichens", *Bull. Soc. Bot. France*, 1969.
 - [18] J.R. De Sloover, F. Leblanc, "Mapping atmosphérique pollution on the basis of lichen sensitivity", *Proc. Symp. Recent Advances in Tropical Ecology*, Varanasi, 1968.
 - [19] C.C. Brîndușa, P. Dondon, C.A. Bulucea, "Numerical Simulation Based on Transfer Function Specific to Proliferation of Tumor Cell Lines", *WSEAS Transactions on Biology and Biomedicine*, Volume 11, 2014, Art. #19, pp. 140-146
 - [20] C.C. Brîndușa, C.A. Bulucea, E.N. Mastorakis, "Determination of the kinetic model for cell line on the duration of action of an inhibitor of tyrosine kinases receptors", *Proc. of 2014 International Conference on Applied Mathematics, Computational Science and Engineering, AMCSE 2014*, Varna, Bulgaria, 13-15 September 2014, pp.82-91.
 - [21] A. Kaufmann, *Metode și modele ale cercetării operaționale*, Editura Științifică București, București, 1977.
 - [22] G.I. Nastase, *Rolul interactiv al informației între factorii fluizi (apă, aer) și cei biologici ai mediului înconjurător*, Editura Rampa București, București, 2001.
 - [23] Ed. Rădăceanu, *Limbaje de simulare*, Editura Militară, București, 1991.

Optimization of Bait Sprays Against *Dacus oleae* Using Embedded Systems, GIS and Web-Based Applications

George N. Fouskitakis, Lefteris D. Doitsidis, Iraklis I. Rigakis, Kyriaki N. Varikou, Ioannis V. Sarantopoulos, Androniki K. Papafilippaki, Kyriaki G. Maniadaki, Athanasia E. Mpirouraki, and Emmanuel N. Antonidakis

Abstract—Olive fruit production is of crucial importance for Greece as it consists the third biggest olive oil producer worldwide, as well as the biggest extra virgin oil producer. Bait sprays applied from the ground are known to be the most effective protection method of olive trees against *Bactrocera oleae*. Nevertheless, its effectiveness highly depends upon its proper application. The proposed study focuses on the design and development of a prototype integrated system for the automation, optimization, and the assurance of proper application of bait sprays. It consists of: (a) a gun sprayer and its nozzle providing precise pressure, flow rate and spraying duration adjustment, thus allowing for spraying specific mixture quantity, (b) an embedded system for fully recording the bait spray procedure in terms of both space (geographic position and route of the tractor equipped with the spraying mechanism) and quantity, and, (c) a web-based application for representing the spraying procedure on suitably modified digital maps using GIS techniques, enabling remote monitoring and control of bait sprays by the surveillance authority and its personnel, thus providing on-time decision making. The results of the study, though at a preliminary stage, were found to be promising.

Index Terms—Bait sprays, *Bactrocera oleae*, embedded systems, GIS, web-based applications.

I. INTRODUCTION

O LIVE fruit production is of crucial importance for Greece as it consists the third bigger olive oil producer worldwide, as well as the biggest extra virgin oil producer, thus offering more than 1.6 billions € of revenue per year to the Greek economy.

Monitoring and control of *Bactrocera oleae* [Fig. 1 (on the left)] is a major parameter for olive growers living. *Bactrocera oleae* (Gmelin) or *Dacus oleae* (Gmelin) (Diptera: Tephritidae) causes high damages to olive fruit production (5 - 15% of the olive oil production) to all countries in the Mediterranean basin. Currently, several protection methods against *B. oleae* are applied including - but not limited to - the following:

Cover sprays from the ground applications: It is a curative method and aims to kill the immature stages of *B. oleae* that are inside the mesocarp of the olive fruit. The entire tree canopy is sprayed with an organophosphorous or with a pyrethroid insecticide until run off. The method's disadvantage

G. Fouskitakis, L. Doitsidis, I. Rigakis, I. Sarantopoulos, A. Papafilippaki, K. Maniadaki and M. Antonidakis are with the Department of Electronic Engineering, Technological Educational Institute of Crete, Chania, 73133, Greece e-mail: (fouskit@chania.teicrete.gr).

K. Varikou and A. Mpirouraki are with the Institute of olive tree, Subtropical plants & Viticulture (ELGO-DIMITRA), Chania, 73100, Greece.

is that a serious number of beneficial species are also killed except flies [1], which results to the break down of other secondary olive pests such as *Saissetia oleae*, *Aspidiotus nerii* etc. In addition, insecticide residues are usually found in the produced olive oil.

Bait sprays from the ground applications: They were based on the Berlesse method, and although they were proved to be effective, the used insecticide was found to be toxic.

Bait sprays from air: It was applied in olive orchards for many years. Nowadays, bait sprays from the air applications are not used any more, due to serious side effects in the beneficial entomofauna of the orchard [2].

Steril Insect Technique (SIT): The aim of SIT method is the destruction of olive fruit fly agroecosystem balance by continuously releasing sterilized males. This method has been studied for many years in Greece and the results indicated its effectiveness when orchards were isolated and olive fruit fly population was low [2]. However, a series of problems concerning the quality of the mass produced insects were also noticed.

Mass trapping: It is widely used against olive fruit fly especially in organic farming although it is not proved to be an effective method [4], [5].

Biological control: The olive fly is attacked by a number of beneficial insects (parasitoid and predator species) in the Mediterranean and also in sub-Saharan Africa, where the fly is thought to have been originated [2]. However, the complex of parasitoids seemed not to be quite effective against olive fruit fly because their impact is constrained only during summer period and not during autumn, where olive flies increase in high population densities.

The use of ground applications with protein baits mixed with insecticides against *Bactrocera oleae* is strongly recommended. With this method only a small part of the tree canopy is sprayed with the insecticide solution (spraying solution of 300cc/tree) and the half number of the trees of the orchard. Generally three (3) bait sprays are applied during summer and two (2) sprays during autumn depending on the olive fruit fly population and infestation. Every year from September and afterwards, only water soluble insecticides are used in order to avoid residues in the produced olive-oil.

To monitor the olive fly population a standard glass or a plastic McPhail trap is used [Fig. 1 (on the right)]. It contains a 2% of ammonium or protein solution as well as borax in order to attract the flies. It is placed within tree canopy, and

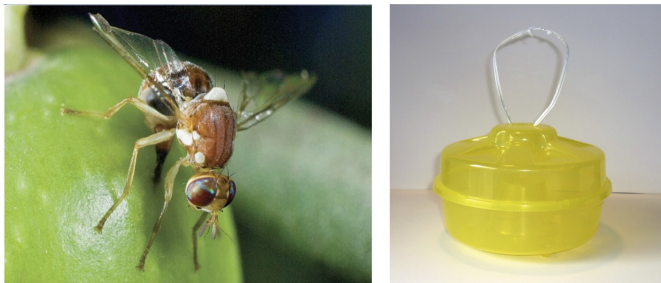


Fig. 1. The olive fruit fly *Bactrocera oleae* (Gmelin) (Diptera: Tephritidae) or *B. oleae* insect.

the captured insects are counted every 5 or 7 days. When the mean number of captured adults per trap and per week is more than 8-10, bait sprays are applied with the registered insecticide. The attractiveness of such a trap is about 20 m, but it is significantly reduced in a distance of 40 m. The attractiveness of the trap increases when humidity decreases or when temperature increases. In Greece, olive fruit fly control is funded by the Ministry of Rural Development and Food and applied by local tractors or back sprayers with specific nozzles, to almost all olive orchards that olive fruit production is more than 25 and 20% of a full production for oil and table olives, respectively. The spraying solution consists of the registered product - such as a-cypermethrin, dimethoate, l-cyhalothrin, etc. - mixed with 2% hydrolyzed protein. A detailed evaluation of the attractiveness of various bait spraying solutions, and the obtained results can be found in [6].

However, the application of the method has many disadvantages. It is not certified and the sprays are totally based on the experience of the sprayers. Specialized staff is required for the supervision of the method. It has been also recorded high loss of insecticide quantity by the people who apply the method, the sprayers. Several disadvantages of the current spraying method have been recorded, including but not limited to: (a) Higher than the recommended (300cc/tree) spraying solution quantity is applied per tree, (b) The entire tree is sprayed instead of a small part its canopy, (c) The spraying solution is not applied only to the olive trees but also to the rest agroecosystem (soil) because of leaks from the nozzle of the gun sprayer, either by improper use from the sprayers, or by use of improper equipment, (d) Spraying solution is applied to forbidden isolated agroecosystems such as rivers, lakes etc, with heavy consequences to the environment, (e) Protection measures of the human-sprayers are neglected, (f) The control of bait sprays is based on sampling by scientific staff.

Bait sprays are found to be of crucial importance. Nevertheless, they aren't systematically applied, they aren't efficiently monitored and they aren't certified. Efforts to automate the process may be found in the literature, as the spray process of trees has been addressed in the past, without accounting for ground (soil) difficulties and for afforestation (as it is inhomogeneously applied in Greece) [7], [8]. In addition, the existing studies do not present any impacts of the proposed methods on the final product. The use of modern GIS techniques for mapping olive fly population - captured in

McPhail traps - has been also presented [9]. This method necessitates the participation of staff within the olive grove, while the input of the obtained data and its mapping upon the GIS maps is manually done and is time-consuming. Recently Potamitis *et al.*, presented an electronic McPhail trap for monitoring *Bactrocera oleae* population based on an array of phototransistors receiving light from an infrared LED, the wing-beat recording is based on the interruption of the emitted light due to the partial occlusion from insects wings as they fly in the trap and the insect detections are transmitted from the field using a smartphone [10].

Based on the above, there is a profound need for the optimization and certification of the bait spraying process as well as the minimization of the human intervention, in order to achieve:

- 1) Effective protection against *B. oleae*,
- 2) Improvement of olive oil productivity,
- 3) Environmental protection, and,
- 4) Improvement of health and safety working conditions.

To address the aforementioned issues, a novel prototype integrated system has been developed able to monitor the insect population, assist the expert entomologists into taking on-time decisions concerning the bait sprays, and further apply bait sprays with an optimal manner. The core components of the system are:

- 1) A prototype McPhail trap equipped with an embedded system able to automatically picture the insect population and further transmit the related information,
- 2) A gun sprayer and its nozzle allowing for precise pressure, flow rate and spraying duration adjustment, thus enabling the application of very specific amount of mixture at each single spray,
- 3) A device for fully recording the bait spray procedure in terms of both space and quantity, and,
- 4) A web-based platform for mapping, remote monitoring and control of bait sprays allowing for real-time decision making.

The proposed approach provides a framework able to assure the proper application of bait sprays by minimizing human intervention, thus improving the health and safety at work, enhancing environmental protection, offering more effective and efficient protection of the olive fruit production against *B. oleae*, and hopefully, leading to a relevant improvement of the produced olive oil in terms of both quantity and quality.

The proposed approach will form the basis for the study of various other automation applications to agriculture, while the resulted know-how and conclusions will be utilized for educational purposes to higher-level education and to any interested organization.

The rest of the paper is structured as follows: The basic components of the proposed prototype integrated system are described in Section II. The results from its effectiveness evaluation are discussed in Section III, and finally the conclusions of the study are summarized in Section IV.

II. THE PROPOSED PROTOTYPE INTEGRATED SYSTEM

In this study, a novel prototype integrated system has been developed for the automation, optimization, and the assurance

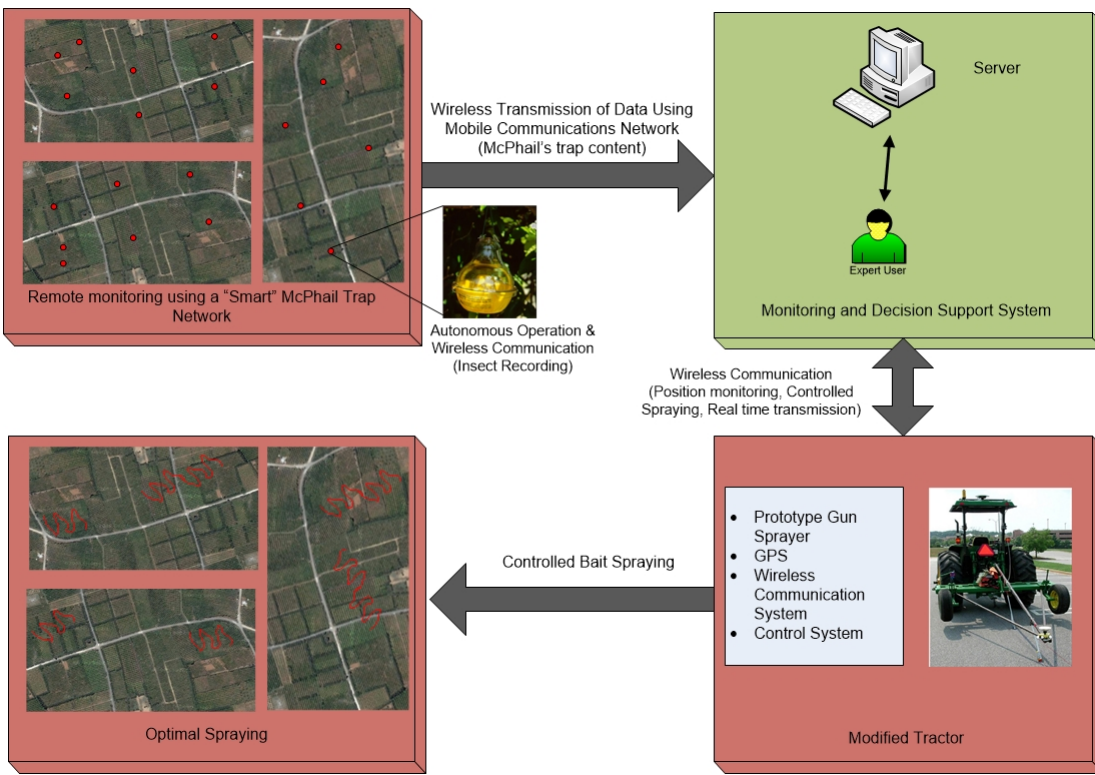


Fig. 2. The proposed prototype integrated system.

of proper application of bait sprays. Its main components are: (a) A prototype "smart" McPhail trap, (b) a gun sprayer and its nozzle enabling the implementation of accurate bait sprays, (c) a device for fully recording the bait spray procedure in terms of both space and quantity, and, (d) a web-based platform for mapping, remote monitoring and control of both the insect population within the smart McPhail traps, as well as of bait sprays. Its operation is schematically depicted in Figure 2.

Initially, a network of "smart" McPhail traps was developed providing wireless (using the GSM network) transmission of the related information. By using a camera installed in every smart trap, its interior was pictured and a series of photos was regularly taken and transferred to a remote server. The information was accessible thru a web-based system. Thus, olive fruit fly population was remotely monitored allowing the expert scientists to plan and schedule bait sprays on-time. These, were performed by a modified tractor equipped with a custom spraying system, being able to completely control the spraying process and simultaneously record both the trajectories route within the olive grove, as well as each single spray (quantity).

A. The "Smart" McPhail Trap

The "smart" McPhail trap, consists of a proper modification of its plastic counterpart shown in Figure 1. A number of components have been added such as an MSP430F5436 microcontroller (16-bit ultra-low-power microcontroller, 192 KB flash, 16 KB of RAM, 12-bit ADC, 4 USCI's), a GSM module (model: GM862 TELIT with GPRS support), a 2 MP

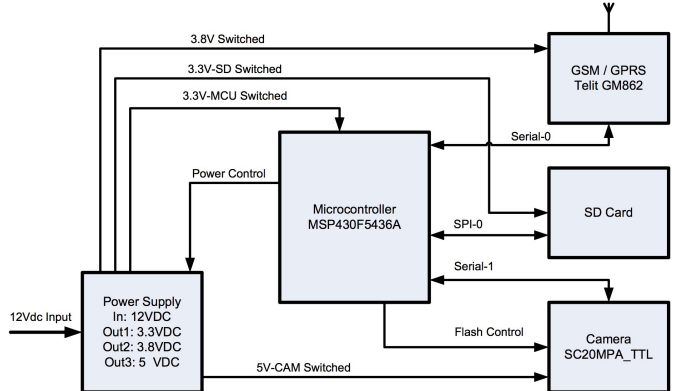


Fig. 3. Block diagram of the "smart" McPhail trap's embedded system.

digital camera supporting JPEG format, a LED light array for internal lighting, three (3) power supply modules (3.3, 3.8 and 5.0 Volts), an SD card slot for additional local data storage and a single 12 Volts battery (7000 mAh), and an embedded system providing automatic monitoring of *B. oleae* population in the field, was developed. Its block diagram is shown in Figure 3. The final version of the trap - after a series of modifications and improvements - installed in the olive grove and a photo of its interior are shown in Figure 4.

B. The Spraying Device

The proposed spraying device is based on an ordinary spraying mechanism. Indeed, a simple magnetic switch (regularly



Fig. 4. The “smart” McPhail trap installed in the field and a picture of its interior.



Fig. 5. The developed spraying device.

used in alarm systems), is installed beneath the trigger of a common spraying gun. An electromagnetic valve (suitable for water-based applications, brass-type, model: CEME 8514, 1/2", normally closed, 12 Volts DC, 30 bar maximum pressure) is installed at the tractor’s pump output. After the electrovalve and before the spraying gun, an extremely accurate (maximum flow rate of 18.3 lt/sec, linearity deviation $< \pm 0.5\%$, measurement error $< 0.05\%$, response time < 50 ms) AISI-316 stainless steel flow meter sensor is installed (model: SIKA VTR 1010, 1/2") along with its VSAPPS NPN/PNP signal transducer and its XVT2053 connection probe. Between the electrovalve and the spraying gun, an AISI-306 stainless steel pipe of approximately 1 meter length is introduced in order to reduce turbulence effects. The proposed spraying device is shown in Figure 5.

Once the spraying gun’s trigger is pressed, the electrovalve opens and allows the mixture to flow within the pipe. The flow meter sensor measures the flow and the mixture then exits the gun. The electrovalve remains open for as long as the electronics allow (see next Section where the recording device is presented). The spraying duration is completely controllable via a potentiometer which is installed on the recording device. Due to the by-pass system already installed on the tractor’s pump, the pressure is approximately constant throughout the spraying process, the sprayed quantity is effectively adjusted by only the duration potentiometer.

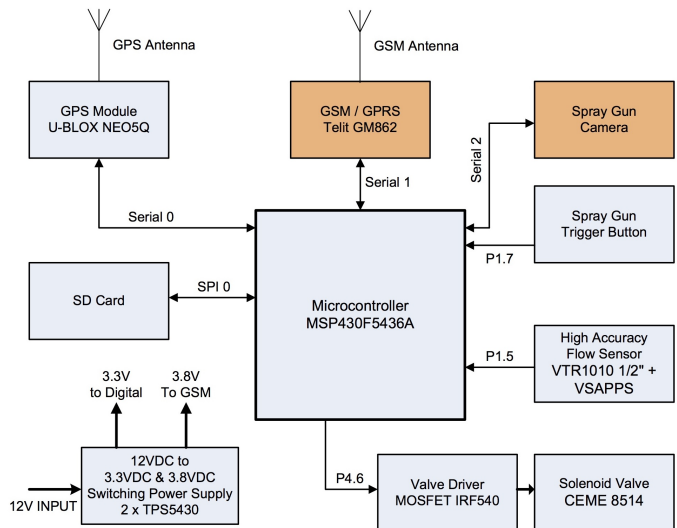


Fig. 6. Block diagram of the recording device’s embedded system.

C. The Recording Device

The aim of the recording device is twofold: (a) To fully control the spraying duration time by opening/closing the electrovalve, and (b) to fully record both the tractor’s path and route within the olive grove and the sprayed mixture quantity for each single spray. Its main components are: (a) an MSP430F5436 microcontroller used also on the “smart” trap, (b) a GPS module, type: U-Blox NEO5Q along with its antenna, (c) a mosfet IRF540 driver for controlling the electrovalve, (d) two (2) power supply modules (3.3, 3.8 Volts), and, (e) an SD card slot for additional local data storage. A GSM module may be easily added for real-time data transmission. This option is currently disabled as the GSM network in the test olive grove is sometimes characterized by poor signal power. A proper (fast focus) camera may be also introduced for monitoring that a specific part of the tree canopy is sprayed. This option is also disable to reduce data load. The recording device is power supplied by the tractor’s electrical power system. The block diagram of the developed embedded system is shown in Figure 6, and its final version, though being still a prototype is shown in Figure 7.

The tractor’s path and route (geographical position, and time) is recorded once a second ($f_s = 1$ Hz). Since the gun’s trigger is pressed, the valve driver mosfet activates the electrovalve and the PWM signal produced by the flow meter sensor is recorded, providing an accurate measurement of the sprayed mixture quantity.

D. The Web-Based Application

The aim of the developed web-based application is to provide the ability of a complete representation of both the information (images) available by the McPhail traps network, as well as the information recorded and stored during the spraying procedure. For this purpose, a suitable web-based application is developed using web pages techniques, Geographical Information Systems (GIS) and Data Base techniques.



Fig. 7. The recording device.

Its usage may significantly facilitate the work of specialized scientists such as agriculturists. Indeed, they can easily monitor the insect population evolution within the “smart” traps, thus being able to be proactive and - on-time - order the bait sprays when needed. Additionally, they can monitor the tractor’s route within the olive grove and control its potential coverage during the spraying procedure.

The Server uses a Linux-based operating system (distribution Debain 8) which was created in order to facilitate web services, which are based on Apache 2 Web Server. The available information is stored and managed via a MYSQL data base. Data management, its interconnection with the data base as well as dynamic web-page creation are based upon PHP 5. Back-end development is based on the Laravel 5.1 PHP framework. The Server’s security is supported by an IPTable filter, sshguard, openssl and other utilities. The user’s front-end management utilizes HTML5 and Javascript, while the front-end development is based on the Angularjs and JQuery Javascript Frameworks. The site’s appearance utilizes the bootstrap prototype. Data transfer between the server and the web-site are based on the RestFul protocol. All maps are based on google maps and google map api 3. All the above are based on open source software except google maps. Its operational block diagram is shown in Figure 8. The main web-page may be accessed at: <http://edakos.chania.teicrete.gr>. A login system for user authentication purposes is employed, offering three levels of access (web site user, super user and administrator).

E. System Evaluation

The proposed system is under evaluation since last July (2015). For this purpose, a large scale experiment is employed using a test olive grove comprising of eight (8) sectors of about a thousand (1000) olive trees each, see Figure 9. The attractiveness of the “smart” trap is evaluated by simultaneously placing three McPhail traps in each sector: a plastic, a glass, and a “smart” one, with the first two kinds already known to be certified. The images taken from the “smart” traps are found to provide adequate information for accurate insect population estimation, see Figure 4 (left subfigure). Nevertheless, the attractiveness of the “smart” trap was found to be significantly lower than its other two counterparts. To build a McPhail trap of adequate attractiveness is a well-known hard task, thus, a

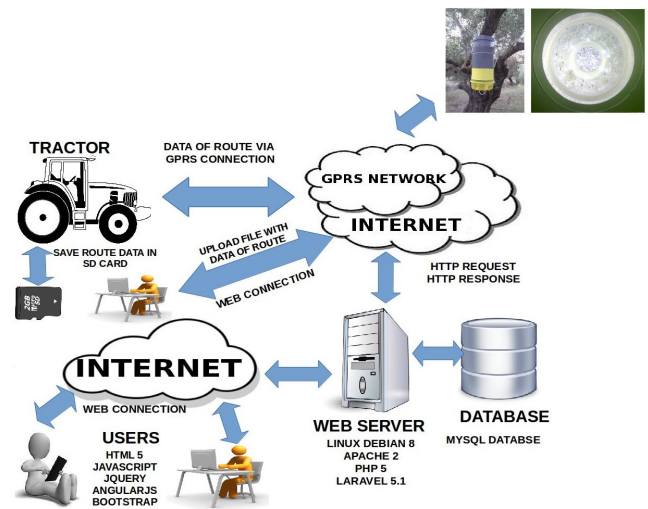


Fig. 8. Block diagram of the web-based application.

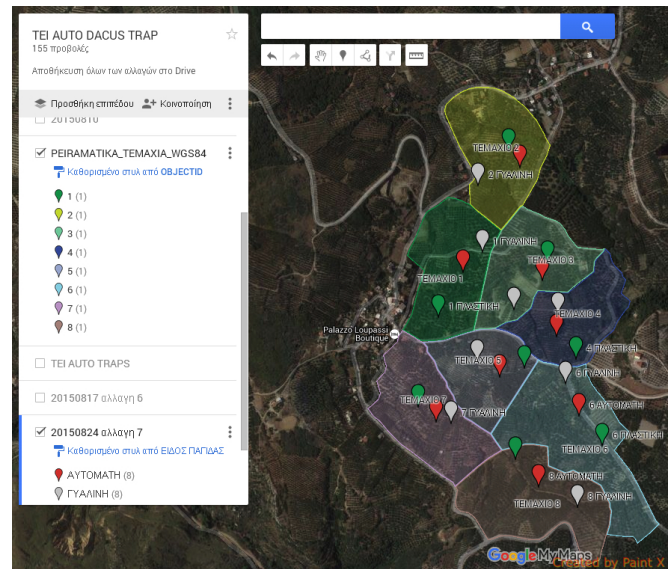


Fig. 9. The test olive grove.

few modifications could still be applied in the future to further enhance the attractiveness of the proposed “smart” trap.

Bait sprays are performed using the developed spraying device. The spraying procedure is continuously recorded/controlled via the embedded system in terms of both space (geographical position) and quantity. The recorded information is subsequently depicted on the properly modified digital map. Data representation is quite informative allowing for adequate monitoring the tractor’s route and the coverage of each sector. The details of each single spray is also available on the computer screen, see Figure 10.

Olive-oil qualitative analysis is still to be implemented, based on crop collected by the sectors sprayed by the proposed system, in terms of acidity, superoxides, K232, K270, according to the 2568/1991 E.C. regulation, and total phenols, hopefully indicating an improvement of the produced olive oil’s quality.

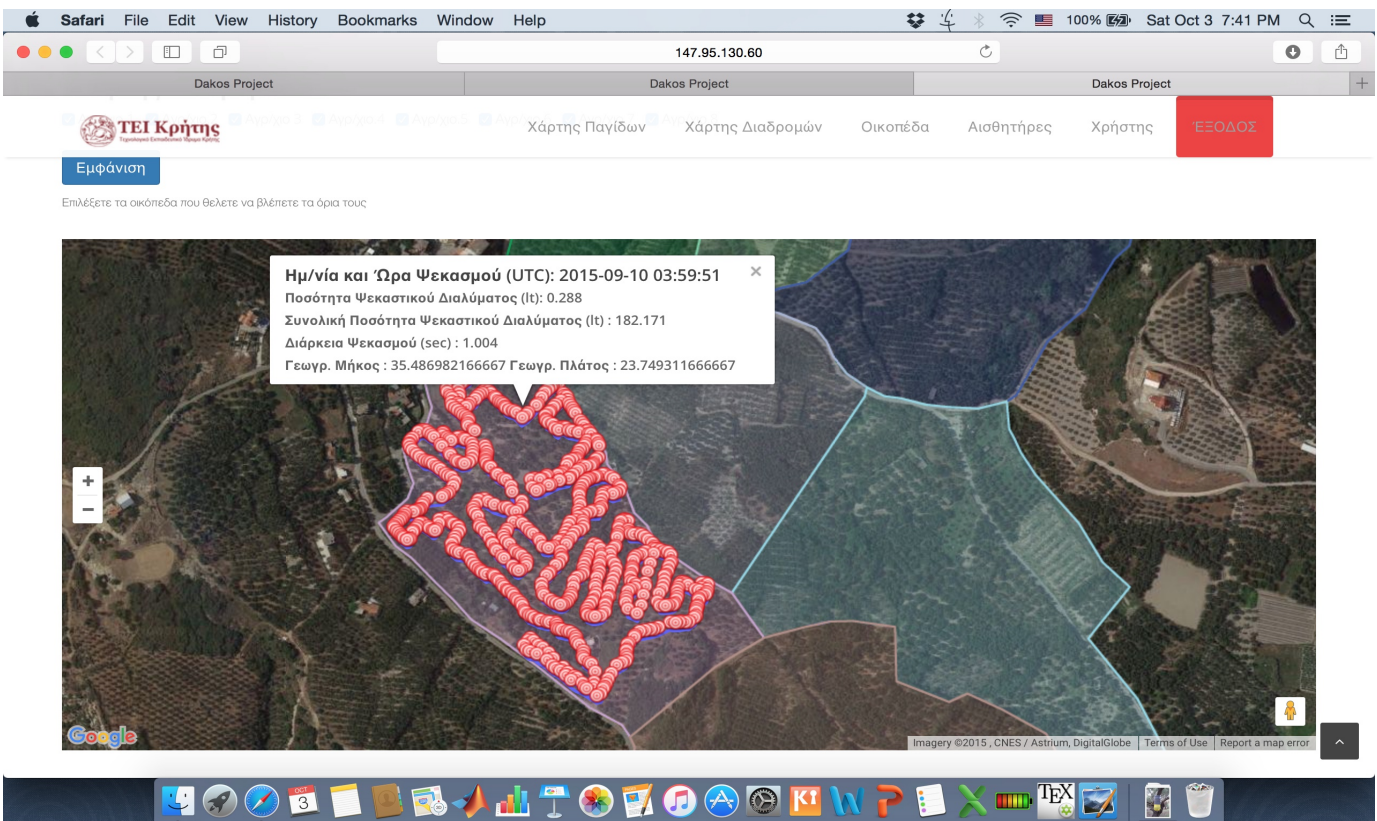


Fig. 10. A view of the developed web-based platform for monitoring bait sprays.

III. CONCLUSION

In this study, embedded systems, GIS's and a web-based application were designed for the development of a prototype integrated system for the automation, optimization and the assurance of proper application of bait sprays against *B. oleae*. Its application to a large scale olive grove, indicated - to an acceptable extent - that it significantly reduced human intervention, and proved capable to achieve: 1) effective protection against *B. oleae*, 2) improvement of olive oil productivity, 3) enhanced environmental protection, and, 4) improvement of the health and safety at work (compare with the required achievements posed in the Introduction). The results of the study, though at a preliminary stage, indicated that the proposed system was fully operational, while its effectiveness could significantly improve the proper application of bait sprays.

ACKNOWLEDGMENT

This work is implemented within the context of the Operational Program "Education and Lifelong Learning" action Archimedes III, Project 25, and is co-financed by the European Union (European Social Fund) and Greek national funds (National Strategic Reference Framework 2007 - 2013). The authors would like to thank BASF for providing specific chemicals and Vodafone for providing GSM SIM cards.

REFERENCES

- [1] Th. Broumas, "Olive fruit fly. Review of its biology and its chemical control," *Agrotypos*, vol. 8, pp. 26-31, 1994.

- [2] Th. Broumas, "Olive fruit fly. Iological and Biotechnical control methods," *Agrotypos*, vol. 1, pp. 44-54, 1995.
- [3] A. P. Economopoulos, N. Avtzis, G. Zervas, J. Tsitsipis, G. Haniotakis, G. Tsironopoulos, A. Manoukas, "Experiments on the control of the olive fly, *Dacus oleae* (Gmel.), by the combined effect of insecticides and releases of gamma-ray sterilized insects," *Zeitschrift fr Angewandte Entomologie*, vol. 83, pp. 201-215, 1977.
- [4] K. Varikou, V. Alexandrakis, et al., "Study of the effectiveness of Mass Trapping and new products for the control of the olive fruit fly *Bactrocera oleae* (Gmelin) (Diptera: Tephritidae) in organic olive groves," in *Proceedings of the Premier Seminaire International sur les Biotechnologies et Qualite des produits de l'Olivier dans le bassin Mediterraneen*, 2004.
- [5] K. Varikou, V. Alexandrakis, et al., "New records for control of Olive fruit fly *Bactrocera oleae* Gmelin," in *Proceedings of the the 5th International Symposium on Olive Growing*, 2004.
- [6] K. Varikou, N. Garantonakis, A. Birouraki, "Residual attractiveness of various bait spray solutions to *Bactrocera oleae*," *Crop Protection*, vol. 68, pp. 60-66, 2015.
- [7] S. Gan-Mor, R. L. Clark, et al., "New records for control of Olive fruit fly *Bactrocera oleae* Gmelin," in *Proceedings of the the 5th International Symposium on Olive Growing*, vol.59, pp. 31-38, 2007.
- [8] G. J. Nistala, "Development of an inexpensive guidance system for agricultural purposes," Biological and Agricultural Engineering, Louisiana State University. M.Sc Thesis, 2006.
- [9] A. Papafilippaki, K. Nikiforakis, et al., "Optimisation of the *dacus olea* control (*Bactrocera oleae*) with the use of Geographical Information Systems," in *Proceedings of the the 12th Panhellenic Conference of Endomology*, 2007.
- [10] I. Potamitis, H. Rigakis, K. Fysarakis, "The Electronic McPhail Trap," *Sensors*, vol. 14, pp. 22285-22299, 2014.

Monospecific dominance in a Alluvial Mixed Ombrophylous Forest in southern Brazil

J. Carvalho, F. Galvão, R. Rios, S. J. E. Velazco

Abstract — The Alluvial Mixed Ombrophylous Forest due to its importance and fragility is protected by law, however, remains uncharacterized and suppressed throughout its range due to human activities. The work was conducted in the Araucaria city of Paraná state of Brazil. We used 18 fixed plots of 10 m x 10 m where the following information was collected: breast height diameter (bhd), total height, botanical identification of all trees ≥ 5 cm bhd. The species were grouped considering the water restriction and the requirement brightness. Chi-square test to detect correlations between these two species groups was used. The forest showed 13 families, 21 genera and 27 tree species. *Sebastiana commersoniana* stands out as monodominant to present more than 60% of the relative density. The monodominance, in this environment, possibly, is subject to the soil water saturation.

Keywords—hydromorphic, ecological groups, phytosociological parameter.

I. INTRODUCTION

THE Alluvial Mixed Ombrophylous Forest occurs on the banks of rivers, running into a plan or wavy geomorphology of land [35]. Occurs in the southern highlands of Brazil in areas subject to periodic flooding pulse. *Sebastiana commersonia*, *Allophylus edulis*, *Lithraea brasiliensis*, *Schinus terebinthifolius*, *Podocarpus lambertii*, *Drimys brasiliensis*, *Capsicodendron dinisi*, *Blepharocalyx salicifolius*, *Luehea divaricata*, *Vitex megapotamica* are the mainly species of this community [6] [12] [22]. These forests have own structure and functionality and it is depending on geological variations, geomorphological and pedological processes [12] and fluctuations of the water table [19]. the distribution of species is related to microtopography due to variation of the requirements for tolerance to water saturation [20].

This forest is considered by a resolution [30], as wetland, so in the case of a fragile ecosystem, highly complex ecological, important to the process of environmental stability and maintenance of biodiversity, which, being in relief plans or lowlands, meet frequently

This work was supported by Coordenação de Aperfeiçoamento de Pessoal de Nível Superior – Capes.

J. Carvalho. Is doutorated student of the Federal University of Paraná. Curitiba, Paraná, Brazil. CEP 80210170 (corresponding author to provide phone: 55-41-30690518; e-mail: joemacarvalho@gmail.com).

F. Galvão, is professor of the Department of Ecology, Federal University of Paraná. Curitiba, Paraná, Brazil (e-mail: fgalvao@lufpr.br).

R. Rios is professor of the Department of Ecology, Federal University of Paraná. Curitiba, Paraná, Brazil (e-mail: rioselva@gmail.com).

S. J. E. Velazco. Is doutorated student of the Federal University of Paraná. Curitiba, Paraná, Brazil. CEP 80210170 (corresponding author to provide phone: 55-41-30690518; e-mail: joemacarvalho@gmail.com).

with high levels of water saturation, determining a situation that a high carbon fixing ability which, in turn, results in high water holding capacity and ions in soil, increasing the filtering capacity and water-tuning the flow of rivers. The adaptations of the species allows their classification according to the requirements of specific conditions and resources. There is still no consensus in academic regarding the most appropriate classification and also the framework of some species. The most important factors that act in river environments are the light and the water regime. Therefor, [38], they group the species in pioneer and climax. Considering the water regime, [39] distinguish the tree species into three groups: general, preferred and exclusive.

The alluvial forests are characterized by having lower plant diversity that the slope [21], presenting monodominance by a species in various situations. [9] define this characteristic as one where a single species is more than 60% of the number of canopy individuals or basal area and that persists in the environment when recruits and regenerates below his own shadow. [15] describes the factors that control the diversity of species in tropical forests and analyzes the causes of monodominance in forests subject to flooding in Central America. In Brazil numerous studies report that analysis [28] [2] [1].

In the present study we evaluated the qualitative and quantitative characteristics of a Alluvial Mixed Ombrophylous Forest in Araucaria municipality in Paraná state of Brazil. In this forest, possibly monodominance it appears a pioneer and preferred species to flooding environments, being the main factor soil waterlogging.

II. MATERIAL AND METHODS

The study site is located in the areas of Mixed Ombrophylous Forest associated with the Iguaçu River basin, south-central portion of the First Paraná Plateau, at an average height of 920 m asl. It is located in the Metropolitan Region of Curitiba, in Araucaria city of Paraná state of Brazil (FIGURE 1), near the Presidente Getúlio Vargas Refinery - REPAR, next to the coordinates 25°34'02,5 "S and 49°20'53,5 "W .

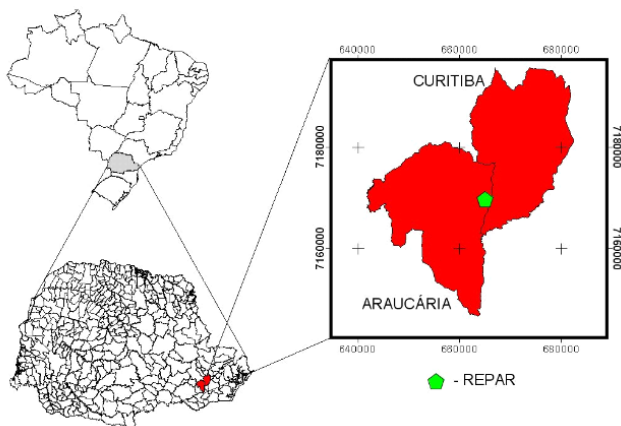


Fig. 1 Study site localization

The site is in the region of humid subtropical climate mesothermal the Cfb, with the occurrence of severe and frequent frosts without a dry season. The annual rainfall is between 1,400 and 1,600 mm, the average annual temperature between 16 and 18 °C and the relative humidity ranges 80-85% [16]. The average annual precipitation over the basin of the Iguaçu river is of 1500 mm year order, and the rain distribution is quite irregular in time and space, therefore there is no well-defined wet season. Annual changes alter the distribution pattern of the same, as the presence of El Niño. The cold front entry can quickly change the height of the water table [26].

The alluvial plains of the Metropolitan Region of Curitiba, in general, have clay-silty-sandy sediments, occupy about 490 km², or 20% of the basin area Curitiba city, mainly covering the Iguaçu River floodplain and its major tributaries. Soils are characterized as mineral hydromorphic the order of Gleyssolics Melanic and Haplic [3]. The Gleyssolic Melanic soil presents very slow permeability rates and low base saturation due to clayey textures and poorly developed structures. The Gleyssolic Haplic soil has medium texture also hindering drainage [11].

The drainage system of the study area is represented by the feeder rivers of the Paraná River basin, and the Iguaçu river as collector master and its tributaries, among them and as a highlight, the river Barigui, present in the study area. The latter river is located along the right or northern Iguaçu and runs for a length of 64.9 kilometers through several municipalities in the region, making a drainage area 272,5 km² [25].

This was a new phytosociological survey in 2012, based on 18 permanent plots of 10 x 10 m, allocated since 2001. All individual trees with perimeter at breast height less than 15 cm were sampled. The number of individuals per species and sociological position (canopy, middle strata and understory) was observed.

We considered three ecological groups regarding the requirement in light, framing the species as pioneers, light demanding climax and shade tolerant climax [39]. Regarding tolerance to water saturation, common to these environments, species were grouped in general, preferred and exclusive [39].

Chi-square test was used in contingency tables of two factors to determine possible associations between these groups of variables.

Table I – Species, numbers of individuals, sociological position and ecological groups in a Alluvial Mixed Ombrophylous Forest in southern Brazil

The botanical material was collected and is available in the Herbarium of Forestry Course (EFC) of the Federal University of Paraná. The verification of scientific names, and abbreviations authors were performed according Missouri Botanical Garden [27].

III. RESULT

The community had 13 families, 21 genera and 27 species, 436 individuals sampled.

It was found that most individuals belong pioneer (70%), followed by shade tolerant climax (19%) and light demanding climax (11%). Considering the total number of species (27), the most is light demanding climax (44%), followed by shade tolerant climax (30%) and pioneer (26%) groups (see Table I).

Sebastiana comersoniana, *Schinus terebinthifolius* and *Hovenia dulcis* were the species that highlighted the ecological group of pioneer species. *Edulis Allophyllus*, *Myrrhinium atropurpureum* and *Eugenia uniflora* were the main species in the group of shade tolerant climax and *Blepharocalyx salicifolius*, *Myrciaglia glaucescens* and *Guettarda uruguensis* belong the group of light demanding climax.

According to the sociological position, the largest number of individuals (45%) lies middle strata, followed by the canopy (37%) and understory (18%).

Considering the community, most of the species are generalists (70%) and the others are preferred (30%). The opposite occurs individuals is most preferred (83%), followed by general (17%). It was observed that all species light demanding climax are general. Regarding pioneer species, the most is general (57%) followed by the preferred (43%). The reverse was found in the shade tolerant climax species, the most is preferred (63%), followed by general (37%). Exclusive species were not observed in the community.

According to the chi-square test, the data showed that there is a significant relationship ($p < 0.05$) between the ecological group related to water tolerance associated with the light (Figure 2). Correlating the sociological position with the two types of ecological groups was detected a strong association for light-related groups ($p < 0.05$). In this community, most preferred pioneer behaves as a hydromorphic environments, however, the light demanding climax is the most general comprises (Figure 2). Individuals characterized as pioneers and light demanding climax are well represented in middle strata and the shade tolerant climax in the just below the canopy strata and the understory. It can be considered that there is no significant association between the variables of sociological position and groups regarding tolerance to water, since the p-value was very close to 0.05 (Figure 3).

EG	Species	Families	NI	SP			RD	IP
				1	2	3		
Light demanding climax and generalists	<i>Blepharocalyx salicifolius</i> (Kunth) O. Berg	Myrtaceae	13	10	3		3,2	5,2
	<i>Myrceugenia glaucescens</i> (Cambess.) D. Legrand & Kausel	Myrtaceae	9	5	3	1	2,1	1,5
	<i>Guettarda uruguensis</i> Cham. & Schltld.	Rubiaceae	6	1	5		1,2	0,7
	<i>Lithraea brasiliensis</i> Marchand	Anacardiaceae	5	3	2		1,2	1,1
	<i>Campomanesia xanthocarpa</i> Mart. ex O. Berg	Myrtaceae	4	3	1		0,9	1,1
	<i>Machaerium paraguariense</i> Hassl.	Leguminosae - Faboideae	4	3	1		0,9	08
	<i>Machaerium brasiliense</i> Vogel	Leguminosae - Faboideae	1		1		0,2	0,1
	<i>Dalbergia frutescens</i> (Vell.) Britton	Leguminosae - Faboideae	2		2		0,5	0,3
	<i>Machaerium stipitatum</i> (DC.) Vogel	Leguminosae - Faboideae	1			1	0,5	0,3
	<i>Inga marginata</i> Willd.	Leguminosae - Mimosoideae	1	1			0,2	0,2
Total	<i>Calyptranthes concinna</i> DC.	Myrtaceae	1		1		0,2	0,1
	<i>Myrcianthes gigantea</i> (D. Legrand) D. Legrand	Myrtaceae	1		1		0,2	0,2
Total				48	26	20	2	
Shade tolerant climax and preferred	<i>Allophylus edulis</i> (A. St.-Hil., A. Juss. & Cambess.) Hieron. ex Niederl.	Sapindaceae	43	1	19	23	9,5	7,1
	<i>Myrrhinium atropurpureum</i> Schott	Myrtaceae	22	2	12	8	5,1	3,4
	<i>Sebastiania brasiliensis</i> Spreng.	Euphorbiaceae	3		2	1	0,7	0,4
	<i>Scutia buxifolia</i> Reissek	Rhamnaceae	2			2	0,3	0,2
	<i>Myrciaria tenella</i> (DC.) O. Berg	Myrtaceae	2		1	1	0,5	0,6
Shade tolerant climax and generalists	<i>Eugenia uniflora</i> L.	Myrtaceae	6		2	4	1,4	0,8
	<i>Casearia decandra</i> Jacq.	Flacourtiaeae	3		1	2	0,5	0,3
	<i>Eugenia uruguayensis</i> Cambess.	Myrtaceae	1			1	0,2	0,1
Total				82	3	37	42	
Pioneers and preferred	<i>Sebastiania commersoniana</i> (Baill.) L.B. Sm. & Downs	Euphorbiaceae	285	120	134	31	66,3	67,9
	<i>Syagrus romanzoffiana</i> (Cham.) Glassman	Arecaceae	2	1		1	0,2	0,1
	<i>Vitex megapotamica</i> (Spreng.) Moldenke	Verbenaceae	2		2		0,5	0,3
Pioneers and generalists	<i>Schinus terebinthifolius</i> Raddi	Anacardiaceae	11	8	1	2	2,3	3,5
	<i>Hovenia dulcis</i> Thunb.	Rhamnaceae	3	1	1	1	0,7	1,2
	<i>Luehea divaricata</i> Mart.	Malvaceae	2	2			0,5	1,7
	<i>Ligustrum lucidum</i> W.T. Aiton	Oleraceae	1				0,2	0,5
Total				306	132	138	35	100

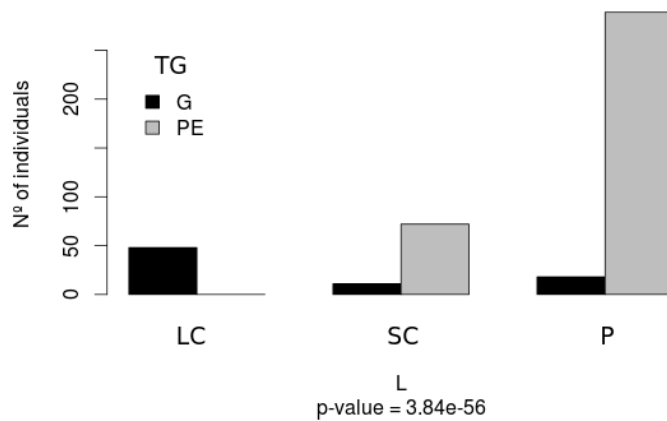


Fig. 2 Relationship between environmental group about the tolerance to water and in relation to light. TW: ecological group for tolerance to water (G - general, PE - preferred). L: ecological groups in relation to light (LC – light demanding climax, SC – shade tolerant climax, P - pioneer)

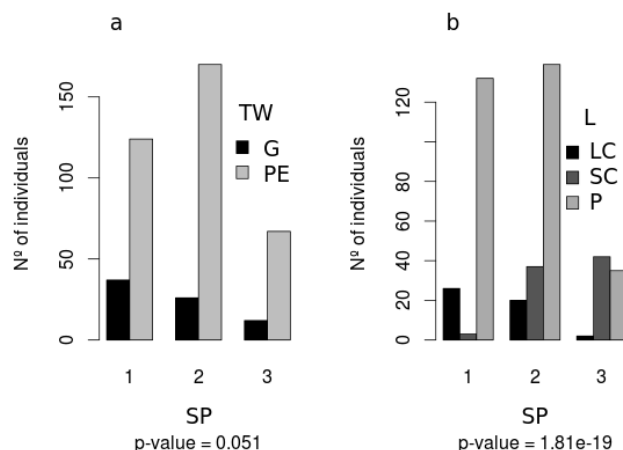


Fig. 3 Relationship between the different ecological groups (a) and the sociological position (b). SP: sociological position. TW: ecological group for tolerance to water (G - general, PE - preferred). L: ecological groups in relation to light (LC – light demanding climax, SC – shade tolerant climax, P - pioneer)

I. DISCUSSION

Most observed individuals in this community are pioneers and preferred, however, the smallest of the species are these two ecological groups. Thus, few species dominate the community, featuring a homogeneous environment. It is therefore a remnant of Alluvial Mixed Ombrophylous Forest [17], defined as climax edaphic [34], constituting a hydrosere [24], characterized by a natural disturbance processes, which in this case is the main factor that works in the natural selection of species [19]. After a peak flood, when the water table is near the soil surface, it is restrictive to the development of tree species [23] [4] [8] [12]. The Gleysol which is typical of where this situation is verified, is the predominant site of the study, mostly suitable for hydrophilic species [11].

Considering the number of individuals in the community, *Sebastiania commersoniana* has 65% of the total and 50.8% of the importance of percentage. It is a pioneer species, selective swamp, very frequent and abundant, almost exclusively of floodplains, where usually becomes dominant, constituting 60-80% of continuous canopy strata [6] [3] [37] [32]. In poorly drained tropical forests there is a tendency to dominance by a few species or a single species

[34]. The expansion of forests in temperate areas during the Lower Holocene, caused by increased heat, has created unfavorable conditions, highly shaded for many of the plants that had previously been dispersed near the glacial stage. Climate change after this stage, were harmful to these species and many of them have become restricted high altitudes, especially at low latitudes. Certain plant species are more tolerant of higher temperatures, but are unable to survive under dark shadows. For these species there were other opportunities, as is the case of environments that for some reason do not harbor forests and provided safe havens, such as habitats disturbed by periodic flooding [10].

The largest number of individuals present in the middle strata and canopy was also *Sebastiania commersoniana*. Due to its requirement in light and dominates the canopy. It can be considered that their presence in middle strata is stock of individuals that future will be recruited for the canopy before a disturbance, determining opening clearing. Thus, the species which occur together with recruiting are species that are already established and are typical of this strata [6].

The representativity of this specie makes the environment to be monodominant because a single specie has greater number of individuals to 60% of the total [9]. Thus, the monodominance is common in alluvial forests of the Brazilian southern plateau.

In studies conducted in a floodplain in cities of Paraná state of Brazil, like Jaguariaiva, found in one of the situations with higher water saturation, the predominance of *Sebastiania commersoniana*. The species showed 59.7% compared to the number of individuals and occupied the dominant strata [29]. In two compartments of the Iguaçu River, in Araucaria, the density of this species ranged from 45% to 63.5% [31]. Similar relationship in the floodplain of the Iguaçu River in São Mateus do Sul, where 60-80% of the canopy was composed of this species [36]. In a remnant of alluvial forest in São José dos Pinhais was observed *Sebastiania commersoniana* with the highest number of individuals occupying the canopy and the middle strata [5]. In the same forest in Irai, the canopy was between 10 and 14 m, where stood out *Sebastiania commersoniana*, with six times more individuals than the other species [40].

In alluvial forests of the Iguaçu River in a fragment of Paraná state, the relative density of *Sebastiania commersoniana* ranged from 96% to 64.6% and the other fragments of this type of forest in the state of Santa Catarina ranged from 79.6% to 44%. Possibly this parameter is correlated with the evolutionary stage of the forest. Gradually, the pioneers are replaced by climax species. Thus, the low relative density of the species show the evolution of successional stage [11]. As these authors, this species is closely tied to the luminous intensity zones, identified bad and regular states for bands below the canopy (below 6 m high), featuring suppression process in succession dynamics. They consider that the patterns of soil drainage is essential importance in the dynamics of occupation of the tree.

This species gives the vegetation a very typical face, the green-white color, high on the physiognomy and structural characterization of alluvial forests of southern Brazil, mainly in the region of occurrence of Mixed Ombrophylous Forest in unstructured soils [13].

The representativity of other species is much less than *Sebastiania commersoniana*. Following this specie, the most representative in the community is *Schinus terebinthifolius*. It is a pioneer and abundant on the edge of the alluvial forest fragments [3] [32] *Hovenia dulcis*, native to Japan and China also pioneer, therefore intolerant to shade [7], considered as alien specie in Brazil [18]. *Allophylus edulis*, *Myrrhinium atropurpureum* and *Eugenia uniflora* were the main species in the group of shade tolerant climax and *Blepharocalyx salicifolius*, *Myrceugenia glaucescens* and *Guettarda uruguensis* the group of light demanding climax species, are selective hygrophilous and that develop in floodplains [32] [33], where the environment is semi-hydromorphic or hydromorphic [11].

II. CONCLUSION

The Alluvial Mixed Ombrophylous Forest studied has monodominance of *Sebastiania comersonia*, most remarkable species in the two upper strata. Belongs to the group of the pioneers and the preferred and may be concluded that these are environmental groups that determine the physiognomy of the forest in question. Possibly in this forest, the dominance of a single species is a result of soil waterlogging.

Studies in other alluvial areas are needed given the continuing strongly changed that are suffering and its importance in relation to quality of water resources. Long-term follow-up will give the possibility to understand the dynamics of these environments, which is a subsidy for the management and the management of these ecosystems.

III. REFERENCES

- [1] G. A. Amador, G. A. Damasceno-júnior, J. C. Casagrand and A. L. B. Sartori. Structure of two communities dominated by *Copernicia Alba* and associations with soil and inundation in Pantanal Wetland, Brazil. *Oecologia Australis*, vol. 16, no. 4, pp. 846-858, 2012.
- [2] J. Arieira and C. N. Cunha. Population structure of cambará (*Vochysia divergens* pohl, Vochysiaceae), monodominant species in floodable forest in the Pantanal Mato-Grossense). *Oecologia Australis*, vol. 16, no. 4, pp. 819-831, 2012
- [3] M. L. Barddal, C. V. Roderjan, F. Galvão, G. R. Curcio. Floristic and phytosociologic characterization of a floodplain forest, at Araucaria, PR. *Ciência Florestal*, vol. 14, no. 2, pp. 37-50, 2004.
- [4] M. M. Brinson. Riverine forests. In: A. E. LUGO, M. BRINSON, S. BROWN, S. Ecosystems of the world 15 – Forested wetlands. Amsterdam: Elsevier Science, 1990, pp. 87-142.
- [5] A. M. Bufren. "Caracterização fitossociológica de um remanescente da floresta ripária do rio Pequeno, São José dos Pinhais – PR. (Dissertation), PhD dissertation, Setor de Ciências Agrárias, Univ. Fed. do Paraná, Curitiba, PR, 1997.
- [6] J. Carvalho, M. C. M. Marques, C. V. Roderjan, S. G. A. Sousa, M. Barddal. Species distribution relationships of different strata and soil characteristics in an alluvial forest in Paraná State, Brazil. *Acta Botanica Brasilica*, vol. 23, no. 1, pp. 1-9, 2009.
- [7] P. E. R CARVALHO. Espécies Florestais Brasileiras : recomendações silviculturais, potencialidades e uso da madeira. Colombo: Embrapa. 1994. 640 p.
- [8] M. T. Casanova and M. A. Brock. How do depth, duration and frequency of flooding influence the establishment of wetland plant communities? *Plant Ecology*, Dordrecht, no. 147, pp. 237-250, 2000.
- [9] J. H. Connell and M. D. Lowman. Low-diversity tropical rain forests: some possible mechanisms for their existence. *American Naturalist* vol. 134, pp. 88-119, 1989.
- [10] C. B. Cox and P. D. Moore, P. D. Biogeography: An Ecological and Evolutionary Approach. John Wiley & Sons, 2010. 506p.
- [11] G. R. Curcio, F. Galvão, A. Bonnet, M. L. Barddal and R. A. A. Dedecek. The riparian forest on two compartments of Iguaçu river, Paraná, Brazil, vol. 37, pp. 125-147, 2007.
- [12] G. P. Curcio, A. Bonnet, D. Pestana, L. Souza, L. G. Socher, F. Galvão and C. V. Roderjan. Toposequence segmentation and phytosocial characterization of a copse from a Mixed Ombrophilous Forest., vol. 36, no. 3, pp. 361-369, 2006
- [13] M. C. Dias, A. O. S. Vieira and M. R. C. Paiva, Florística e fitossociologia das espécies arbóreas das florestas da bacia do rio Tibagi. In: A bacia do rio Tibagi. Ed: M. E. Medri, E. Bianchini, O. A. Shibatta, J. A. Pimenta. Cap. 8, pp. 109-124, 2002.
- [14] G. Durigan, R. R. Rodrigues and I. A. Schiavini. Heterogeneidade ambiental definindo a metodologia de amostragem da floresta ciliar. In: R. R. Rodrigues and H. F. Leitão-Filho. Matas Ciliares: conservação e recuperação. 2. ed. São Paulo: Edusp, Fapesp, 2001. Cap. 10
- [15] P. J. Hart. Patterns of Tree Mortality in a Monodominant Tropical Forest, 1990
- [16] Instituto Agrônomico Do Paraná. Cartas climáticas do Paraná [cited 2014 jul. 19]. Available from: <http://www.iapar.br/modules/conteudo>.
- [17] Instituto Brasileiro De Geografia E Estatística – IBGE. Manual Técnico da Vegetação Brasileira. Série Manuais Técnicos em Geociências. Rio de Janeiro, 2012.
- [18] Instituto De Recursos Mundiais; União Mundial Para A Natureza; Programa Das Nações Unidas Para O Meio Ambiente. A estratégia global para a biodiversidade - diretrizes de ação para estudar, salvar e usar de maneira sustentável e justa a riqueza biota da Terra. Curitiba: World Resources Institute e Fundação O Boticário de Proteção à Natureza, 1992, 232 p.
- [19] N. M. Ivanauskas, R. R. Rodrigues and A. G. Nave. Ecological aspects of a swamp forest at Itatinga, SP: floristics, phytosociology and species selectivity. *Revista Brasileira de Botânica*, São Paulo, vol.20, no.2, pp.139-153, 1997.
- [20] C. A. Joly. Flooding tolerance in tropical trees. Pp. 23-34. In: M.B. Jackson; D.D. Davies and H. Lambers (eds.). Plant life under oxygen deprivation: ecology, physiology and biochemistry. SBP Academic Publishing, The Hague, 1991.
- [21] P. C. Lobo and C. A. Joly. Aspectos Ecofisiológicos da Vegetação de Mata Ciliar do Sudeste do Brasil, pp. 143-157. In: R. R. Rodrigues and H. F. Leitão Filho (eds.). Matas ciliares: conservação e recuperação. 2a ed. São Paulo, EDUSP e FAPESP, 2001.
- [22] R. M. Klein and G. Hatschbach. Fitofisionomia e notas sobre a vegetação para acompanhar a planta fitogeográfica do município de Curitiba e arredores. *Boletim da Universidade Federal do Paraná. Geografia Física*, v. 4, no. 30, 1962.
- [23] T. T. Kozlowski. Extent, causes and impacts of flooding. In: T. T. Kozlowski. Flooding and plant growth. Orlando: Academic, pp.1-7, 1984.
- [24] Y. S. Kuniyoshi. Sucessão Ecológica. A Vegetação Natural do Estado do Paraná. Curitiba: IPARDES and IAP, 1994.
- [25] E. J. Manassés, J. L. Vaine and T. L. G. Miranda. Estudo estatístico do risco de ocorrência das vazões e níveis no rio Barigüi. In: II Seminário do rio Iguaçu. Araucária: Ações implementadas pela UMR-REPAR/Petrobras, 2001.
- [26] M. R. M. Mine, C. E. M. Tucci. Gerenciamento da produção de energia e controle de inundação: Foz do Areia no rio Iguaçu. RBRH - Revista Brasileira de Recursos Hídricos, vol. 7, no. 3, pp. 85-107, Jul/Set 2002,
- [27] Missouri Botanical Garden. Vascular Tropicos (VAST) nomenclatural database and associated authority files, 1968. Disponível em: <http://www.mobot.org/w3t/search/vast.html>.
- [28] M. T. Nascimento and J. Proctor. Soil and plant changes across a monodominant rain forest boundary on Maracá island, Roraima, Brazil. *Global Ecology and Biogeography Letters*, 6, pp. 387-395, 1997. <http://dx.doi.org/10.2307/2997339>
- [29] M. K. F. S Nogueira, G. R. Curcio, R. S. Moro and F. Galvão. Phytosociological and pedological characterization of tree and shrub strata in a flood plain in Jaguariaíva, state of Paraná, Brazil. *Terr@Plural*, Ponta Grossa, vol.4, no.2, pp.193-215, jul./dez. 2010.
- [30] PARANÁ. Resolução conjunta IBAMA / SEMA / IAP nº 45, de 25 de setembro de 2007: define critérios para avaliação das áreas úmidas e seus entornos protetivos, normatiza sua conservação e estabelece condicionantes para o licenciamento das atividades neles permissíveis no estado do Paraná. Diário Oficial do estado do Paraná, edição no. 7570, pp. 18-19, out. 2007.
- [31] A. L. PASDIORA. "Florística e fitossociologia de um trecho de floresta ripária em dois compartimentos ambientais do rio Iguaçu, Paraná, Brasil". (Dissertation), PhD dissertation, Setor de Ciências Agrárias, Univ. Fed. do Paraná, Curitiba, PR, 2003
- [32] R. Reitz, R. M. Klein and A. Reis. Projeto madeira do Rio Grande do Sul. Sellowia no. 34 and 35, 525p., 1983.
- [33] R. Reitz, R. M. Klein and A. Reis. Projeto madeira – Santa Catarina. Florianópolis. Lunardelli, 1979.
- [34] M. A. Richards. The Tropical Rain Forest: an ecological study. London, Cambridge, Cambridge University Press, 1979.
- [35] C. V. Roderjan, F. Galvão, Y. S. Kuniyoshi, G. G. Hatschbach. As Unidades Fitogeográficas do Estado do Paraná. Ciência & Ambiente. Fitogeografia do sul da América. Santa Maria, vol. no., 24, pp. 75-92, 2002.
- [36] S. M. Silva, R. M. Brites and W. S. Souza, J. T. W. Motta. Levantamento florístico em área de várzea do rio Iguaçu, São Mateus do Sul – PR – Brasil. Arquivos de Biologia e Tecnologia, Curitiba, vol. 40, no. 4, pp. 903 – 913, 1997.

- [37] L. B. Smith, J. Downs and R. M. Klein. As plantas eufo: Euphorbiaceaeas. R. Reitz (ed.). Flora Ilustrada Catarinense. Sellowia, pp. 308-313, 1988.
- [38] M. D. Swaine and T. C. Whitmore. On the definition of ecological species groups in tropical rain forests. Vegetation vol. 75, pp. 81-86. Netherlands: Kluwer Academic Publishers, Dordrecht, 1988.
- [39] B. M. T Walter, J. F. Ribeiro. Spatial floristic pattern in gallery forest in the cerrado region, Brazil. In: J. I. Encina, J. I.; C. Kleinn. Proceedings of the international symposium on assessment and monitoring of forests in tropical dry regions with special reference to gallery forests. Brasília: EDUNB, pp. 339-349, 1997.
- [40] S. R. Ziller. As Formações Vegetais da Área de Influência do Futuro Reservatório do Rio Irai - Piraquara / Quatro Barras - PR. Curitiba, Relatório Técnico. 93p., 1993.

New Technology of Renewable Energy Generation

S. Tounsi

Abstract— In this paper we present a modelling approach of an automated renewable energy system including the losses of the power chain. The choice of the energy generation chain components is conducted taking account of the possibility to achieve high current to recover high power in the one hand and the simplicity of the chain structure and of its components in order to reduce the cost of production in the other hand. Indeed, a synchronous motor with coiled rotor and reduced production cost is chosen for the electric energy generation. To enable continuous energy recovery, excitation current is increased at low speeds and reduced at high speeds to prevent over-current problem. In addition, an automated braking system, provided by pulse width modulation control of an electromagnet, limits the charging current of the batteries to protect the energy generation chain.

The implementation of the global model in the simulation environment Matlab-Simulink has led to very good results of simulations encouraging the industrialization process of this chain.

Keywords— Coiled Rotor Generator, Rectifier, Modeling, Battery, Braking Torque, Recovered Energy.

I. INTRODUCTION

This paper presents a parameterized model of the generation chain of renewable energy. A coiled rotor generator design program based on the analytical method is developed [1-3]. This generator is modular, allowing to generate high currents without destroying the quality of the waveform of back electromotive force by adding additional modules. In this way, the total flux received by the coil keeps a shape close to a sinusoidal shape, and its amplitude depend essentially that of the excitation current (reduction of the magnetic armature reaction). This type of generator has the following advantages:

- A variable excitation allowing a continuous recovery of energy.
- Modularity permitting to generate strong currents especially at high propeller speeds.

Little research illustrates and addresses the problem of energy generation using this type of generator, making this study innovative solution for the energy production. Energy generation chain is subdivided into modules and each module is modeled at Matlab-Simulink simulation environment. The

S. TOUNSI, is with the National School of Electronics and Telecommunications of Sfax, Sfax university (B.P. 1163, 3018 Sfax-Tunisie, Tel.: 74 863 047, 74 862 500 – Fax: 74 863 037; e-mail: souhir.tounsi@enetcom.rnu.tn).

coupling of different models leads to overall power generation chain model.

This paper is mainly articulated around the following points:

- A presentation of the model approach of the different modules of the energy generation chain.
- Implementation of the global model in the Matlab-Simulink simulation environment.
- A description of the simulations results.

II. CONVERSION CHAIN STRUCTURE

Conversion chain (figure 1) has a propeller to recover the energy generated by wind. This mechanical energy is converted into an alternating electrical energy via a gear speed amplifier and a coiled rotor synchronous generator. The electrical energy developed is also converted into DC power through a three-phase rectifier. An automated braking system, provided by pulse width modulation control of an electromagnet, limits the charging current of the batteries to protect the energy generation chain.

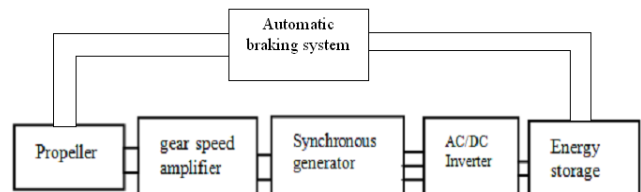


Fig.1 Power chain structure

III. DESIGN OF THE SYNCHRONOUS GENERATOR

Our choice fell on the analytical method since it has the following key benefits [4-12]:

- It produces solutions quickly and without iterations.
- It leads to highly parameterized design models leading to performance optimization problems.
- It provides acceptable precisions on the results for it is based on simplifying assumptions well argued and proper to address a design problem of an electrical device.

The generator design problem by the analytical method is completely reversed to facilitate resolution. Generally, we starts from the generator dimensions to the power requirement and in this case a series of simulations is needed to converge to a satisfactory solution. In our case, we start from the generate power (maximum speed and maximum torque of the generator

shaft) to the dimensions. The analytical method is set by the finite element simulations.

The coiled rotor axial flux generator structure is illustrated by the figure 2:

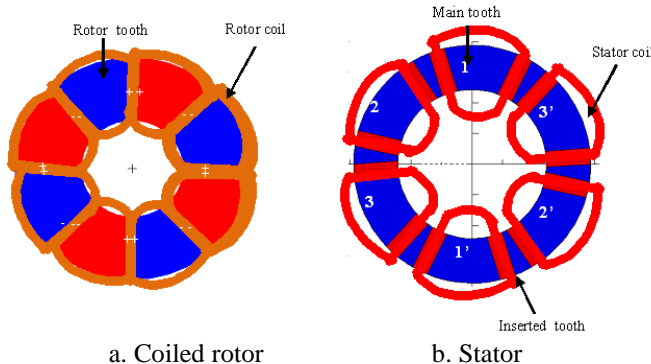


Fig. 2 The coiled rotor axial flux generator structure

IV. MONITORING STRATEGY

The energy generating system allows continuous and secure recovery of energy. Indeed, at low speeds the generator excitation current is increased to make the energy recoverable and for high speeds this current is reduced to limit the current and protect the chain against over-current. To a very high speed adjustable brake torque is applied on the propeller shaft to ensure the reduction of the speed of the generator shaft to limit the charging current of the batteries. This torque is generated by means of an electromagnet controlled by voltage pulses modulated in pulse width to adjust the braking torque to a value setting the speed of the generator relative to the maximum permissible current. The control signal of the electromagnet is find by comparing the reference battery load current fixed to 2600 A to the load current. The comparator output drives a proportional-integral regulator type. The output of the proportional-integral is compared with a triangular wave signal with high frequency. The comparator output drives a hysteresis reproducing the control signal of the electromagnet.

V. MODEL OF THE BATTERY

The energy accumulator comprises batteries in parallel with super-capacity to increase storage capacity. The Simulink model of the battery is shown in Figure 3 [1, 2].

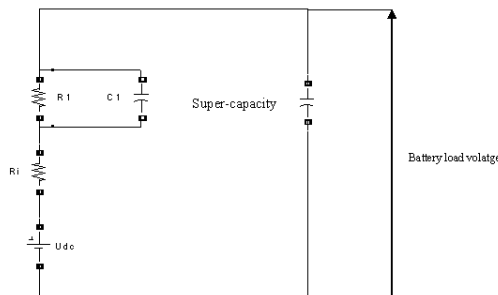


Fig. 3 Simulink model of the batteries

C_1 is a capacity to take into account the transitional arrangements.

R_i is the internal resistance

VI. EQUATIONS OF MOTION

The equation that governs the motion of the rotating parts of the energy generation chain is derived from the fundamental dynamics relationship:

$$J \times \frac{d\Omega}{dt} = T_m - r_d \times (T_{em} - \text{sgn}(T_{em}) \times T_{mec} - \text{sgn}(T_{em}) \times T_{fer}) \quad (1)$$

Where J is the moment of inertia of the rotating parts, r_d is the speed amplification ratio, T_m is the torque imposed on the motor shaft caused by the movement of wind, T_{em} is the electromagnetic torque, T_{mec} is the torque due to mechanical losses and T_{fer} is the torque due to iron losses [4-12].

$$T_m = \frac{1.918 \times R_p^2 \times V_{vent}^3}{\Omega} \quad (2)$$

$$T_{em} = \frac{1}{\Omega} \sum_{i=1}^3 e_i \times i_i \quad (3)$$

Where e_i and i_i are respectively the induced electromotive force and the current of the phase i .

Where 1.918 is a coefficient that depends on the kinetic energy of the wind and pale properties, R_p is the pale ray and V_{vent} is the wind speed.

The implementation of this equation in the environment MATLAB / Simulink is illustrated in Figure 4:

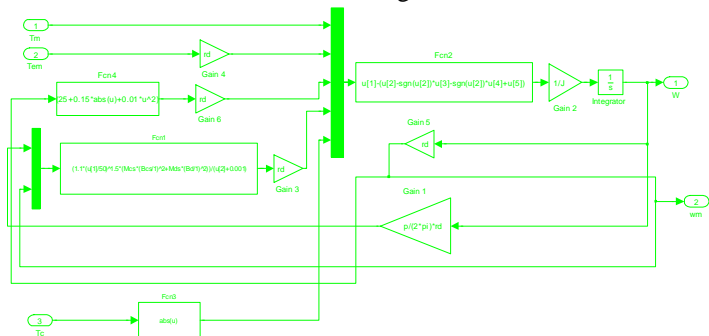


Fig. 4 Simulink model of the motion equation

VII. MODEL ELECTROMOTIVE FORCES

The three induced electromotive forces are estimated from the following three equations [4-12]:

$$e_1 = \frac{2}{3} \times K_e \times \Omega \times \cos\left(p \times \Omega \times t + \frac{\pi}{2}\right) \quad (4)$$

$$e_2 = \frac{2}{3} \times K_e \times \Omega \times \cos\left(p \times \Omega \times t - \frac{2 \times \pi}{3} + \frac{\pi}{2}\right) \quad (5)$$

$$e_3 = \frac{2}{3} \times K_e \times \Omega \times \cos\left(p \times \Omega \times t - \frac{4 \times \pi}{3} + \frac{\pi}{2}\right) \quad (6)$$

Where K_e is the electromotive constant and Ω is the angular velocity of the generator.

The Simulink model of the electromotive forces is illustrated by the figure 5:

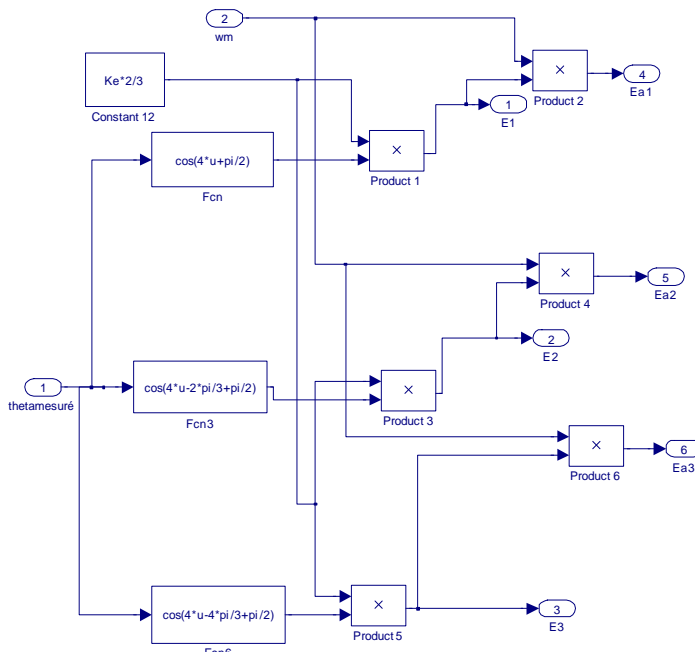


Fig. 5 Simulink Model of the electromotive forces

VIII. MODEL OF GENERATOR-RECTIFIER UNIT

The generator phase voltages are given by the following relationships [4-12]:

$$v_1 = R \times i_1 + (L - M) \times \frac{di_1}{dt} + e_1 \quad (7)$$

$$v_2 = R \times i_2 + (L - M) \times \frac{di_2}{dt} + e_2 \quad (8)$$

$$v_3 = R \times i_3 + (L - M) \times \frac{di_3}{dt} + e_3 \quad (9)$$

Where R , L and M are respectively the phase resistance, phase inductance and phase mutual inductance.

The three phase voltages are converted into a DC voltage through a PD3 rectifier. The rectified voltage is filtered by a capacitor. The output voltage of the rectifier attacks directly the batteries for recharging:

The Simulink model of the generator-rectifier assembly is shown in Figure 6 [1, 2].

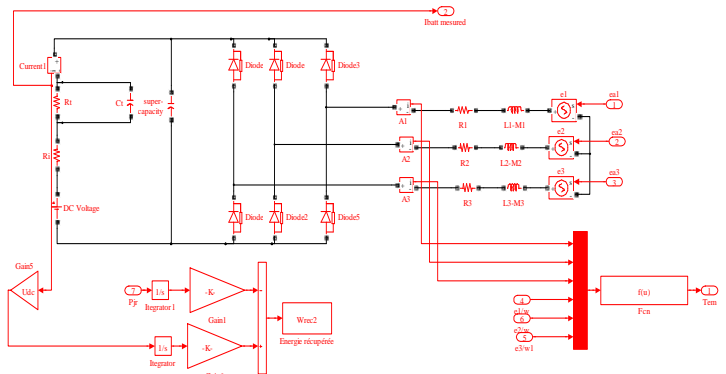


Fig. 6 Simulink model of the generator-rectifier

IX. EXCITATION SYSTEM

The optimization system of the excitation current (figure 7) makes it possible to increase the excitation current for low speed for continuous recovery of energy on the one hand and on the other hand reduces the excitation current for high speeds to avoid the burning problem of energy generation system.

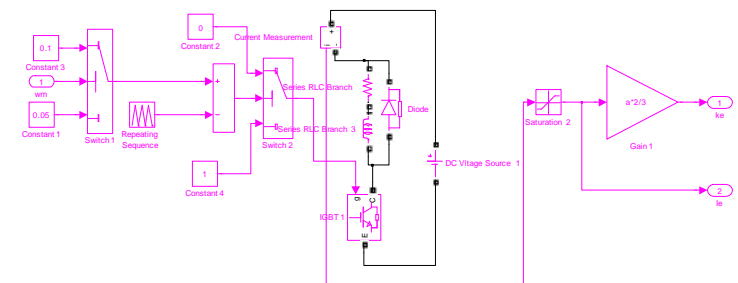


Fig. 7 Simulink model of the optimization system of the excitation current

X. BRAKING TORQUE REGULATOR

The batteries current regulator (Figure 8) limits the charging current of the battery to a value equal to 2600 A, to protect the energy generation chain against the burn. This value is held into account by the design approach of the power chain.

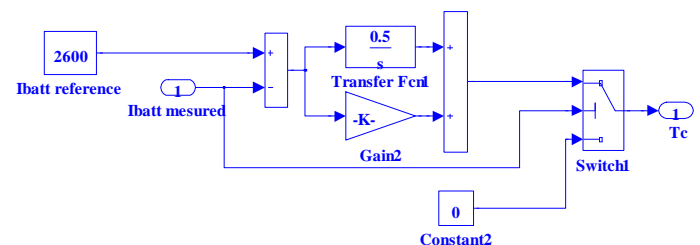


Fig. 8 Recharge current regulator

XI. GLOBAL MODEL OF THE POWER CHAIN

The global model of the energy generation system is based on the connection of the different Simulink models of the chain components make up this chain according to Figure 9 [1-3]:

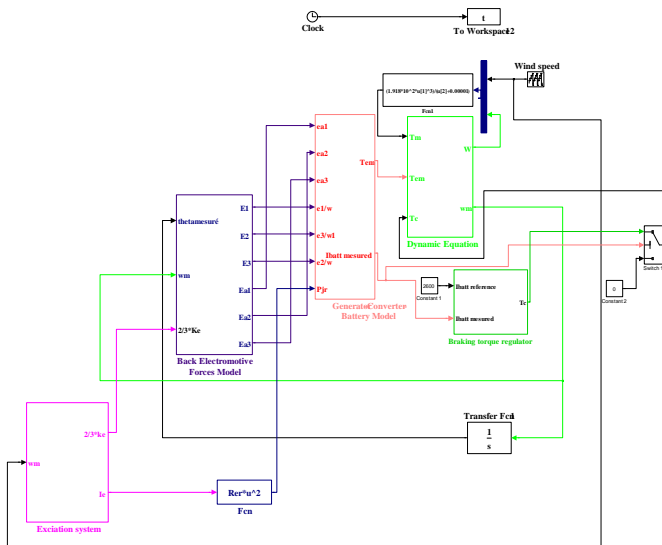


Fig. 9 Simulink model of the global energy generation chain

XII. DESCRIPTION OF SIMULATION RESULTS

Simulation parameters calculated from a generator sizing program are illustrated in Table 1 [12-20].

Tab. 1 Simulation parameters

Nomenclatures	Value	Unit
Phase resistance (R)	0.882	mΩ
Phase inductance (L)	2.247098	mH
Mutual inductance (M)	0.841539	mH
Moment of inertia of the rotating parts (J)	25081.455	Kg.m^2
Supper capacity (C)	15	Farads
internal resistance of the battery (R _i)	0.02	Ω
Resistance modeling the transitional arrangements for charging and discharging of batteries indentified by experimental test (R1)	0.001	Ω
Capacity modeling the transitional arrangements for charging and discharging of batteries indentified by experimental test (C1)	1	Farad
Gear ratio (r _d)	8	/
Batteries nominal voltage (Udc)	220	Volts
Inductor inductance (L _e)	41.880	mH
Inductor resistance (R _e)	0.295	Ω

Figure 10 shows the wind speed profile:

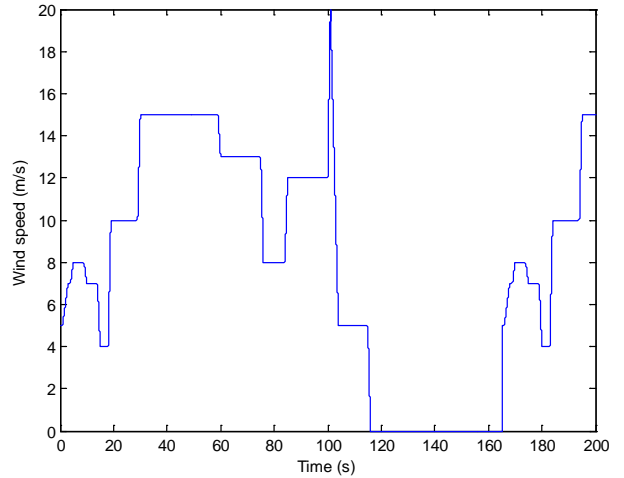


Fig. 10 Wind speed profile

The pace of this speed is chosen randomly and strongly with operating constraints such as speed limit, to test the performance of the control algorithm of the energy generation chain.

The angular speed of the generator is illustrated by the figure 11:

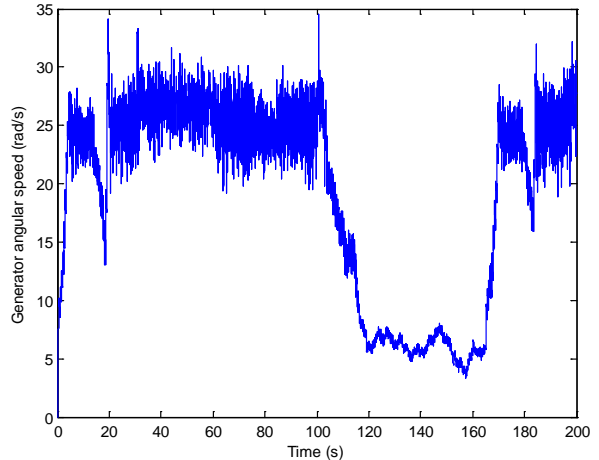


Fig. 11 Generator angular speed

Figure 11 shows that after training in movement of the generator shaft, the wind stopping does not immediately causes the stop of the generator shaft as a result of the inertia of the rotating parts.

Figure 12 shows the electromotive forces induced by the generator:

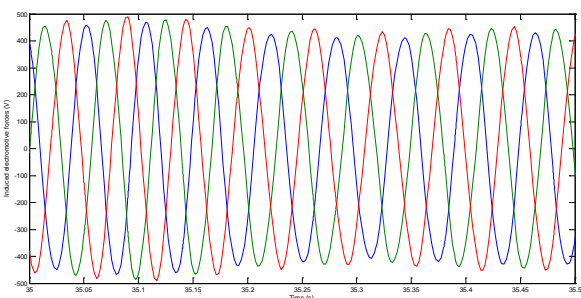


Fig.12 Induced electromotive forces

The amplitude of the electromotive forces is relatively high, which is explained by the insert made of a gear amplifier with amplifying ratio $r_d = 8$. This is to compensate the drop of phase voltages of the generator at battery charging phase.

Figure 13 illustrates the phase voltages of the generator:

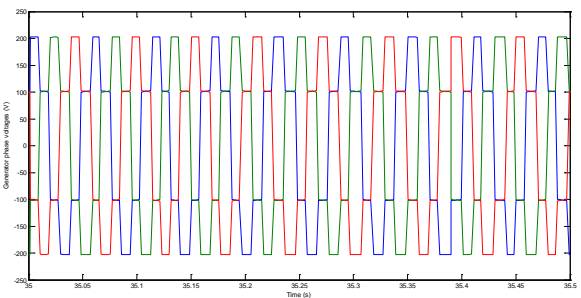


Fig. 13 Phase voltages of the generator

The amplitude of the phase voltages is reduced relative to the amplitude of the electromotive forces since the voltage drop across the phase resistance is important.

Figure 14 illustrates the phase currents begun by the generator:

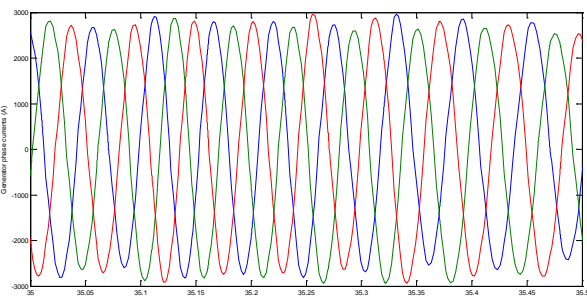


Fig. 14 Phase currents of the generator

The amplitude of the generator phase currents depends primarily on the internal resistance of the battery and of the rectified voltage.

The evolution of the braking torque is illustrated by the figure 15:

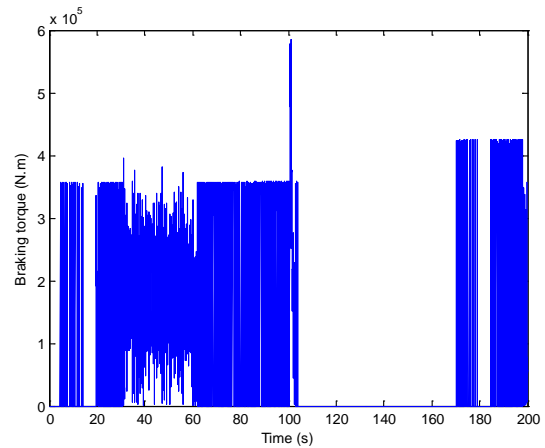


Fig. 15 Evolution of the braking torque

The figure 15 shows that the braking torque is high for high speed values, which is explained by the fact that the battery charging current exceeded the limit set at 2600 A.

The battery charging voltage is shown in Figure 16:

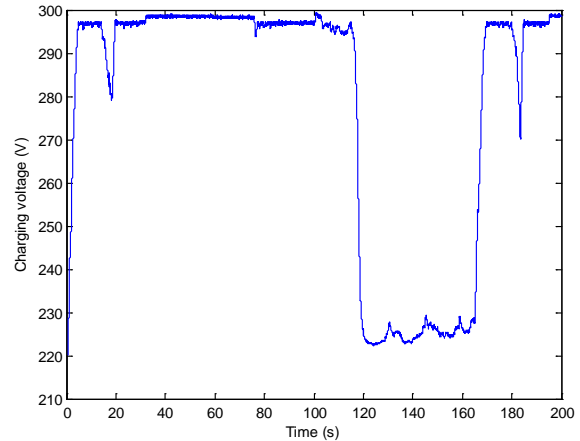


Fig. 16 Battery charging voltage

This voltage is maintained continuously since it is applied directly to a super-capacity. The amplitude of this voltage allows a continuous charging of the batteries as the nominal battery voltage is 220V significantly below to this voltage.

The current charging the batteries is shown in Figure 17:

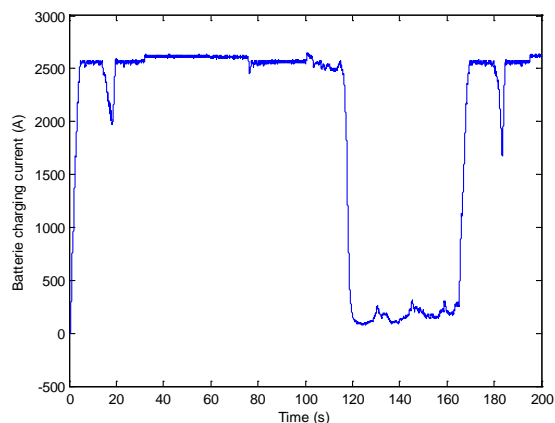


Fig.17 Battery charging current

The figure 17 shows that battery charging takes place at constant current maintained equal to 2600 A, which shows the effectiveness of the protection system of energy generation chain.

The iron and the mechanical losses of the generator are illustrated by the figure 18:

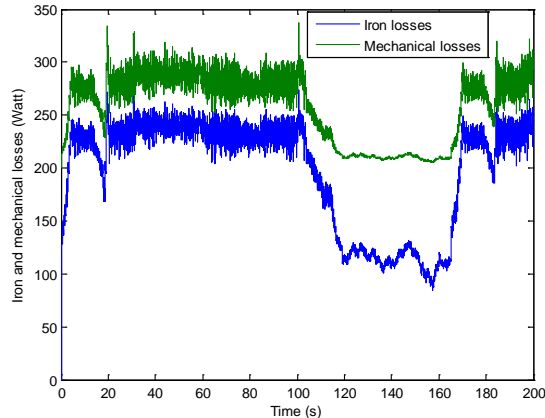


Fig.18 Evolution of the iron and the mechanical losses of the generator

Figure 18 shows that the mechanical and iron losses are proportional to the speed of the generator shaft.

The copper losses are illustrated by the figure 19:

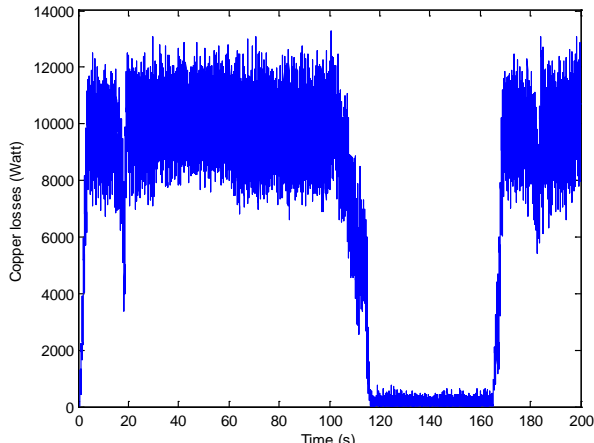


Fig.19 Evolution of copper losses of the generator

The copper losses are relatively high compared to iron and mechanical losses view that the current delivered by the generator is important.

The power generated by the wind and the power recovered by the batteries are illustrated by the figure 20:

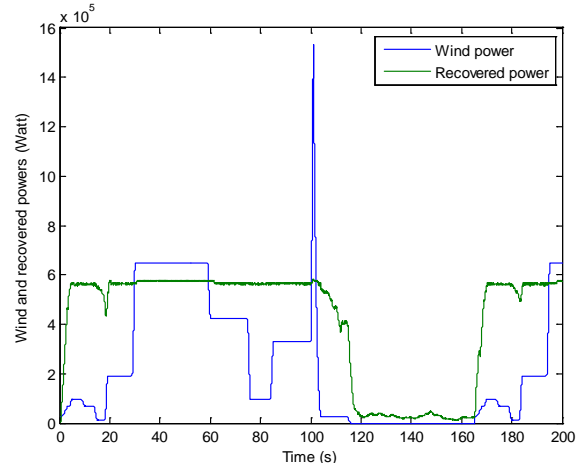


Fig.20 Wind and recovered power

The figure 20 show that the power transferred to the batteries is lower than that developed by the wind, which is explained by the different losses of energy generation chain.

The energy recovered by the batteries is shown in Figure 21:

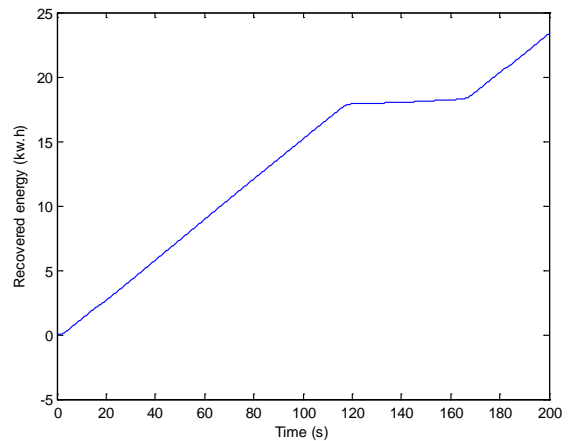


Fig. 21 The energy recovered by the batteries

This recovered energy is approximately equal to 23 kw.h, important value which validates the performance of the designed generation chain.

XIII. CONCLUSION

In this paper we have described a modeling approach of an automated renewable energy generation systems with coiled rotor synchronous generator, implanted under the Matlab Simulink simulation environment. This approach is parameterized consistent in consequence with optimization algorithms, for example, of the recovered energy. Simulation results are with good scientific level and validate the synchronous generator design approach dedicated to the generation of renewable energy. As future work, it is interesting to validate this modeling approach experimentally.

REFERENCES

- [1] Souhir Tounsi, Design and Optimization of Axial Flux Brushless DC Generator Dedicated to Generation of Renewable Energy, American Journal of Electrical Power and Energy Systems. Special Issue:Design and Monitoring of Renewable Energy Systems (DMRES). Vol. 4, No. 3-1, 2015, pp. 1-5. doi: 10.11648/j.epes.s.2015040301.11.
- [2] Wiem Nhidi, Souhir Tounsi, Mohamed Salim Bouhlel, Design and Modeling of a Synchronous Renewable Energy Generation System, American Journal of Electrical Power and Energy Systems. Special Issue:Design and Monitoring of Renewable Energy Systems (DMRES). Vol. 4, No. 3-1, 2015, pp. 6-11. doi: 10.11648/j.epes.s.2015040301.12.
- [3] Mariem Ben Amor, Souhir Tounsi, Mohamed Salim Bouhlel, Design and Optimization of Axial Flux Brushless DC Motor Dedicated to Electric Traction, American Journal of Electrical Power and Energy Systems. Special Issue:Design, Optimization and Control of Electric Vehicles: (DOCEV). Vol. 4, No. 2-1, 2015, pp. 42-48. doi: 10.11648/j.epes.s.2015040201.16.
- [4] Chaithongsuk, S., Nahid-Mobarakeh, B., Caron, J., Takorabet, N., & Meibody-Tabar, F. : Optimal design of permanent magnet motors to improve field-weakening performances in variable speed drives. Industrial Electronics, IEEE Transactions on, vol 59 no 6, p. 2484-2494, 2012.
- [5] Rahman, M. A., Osheiba, A. M., Kurihara, K., Jabbar, M. A., Ping, H. W., Wang, K., & Zubayer, H. M. : Advances on single-phase line-start high efficiency interior permanent magnet motors. Industrial Electronics, IEEE Transactions on, vol 59 no 3, p. 1333-1345, 2012.
- [6] C.C Hwang, J.J. Chang : Design and analysis of a high power density and high efficiency permanent magnet DC motor, Journal of Magnetism and Magnetic Materials, Volume 209, Number 1, February 2000, pp. 234-236(3)-Publisher: Elsevier.
- [7] MI. Chunting CHRIS : Analytical design of permanent-magnet traction-drive motors" Magnetics, IEEE Transactions on Volume 42, Issue 7, July 2006 Page(s):1861 - 1866 Digital Object Identifier 10.1109/TMAG.2006.874511.
- [8] S.TOUNSI, R.NÉJI, F.SELLAMI : Conception d'un actionneur à aimants permanents pour véhicules électriques, Revue Internationale de Génie Électrique volume 9/6 2006 - pp.693-718.
- [9] Sid Ali. RANDI : Conception systématique de chaînes de traction synchrones pour véhicule électrique à large gamme de vitesse. Thèse de Doctorat 2003, Institut National Polytechnique de Toulouse, UMRCNRS N° 5828.
- [10] C. PERTUZA : Contribution à la définition de moteurs à aimants permanents pour un véhicule électrique routier. Thèse de docteur de l'Institut National Polytechnique de Toulouse, Février 1996.
- [11] S. TOUNSI, R. NEJI and F. SELLAMI: Mathematical model of the electric vehicle autonomy. ICEM2006 (16th International Conference on Electrical Machines), 2-5 September 2006 Chania-Greece, CD: PTM4-1.
- [12] R. NEJI, S. TOUNSI, F. SELLAMI: Contribution to the definition of a permanent magnet motor with reduced production cost for the electrical vehicle propulsion. Journal European Transactions on Electrical Power (ETEP), Volume 16, issue 4, 2006, pp. 437-460.
- [13] Aicha Khlissa, Houcine Marouani, Souhir Tounsi, Systemic Design and Modelling of a Coiled Rotor Synchronous Motor Dedicated to Electric Traction, American Journal of Electrical Power and Energy Systems. Special Issue:Design, Optimization and Control of Electric Vehicles: (DOCEV). Vol. 4, No. 2-1, 2015, pp. 1-7. doi: 10.11648/j.epes.s.2015040201.11.
- [14] Houcine MAROUANI and Souhir TOUNSI : Design of a Coiled Rotor Synchronous Motor Dedicated to Electric Traction. Journal of Electrical Systems (JES), Volume 10, Issue 3, (September 2014), Indexed in SCOPUS.
- [15] Ajmia BEGACEM, Mohamed Amine FAKHFAKH and SouhirTOUNSI : « OPTIMAL DESIGN AND CONTROL OF ELECTRIC VEHICLE POWER CHAIN » Journal of Electrical Engineering (JEE), Edition 2, juin 2015, Indexed in SCOPUS.
- [16] S. TOUNSI "Losses of the electromagnetic modeling and IGBT converters," International Int. J. Electric and Hybrid Vehicles (IJEHV)-InderSciences publisher, Vol. 5, No. 1, 2013, pp: 54-68.
- [17] Amal Suilah, Nadia Graja, Amal Boudaya, Souhir Tounsi, Modelling of Synchronous Generation System for Renewable Energy, International Journal of Electrical Components and Energy Conversion. Vol. 1, No. 1, 2015, pp. 36-43. doi: 10.11648/j.ijecce.20150101.14.
- [18] Marwa Sellami, Souhir Tounsi. Control of Axial Flux DC Motor with Permanent Magnet Dedicated to Electric Traction. International Journal of Electrical Components and Energy Conversion. Vol. 1, No. 1, 2015, pp. 44-48. doi:10.11648/j.ijecce.20150101.15.
- [19] Moez Hadj Kacem, Souhir Tounsi, Rafik Neji. Losses Modeling of the Electric Vehicles Power Chain. International Journal of Electrical Components and Energy Conversion. Vol. 1, No. 2, 2015, pp. 49-54. doi: 10.11648/j.ijecce.20150102.11.
- [20] S. TOUNSI , N. Ben Hadj, R. and F. Sellami Neji: "Optimization of Electric Motor Design Parameters Maximizing the autonomy of electric vehicles", International Review of Electrical Engineering (IREE), ISSN 1827-6660, Volume 2 No. 1, January-February 2007, pp. 118-126, Indexed in SCOPUS.

Effects of Gamma Radiation on Some Hematological Parameters in Female Rats

Ali Abid Abojassim

Haider Salih Jaffat

Adhraa Baqir Hassan

Abstract— The effect of low exposure doses of gamma ray at doses of 0.055 Gy, 0.11 Gy and 0.165 Gy on the some hematological parameters of albino female rats were investigated. At the end of exposure periods and Blood samples were collected for analyses. The results obtained when increases of gamma ray doses of rats caused significant ($p \leq 0.05$) decrease in the RBCs, Hb and Ht%. Also it was found elevation in MCV and MCH with increased exposure dose as well as significant decreases ($p \leq 0.05$) Platelets in decreasing with increasing of doses rate and while MCHC% did not change significantly. But it was found when increases of gamma ray doses of rats caused significant ($p \leq 0.05$) decrease in WBCs count, lymphocytes count, monocytic, neutrophils, esinophiles and basophiles respective controls. These findings on the some hematological parameters suggest that the changes in blood parameters of the treated rats were due to the exposure of low doses of gamma ray.

Keywords— Cesium-137, Hematological parameters, gamma irradiation and female rats.

INTRODUCTION

IONIZING radiation affects people by depositing energy in body tissue, which can cause changes in the chemical balance of cell [1]. The energy associated with ionizing radiation is significantly greater than the bond energies of many molecules and can cause homolytic bond scission and the generation of secondary electrons. The time scale of the initial steps of energy deposition and molecular bond scission is on the order of 10-13 s [2]. The effect degree of the ionizing radiations depends on the type of radiation, energy of radiation, intensity of radiation and exposure time. The Radiation is thus seen to produce a biological effect by two mechanisms, directly by dissociating molecules following their excitation and ionization; and indirectly by the production of free radicals and hydrogen peroxide in the water of the body fluids [3]. The Gamma ray has no charge, and it has very high ionizing energy. Because of their high energy, gamma photons travel at the speed of light and can cover hundreds to thousands of meters in air before spending their energy. They can pass through many kinds of materials, including human tissue [4]. Physiological criteria such as the ability to degrade

different substrates, casine, and xanthine were used for genus determination. Streptomyces are obligate aerobes, chemoorganotrops that need only an organic carbon source (such as glucose, starch, and glycerol), an inorganic nitrogen source, and a few mineral salts for grow. However, faster growth can be obtained in complex media containing, for instance, yeast extract, or other organic nitrogen sources. Trace elements contained in tap water are generally sufficient, but addition of iron manganese, zinc and ions can be beneficial [5]. The destructive effects and mutations from radiation were originally thought to be due primarily to direct content of high-energy rays and particles with vital centers of microbial cells. Highly free radicals resulting from water hydrolysis are most important factors contributing to lethal and sublethal changes in microbial cells [6]. There are some scientists modernly study effects of irradiation on different parts of rats. Allehyanim et al.[7] studied the effects of gamma rays in the dose rate range 0- 5.6Gy on RBCs membrane solubilization, of rats erythrocytes using sodium dodecyl sulfate (SDS). Omar Mohamed et al. [8] studied the effects of gamma rays in the dose rate 8Gy on Whole Body of rats Induced Early Alterations in Biliary Secretion. Asrar M. Hawas[9] studied the effect of low dose (0.055 Gy) gamma-rays on certain essential metals namely Fe, Cu, Zn and Ca levels in various tissues (liver, kidney, testis, spleen, intestine, heart and brain) in rats. Also, lipid peroxidation as malondialdehyde (MDA) and metallothionein (MT) levels were measured in liver, kidney and testis. The aim of this study was estimated the effects of gamma rays in the low dose rate range 0-.012 Gy on Physiological Criteria in Female Rats
Procedure for Paper Submission

Materials and Methods

A. Experimental Animals and Irradiation

12 rats were divided into 4 groups with 3 rats (R1) First group as control group did not receive any radiation, (R2) was irradiated with 0.055Gy, (R3) was irradiated with 0.11Gy and (R4) was irradiated with 0.165Gy. Animals were housed under standardized conditions for light and temperature. A commercially prepared diet and clean drinking water were provided ad libitum. Irradiation was performed through the use of Cesium-137 source with 5 μ Ci from the International Atomic Energy Agency in a close system. The Cesium-137 radiation was taken in place was used so that three animals could be simultaneously irradiated.

Ali Abid Abojassim, University of Kufa, Faculty of Science, Department of Physics, Al-Najaf/ Kufa, box (221) Najaf , Iraq (Corresponding Author : +009647801103720, e-mail: ali.alhameedawi@uokufa.edu.iq).

Haider Salih Jaffat, University of Kufa, Faculty of Science, Department of Biology (e-mail: TUhaider_salah1968@yahoo.com).

Adhraa Baqir Hassan, University of Kufa, Faculty of Science, Department of Biology (e-mail: abh_mscph@yahoo.com).

B. Blood sample collection method

At the end of exposure periods, each group of animals was anaesthetized with ether, and then blood samples were collected by heart puncture on heparin containing tubes. One part of blood was taken for whole blood viscosity measurement.

C. Determination of Hematological Parameters

The red blood cells (RBC) and white blood cells (WBC) counts were determined by the improved Neubauer haemocytometer method. The haemoglobin (Hb) concentration was determined according to [10], using the cyanomethaemoglobin method. The packed cell volume (PCV) was determined by the micro-haematocrit method according to [11]. Schilling method of differential leucocyte count was used to determine the distribution of the various white blood cells [12]. Mean corpuscular volume (MCV), mean corpuscular haemoglobin (MCH) and mean corpuscular haemoglobin concentration (MCHC) were computed according to [12].

D. Statistical evaluation

Statistical analysis for evaluation of the results was done by calculating arithmetic mean and standard deviation for red blood cells and hemoglobin measurements. All these measurements had been done for all groups. Results were expressed as mean \pm standard deviation for each group. The results were evaluated by Student's unpaired t-tests.

Results and discussions

Figures (1-7) show the effect of gamma irradiation on the Hematological parameters in female rats. There are significant decreases ($P \leq 0.05$) in RBCs, Hb and Ht% in groups exposed to 0.055 Gy, 0.11 Gy and 0.165 Gy gamma irradiation when compared to the control (4.9, 13.7 and -40) for low respectively. MCV and MCH increased significantly ($P \leq 0.05$) with irradiation doses compared to the control group, while MCHC% did not change significantly in most treated groups. Platelets count decreased significantly ($P \leq 0.05$) in the group exposed to irradiation dose (0.165Gy).

The formation of superoxide partially accounts for the well-known oxygen enhancement of radiation induced biochemical changes and cell damage. After whole body gamma irradiation at a low dose level a significant decline in RBCs, Hb, Ht% and WBCs count was observed in rats [13].

Data presented in Figure (8) Showed that WBCs count was significantly decreased ($P \leq 0.05$) in rats treated with low (0.165Gy) of gamma irradiation. The higher dose (0.165Gy) caused a significantly higher reduction in the lymphocytes count, monocytic count and neutrophils exhibited the same significant ($P \leq 0.05$) level observed with the WBCs count (see Figures (9-11)). In regard to the esinophiles and basophiles, they all decreased significantly at both irradiation exposure levels with a significant dose effect (Figures (12 and 13)).

Gamma irradiation results in a decrease of the total count of WBCs, Lymphocytes, monocytes, neutrophils, basophils and esinophils [14]. The results are consistent with the previous findings that irradiation induced leucopenia [15] and reduces

lymphocytes, neutrophils and monocytes count [14, 16]. The decreases could be attributed to high radio sensitivity of haematopoietic tissue [17] and a reduction in the viability of spleen hematopoietic stem cells [18].

Conclusions

In conclusion, this study has shown that the low doses of gamma ray could have dangerous on the some Hematological Parameters for blood of female rats. Exposures to ionizing radiation in the permissible range(ICRP-60) still have hazardous effects on RBCs and WBCs, therefore It is necessary to review the dose limits recommended by the ICRP-60 for radiation workers based on the present findings.

Acknowledgments

A.A. would like to acknowledge all those who have contributed in this issue. Special thanks to the staff of the Department of Physics and Department of Biology at Kufa University.

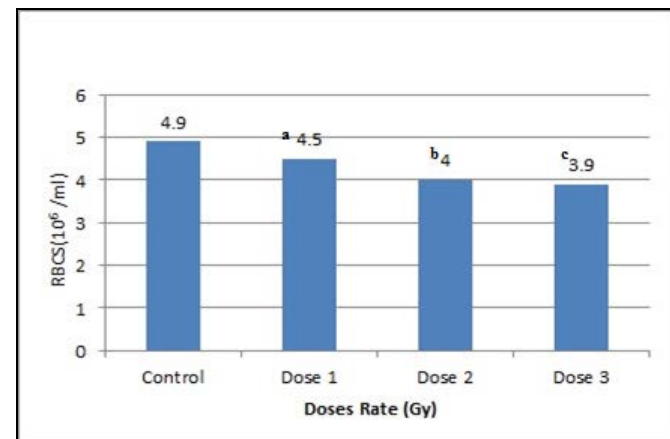


Figure (1): Effect of low doses of gamma ray on RBCS counts in female rats (a, d and c: means significant difference at $P \leq 0.05$)

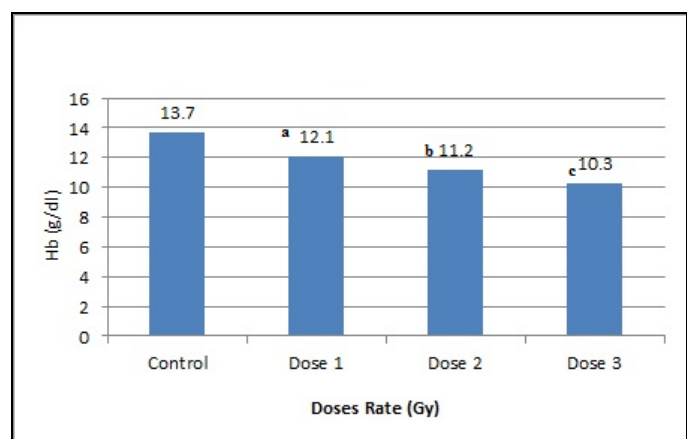


Figure (2): Effect of low doses of gamma ray on Hb(g/dl) counts in female rats . (a, b and c: means significant difference at $P \leq 0.05$)

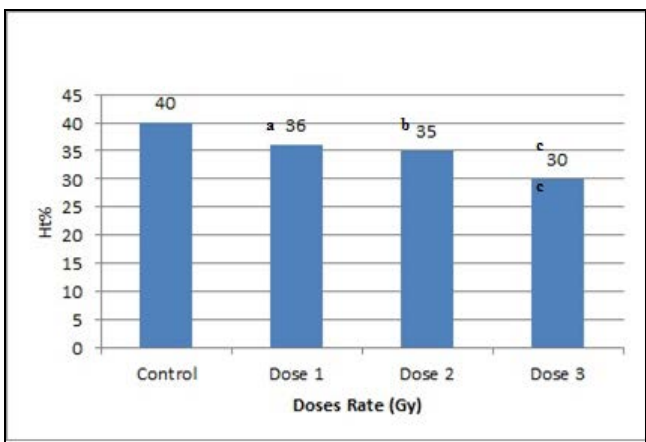


Figure (3): Effect of low doses of gamma ray on Ht% counts in female rats . (a, d and c: means significant difference at $P \leq 0.05$)

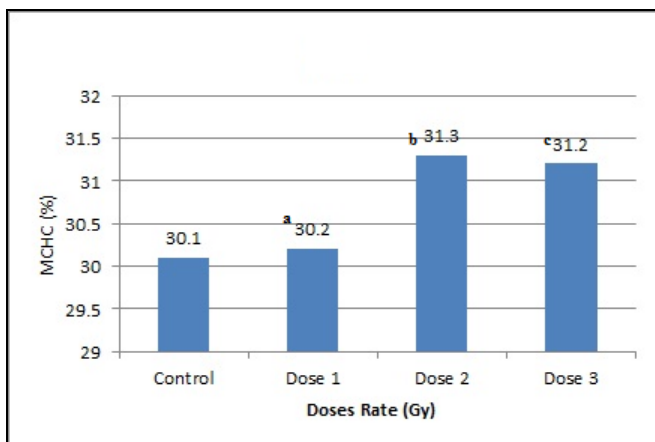


Figure (6): Effect of low doses of gamma ray on MCHC(%) counts in female rats. (a, b and c:means no change in significant)

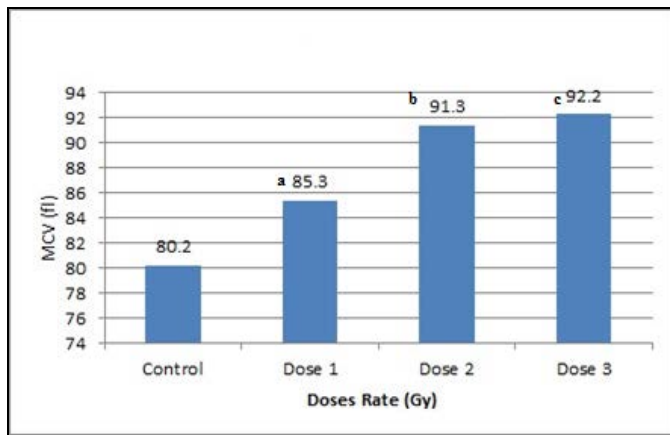


Figure (4): Effect of low doses of gamma ray on MCV(fl) counts in female rats . (a, b and c :means significant difference at $P \leq 0.05$)

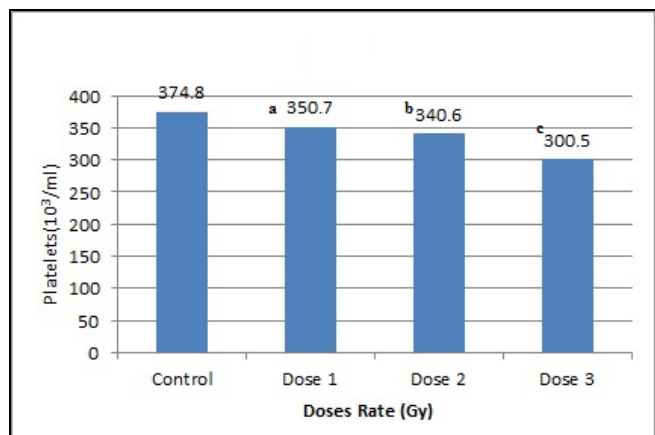


Figure (7): Effect of low doses of gamma ray on Platelets counts in female rats . (a, b and c: means significant difference at $P \leq 0.05$)

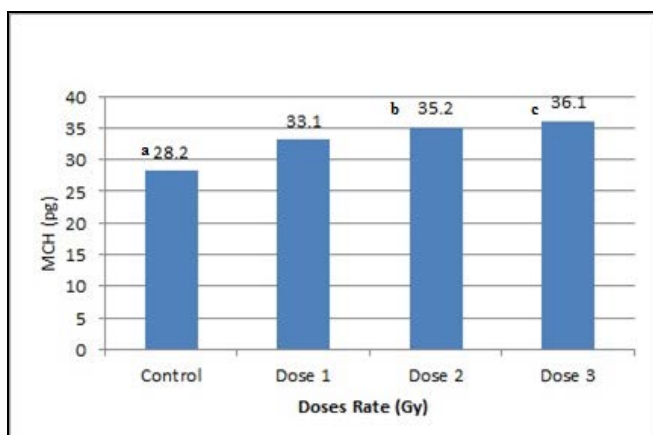


Figure (5): Effect of low doses of gamma ray on MCH(Pgl) counts in female rats . (a, b and c:means significant difference at $P \leq 0.05$)

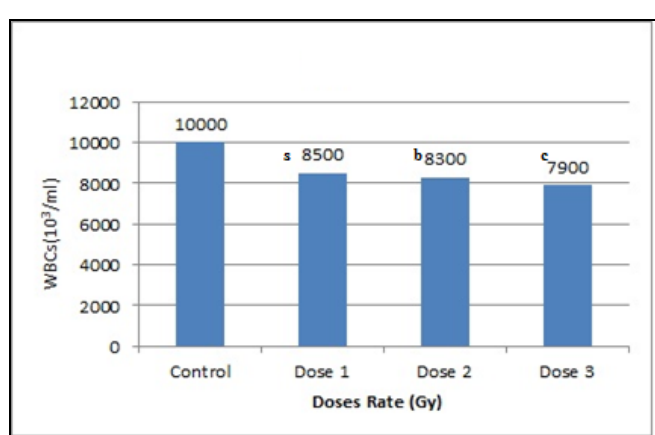


Figure (8): Effect of low doses of gamma ray on WBCs counts in female rats . (a, b and c:means significant difference at $P < 0.05$)

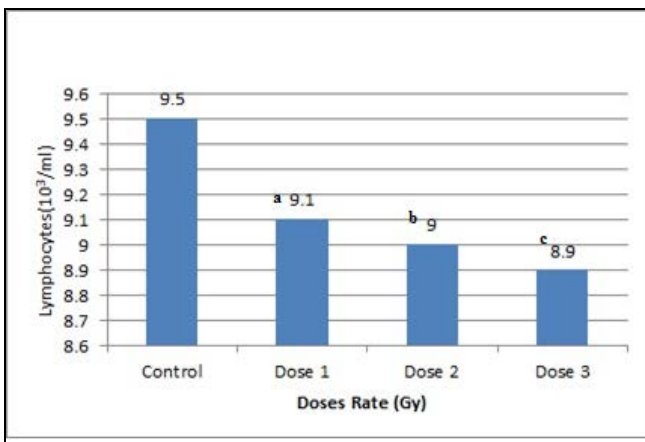


Figure (9): Effect of low doses of gamma ray on Lymphocytes counts in female rats. (a, b and c: means significant difference at $P \leq 0.05$)

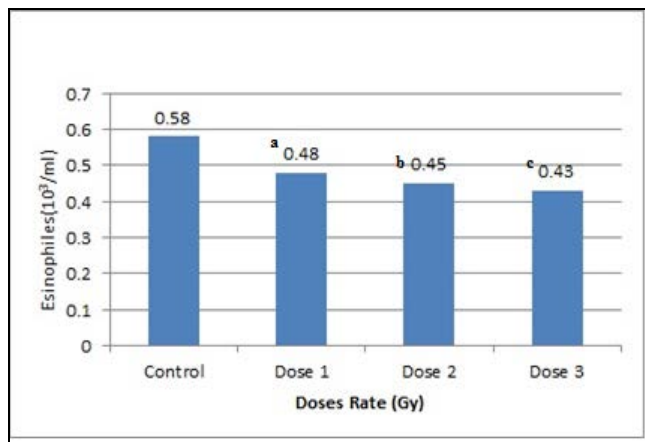


Figure (12): Effect of low doses of gamma ray on Eosinophiles counts in female rats. (a, b and c: means significant difference at $P \leq 0.05$)

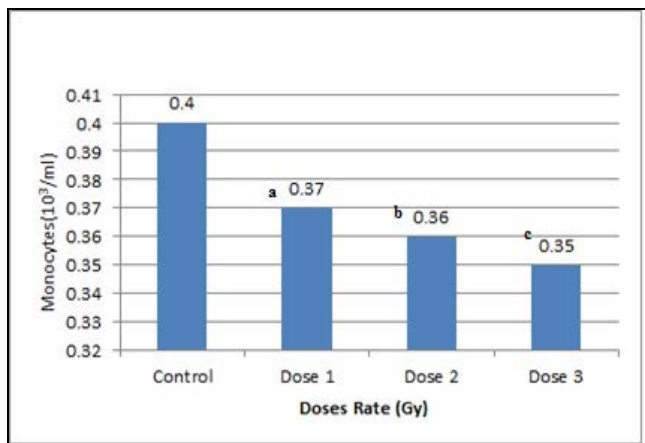


Figure (10): Effect of low doses of gamma ray on Monocytic counts in female rats . (a, b and c: means significant difference at $P \leq 0.05$)

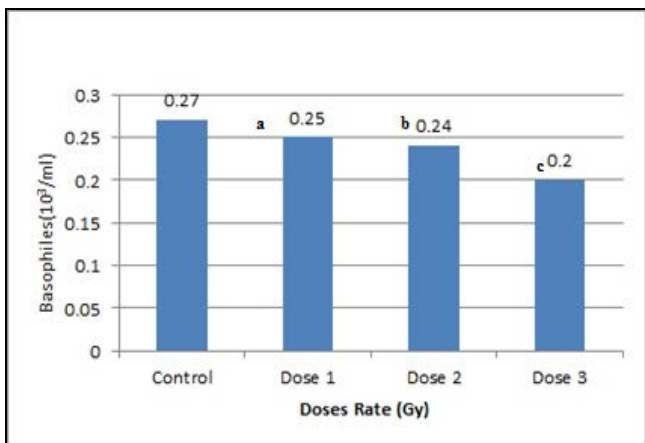


Figure (13): Effect of low doses of gamma ray on Basophiles counts in female rats. (a, b and c: means significant difference at $P \leq 0.05$)

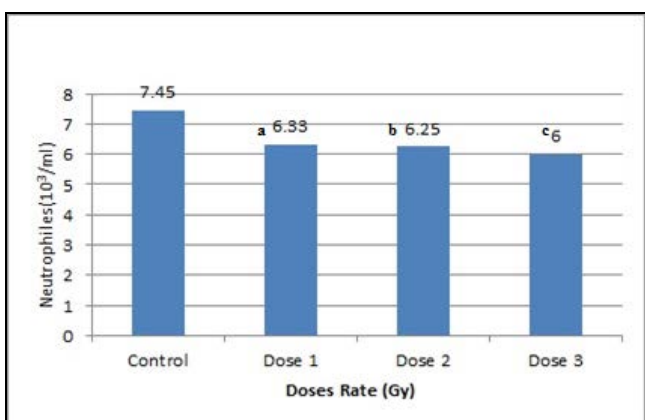


Figure (11): Effect of low doses of gamma ray on Neutrophils counts in female rats. (a, b and c: means significant difference at $P \leq 0.05$)

References

- [1] U.S. Environmental Protection Agency, (2005), "Radiation Information: Fact Sheets Series on Ionizing Radiation", No. 2.
- [2] Soule, B. P., Hyodo, F., Matsumoto, K. I., Simone, N. L., Cook, J. A., Krishna, M. C., et al. (2007). The chemistry and biology of nitroxide compounds. *Free Radical Biology and Medicine*, 42(11), 1632.
- [3] Camber H., (1987), "Introduction to Health Physics", 2nd edition. Pergamon Press. New York.
- [4] U.S. Environmental Protection Agency, (2005), "Understanding Radiation: Health Physics".
- [5] Gottlieb, D. and E.B. Shirling, (1967). Cooperative description of type cultures of streptomyces. I. The International of Streptomyces Project. *Int. Syst. Bacteriol.*, 17: 315–76 .
- [6] Ingram, M. and T.A.C. Roberts, (1980). Ionizing irradiation. In: *Microbial Ecology of Foods*, Vol. 1, pp. 46–69. ICMSF, Academic Press, New York.
- [7] Allehyanim S.H. and sultan Monem. (2003), " Membrane solubilization and hemoglobin gelation as biomarker of radiation exposure to gamma-rays Egyptian biophysics journal, vol.9,p.234-244.
- [8] Omar Mohamed, Ihsan Hadajat, Ayman Ragab, Siham EL-Shinawy, (2006), "Exposure of Rats to Whole Body Gamma Rays Induces Early Alterations in Biliary Secretion", *Turk J Med Sci* ; 36 (5): 263-269

- [9] Asrar M. Hawas, (2013), " Effect of low dose gamma rays on certain essential metals and oxidative stress in different rat organs", journal of radiation research and applied sciences 6, p.38-44.
- [10] Jain NC. Schalm's Veterinary Haematology (1986),4th ed. Lea and Fabiger, Philadelphia.
- [11] Dacie JV, Lewis SM. Practical haematology, 7th edition (1991), ELBS with Churchill Livingston, England, pp 37-85.
- [12] Mitruka BM, Rawnsley H. Clinical, (1977) biochemical and haematological references values in normal experimental animals. Masson Publishing USA Inc., P. 53-54.
- [13] Abou-Seif, M.A., M.M. El-Naggar, M. El-Far, M. Ramadan and N. Saleh, (2003). Prevention of biochemical changes in gamma-irradiated rats by some metal complexes. *Clin. Chem. Lab. Med.*, 41(7): 926-933.
- [14] Ezz, M.K., (2011). The ameliorative effect of *Echinacea purpurea* against gamma radiation induced oxidative stress and immune responses in male rats. *Aust. J. Basic & Appl. Sci.*, 5(10): 506-512..
- [15] Mishima, S., K. Saito, H. Maruyama, M. Inoue, T. Yamashita and Y. Gu, (2004). Antioxidant and immuno-enhancing effects of *Echinacea purpurea*. *Biol. Pharm. Bull.*, 27: 1004-1009.
- [16] Hari, K., M. Sabu, P. Lima and R. Kuttan, (2004), Modulation of haematopoietic system and antioxidant enzymes by *Emblica officinalis* gaertn and its protective role against gamma-radiation induced damages in mice *J. Radiat. Res.*, 45: 549-555.
- [17] Chew, B. and J. Park, (2004). Carotenoid action on the immune response. *J. Nutr.*, 134(1): 257S-261S.
- [18] Miura, N., M. Satoh, N. Imura and A. Naganuma, (1998). Protective effect of bismuth nitrate against injury to the bone marrow by gamma-irradiation in mice: Possible involvement of induction of metallothionein synthesis. *The Journal of Pharmacology and Experimental Therapeutics*, 286: 1427-1430.

Risk of Acid Attack on Plants: A Review

S. Behera, B. Mallick, T. N. Tiwari, and P. C. Mishra

Abstract— Acid rain in reality has been well documented for many places, viz. the eastern USA, Canada, Bermuda, etc. Plants are drastically affected by acid rain (AR)-caused acid deposition. One of the main effects of acid rainfall on plants is the leaching of nutrients and cations from leaves. The literature review of acid rain-induced effects on various plants is described in the present paper, which gives the detailed description of different AR-induced effects observed in herbs, crop and vegetable plants, trees and forest, etc.

Keywords— Acid rain, Herbs, Plant materials, Trees.

I. INTRODUCTION

ACID rain (AR) [1] was discovered in the year 1852 by Robert Angus Smith (Father of acid rain), a pharmacist from Manchester (England), who measured high levels of acidity in rain falling over industrial regions of England and contrasted them to the much lower levels he observed in less polluted areas near the coast [2]. Little attention was paid to his work until the 1950s, when biologists noticed an alarming decline of fish populations in the lakes of southern Norway and traced the problem to AR. Later, these findings spurred intense research to understand the origin of the AR phenomenon.

AR is caused by emissions of SO_2 and NO , which react with the water molecules in the atmosphere to produce acids. These pollutants (SO_2 , NO_x), once released into the atmosphere, can be converted chemically (under the influence of sunlight and moisture) into secondary pollutants such as sulphuric acid (H_2SO_4) and nitric acid (HNO_3). Both H_2SO_4 and HNO_3 can dissolve easily in clouds and water. Ambient concentrations of the primary pollutants, SO_2 and NO_x , and the secondary pollutants, ozone (O_3) and acidic wet deposition have been reported. The effects of the above gaseous pollutants (O_3 , SO_2 , NO_x) and AR have been assessed and compared for a wide variety of crop cultivars and species. Such a comparison is

S. Behera is with the Department of Environmental Science, Sambalpur University, Jyoti Vihar Burla 768019, Odisha, India (e-mail: shradhanjali_botany@rediffmail.com).

B. Mallick, is with the Institute of Physics, Bhubaneswar 751005, India (corresponding author; phone: +91-674-2306466; fax: +91-674-2300142; e-mail: bmallickr@iopb.res.in)

T. N. Tiwari is with the Unique Research Centre, Rourkela 769014, India (e-mail: urctntrkl@gmail.com).

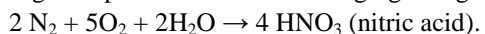
P. C. Mishra is with the National Green Tribunal, Eastern Zone Bench, Finance Centre, 3rd Floor, New Town, Kolkata-700156, India (e-mail: pcm_envsu@rediffmail.com)

useful for evaluating the need and the strategy for controlling pollutant emissions.

The normal rainwater is acidic in nature; the reason is that water reacts to a slight extent with the atmospheric carbon dioxide (CO_2) to produce carbonic acid. Carbonic acid forms naturally in the atmosphere due to the reaction of water (H_2O) and carbon dioxide (CO_2):



Small amount of nitric acid is also responsible for the acidity of normal rainwater, which is produced by the oxidation of nitrogen in presence of water during lightning storms.



Rain water that presents a concentration of H^+ ion greater than $2.5 \mu\text{eq}^{-1}$ and pH value less than 5.6 is considered to be acidic [3]. The degree of acidity is measured by pH value, which is shorthand version of potential hydrogen. Actually, the degree of acidification is the pH of the water, which is defined as the negative logarithm of the concentration of hydrogen ion (H^+), or $\text{pH} = -\log [\text{H}^+]$.

II. EFFECT ON HERB

To the best of my knowledge is concerned, there are only a few reports available on the effect of medicinal herbs due to acid rain. Punam Kumari and Tomar [4] studied the effects of simulated acid rain (SiAR) of pH 2.5, 3.5, 4.5 and 5.5 on chlorophyll and ascorbic acid contents of two cultivars (cv. Himalaya and cv. Kaushik) of a medicinal herb *Mentha piperita*. In the above study, they found that chlorophyll and ascorbic acid contents of the leaves were adversely affected (at pH 2.5 and 3.5), and chlorophyll-a showed more reduction than chlorophyll-b. In both the cultivars, cv. Himalaya was more sensitive than cv. Kaushik on chlorophyll and ascorbic acid contents.

Various aluminium-based new phases formed due to the substitution of sulphur via SiAR in Brahmi (*Bacopa Monnieri* L.), which have been analyzed using X-Ray diffraction technique have been reported in Behera et al [5]. In this study, an attempt has been made to analyze the various aluminium phase (salt) formations due to the substitution of sulphur via SiAR in *B. Monnieri* because of their toxicological importance. The new phases like $\text{AlH}(\text{SO}_4)_2$ and Al_2S_3 along with usual Al_2O_3 ; H_2O , MgO , $\text{FeAl}_2(\text{PO}_4)_2(\text{OH})_2$; $8\text{H}_2\text{O}$, and $(\text{K}_2\text{Ca}(\text{SO}_4)_2$; H_2O , have been observed in *B. Monnieri* when treated with sulphur-simulated acid rain (S-SiAR) of two different pH (3.39 and 5.45) for 20 weeks.

The effects of simulated acid rain (pH 3 and 4) and control (rain with pH 5.7) on physiological and biochemical processes in *Lolium perenne* have been studied by Vicas et al. [6]. In

that work, S-SiAR and normal rain had been applied by spraying daily for 10 days from the beginning of the experiment. In that analysis, they have concluded that, under stress of SiAR (pH 3 and 4), the germination and the growth decreased with the decline in of pH values of the acid rain.

Wang *et al.* [7] studied the major invasive weed *Wedelia trilobata* in southern China to examine the possible effects of acid rain on the allelopathic potential of invasive plant species. In that report, they have investigated the phytotoxicities of aqueous leachates and dried leaf litter of field-grown *W. trilobata* plants exposed to SiAR (pH 2.5, 4.0, 5.6, 7.0 water control) in *in-vitro* assays on two receptor species: *Brassica campestris* and *Raphanus sativus*. Again, substantial increase in the phytotoxicity of the leachates as well as leaf litter have been observed as a function of decreasing SiAR pH. Additionally, glasshouse experiments have been carried out to determine the effects of various SiAR treatments on *W. trilobata* biomass accumulation and shoot height; both parameters showed modest increases at SiAR pH 4.0 and decreases at SiAR pH 2.5 than control (pH 7.0) plants. Authors claimed that the acidic conditions increased the allelopathic potential of *W. trilobata*, suggesting that acid rain exposure may increase the invasiveness of this weed.

III. EFFECT ON CROP AND VEGETABLE PLANTS

Crop and vegetable plants have shown a wide range of sensitivity to the acidity of rain water. As reported by Ferenbaugh [8], the effects of SiAR (pH < 3) on *Phaseolus vulgaris* L. plants exhibited a failure to attain normal height, had necrotic and wrinkled leaves, excessive and adventitious budding, and premature abscission of primary leaves. Again, apparent rates of photosynthesis, however, increased dramatically. Both carbohydrate production and root biomass were reduced by low pH treatments, and application of Congo red indicator to the acid-treated leaf tissue showed that the cell contents were acidified to a pH of below 4.0.

In an investigation by Lee *et al.* [9], it has been reported that *Arabidopsis* leaves treated with SiAR showed phenotypes similar to necrotic lesions caused by biotic stresses like pseudomonad infiltration. Again, exposure of *Arabidopsis* to SiAR resulted in the up-regulation of genes. In their report, they suggested that SiAR activates at least the salicylic acid pathway, and activation of this pathway is sensitive to sulfuric acid. Verma *et al.* [10] studied the impact of SiAR with pH-levels of 5.0, 4.0 and 3.0 on three most popular vegetable plants species, viz. *Capsicum annuum*, *Lycopersicon esculentum* and *Solanum melongea* of the family *Solanaceae*. From the above study, they have reported that the growth parameters and fruiting were severely curtailed with increasing acidity in all the three species.

A good review work on the effect of AR and its ecological consequences has already been published [11]. In that report, effects of AR on various vegetable plants including various physiological parameters (photosynthetic rate, stomatal conductance, etc.) and morphological characteristics of plants were found to be negatively affected by AR. Norby and Luxmoore [12] found reduction in CO₂ fixation in soybeans

when treated with acid rain of pH 2.6. This decrease was ascribed to the reduction in leaf area. In another report by Singh and Agrawal [13], morphological characteristics of two varieties of wheat (Sonalika and M 213) have been reported and found to be negatively affected by acid rain treatments. In the report by Smol and Glew [14], it has been found that species of diatoms and golden brown algae are also sensitive to the change in water chemistry, and hence can be used as indicator of acidity of water. Findlay and Kasian [15] observed that with acidification of lakes, golden brown algal species are replaced by other chlorophycean like *Chlorella mucosae*.

In an investigation by Liao *et al.* [16], complex toxic effects of Cd²⁺, Zn²⁺, and AR on the growth of kidney bean (*Phaseolus vulgaris* L) have been studied. In this report, the effect on weights of the plants, superoxide dismutase (SOD), peroxidase (POD), and lipid peroxidation such as malonydialdehyde (MDA) in the plant organs, and the injury symptoms have been studied. Again, they demonstrated that all treatments of Cd²⁺, Zn²⁺, and/or AR significantly decreased fresh weights of kidney beans and caused toxic effects on the growth of the plants, especially higher amounts of Cd²⁺ and Zn²⁺ and higher acidity of AR. Combination of these three pollutant factors resulted in more serious toxic effects than any single pollutant and their combinations of any two pollutants.

Again, the effect of SiAR (pH 1.8) on H₂O₂ and malonydialdehyde (MDA) levels and activities of peroxidase and catalase in bean plants have been investigated by Velikova *et al.* [17]. The influences of exogenous polyamines spermidine and spermine on these parameters have been studied. In the report, it has been observed that the protective effect of spermine was higher than that of spermidine. Again, the impact of polyamines could be attributed to their acid-neutralizing and antioxidant effects, as well as to their ability to stabilize membranes by associating with negatively charged phospholipids. It has been also found that AR significantly increased peroxidase and decreased catalase activities at the first hours after treatment.

The Effects of soil acidity on the uptake of trace elements (Co, Zn, Se, Rb, Sr, Y, Zr, Tc, Ru, Rh and Re) in soybean and tomato plants have been studied by Wang *et al.* [18] applying a multi-tracer technique. They found that the uptake of cationic elements in the leaves and stems of soybean plants cultivated on acid soil (pH= 4.2) became higher than those of plants cultivated on normal soil (pH=6.4) during the late period of growth. However, they found that the effect on the element Se was quite different from that on the cationic elements. The uptake of Se by the plants cultivated on normal soil was higher than that of the plants cultivated on acid soil.

Again, the effects of SiAR (pH 1.8) on the ultrastructure of chloroplasts and mitochondria as well as antioxidant defense system were investigated in tomato (*Lycopersicon esculentum* Mill) by Gabara *et al.* [19]. The tomato leaves were sprayed with AR of pH 1.8. The analyses carried out at 0.5, 3.0, 24, 48, 72 and 96 h after a single spraying of AR indicated alterations in 13% of chloroplasts and 95% of mitochondria.

Irving [20] in his report studied the effects of gaseous pollutants (O₃, SO₂, NO₂) and acidic rain on a wide variety of crop cultivars and species. In his investigation, he found that

exposures of SO₂ and combinations of SO₂ and NO₂ may reach concentrations and frequencies that could reduce crop productivity, but effects from these pollutions are not significant on a national scale. Also, the author claimed that O₃ at ambient levels during the growing season tends to reduce the yield by an average of 5-10% for the majority of crops tested.

As reported by Wyrwicka and Sklodowska [21], the effect of repeated treatment with SiAR on antioxidative enzyme activities, lipid peroxidation and chlorophyll concentration in cucumber plants (*Cucumis sativus* L.) was investigated. Measurements were carried out for short period (one, five and seven days) after triple spraying. They found that ascorbate peroxidase (APx) and glutathione transferase (GST) activities increased considerably after the exposure to AR stress, indicating a direct correlation with pH of the used solution. Again, both enzyme activities were enhanced till the end of the experiment, which could contribute to the scavenging of reactive oxygen species (ROS) and detoxification of potentially toxic products originating from AR stress. Contrary to APx and GST activities, increases in catalase (CAT) and glutathione peroxidase (GSH-Px) activities were observed shortly after AR stress only. Changes in chlorophyll concentration were strongly dependent on pH of the applied AR. It was also found that lipid peroxidation (POD), measured as 2-thiobarbituric acid reactive substances (TBARS) concentrations, was increasing in cucumber plants to the fifth day after AR treatment. Leaf bleaching and increased TBARS concentration suggested premature senescence of the AR-treated plants. Also, in the same report, they have quoted that antioxidant enzymatic response to AR stress was quite sufficient in leaf tissue exposed to AR pH 4.4, but was not effective at pH below 3.0.

Munzuroglu *et al.* [22] studied the effect of acid rain implementation including pH 2-5 on the vitamins (A, E and C) of matured strawberry fruit using High Performance Liquid Chromatography (HPLC). It has been found that vitamin levels of plants sprayed with SiARs decreased with respect to pH and time when compared with control. Again, sprayed roots were more affected in respect of vitamin levels than untreated plants.

IV. EFFECT ON TREE AND FOREST

The effect of AR on higher plants viz. pine [23-31], Beech and Holm Oak [32], apple tree [33], litchi [34], and even forest [35-40] is highly adverse due to acid deposition. Leaf is the most sensitive organ to AR-caused pollutant damage, and has been the target of many studies. Usually, the effect of acid depositions on higher plants arises in two ways-either through foliage or through roots. The symptoms include direct damage to the plant tissue (especially roots and foliage), reduced canopy cover, crown dieback and whole tree death [41]. The germination rate of Norway spruce, Scots Pine and silver birch seeds was found to be moderately inhibited at pH 3.8 and 5.4 [42].

Shan [23] studied the effects of SiAR on the chlorophyll contents of leaves of *Pinus densiflora*, on the net

photosynthetic rate on a unit chlorophyll basis, and on chlorophyll degradation. When NO₃⁻ concentrations in rain water increased, the chlorophyll a+b contents of the leaves increased in parallel, even though the pH of the simulated rain decreased. The nitrogen content of the rain was sufficient to stimulate the production of chlorophyll and was able to override any degradative effect expected due to the H⁺ input from AR. The AR does, therefore, simultaneously increase chlorophyll content and reduce the efficiency of the use of chlorophyll in photosynthesis. This reduced efficiency may be linked to the increase in the rate of degradation of chlorophyll to pheophytin.

However, in the study of Shumejko *et al.* [24] the effects of prolonged SiAR on the biochemistry of Scots pine needles were reported in Finnish Lapland. In this report, pine trees were exposed by spraying the foliage and soil with either clean water or SiAR (both sulphuric and nitric acids) over the period 1985-1991. The concentrations of carbohydrates (starch, glucose, fructose, and sucrose) in one-year-old pine needles were not affected by SAR-treatments. The SAR-treatments did not have significant effects on protein-bound amino acids, which was true also for most of the free amino acids. However, the citrulline concentration was over three-fold greater in the foliage of pines exposed to SAR of pH 3 compared to irrigated controls. The concentrations of total phenolics, individual low-molecular-weight phenolics and soluble proanthocyanidins were not affected by the treatments, but insoluble proanthocyanidins had increased in acid-treated trees. Some of the studied biochemical compounds showed significant differences between two sub-areas (similar treatments) only 120 m apart.

As reported by Shan *et al.* [25], the seedlings of *Pinus armandi* Franch were exposed to ozone (O₃) at 300 ppb for 8 h a day, 6 days a week, and SiAR of pH 3.0 or 2.3, 6 times a week, alone or in combination, for 14 weeks. The control seedlings were exposed to charcoal-filtered air and simulated rain of pH 6.8 during the same period. Significant interactive effects of O₃ and SiAR on whole-plant net photosynthetic rate were observed, but not on other determined parameters. The exposure of the seedlings to O₃ caused the reductions in the dry-weight growth and root dry weight relative to the whole-plant dry weight, net photosynthetic rate, transpiration rate in light, water-use efficiency and root respiration activity, and increases in shoot/root ratio, and leaf dry weight relative to the whole plant dry weight without an appearance of acute visible foliar injury, but did not affect the dark respiration rate and transpiration rate in the darkness. The decreased net photosynthetic rate was considered to be the major cause for the growth reduction of the seedlings exposed to O₃. On the other hand, the exposure of the seedlings to SiAR reduced the net photosynthetic rate per unit chlorophyll a + b content, but did not induce the significant change in other determined parameters.

Helander *et al.* [26] studied the variation in assemblages of endophytic fungi in Scots pine (*Pinus sylvestris*) needles in a subarctic area, where background pollution values are low: The effects of tree density and prolonged SiAR on the occurrence of endophytic fungi were investigated. The needle

endophyte most frequently isolated was *Cenangium ferruginosum*, accounting for 64% of all fungal individuals, followed by *Cyclaneusma minus* (12% of all individuals). Old needles were colonized more frequently by endophytes than young ones. In young needles, the colonization by endophytes increased during the summer, whereas in old ones no seasonal variation was detected. Endophyte colonization was positively correlated with stand density and was reduced on pines treated with spring water acidified with either sulphuric acid alone or in combination with nitric acid. In contrast, nitric acid alone did not affect endophyte colonization.

In another report by Reich *et al.* [27], experiments were conducted to assess the response of potted white pine (*Pinus strobus L.*) seedlings to combined AR, ozone, and soil treatments. In that study, seedlings had been grown in five forest soils and exposed for 4 months to realistic levels of AR and ozone. Acid rain treatments consisted of exposure to simulated rain of pH 5.6, 4.0, 3.5, or 3.0, while ozone treatments consisted of exposure to 0.02 and 0.06, ppm ozone. Minimal interaction between AR and ozone 0.10, or 0.14 was observed with regard to photosynthesis or growth. Acid rain and soil type had a strong interaction in determining plant response. They found that the extent of this response was inversely correlated with the availability of nitrogen in each soil. Ozone treatments caused decreased net photosynthesis in pine seedlings.

Nutrient cycling and decomposition rate is also negatively affected by acidification of soil due to AR. It has been shown that strong acidification retards the decomposition of litter of spruce, pine, birch and other cellulose-rich materials, as reported by Francis [28] and Kilham *et al.* [29]. Soil acidification led to changes in soil quality from podzol, podzolic soil, dernopodzolic soil and brown earth to Pararendzina that changes the floristical composition, followed by changing of pine and spruce forest to mixed and birch forest, as reported by Kopstik *et al.* [30].

The additive and interactive effects of SiAR and elevated ozone on C and N contents, the C-N ratio of one-year-old, current-year foliage of field-grown mature trees and their half-sib seedlings of a stress-tolerant genotype of ponderosa pine have been studied by Momen and Helms [31].

In his report, Paoletti [32] observed that Beech (*Fagus sylvatica L.*) and holm oak (*Quercus ilex L.*) leaves were subjected to SiAR and UV-B radiation for 10 days. The almost glabrous beech leaves revealed a greater predisposition to developing macroscopic necrotic lesions than the pubescent holm oak leaves.

Bellani *et al.* [33] studied the viability, germination and tube length in pollen grains of field-grown ‘summered’ apple trees (*Malus domestica Borkh*) exposed to deionized water, rainfall or SiAR at pH 5.6, 4.0 and 3.0. Pollen viability and germination significantly decreased with lower values of pH and with increasing number of treatments. Also, it has been observed that the effects of pH 5.6 and natural rainfall were not significant. Electron microscope investigation of vegetative pollen cells of plants exposed to acid rain at pH 4.0 and 3.0 showed modified features in mitochondria, plastids and endoplasmic reticulum.

The regulatory role of calcium in fertility of pollen and pistil under SiAR was investigated by Dong-Liang *et al.* [34]. The germination percentage of pollen treated with AR of pH 4.5 was 9.42% lower than that of control, and that of pH 3.5, pH 2.5 and pH 1.5 was lower by 22.47%, 45.49% and 71.62%, respectively. AR- induces changes in the cellular biochemistry and physiology of the whole plant. AR-caused effects including visible symptoms of injury (chlorosis and/or necrosis), and invisible effects such as reduced photosynthesis, nutrient loss from leaves, altered water balance, variation of several enzyme activities, changes of pollen physiology and ultrastructure. Due to the need for further evidence regarding atmospheric pollution in the form of AR and its interaction with and influence upon the reproductive processes of litchi, the study was undertaken concentrating on one stage of reproduction. It is known that pollen germination is significantly regulated by the transport Ca^{2+} , K^+ and other inorganic ions across the plasma membranes of pollen.

In the 1985 report by Tift [35], 7.7% of 7.4 million hectares of West Germany’s forests were visibly damaged; within a year 34% of trees had suffered discolouration and some loss of needles and leaves; by late 1984 around half the country’s woodlands showed symptoms of the disease.

Bardy [36] developed the nitrous acid hypothesis, which could explain the triggering effect of drought on forest decline. The first rainfall after summer drought (FRAD) receives the nitrifiers which gives rise to an acidification push with nitric acid production. But also denitrifiers are rapidly received in anaerobic micro-sites. Also, it has been observed that, during this climatic event, intermediate NO_2^- of nitrification-denitrification (as undissociated HNO_2 species) would react drastically and without discrimination on dead and living organic matter, thus altering roots and mycorrhizas, particularly in the direct vicinity of aggregates.

Ruuholo *et al.* [37] examined how long-term (19yr) AR pollution affects (i) the oxidative responses in mountain birch foliage, and (ii) the growth and immune responses of autumnal moth larvae. They found that pollution caused a 50% increase ($p<0.05$) in the peroxidase activities (PODs) in birch leaves, whereas polyphenoloxidase (PPO) or catalase (CAT) activities were not affected, suggesting that PODs play an important role in the quenching of the oxidative stress in birches. In polluted trees, phenoloxidases probably acted as antioxidative, not prooxidative enzymes. Although AR pollution did not have any direct effect on either pupal weight or the length of larval period, the stronger AR treatment reduced slightly (6% in females) the encapsulation response of pupae. A decrease of this magnitude might be too small to have measurable effects on the incidence of moth outbreaks.

Anna-Santos *et al.* [38] reported the correlation between symptomatology with anatomical alterations caused by AR in leaves of tropical species, seedlings and saplings of *spondias dulcis* Forst F., *Mimosa artemisiana* Heringer and Paula and *Gallesia integrifolia* (Spreng.) Harms exposed to simulated low-pH AR (pH 3.0). It has been observed that the necrotic spots on the leaf blade occurred and most of the injuries onset on the epidermis in all species studied. *S. dulcis* displayed epicuticular wax erosion and rupture of epidermis. The abaxial

surface of *M. artemisiana* was colonized by a mass of fungi hyphae, and stomatal outer ledge rupture occurred. Some epidermal cells of *G. integrifolia* showed appearance similar to plasmolysis. The plants accumulated phenolic compounds in necrotic areas. Afterwards, leaves presented injuries in the mesophyll and collapsed completely. Cells surrounding the injured areas accumulated starch grains in *S. dulcis*. *M. artemisiana* showed more drastic symptom intensity in response to AR. Also, it was found that AR caused anatomical alterations in the leaves of tropical species, seedlings and sapling of *Spondias dulcis* Forest. When exposed to simulated acid rain with low pH (3.0), necrotic spots on the leaf blade occurred, which were mostly restricted to epidermis in all the species. *S. dulcis* displayed epicuticular wax erosion and rupture of epidermis.

Pritsch *et al.* [39] showed the influence of a moderate contamination with heavy metals (HM) viz Cu, Zn, Cd, Pb /640, 3000, 10, 90 mg kg⁻¹ of HNO₃-extractable metals, AR (pH 3.5), and the combined treatment was studied in model forest ecosystems. Extracellular enzymatic activities were measured in soil samples and on absorbing fine roots of seven different tree species (*Betula pendula*, *Fagus sylvatica*, *Populus tremula*, *Picea abies*, *Salix viminalis*, *Alnus incana*, and *Acer pseudoplatanus*). The five studied enzymes represent the carbon, phosphorus and nitrogen cycle, and include phosphatase, glucosidase, cellobiohydrolase, chitinase, and xylosidase. AR alone had no effect on soil enzyme activities, while heavy metals strongly reduced activities of all enzymes. Surprisingly, this reduction was less pronounced in the combined treatments with HM and AR. The absorbing fine roots of the seven different tree species exhibited a broad range of reactions to both stressors. Overall, the results suggest that studies on heavy metal reactions in woody plants should consider species effects as well as other environmental factors such as AR. Again, AR- caused reduction in protein concentration of *Betula alleghaniensis* and white spruce [40].

V. CONCLUSION

In conclusion, soil and aquatic ecosystem are two very important environmental components and are directly affected by acid rain. Since soil and water are two essential components for the plant growth, they are directly related to plant kingdom. AR-induced pollution of soil and water impacts an adverse effect on plants. Hence, polluted and water highly affect the plants; this indirect effect may cause even more impact on plants rather than the direct acid rain.

ACKNOWLEDGMENT

Authors would like to thank Professor S. Panigrahi of the Department of Physics, and Professor S. C. Mishra of the Department of Metallurgical and Material Engineering of National Institute of Technology, Rourkela, India for their help and encouragement.

REFERENCES

- [1] J. A. W. Fairfax and N. W. Lepp, Effect of simulated acid rain on cation loss from leaves, *Nature*, vol. 255, pp. 324-325, 1975.
- [2] J. H. Seinfeld, S. N. Pandis, *Atmospheric Chemistry and Physics—From Air Pollution to Climate Change*. New York: John Wiley and Sons, Inc. 1998.
- [3] L. S. Evans, Botanical aspects of acidic precipitation, *Bot. Rev.*, vol. 50, pp. 449-490, 1984.
- [4] Punam Kumari, Y.S. Tomar, Effect of simulated acid rain on chlorophyll and ascorbic acid contents of *Mentha piperita* L. (Peppermint), *Agric. Sci. Dig.*, vol. 29, pp. 1-6, 2009.
- [5] S. Behera, B. Mallick, T. N. Tiwari and P.C. Mishra, X-Ray Characterization of Various Aluminium Phases in the Medicinal Herb Bacopa Monnier Affected by Simulated Acid Rain, *J. Biomed. Phar. Res.*, vol. 1 (1), pp. 08-15, 2012.
- [6] S. I. Vicas, E. Grosu, V. Laslo, The effects of simulated acid rain on growth and biochemistry process in grass (*Lolium perenne*), *Lucrări Științifice*, vol. 52, pp. 277-283, 2009.
- [7] Ruilong Wang, Shafiq Ur Rehman , Xiaoting Liang, Yuanyuan Song, Yijuan Su, Scott R Baerson And Rensen Zeng, Effects of simulated acid rain on the allelopathic potential of invasive weed *Wedelia trilobata*, *Allelopath. J.*, vol. 30 (1), pp. 23-32, 2012.
- [8] R. W. Ferenbaugh, effects of simulated acid rain on *Phaseolus vulgaris* L. (FABACEAE), *Amer. J. Bot.*, vol. 63(3), pp. 283-288, 1976.
- [9] Youngmi Lee, Jongbum Park , Kyunghoan Im , Kiyoon Kim , Jungwoo Lee , Kyungyeoll Lee , Jung-An Park , Taek-Kyun Lee , Dae-Sup Park , Joo-Sung Yang , Donggiun Kim , and Sukchan Lee , Arabidopsis leaf necrosis caused by simulated acid rain is related to the salicylic acid signaling pathway, *Plant Physiol. Biochem.* (Paris), vol. 44, pp. 38-42, 2006.
- [10] Arti verma, Ashish Tewari, Abdullah Azami, An impact of simulated acid rain of different pH-levels on some major vegetable plants in India, *Report and Opinion*, vol. 2(4), pp. 38-40, 2010.
- [11] Anita Singh and Madhoolika Agrawal, Acid rain and its ecological consequences, *J. Environ. Biol.*, vol. 29(1), pp. 15-24, 2008.
- [12] R.J. Norby and R.J. Luxmoore, Growth analysis of soybean exposed to simulated acid rain: Damage, growth and gas exchange, *New Phytol.*, vol. 99, pp. 389-405, 1983.
- [13] Singh, B. and M. Agrawal: Impact of simulated acid rain on growth and yield of two cultivars of wheat, *Water Air Soil Pollut.*, vol. 152, pp. 1-4 2004.
- [14] J.P. Smol, and J.R. Glew, Palcolimnology, In: *Encyclopedia of earth system science* (Ed.: W. Nierenberg). London: Taylor and Francis, 1992, pp. 95-107.
- [15] D.L. Findlay, and S.E.M. Kasian, Phytoplankton biomass, succession and composition in lake 223. Experimental lakes area, north eastern Ontario, *Can. J. Fish Aquat. Sci.*, vol. 44, pp. 35-46, 1986.
- [16] Liao, Bo-han, Liu, Hong-yu, Zeng, Qing-ru, Yu, Ping-zhong, Probst, Anne and Probst, Jean-Luc, Complex toxic effects of Cd²⁺, zn²⁺, and acid rain on growth of kidney bean (*Phaseolus vulgaris* L), *Environ. Int.*, vol. 31, pp. 891-895, 2005.
- [17] V. Velikova, I. Yordanov, and A. Edreva, Oxidative stress and some antioxidant systems in acid rain-treated bean plants protective role of exogenous polyamines, *Plant Sci.*, vol. 151, pp. 59-66, 2000.
- [18] Hai Fang Wang , Noburu Takematsu , Shizuko Ambe , Effects of soil acidity on the uptake of trace elements in soybean and tamato plants , *Appl. Rad. Isot.*, 52 , 803-811, (2000).
- [19] Barbara Gabara, Maria Sklodowska, Anna Wyrwicka, Slawa Glinska, and Magdalena Gapinska, Changes in the ultrastructure of chloroplasts and mitochondria and antioxidant enzyme activity in *Lycopersicon esculentum* Mill. Leaves sprayed with acid rail, *Plant Sci.*, vol. 164, pp. 507-516, 2003.
- [20] Patricia M. Irving, Gaseous Pollutant and Acidic Rain Impacts on Crops in the United States" A Comparison, *Environ. Technol. Lett.*, vol. 8, pp. 451-458, 2008.
- [21] Anna Wyrwicka and Maria Sklodowska, Influence of repeated acid rain treatment on antioxidative enzyme activities and on lipid peroxidation in cucumber leaves, *Environ. Exp. Bot.*, vol. 56, pp. 198- 204, 2006.
- [22] Omer Munzuroglu , Erdal Obek , Fikret Karatas and Sule Yoksei Tatar , Effects of Simulated Acid Rain on Vitamins A, E and C in Strawberry (*Fragaria Vesca*), *Pak. J. Nutrition*, vol. 4, pp. 402-406, 2005.

- [23] Y. Shan, Effects of Simulated Acid Rain on *Pinus densiflora*; Inhibition of Net Photosynthesis by the pheophytization of Chlorophyll, *Water, Air, and Soil Pollut.*, vol. 103, pp. 121-127, 1998.
- [24] Pavel Shumejko, Vladimir Ossipova, and Seppo Neuvonen, The effect of simulated acid rain in the biochemical composition of scots pine needles, *Environ. Pollut.*, vol. 92, pp. 315-321, 1996.
- [25] Yunfeng Shan, Zongwei Feng, Takeshi Izuta, Masatoshi Aoki and Tsumugu Totsuka, The individual and combined effects of ozone and simulated acid rain on growth, gas exchange rate and water-use efficiency of *pinus armandi* Franch., *Environ. Pollut.*, vol. 91, pp. 355-361, 1996.
- [26] M. L. Helander, T. N. Sieber, O. Petrini, and S. Neuvonen , Endophytic fungi in Scots pine needles: spatial variation and consequences of simulated acid rain, *Can. J. Bot.*, vol. 72(8), pp. 1108-1113, 1994.
- [27] Peter B. Reich, Anna W. Schoettle, Hans F. Stroo, John Troiano, Robert G. Amundson, Effects of ozone and acid rain on white pine (*Pinus strobus*) seedlings grown in five soils. I. Net photosynthesis and growth, *Can. J. Bot.*, vol. 65(5), pp. 977-987, 1987.
- [28] A.J. Francis, Effects of acidic precipitation acidity on soil microbial processes, *Water Air Soil Pollut.*, vol. 18, pp. 375-314, 1982.
- [29] K. Kilham , M.K. Firestone and J.G. McColl, Acid rain and soil microbial activity, Effects and their mechanisms, *J. Environ. Qual.*, vol. 12, pp. 133-137, 1983.
- [30] G.N. Kopstik, S.V. Kopstik and D. Aamlid, Pine needle chemistry near a large point SO₂ sources in northern Fennoscandia, *Water Air Soil Pollut.*, vol. 130, pp. 929-934, 2001.
- [31] B. Momen and J.A. Helms, Effects of Simulated Acid Rain and ozone on foliar chemistry of field-grown *pinus ponderosa* seedlings and mature trees, *Environ. Pollut.*, vol. 91(1), pp. 105-11, 1996.
- [32] E. Paoletti, UV-band and acid rain effects on beech (*Fagus sylvatica L.*) and holm oak (*Quercus ilex L.*) leaves, *Chemosphere.*, vol. 36, pp. 835-840, 1998.
- [33] L.M. Bellani, C. Rinallo, S. Muccifora and P. Gori, Effects of simulated acid rain on pollen physiology and ultrastructure in the apple, *Environ. Pollut.*, vol. 95, pp. 357-362, 1997.
- [34] Qiu Dong-Liang, Liu Xing-hui, Guo Su-Zhi, Effects of simulated acid rain on fertility litchi, *J. Environ.l Sci.*, vol. 17, pp. 1034-1037, 2005.
- [35] S. Tift, Requiem for the forest, *Time*, vol. 126, pp. 46-53, 1985.
- [36] Jean-Alexis Bardy, Acid Depositions, Summer Droughts, Forest Decline: Development of the Nitrous Acid Hypothesis, *Environ. Technolol.*, vol. 11, pp. 765-776, 1990.
- [37] Teija Ruuhola , Liisa M. Rantala, Seppo Neuvonen, Shiyong Yang, Markus J. Rantala, Effects of long-term simulated acid rain on a plant – herbivore interaction, *Basic Appl. Ecol.*, vol. 10, pp. 589-596, 2009.
- [38] Bruno Francisco Sant' Anna-Santos, Luzimar Campos da Silva, Aristea Alves Azevedo, Joao Marcos de Araujo , Ericka Figueiredo Alves , Eldo Antonio Monteiro da Silva, Rosane Aguiar, Effects of simulated acid rain on the foliar micromorphology and anatomy of tree tropical species, *Environ. Exp. Bot.*, vol. 58, pp. 158-168, 2006.
- [39] Karin Pritsch, Madeleine S. Günthardt-Goerg, Jean Charles Munch, and Michael Schloter, Influence of heavy metals and acid rain on enzymatic activities in the mycorrhizosphere of model forest ecosystems, *For. Snow Landsc. Res.*, vol. 80, pp. 289-304, 2006.
- [40] T. Scherbatskoy and R.M. Klein, Response of spruce and birch foliage to leaching by acidic mist, *J. Environ. Qual.*, vol. 12, pp. 189-195, 1983.
- [41] G. Tomilnson, Air pollutants and forest decline, *Environ. Sci. Tech.*, vol. 17, pp. 246-256, 1983.
- [42] G. Abrahamsen, A.O. Stuanes and B. Tveite, Effects of long range transported air pollutants in Scandinavia, *Water Qual. Bull.*, vol. 8, pp. 89-95, 1983.

In-Vitro Evaluation of Cytotoxicity, Antiviral and Virostatic Activity of PMF Derived from Camel Urine

Noor S.O, AlAttas S.G, Khorshid F.K, Elsourojy Y.A and Tawfik N
King Abdulaziz University, Jeddah, Saudi Arabia

Abstract—Although many antiviral and anticancer drugs are produced, no cure can be ensured. Many trials to produce antiviral / anticancer drugs from different sources, either synthetic or natural, could not achieve their goal. In the present study we tried to produce an antiviral / anticancer drug and data revealed that PMF derived from camel urine showed a relative cytotoxicity (IC₅₀) to normal and cancerous cell line; 90 and 140 µg respectively. PMF, as a camel urine derived drug, could prove to be a promising virucide .The VSV virus model was completely inhibited 75 minutes post treatment with PMF. Further investigation of antiviral and anticancer activities relative to gene expression to confirm the biological activity are a must.

Keywords—VSV, PMF, camel urine, anticancer drug; antiviral activity

I. INTRODUCTION

Natural products play an important role in our healthcare system (Pezzuto, 1997 and Schwartsmann, 2000). They offer a valuable source of potent compounds with a wide variety of biological activities and novel chemical structures, many of which are important for novel drug development (Vuorela, et al., 2004). Camel urine is a

This work was supported by King Abdulaziz University and A-lZamel research chair.

Noor S.O is an Assistant Professor of Medical and Molecular Microbiology, Department of Biology, Faculty of Science, King Abdulaziz University, Saudi Arabia (corresponding author , phone: +966595352531; fax: +966126963367; e-mail: sonoor@kau.edu.sa).

AlAttas S.G is a Post Doc at CEE department –MIT Boston USA ,Assistant Professor of Medical Virology, Department of Biology, Faculty of Science, King Abdulaziz University Saudi Arabia (E-mail: sangtas@mit.edu)

Khorshid F.K Prof. of Cell Biology & Cell Engineering, Department of Biology, Faculty of Science, King Abdulaziz University, Saudi Arabia (E-mail: fatenkhorshid@yahoo.com).

Elsourojy Y.A is a General Manager of Development Research ,Vacsara egyptian company for production of Vaccines, Sera & Drugs Egypt (E-mail: ceo@egyvac.com)

Tawfik N is a Senior Technician, Vacsara egyptian company for production of Vaccines, Sera & Drugs, Egypt, (E-mail: ceo@egyvac.com)

physiological catabolic product, it has been used traditionally in the treatment of many diseases in Arabic countries (Alhaider et al., 2011). It is used both externally and internally as a medicine. Amer and Al-hendi (1996) analyzed urine of mature camels between 5 - 10 years old, and found that its relative density ranged from 1.022 to 1.07 gm/dL, while pH values varied to be either acidic or alkaline. Urea level ranged from 18-36 gm/dL. Keratin was recorded at 0.2 - 0.5 gm/L. Microscopical analysis proved the presence of phosphorus, calcium oxalate, and ammonium urate; some epithelial and granular cells appeared. Al-Attas (2008), using neutron activation analysis, estimated the amount of some essential elements within milk and urine of camels and discovered that they contain large amounts of Na and K, which can substitute for the loss of such elements in humans in the case of diarrhea. PMF is a new pharmaceutical drug prepared by extracting lyophilized camel urine and was proved to have selective toxicity and anticancer substrates and to exert negligible effects on vital organs (Khorshid, 2008). The extracted fraction of PMF was found in 150 mg /g of lyophilized PM 701 (camel urine) and it was able to inhibit the proliferation of cancer cells significantly without affecting the normal cells at cell culture level (Khorshid et al., 2005, 2008, Khorshid, 2009, Moshref et al., 2006 and El-Shahawy et al., 2010). Cell culture and animal models play a crucial role in the development of new therapies. A novel treatment cannot be applied directly to humans. Treatments (both pharmacological and non-pharmacological) can be potentially dangerous. Cell culture can verify the mechanism of the new therapy and aid in establishing a safe human dose range (Giaever & Keese, 1986; Khorshid & Mosherf, 2006). A reliable and predictive animal model must be employed to assess the safety and efficacy of treatment prior to its use on humans. In addition, cell culture and animal models are far less expensive than clinical studies (Giaever & Keese, 1986; Khorshid & Mosherf, 2006). So, the present work aimed to evaluate both cytotoxicity and antiviral activity of PMF from camel urine using the virus model that is used for evaluation of current recombinant Interferon as an antiviral drug despite the lack of results.

II. MATERIAL AND METHODS

A. Maintenance of cell lines

Both African green monkey cells (Vero) and Human Hepato cellular Carcinoma cells HpeG2 cell line (ATCC-HB-8065) were cultured in 75-cm² tissue culture flasks using EMEM and medium 199E (GIBCO-USA) supplemented with 10% (FBS) fetal bovine serum (GIBCO-USA). Cell lines were maintained according to the method described by Thomson (1998) where cells were grown until they reached confluent monolayer. Cells were incubated with trace trypsin in the incubator at 37°C until the cells detached from the surface. Cells were resuspended in growth medium to the desired concentration according to cell count. Cell suspension was incubated in new culture growth media in new flasks and incubated at 37°C until confluence. The cell number in the suspension was calculated by using trypan blue exclusion assay according to Steven et al., (1993).

B. Vesicular stomatitis virus (VSV) propagation onto cell culture

Sterile VSV was inoculated into pre-cultured Vero cells tissue culture flask. Infected flasks were incubated at 37°C (Jouan-France) for an adsorption period of 1-1.5 hr with gentle mixing at timed intervals of 15 min. Maintenance medium was added to infected flasks(Joseph 1994). Non-infected cell culture control, were included. Cultures were incubated at 37°C and examined daily under the inverted microscope (Hund-Germany) until the initial detection of cytopathic effect. Flasks that showed 90% CPE were frozen and thawed three successive times for virus extraction according to (Abd el-razek et al., 2011).

C. Virus infectivity titer assessment

The virus infectivity titer was assessed according to Reed and Muench (1938) to determine the highest dilution of the virus that produced CPE in 50% of the infected cells (TCID50). VSV was 10 fold diluted in culture medium. Vero cells precultured on 96 well plates (10^4 cells/well) were infected using the serially diluted VSV on the reciprocal wells. On confluence, the medium was decanted 100 µl/well of each dilution of the virus suspension into 8 wells (using separate tips for each dilution). Two successive columns of non inoculated wells were maintained as negative control. Plates were incubated at 37°C, seven days post incubation, the number of wells per each dilution showed CPE were recorded. The 50% endpoint was determined according to the method cited from Reed and Muench (1938) as follows: 50% endpoint = (percentage of CPE of >50% – 50) / (percentage of CPE of >50 % – percentage with CPE of < 50%) X log dilution.

D. Evaluation of PMF cytotoxicity using MTT assay

The MTT (3-[4, 5-dimethylthiazol-2-yl]-2, 5 diphenyltetrazolium bromide) assay is based on the conversion

of MTT into formazan crystals by living cells, which determines mitochondrial activity. Since for most cell populations the total mitochondrial activity is related to the number of viable cells, Van Meerloo et al (2011). Cellular cytotoxicity was determined using MTT assay as described by Takahashi et al.,(1989). PMF was dissolved in EMEM, at the concentrations of 24 µg/ml and 120 µg/ml. Double fold dilutions were prepared of both concentrations. Cell lines were counted as 10^5 cells/ml and cultured in 96-well tissue culture plates. On confluence, growth media were discarded and 100 µl of each dilution of PMF was inoculated into 8 wells of the plates. The plates were incubated at 37°C for 24 hrs. Media containing PMF of different dilutions were decanted and plates were washed with PBS 3 times. Plates were stained using MTT (0.05 ml/well) for 4 hrs at 37°C. Developed MTT-Formazan complex was dissolved using 0.05 ml of DMSO. Plates were incubated for 30 minutes at 37°C for cell lysis. Optical density (OD) was measured using ELISA reader at wavelength of 550-570 nm. The percentage of viability was determined according to the method described by Ho-Joon et al., (2000) as follows:

$$\text{Number of residual living cells} = (\text{OD of treated cells} / \text{OD of untreated cells}) \times \text{Number of negative control cells} (10^4 \text{ cells}/0.1\text{ml}).$$

$$\text{Percentage viability} = (\text{Number of residual living cells} / \text{Number of negative control cells}) \times 100.$$

E. Evaluation of anti-viral activity of PMF against VSV

The antiviral activity of PMF against VSV was determined according to the method described by Shinji (2005) where non toxic concentrations of PMF was prepared in EMEM to contain 60, 30, 15µg/ml respectively. Vero cells were counted as 10^5 cells/ml and cultured in 96-well tissue culture plates. On confluence, growth media were discarded. Pre cultured plates 100 µl/well PMF (under test for antiviral activity) were dispensed to the reciprocal wells..One PMF non treated plate was maintained for viral control titration. All plates were incubated at 37°C for 24 hrs. VSV was 10 fold serially diluted in EMEM (6 dilutions 10^{-2} - 10^{-8}). Growth/ treatment media were decanted; each virus dilution was inoculated at 100µl /well. Plates were incubated at 37°C and examined daily under the inverted microscope. Three days post incubation, the virus titer was calculated in each plate. The antiviral activities were calculated by determining VSV mean titer in treated and untreated cells. The difference between both titers refers to the antiviral activity.

F. Virucidal activity

Virucidal activity was monitored based on the evaluation of direct contact of VSV with PMF follow by collecting samples from 37°C incubated PMF–virus mix. Collected samples were titrated the treatment test was repeated in triplicates and the mean depletion rate was calculated according to (Reed and Muench 1938).

G. Statistical analysis

Data were represented as mean \pm SD. Statistical significance between treated and untreated cells was determined using one way ANOVA. Differences at P values less than 0.05 were considered significant

III. RESULTS AND DISCUSSION

Cytotoxicity of natural products may be based on the effect of toxic materials on cell organelles including mitochondrial, nuclear and cellular membrane damage. This damage leads to breakage of cellular and mitochondrial membranes enhancing cell death and viral protein assembly ceasing in cases of viral infection. Cancer is a disease characterized by uncontrolled cellular proliferation and differentiation. Nearly all conventional cancer treatments have undesirable negative impacts; safer chemotherapeutics would be advantageous. We evaluated the cytotoxicity of PMF as a natural product by using a cancer cell line model compared to a normal one, namely HEPG-2 and vero cells respectively. Data revealed that the toxicity of PMF was relative to PMF concentration. It was clear that toxicity inducing concentration of PMF to vero cells was significantly less than that of hepatic cancer cell line toxicity ($p<0.05$). Our data showed that the inhibitory concentration for 50% of treated cells [IC50] was 144 μ g for vero cells and 90 μ g for HEPG-2 cell lines Fig (1) and (2) that were evaluated using Masterplex Reader fit (2010) software. Viability was compared to non treated cell controls under the same conditions. Cytotoxic effect may be attributed to HEPG-2 cells apoptotic enhancing activity under the effect of camel urine derived PMF, also the PMF may enhance cell and mitochondrial membrane rupture. In our recent work, El-shahawy et al (2010) recorded that camel urine, which coded PM701, is a natural product and is free of toxicity.

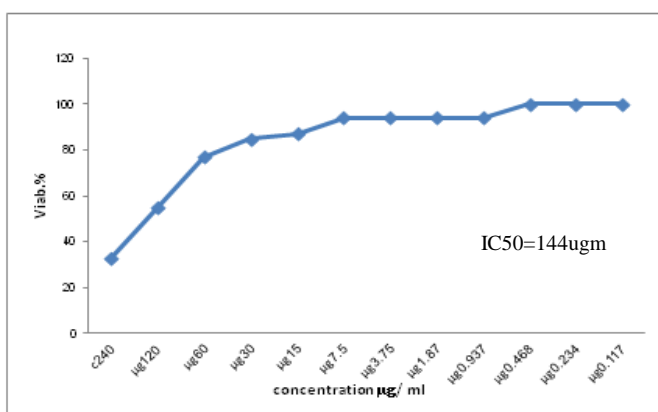


Fig (1) : Evaluation of viability of Vero cell line post treatment with PMF relatively to concentration using MTT assay

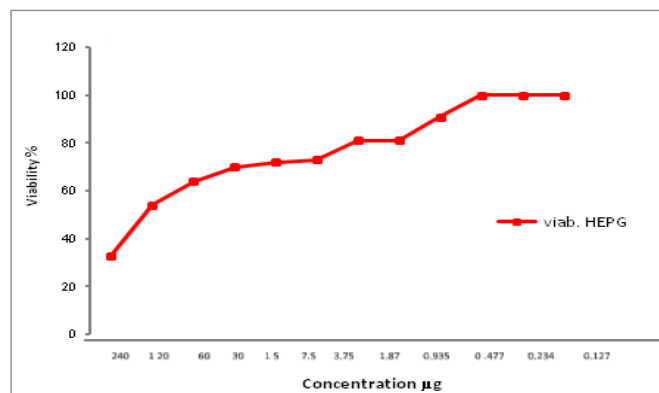


Fig (2) : Evaluation of viability % of HEPG-2 cell line post treatment with PMF relatively to concentration using MTT assay

The extracted fraction, which was coded PMF, was found in 150 mg /g of lyophilized PM701 and it was able to significantly inhibit the proliferation of cancer cells without affecting the normal cells at cell culture level. The PMF has been fractionated from a PM701 sample and this fractionated sample has anti-carcinogenic effect on lung cancer and leukemic cells. These data coincided with Nujoud et al (2011) despite the use of different cell lines and their attention to immune reactivity; they recorded that camel urine showed cytotoxicity against various human cancer cell lines, with only marginal effects on non-tumorigenic epithelial and fibroblast cells. Interestingly, 216 mg/ml of lyophilized Camel Urine (CU) inhibited cell proliferation and triggered more than 80% of apoptosis in different cancer cells, including breast carcinomas and medulloblastomas. Apoptosis was induced in these cells through the intrinsic pathway via a decrease in Bcl-2 -2. Furthermore, CU down-regulated the cancer-promoting proteins survivin, β -catenin and cyclin D1 and increased the level of the cyclin-dependent kinase inhibitor p21. In addition, they have shown that CU has no cytotoxic effect against peripheral blood mononuclear cells and has strong immune-inducer activity by inducing IFN- γ and inhibiting the Th2 cytokines IL-4, IL-6 and IL-10. Our results were consistent with Al-harbi et al., (1996) who reported the cytotoxic effect of CU constituents to cancer cell lines. They recorded that CU treatment was found to cause a significant cytotoxic effect in the bone marrow cells of mice and mentioned that the cytotoxicity appeared at higher doses comparable with that of cyclophosphamide (CP), standard drug. However, unlike CP, the camel urine treatment failed to induce any clastogenicity. Also, they reported that the cytotoxicity induced by camel urine treatment was substantiated by the reduction of liver nucleic acids and glutathione levels and increased malondialdehyde (MDA) contents in the same animals. CP treatment was found to be highly clastogenic, cytotoxic, able to reduce the levels of nucleic acids, proteins, glutathione and increased malondialdehyde concentration due to its prooxidant nature. Al-harbi et al., (1996) returned the non-clastogenic nature of camel urine to the antioxidant and antimutagenic compounds present in camel urine. They stated that the pretreatment with camel urine increased the cytotoxicity of CP

and intensified the CP induced reduction of liver nucleic acids, and glutathione and increased the MDA concentration. The increase of CP induced cytotoxicity appears to be partly due to the additive effect of the two treatments on cellular lipid peroxidation.

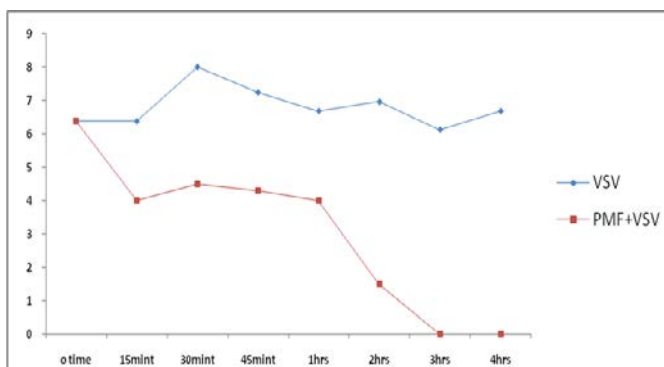


Fig (3): Evaluation of VSV titer post treatment at 37 °C comparing with negative control

Urine constituents showed a variable reactivity to cancer cell lines / apoptotic activity relative to age and sex of camels (Alghamdi; Khorshid, 2012). At the same time Abdulqader et al., (2011) recorded that all types of camel; but not bovine; urine differentially inhibited the induction of Cyp1a1 gene expression by TCDD, the most potent Cyp1a1 inducer known as a carcinogenic chemical. They added that the virgin camel urine showed the highest degree of inhibition at the activity level, followed by lactating and pregnant camel urines. Furthermore, they have shown that virgin camel urine significantly inhibited the TCDD-mediated induction of Cyp1a1 at the mRNA and protein expression levels.

The ability of virgin camel urine to inhibit Cyp1a1 was strongly correlated with its ability to inhibit AhR-dependent luciferase activity and dna binding as determined by EMSA, suggesting that AhR-dependent mechanism is involved. Also Abdulqader et al., (2011) concluded that their work provides the first evidence that camel urine, but not that of bovine, inhibits the TCDD-mediated toxic effect by inhibiting the expression of Cyp1a1, at both transcriptional and post-transcriptional levels through an AhR-dependent mechanism. This agrees with our data that camel urine proved its anticancer activity based on its toxic effect on human hepatoma cell line. Safe concentrations of PMF could not be proven where virus infectivity titer showed no change 24 hrs after on pretreated cells infection compared to virus control infectivity titer. Virucidal activity was evaluated; the data revealed that VSV showed a significant depletion rate in virus infectivity titer 15 minutes post treatment ($p<0.05$), while an almost stationary phase was detected through the 30 - 45 minutes mark followed by a sharp declining phase of virus infectivity titer, VSV could not be detected 75 minutes post treatment recording a depletion rate of VSV in the order of $0.49 \log_{10}/ 15$ minutes. Finally, 75 minutes post treatment, the virus could not be detected compared to the control Fig (3)

and (4). Antiviral activity may be attributed to the lysozyme enzyme found in urine that enhances its antimicrobial activity in general and it may work on the viral epitopes denaturation preventing the adhesion potential of virus to cell receptors. Our data shows agreement with El-shahawy et al., (2010) that the antimicrobial activity of PMF derived from camel urine could significantly inhibit VSV virus infectivity titer in 60 minutes. PMF may affect viral epitopes integration due to its chemical structure which affects virus replication enzymes. Abdulqader et al., (2012) supported our results from the first survey of the dromedary camel urinary proteome with the absence of a complete camel genome sequence. The number of protein identifications was maximized by searching three primary sequence databases: swiss-prot, alpaca and camel EST.

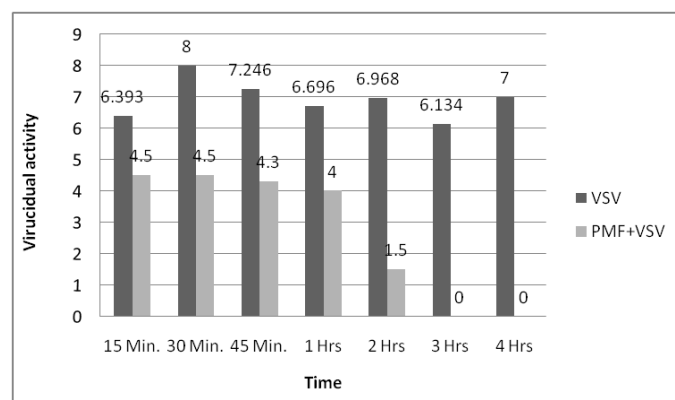


Fig (4): Comparative evaluation of Virucidal activity of PMF to Vesicular stomatitis virus [VSV] relatively to time

This search strategy enabled the identification of 1274 peptide sequences, of which 735 were found in at least two independent samples. Functional annotations for proteins identified from alpaca and camel EST sequences were mapped from basic local alignment protein search tool. These 735 peptides, which included many novel sequences found only in the camel EST database, were grouped into 147 protein descriptors. Gene ontology term analysis of human proteins with sequence similarity showed that camel urine may be particularly enriched in proteins from extracellular compartments and vesicles, and with functions that include carbohydrate-binding and peptidase inhibitor activities. If their biological functions are conserved between species, many of the camel urinary proteins could be involved in various stress and immune responses, and some may have antimicrobial activities.

III. CONCLUSION

Testing the activity of VSV virus post PMF treatment revealed that the log differences are highly significant which means that the treatment by PMF has a powerful effect on the virus replication. The test PMF is a promising bioproduct from

camel urine that has anticancer and antiviral potentials. In addition it needs more studies concerning gene expression profile to prove anti apoptotic activity to explain the anticancer mechanism of action. Also, the promising fast antiviral activity must be enhanced using a wide range of virus models with both DNA and RNA and cancer inducing viruses. We need to trace the antiviral activity expressed by gene profiles namely MX and 2,5 Olygoadenylatesynthetase, as marker genes for antiviral activity, In-Vitro and In-Vivo studies for intensified evaluation of PMF must be done.

REFERENCES

- [1] Alhaider A. Bayoumy N. Argo E. Gader A. Stead D, *Survey of the camel urinary proteome by shotgun proteomics using a multiple database search strategy*. WILEY-VCH Verlag GmbH & Co. KGaA, Weinheim. PROTEOMICS, 2012. **12**(22): p. 3403-3406.
- [2] Al-Harbi MM.Qureshi S. Ahmed MM. RazaM. Baig MZ. Shah AH, *Effect of camel urine on the cytological and biochemical changes induced by cyclophosphamide in mice*. Journal of Ethnopharmacology, 1996. **52**(3): p. 129-137.
- [3] Altman S. Randers L. Govind Rm, *Comparison of trypan blue dye exclusion and fluorometric assays for mammalian cell viability determinations*. Biotechnol. Prog., 1993. **9**(6): p. 671-674.
- [4] Amer HA. Al-Hendi AB, *Physical, biochemical and microscopically analysis of camel urine*. J. Camel Practice Res, 1996. **3**(1): p. 17-21.
- [5] Barber GN, *Vesicular stomatitis virus as an oncolytic vector*. Viral Immunol. , 2004. **17**(4): p. 516-27.
- [6] Benkerroum N. S.a.u.l.m.i.m.a.m.l, *Antimicrobial activity of lysozyme with special relevance to milk*. African Journal of biotecnology And Dolores P, 2008. **124**(5): p. 921-952.
- [7] Carson SD, *Limited proteolysis of the coxsackievirus and adenovirus receptor (CAR) on HeLa cells exposed to trypsin*. FEBS Lett., 2000. **484**(1): p. 149-152.
- [8] deMattos C A. de Mattos CC. Rupprecht CE, *Rhabdoviruses*. Fields virology. Lippincott Williams and Wilkins, Philadelphia, Pa., 2001: p. 1245-1278.
- [9] El-Shahawy A. Elsawi NM. . Baker WS, K.F.G.N., *Spectral analysis, molecular orbital calculations and antimicrobial activity of PMF-G fraction extracted from PM-701*. Int. J. Pharma Biosci., 2010. **1**(1): p. 1-19.
- [10] Fenner FP. Bachmann A. Gibbs EJ. Murphy FA. Studdert MJ. White DO, *Veterinary virology*. Academic Press, Inc., Orlando, Fla., 1987: p. 541-544.
- [11] Gerhäuser C. Lee SK. Kosmeder JW. Moriarty RM. Hamel E. Mehta RG. Moon RC. Pezzuto JM, *Regulation of ornithine decarboxylase induction by deguelin, a natural product cancer chemopreventive agent*. Cancer Res, 1997. **57**(16): p. 3429-35.
- [12] Giaever I. Keese CR, *Use of electric fields to monitor the dynamical aspect of cell behavior in tissue culture*. IEEE Trans Biomed Eng., 1986. **33**(2): p. 242-7.
- [13] Joseph SK, *Biosynthesis of the inositol trisphosphate receptor in WB rat liver epithelial cell*. J Biol Chem., 1994. **269**(8): p. 5673-9.
- [14] Khorshid FA, *Preclinical evaluation of PM 701 in experimental animals*. Int. J. Pharmacol., 2008. **1**(4): p. 443-451.
- [15] Khorshid FA, *Comparative study of keloids formation in human and laboratory animals*. Med. Sci. Monit., 2005. **11**(BR): p. 212-219.
- [16] Khorshid FA, *Potential anticancer natural product against human lung cancer cells*. Trends Med. Res., 2009. **1**(4): p. 8-15.
- [17] Moshref SS. Khorshid FA. Jamal Y, *The effect of PM 701 on mice leukemic cells: I-tissue culture study of L1210 (in vitro) II-in vivo study on mice*. JKAU: Med. Sci., 2006. **13**(1): p. 3-19.
- [18] Nair AB. Kurma R. Harash S. Attimarad M. Al-Dubiab BE. Ahaider IA, *In vitro techniques to evaluate buccal films*. J Control Release, 2013. **166**(1): p. 10-21.
- [19] NEE A. Shoman S. Mohamed A, 2:115.2:115., *Nanocapsulation of Rift valley fever vaccine candidates and relative immunological and histopathological reactivity in out bred vs Swiss mice*. J. vacc. and vaccination 2011. **2**(1): p. 115-118.
- [20] Nujoud A. Gaafar A. Al-Otaibi B. Al-Jammaz I. AlHussein K. Aboussekra A, *Camel urine components display anti-cancer properties in vitro*. Journal of Ethnopharmacology, 2011. **143**(3): p. 819-825.
- [21] Reed LJ. Muench H, *A simple method of estimating fifty percent endpoints*. The American Journal of Hygiene, 1938. **27**(1): p. 493-497.
- [22] Roberts WA. Carter GA, *Essentials of veterinary virology*. Michigan State University Press, East Lansing, Mich, 1976: p. 64-65.
- [23] Rose JK. Whitt MA, *Rhabdoviridae: the viruses and their replication*. Fields virology. Lippincott Williams and Wilkins, Philadelphia, Pa. , 2001: p. p. 1221-1244.
- [24] Schwartmann G, *Marine organisms and other novel natural sources of new cancer drugs*. Ann Oncol, 2000. **11**(Suppl 3): p. 235-43.
- [25] Shinji H, *The broad anti-viral agent glycyrrhizin directly modulates the fluidity of plasma membrane and HIV-1 envelope*. The Biochemical journal., 2005. **392**(Pt 1): p. 191-9.
- [26] Thomson JA. Itskovitz-Eldor J. Shapiro SS. Waknitz MA. Swiergiel JJ, *Embryonic stem cell lines derived from human blastocysts*. Science (New York) 1998. **282** (5391): p. 1145-7.
- [27] Ueda R. Takahashi T. Watanabe H. Kato T. Suyama R. Takahashi T, *Chemosensitivity and radiosensitivity of small cell lung cancer cell line studied by a newly developed 3-(4,5-dimethylthiazol-2-yl)-2,5-diphenyltetrazolium bromide (MTT) hybrid assay*. Cancer Res., 1989. **49**(17): p. 4785-90.
- [28] VanMeerloo H J. Kaspers J, *Cell sensitivity assays: the MTT assay*. Methods Mol Biol. , 2011. **731**(1): p. 237-45.

Safety profile of PMF a fraction derived from camel urine on mice (acute study)

Samar O Rabah¹, Faten A Khorshid², Huda Aboarik³, Nahid H Hajrah⁴; Jamal S Sabir⁵ and Roop S Bora⁶

Abstract— Camel urine, a rich source of natural products with medicinal properties, has been used traditionally for the treatment of various diseases in Middle East. To exploit the therapeutic potential of various ingredients present in camel urine, evaluation of efficacy and safety profile is required. In the present study, we have evaluated the potential of camel urine fraction [PMF] to cause hepatotoxicity and nephrotoxicity in mice. Biochemical tests and complete blood picture [CBC] were performed after oral administration with varying doses of PMF. Blood samples were collected from the orbital sinus of mice after 24hrs of drug treatment. Liver function tests such as measurement of ALT, AST, Alkaline phosphatase, Gamma-glutamyltransferase [GGT], total bilirubin and albumin levels were performed to assess the hepatotoxic potential of PMF. Kidney function tests such as measurement of Na, K, Cl, total protein, creatinine, uric acid, blood urea nitrogen [BUN] and phosphatase level were performed in order to evaluate nephrotoxic effects of PMF in mice. Our study indicated that PMF did not cause any damage to liver and kidney even after treatment with twenty times of the therapeutic dose. The present study clearly suggested that PMF does not have any potential to cause hepatotoxicity and nephrotoxicity and it is safe for therapeutic use in human.

Keywords— Camel urine, drug safety, PM701, PMF.

I. INTRODUCTION

Camel urine has been used traditionally for the treatment of various diseases in many Middle East countries. It is known to be a rich source of several potent compounds with novel many structures and with wide variety of biological functions [1]. Drinking camel urine was shown to be effective in treating numerous cancers in human [2]. Previous studies have

This work was supported in part by ALZAMEL group as a Scientific Chair for Cancer Researches no "429/3/KBM".

1. Faculty of Science, Biology Department, King Abdulaziz University, Jeddah, Kingdom of Saudi Arabia. E-mail: samara@yahoo.com
2. Faculty of Science, Biology Department, King Abdulaziz University, P.O Box 42805, Jeddah 21551, Kingdom of Saudi Arabia
E-mail: fkhorshid@kau.edu.sa
3. Animal House King Fahad Research Center, King Abdulaziz University, Kingdom of Saudi Arabia, email: hudaraki55@yahoo.com
4. Faculty of Science, Biology Department, King Abdulaziz University, Jeddah, Kingdom of Saudi Arabia. E-mail: nhajrah260@gmail.com
5. Faculty of Science, Biology Department, King Abdulaziz University, Jeddah, Kingdom of Saudi Arabia. E-mail: jsabir2622@gmail.com.
6. Faculty of Science, Biology Department, King Abdulaziz University, Jeddah, Kingdom of Saudi Arabia E-mail: roopbora@yahoo.co.in.

suggested that PM701 (dried camel urine), has cytotoxic activity and induces apoptosis in cultured human lung cancer cells. Induction of apoptosis was also observed in cultured leukemia cells. PM701 was also found to be effective in preventing metastasis in animal models [1,3]. Several studies by Khorshid et al., [1;4] identified that Prophet Medicine fraction [PMF] is the biologically active fraction isolated from PM701, which has the potent anticancer activity [4]. The apoptotic effect of PMF in human cancer cell was analysed by TUNNEL method and it was observed that PMF was able to induce apoptosis in dose dependent manner. Cell proliferation study using MTT assay revealed that PMF treatment resulted in dramatic decrease in cell proliferation and cell survival [4]. It was also observed that Cesium [Cs] and Rubidium [Rb] particles are present in PMF as detected by Energy Dispersive X-ray attached to Scanning Electron Microscope. Treatment of lung cancer cell line A549 with PMF induced pores in the nuclear membrane resulting in the internalization of Cs and Rb with subsequent cell death due to elevation of cellular pH [4,5]. These studies clearly suggested that PMF derived from camel urine has tremendous therapeutic potential to treat various types of cancer.

The safety assessment of drug compounds is essential for its therapeutic use in humans. Several drugs have been withdrawn from the market due to the severe adverse effects in patients [6-8]. Most of these drugs have shown potential to cause hepatotoxicity and nephrotoxicity [9-11]. The objective of the present study is to evaluate the safety of PMF administration at high doses in mice and investigate its potential to cause hepatotoxicity and nephrotoxicity.

II. MATERIAL AND METHODS

A. Animals

125 adult mice were kept and maintained at room temperature with an adequate ventilation and normal 12-hours light-dark cycle and free access to food and water. All the studies were conducted in accordance with the laws and regulation of local governing authorities. These animals were divided into five groups, each one having twenty mice.

B. Treatment of mice with PMF

Group one was administered with a therapeutic dose of PMF (0.75 μ l + 75 μ l sterile water) through oral gavage. The second group was administered 2 X of the therapeutic dose (1.5 μ l PMF + 75 μ l sterile water). The third group was given 4 X of the therapeutic dose of PMF (3 μ l + 75 μ l sterile water). The fourth group of mice was administered with 20 X of the

therapeutic dose of PMF (15 µl PMF + 75 µl sterile water). The fifth group was the control group and was administered with 0.2ml sterile water only.

C. Biochemical Analysis

Animals were anaesthetized with ether and blood was collected after 24 hours post- administration from Orbital sinus and the sera of the animals were isolated. Erythrocyte count (RBCs), Haemoglobin concentration (Hb), packed cell volume (PCV), haematological indices {mean corpuscular volume (MCV), mean corpuscular haemoglobin (MCH) and mean corpuscular haemoglobin concentration (MCHC), total leukocytic count (TLC) and lymphocytic count; were estimated by using automated blood cells counter i.e Exigo haematology analyser. Liver function tests for Aspartate aminotransferase (AST) and alanine aminotransferase (ALT) activities were estimated spectrophotometrically by using the test kits supplied from Biodiagnostic Laboratories according to the method of Reitman and Frankel (12). Kidney functions tests including blood urea nitrogen (BUN), total protein (TP), uric acid (URCA) were determined according to Walker et al.,[13]. Multiple Comparisons dependent variable test was performed using software according to Howell [14].

III. RESULTS AND DISCUSSION

The blood components of mice administered with varying doses of PMF did not show any significant differences in the RBC count and platelets count as compared to control group. Similarly there was no significant difference in the concentration of Hb, MCV, MCH and MCHC between PMF treated and control groups as shown in Fig.1 and Table 1. The liver enzymes mainly ALT, AST, alkaline Phosphatase (ALP), albumin (ALB), total bilirubin (TBIL) and Gamma-glutamyltransferase (GGT) did not show any significant differences between treated mice with PMF and control groups as shown in Fig.2 and Tables 2,3 and 4.

In addition the kidney function tests including Na, K, Cl, creatinine, blood urea nitrogen, uric acid, phosphorus and total protein values did not show any significant difference between treated mice with PMF and control groups as shown in Fig.3 and Table 5.

Whereas studies have reported that complete blood cell count (CBC) is one of the most common laboratory test to evaluate the safety of a drug compound. The measurement of these parameters is useful in diagnosis of different types of anemia, autoimmune diseases, neoplasm and inflammation [15]. In the present study, administration of PMF in mice using the doses higher than the therapeutic dose did not show any effect on the blood components as shown by the Multiple Comparisons dependent variable statistical test.

Deursen et al., [2010] showed that liver function abnormalities are frequently observed in patients with heart failure; in particular high levels of bilirubin, LDH and GGT have been detected [16]. Alteration in liver function tests including

bilirubin concentration, AST, GGT and alkaline phosphatase activity were related to liver injury during heart failure. Thus, abnormalities in liver function tests have prognostic importance in chronic heart failure. Although we have no alterations in liver enzymes activity, we could reveal that these results showed the safety of PMF on heart function.

Kluwe [1981] analysed the nephrotoxic potential of various compounds including biphenyl, carbon tetrachloride and mercuric chloride in male rats [17]. Several renal function tests such as measurement of urine specific gravity, pH & volume, urinary excretion of glucose, protein, electrolytes & various enzymes, serum concentrations of urea nitrogen, creatinine & electrolytes, creatinine clearance and kidney weight, were performed after administration of four different doses of each compound. Ability to concentrate urine after water deprivation, kidney morphology and accumulation of organic ions by renal cortical tissue *in vitro* was also examined. In general, it was observed that *in vitro* accumulation of organic ions, urinary concentrating ability and kidney weight were the most sensitive and consistent indicators of nephrotoxicity [17]. On the other hand, standard urinalyses, serum analysis and pathological changes in renal morphology were less sensitive and less consistent indicators of renal injury. The most advantageous tests, therefore, appeared to be those that measured total, functional renal capacity. The administration of different doses of PMF showed none of the previous mentioned signs on the treated animals.

Various studies have indicated that increase in uric acid level is generally associated with the development of hypertension, abdominal obesity, insulin resistance, cardiovascular disease and renal failure [18]. These studies have shown a correlation between increased uric acid concentrations with the oxidative stress, endothelial dysfunction, inflammation, subclinical atherosclerosis and increased risk of cardiovascular disease.

Our study clearly showed that there was no significant difference in liver and kidney function tests in PMF treated group as compared to the control group using the multiple comparisons dependent variable statistical test, suggesting that PMF does not cause liver or kidney injury in mice.

Although our previous work indicted the efficiency of PMF in fighting cancer cells [19-24], this work improved the safety of PMF for administration for human in clinical trial.

Conclusion

In conclusion, our study clearly suggests that PMF derived from camel urine, is a safe drug and does not have potential to cause hepatotoxicity and nephrotoxicity. Hence, PMF has tremendous therapeutic potential as a safe and potent anticancer agent for treatment of various types of cancer in human.

FIGURES AND TABLES

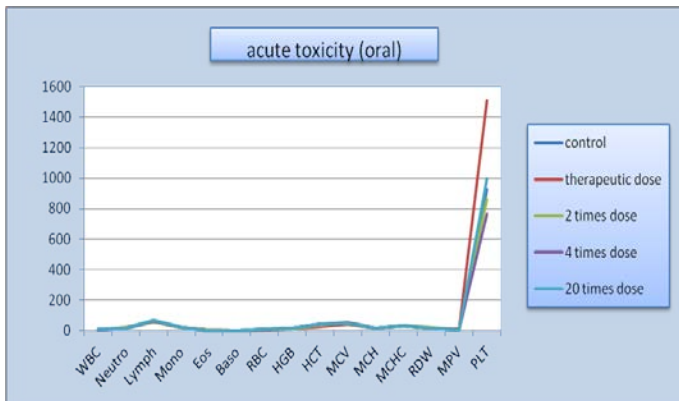


Fig.1. Complete blood picture showing no significant difference in the numbers of different components of blood after oral administration with different doses of PMF in comparison with the control group.

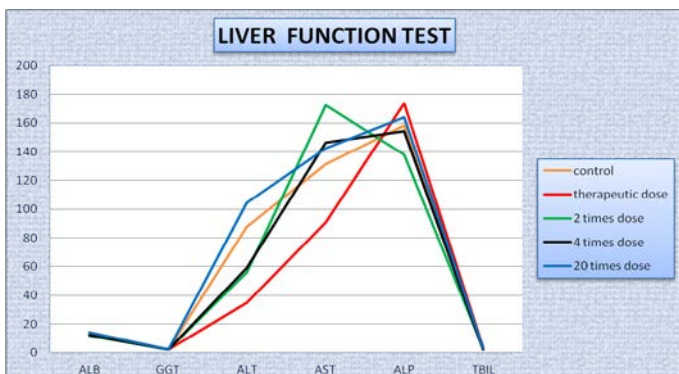


Fig.2. Liver function tests indicating no significant difference in liver enzymes between PMF treated and control groups.

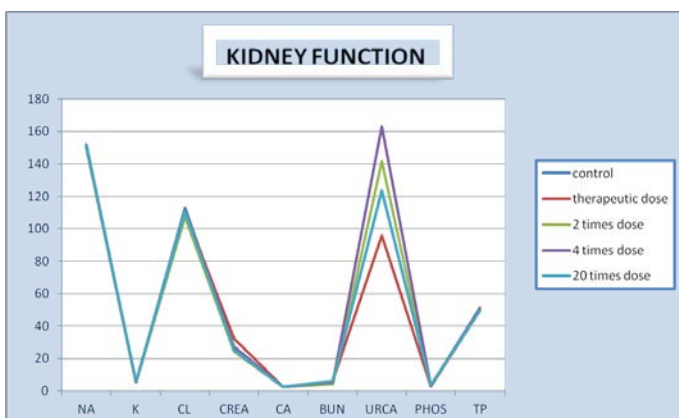


Fig.3: Analysis of Kidney function tests revealed no significant difference in kidney functions parameters between PMF treated and control groups.

Control Group	Exp. Group	Mean	Std. Error	Sig.	95% Confidence Interval	
					Lower Bound	Upper Bound
Control	therapeutic dose	-583.500	202.5998	.035	-1104.2995	-62.7005
	2 times dose	64.000	202.5998	.765	-456.7995	584.7995
	4 times dose	159.000	202.5998	.468	-361.7995	679.7995
	20 times dose	24.5000	202.5998	.908	-496.2995	545.2995

Table 1. Multiple Comparisons dependent variable of PLT showing that the differences between all groups treated with PMF are not significant as compared with control, whereas the significant is (0.005 – 0.0005).

Control Group	Exp. Group	Mean	Std. Error	Sig.	95% Confidence Interval	
					Lower Bound	Upper Bound
Control	Therapeutic dose	52.66667	33.58703	.148	-22.1699	127.5032
	2 times dose	31.66667	33.58703	.368	-43.1699	106.5032
	4 times dose	28.66667	33.58703	.413	-46.1699	103.5032
	20 times dose	-17.0000	33.58703	.624	-91.8366	57.8366

Table 2. Multiple Comparisons dependent variable of ALT showing that the differences between all groups treated with PMF are not significant as compared with control.

Control Group	Exp. Group	Mean	Std. Error	Sig.	95% Confidence Interval	
					Lower Bound	Upper Bound
Control	Therapeutic dose	73.6666	59.1307	.241	-58.0848	205.4182
	2 times dose	-7.6666	59.1307	.899	-139.4182	124.0848
	4 times dose	18.3333	59.1307	.763	-113.4182	150.0848
	20 times dose	22.0000	59.1307	.718	-109.7515	153.7515

Table3. Multiple Comparisons dependent variable of AST showing that the differences between all groups treated with PMF are not significant as compared with control, whereas the significant is (0.005 – 0.0005).

Control Group	Exp. Group	Mean	Std. Error	Sig.	95% Confidence Interval	
					Lower Bound	Upper Bound
Control	Therapeutic dose	73.66667	59.13074	.241	-58.0848	205.4182
	2 times dose	-7.66667	59.13074	.899	-139.4182	124.0848
	4 times dose	18.33333	59.13074	.763	-113.4182	150.0848
	20 times dose	22.00000	59.13074	.718	-109.7515	153.7515

Table 4. Multiple Comparisons dependent variable of ALP showing that the differences between all groups treated with PMF are not significant as compared with control, whereas the significant is (0.005 – 0.0005).

Control Group	Exp. Group	Mean	Std. Error	Sig.	95% Confidence Interval	
					Lower Bound	Upper Bound
Control	Therapeutic dose	28.0000	15.25487	.096	-5.9900	61.9900
	2 times dose	-18.0000	15.25487	.265	-51.9900	15.9900
	4 times dose	-39.3333	15.25487	.027	-73.3233	-5.3434
	20 times dose	.00000	15.25487	1.000	-33.9900	33.9900

Table. 5: Multiple Comparisons dependent variable of URCA showing that the differences between all groups treated with PMF are not significant as compared with control, whereas the significant is (0.005 – 0.0005).

ACKNOWLEDGMENT

F. A. Khorshid Author thanks Prof Soad Shaker Ali for helpful suggestions during this project

REFERENCES

- [1] Khorshid FA. Osman AMM. Abdel-Sattar E, *Cytotoxic activity of bioactive fractions from PM701*. Elect J Environ Agri Food Chem, 2009. **8**(11): p. 1091-1098.
- [2] Alhaider AA. El Gendy MA. Korashy HM. El-Kadi AO, *Camel urine inhibits the cytochrome P450 1a1 gene expression through an AhR- dependent mechanism in HepG2 cell line*. J Ethnopharmacol, 2011. **133**(1): p. 184-190.
- [3] Moshref SS. Khorshid FA. Jamal Y, *The effect of PM 701 on mice leukemic cells: I-tissue culture study of L1210 (in vitro) II-in vivo study on mice*. JKAU: Med Sci 2006. **13**(1): p. 3-19.
- [4] Khorshid FA. Rahimaldeen SA. AL-Amri JS, *Apoptosis study on the effect of PMF on different cancer cells*. Int J Biol Chem 2011. **5**(1): p. 150-155.
- [5] Khorshid FA, *The effect of the viscosity of the medium in the reaction of cells to topography*, in Medicine2001, Glasgow University: UK.
- [6] Bertino J. Fish D, *The safety profile of the fluoroquinolones*. Clin Ther 2000. **22**(1): p. 798- 817.
- [7] Leitner JM. Graninger W. Thalhammer F, *Hepatotoxicity of antibacterials: Patho- mechanisms and clinical data*. Infection, 2010. **38**(1): p. 3-11.
- [8] Sabir JSM. AbuZinadah OA. Bora RS. Ahmed MMM. Saini KS, *Role of toxicogenomics in the development of safe, efficacious and novel anti-microbial therapies*. Infect Disord -Drug Targets, 2013. **13**(1): p. 206-214.
- [9] Liguori MJ. Anderson MG. Bukofzer S. McKim J. Pregenzer JF. Retief J. Spear BB. Waring JF, *Microarray analysis in human hepatocytes suggests a mechanism for Hepatotoxicity induced by Trovafloxacin*. Hepatol, 2005. **41**(2): p. 177-186.
- [10] Thukral SK. Nordone PJ. Hu R. Sullivan L. Galambos E. Fitzpatrick VD. Healy L. Bass MB. Cosenza ME. Afshari CA, *Prediction of nephrotoxicant action and identification of candidate toxicity-related biomarkers*. Toxicol Pathol 2005. **33**(3): p. 343-355.
- [11] Guengerich FP, *Mechanism of drug toxicity and relevance to pharmaceutical development*. Drug Metab Pharmacokinet, 2011. **26**(1): p. 3-14.
- [12] Reitman S. Frankel S, *A colorimetric method for the determination of serum glutamic oxaloacetic and glutamic pyruvic transaminases*. Am J Clin Pathol, 1957. **28**(1): p. 56-63.
- [13] Walker HK. Hall WD. Hurst JW, *Clinical methods: The History, Physical, and Laboratory Examinations*. 3 ed. 1990, Boston, USA: Butterworths.
- [14] Howell DC, *Statistical methods for psychology*. 5th ed. 2002, Canada: Duxbury Press.
- [15] Tefferi A. Curtis AH. Inwards DJ, *How to interpret and pursue an abnormal complete blood cell count in adults: Concise review for clinician*. Mayo Clin Proc, 2005. **80**(7): p. 923-936.
- [16] Deursen VM. Van Damman K. Hillege HL. Van Beek AP. Van Veldhuisen DJ. Voors AA, *Abnormal liver function in relation to hemodynamic profile in heart failure patients*. J Cardiac Failure, 2010. **16**(1): p. 84-90.
- [17] Kluwe WM, *Renal function tests as indicators of kidney injury in subacute toxicity studies*. Toxicol Appl Pharmacol 1981. **57**(5): p. 414-424.
- [18] Gagliardi ACM. Miname MH. Santos RD, *Uric acid: A marker of increased cardiovascular risk*. Atherosclerosis, 2009. **202**(1): p. 11-17.
- [19] Ahmed GA. Khorshid FA. Kumsani TA, *FT-IR Spectroscopy of A549 Cells Treated with PMF: Structural changes in DNA and cell membrane*. Journal of Thoracic Oncology, 2010. **5**(1): p. 46S Abstract.
- [20] Ali A. Khorshid FA. Aboarky H. Osman AM, *Tumor Lung Cancer Model for Assessing Anti-neoplastic Effect of PMF in Rodents: Histopathological Study*. Trends in Applied Sciences Research, 2011. **6**(1): p. 1214-1221.
- [21] Khorshid FA, *The Cytotoxic effect of PM 701 and its fractions on cell proliferation of breast cancer cells, McF7*. American J of Drug Discovery and Development, 2011.
- [22] Khorshid FA. Raouf GA. El-Hamidy SM. Al-amri GS. Alotaibi NA. Kumsani TA, *PMF Cesium & Rubidium Nanoparticles Induce Apoptosis in A549 Cells*. Life Sci. Journal, 2011. **8**(3): p. 15-19.
- [23] Alghamdi Z. Khorshid FA, *Cytotoxicity of the Urine of Different Camel Breeds on the Proliferation of Lung Cancer Cells, A549*. Journal of Natural Sciences Research, 2012. **2**(5): p. 9-16.
- [24] Mahboub FA. Khorshid FA. Emwas AM, *The Cytotoxic Effect of Small and Large Molecules of PMF Fraction Extracted from Camel Urine on Cancer Cells*. British Journal of Medicine and Medical Research, 2014. **6**(4).

Magnetic effects in the thermodynamics of the process of thinking

Aibassov Yerkin Zhakenovich^{1*}, Savizky Ruben², Yemelyanova Valentina¹, Shakieva Tatyana¹, Tussupbaev Nessipbay¹, Bulenbayev Maxat¹, and Blagikh Evgeniy¹

¹*Research Institute of New Chemical Technologies and Materials, Kazakh National University Al-Farabi, Almaty 005012, Kazakhstan*

²*Department of Chemistry the Columbia University, New York, 005012,*

Abstract

We have shown that the process of information and thinking can be modeled on the basis of chemical thermodynamics. We offer general equations to calculate the thinking of the work of judgment the L and of entropy solutions G in the presence of a magnetic field. As a result, studies have shown that the magnetic effects strongly influence the thermodynamics of the process of thinking.

Key words: Magnetic effect, thermodynamics, process of thinking, Shonon equation.

1. Introduction

The human brain is the most mysterious organ that controls thought processes.

In recent years, many works devoted to the thermodynamics of the thinking process [1-6].

We have previously been shown that the thermodynamic functions of internal energy dU and free energy dF in the presence of a magnetic field [5]:

$$dU = TdS + 1/4\pi HdB \quad (1)$$

$$dF = -SdT + 1/4\pi HdB \quad (2)$$

It was also shown that the Nernst equation in a magnetic field change, and is described by the equation [6]:

$$E = E^0 + RT/nF \ln a_{Ox}/a_{Red} + 1/4\pi H dB \quad (3)$$

The purpose of this work is an attempt to study the magnetic effects in thermodynamics thought processes and to find patterns of thinking mechanism in living organisms.

2. Theory

Thinking - certainly a biological phenomenon, and should therefore be subject to the atomic and molecular description. Science has established that the complex DNA and RNA molecules are capable of performing the function of storage n transmission of information is even more faith in the fact that the complex information processes, including thinking, made atomic-molecular mechanisms.

The fundamental thermodynamic properties of Shannon-type thinking is that the solution to

Aibassov Yerkin Zhakenovich*, Professor, research field: metalorganic chemistry of uranium and thorium, As, Sb and Bi. E-mail: erkin53@mail.ru.

the problem of information is not a process of spontaneous and necessary, ie running with decreasing free energy, but, on the contrary, requires the expenditure of work. This expresses the basic property information, that it is not deducible from the known data as a deduction - otherwise it would not be at all necessary, as always could be obtained from these data - but gives the new independent information that do not have believed to be reliable.

The process of logical thinking is similar to spontaneous thermodynamic process: In both cases, the original particle system (information) to be converted to a finite system of new particles or inferences. As spontaneous process in the thermodynamics with decreasing capacity of the free energy, and always leads to a more stable state. Spontaneous logical process flows down the free energy and give the thermodynamically stable as a result of the withdrawal or deduction. The process of thinking is described thermodynamically expression:

$$\text{Work Information: } I_{\text{Inform}} < 0, \Delta\varphi_{\text{Inform}} < 0, \quad (4)$$

$$\text{The work of judgment (solution): } L_{\text{Solution}} \gg 0, \Delta\varphi_{\text{Solution}} \gg 0, \quad (5)$$

where $\Delta\varphi$ - the fall of the free energy in the act of information or diskursii.

Between these extremes there is an intermediate area in which the magnitude of the fall of the free energy is large enough to process the judgment was spontaneous, but not high enough for it to be unique. This is - an ambiguous area of probabilistic thinking.

In connection with the (equation (4)) increase in free energy of the information and hence its instability, it has to be stored in anti-entropy devices - in memory, in the records of a particular type, including a variety of codes - otherwise it will inevitably dissipate.

1. Results and discussion

Energy - is the ability to do the job, but also the ability to create and modify any type of order in nature.

Dynamic energy $E = Z\lambda$ - \exists energy action in a certain space, energy vektorization energy; Ψ - energy of the order.

Dynamic energy is manifested in two forms: vector $E_V = E\eta$, giving direction and displacement of an object in its area of action and Brownian $E_B = E(1 - \eta)$, extending the scope and status of the process.

$$\text{Hence the total energy } U_{\text{Total}} = E_V + E_B + \Psi. \quad (6)$$

The information in contrast to the thinking can not appear as a product of pure inferences from other data. It is impossible, without spending any work, just standing on the platform, by "pure" reasoning to know address of your friend.

Information data are logically independent of each other, it is as if from nowhere output set of "primary", independent data (in physical chemistry - the system of non-interacting particles).

Thinking (especially in its marginal, formal logical form) operates on the information data according to the laws of logic, and it resembles a chemical reaction "dissimilar" of the particles of the gas mixture to react with strictly defined laws.

The result of thinking is the conclusion that can be recorded. They include various elements of the original information.

Thinking there where begins the act of judgment as a result of a conscious selection of the source data come parcels in the form of some data (information), self-evident position (axioms) and certain assumptions (hypotheses), and subjecting them to an algorithm constructed in accordance with the laws of logic '.

With this information system, axioms and hypotheses thinking process always leads to a definite conclusion. This is a very important property of thinking. It is similar to some spontaneous process, the outcome of which, regardless of the physical and chemical properties of the medium, where it occurs, is always the same!

It's like a roller coaster movement of rail road. Point of arrival is not dependent on anything. It is defined only by the desire to move the system to a stable state.

Thus, the thinking process is modeled on the basis of chemical thermodynamics in the form of spontaneous transition ($Z - 1$) varieties of "chances" that are concentrated in a single cell in a k-th some sort of a drop in the free energy and entropy, expressed by the equation of thinking:

The work of judgment (Solution):

$$L = \sum p_i \log p_i + \Delta\phi^o = I_{Vin} + \Delta\phi^o > 0, \quad (7)$$

Entropy judgments (Solutions):

$$G = \sum p_i \log p_i + \Delta H^o = H_{Sannon} + \Delta H^o > 0, \quad (8)$$

We offer general equations to calculate the thinking of the work of judgment L and entropy solution G in the presence of a magnetic field:

$$L = I_{Vin} + \Delta\phi + 1/4\pi H dB, \quad (9)$$

$$G = H_{Sannon} + \Delta H + 1/4\pi H dB, \quad (10)$$

The final result of the act of thinking - a conclusion or inference - and there is a stable state of mind in the thermodynamic sense of the word.

Amazing uniqueness of the final result of mental activity proves it strictly directed, "spontaneous", the vector character, apparently independent from the chaos of Brownian motion of atoms and molecules that make up the substance of the brain or any other mechanism where there is thinking.

Inference can be repeated numerous times with the same result. For example, you can repeat as often as proof of the Pythagorean theorem. This means that the probability of a thermodynamic system, which carries out the process of thinking is always equal to one, which corresponds to the only possible way of thinking of those responsible for the microparticles, their full order and they are not susceptible to thermal chaos.

2. Conclusion

The analysis shows that the thinking process is modeled on the basis of chemical thermodynamics in the form of spontaneous transition ($Z - 1$) varieties of "chances" that are concentrated in a single cell in a k -th some sort of a drop in the free energy and entropy, expressed by the equation of thought.

We offer general equations to calculate the thinking of the work of judgment L and entropy solution G in the presence of a magnetic field:

$$L = I_{Vin} + \Delta\varphi + 1/4\pi H dB, \quad (9)$$

$$G = H_{Sannon} + \Delta H + 1/4\pi H dB, \quad (10)$$

We have shown that the process of thinking can be modeled on the basis of chemical thermodynamics. We offer general equations to calculate the thinking of the work of judgment the Land of entropy solutions G in the presence of a magnetic field. As a result, studies have shown that the magnetic effects strongly influence the thermodynamics of the process of thinking.

The consequence of the above is the ability to save the information entropy and speed of thinking in three dimensions, so the speed of thought to increase by several orders of magnitude.

Research in this direction will be continued.

Acknowledgments

The authors would like to thank Lynn C. Francesconi (Hunter College CUNY), Peter C. Burns (Notre Dame University, Indiana) and Christopher L. Cahill (George Washington University) for discussion of the results.

References

- [1] Claude E. Shannon: *A Mathematical Theory of Communication*, Bell System Technical Journal, Vol. 27, pp. 379–423, 623–656, 1948.
- [2] Claude E. Shannon and Warren Weaver: *The Mathematical Theory of Communication*. The University of Illinois Press, Urbana, Illinois, 1949.
- [3] Claude E. Shannon: *Programming a Computer for Playing Chess*, Philosophical Magazine, Ser.7, Vol. 41, No. 314, March 1950.
- [4] David Levy: *Computer Gamesmanship: Elements of Intelligent Game Design*, Simon & Schuster, 1983.
- [5] Aibassov Yerkin, Yemelyanova Valentina, etc., Study of changes in the thermodynamic functions in a magnetic field, J. Chem. Chem. Eng., 8, (2014), p. 119-122.
- [6] Aibassov Yerkin, Yemelyanova Valentina, etc., Derivation of the equation Nernst-Aibassov in a magnetic field, J. Chem. Chem. Eng., 9, (2015), p. 218-220.

ORGANIC-INORGANIC ION-EXCHANGERS CONTAINING NANOPARTICLES OF ZIRCONIUM HYDROPHOSPHATE FOR ELECTRODEIONIZATION PROCESSES

Yu.S. Dzyazko^a, L.N. Ponomaryova^a, Yu.M. Volkovich^b, V.E. Sosenkin^b, V.N. Belyakov^a

^a*V.I. Vernadskii Institute of General and Inorganic Chemistry of the NAS of Ukraine, acad. Palladin ave. 32/34, Kyiv-142, 03680, Ukraine, dzyazko@gmail.com*

^b*A.N. Frumkin Institute of Physical Chemistry and Electrochemistry of the RAS, Leninskii pr, 31, Moscow, 119071, RF, yuvolf40@mail.ru*

ABSTRACT

A series of organic-inorganic materials based on flexible gel-like cation exchange resin were obtained by means of its modification with zirconium hydrophosphate. The samples were investigated using transmission and scanning electron microscopy, standard contact porosimetry as well as impedance spectroscopy. Both non-aggregated nanoparticles (6-10 nm) and their aggregates (from 25 nm up to several microns) were found inside the polymer. Decreasing of temperature, at which the modifier is precipitated, causes a growth of amount of single nanoparticles, which occupy transport pores. Evolution of porous structure of the polymer constituent affected by the inorganic particles is considered, the modifier has been shown to decrease the content of free water in the polymer, to increase swelling pressure, which is determined according to Gregor model, and also to provide a growth of ion-exchange capacity in a comparison with the pristine resin (from 0.56 up to 2.3 mmol cm⁻³). Thus, the inorganic constituent formally behaves like a cross-linking agent. However, increasing of the modifier amount causes a growth of electrical conductivity of the composites from 0.2 to 0.8 Ohm⁻¹m⁻¹. The ion-exchanger with a maximal content of zirconium phosphate (67 %) was applied to removal of Cd²⁺ ions from a solution containing also hardness ions and organics. The composite provide continuity of the process, the removal degree of toxic ions reaches 96-98%. Redistribution of the nanoparticles in the polymer, which is affected by electric field, has been found.

Key words: electrodeionization, electrodialysis, organic-inorganic ion-exchanger, zirconium phosphate, standard contact porosimetry.

1. Introduction

In opposite to electrodialysis, electrodeionization (EDI) involves not only membranes, but also granulated ion-exchange resins between them: cation-exchanger, anion-exchanger or their mixture [1-3], particularly layered bed [4]. Simultaneous ion exchange and transport of sorbed species through the ion-exchanger bed and membranes provide continuity of the EDI process. This hybrid technique is applied to weakly-concentrated solutions, since the ion-exchanger particles intensify mass transport. The EDI method allows one to solve different tasks, such as treatment of reverse osmosis permeate [4], production of ultrapure water [5], removal of Ni²⁺ [6-12], HCrO₄⁻ [13-16], Cu²⁺ [17-19] ions from electroplating wastes, recovery of Co²⁺ [20, 21] and Sr²⁺ [21] ions from coolant of nuclear reactors, F⁻ anions removal from tap water [22], water softening [23] etc.

Removal of heavy metal ions from diluted solutions is complicated by low selectivity of ion exchange resins and their poisoning with organics [6]. In order to overcome these difficulties, glass-like hydrogel of zirconium hydrophosphate

(ZHP) has been proposed [8]. A disadvantage of this ion-exchanger is gradual fragmentation of grains.

Organic-inorganic ion-exchangers are widely used for removal of heavy metal ions from diluted solutions by means of ion exchange [10, 24-28]. The material based on flexible resin was also applied to the EDI process of Ni^{2+} removal from a combining weakly-concentrated solution [10]. However, the process efficiency was rather low. In order to overcome this disadvantage, functional properties of the ion exchanger, namely electrical conductivity and ion exchange capacity, have to be improved.

These properties are known to be determined by location of nanoparticles in one or other pores of the polymer matrix [26, 28]. Porous structure of swollen ion-exchange polymer includes several types of pores [29-31]. Gel fields of the polymer are riddled with nanosized so called “transport pores” (clusters and narrower channels between them), where functional groups are placed. These pores are responsible for ion movement. Non-aggregated nanoparticles in clusters and channels enhance the transport. Hydrophobic links of the polymer chains are located in voids between gel fields, a size of which is more than 20 nm. The largest pores are the structure defects.

The aim of the investigation is a purposeful control of a state of the inorganic constituent in ion exchange polymer in order to provide maximal content of non-aggregated nanoparticles in transport pores. The purpose of the study is also to establish the influence of the particles on the polymer structure and functional properties of the composites. At last, testing of the materials in the EDI process is necessary.

Flexible gel-like cation exchange resin has been chosen as a polymer matrix, since this material can be used successfully for removal of d-metal ions by means of EDI [6]. Macroporous and rather rigid ion exchange polymers were used earlier for composite preparation, mainly aggregated nanoparticles were found for these materials [24, 25, 28]. In this study, ZHP was used as a modifier, since it provides selectivity of the composites [10, 24, 26-28] due to formation of complexes of sorbed ions with functional groups of this ion-exchanger [32, 33].

The composites were tested for removal of Cd^{2+} ions from multicomponent solution containing also hardness ions and organics. The equipment, which contains details with cadmium coatings, is attractive for petroleum, automotive, electric and electronic industries especially for shipbuilding [34]. This is due to variable properties of cadmium coatings: stability against corrosion, low friction coefficient etc. In owing to high toxicity of cadmium ions, their removal from electroplating wastes is an important task,

2. Experimental

2.1. Ion-exchangers

Such strongly acidic cation-exchanger as (*Dow Chemical*), which contains 2 % DVB, was used as a polymer matrix. Further the resin is marked as *CR*.

The modification procedure involved: (i) swelling a weighted amount of the resin in deionized water; (ii) impregnation with a 1 M ZrOCl_2 solution for 24 h at 353 K followed by separation of solid and liquid by means of centrifugation; (iii) treatment with a 1 M H_3PO_4 solution at 273 K and phase separation, washing with deionized water up to pH 7 of the effluent; (iv) drying under vacuum at 343 K followed by a treatment with ultrasound at 30 kHz using a *Bandelin* ultrasonic bath (*Bandelin*); (v) drying in a desiccator over CaCl_2 at 293 K down to constant mass.

The differences of this technique from [10, 26] is higher temperature of impregnation with a zirconium-containing solution and lower temperature of ZHP precipitation.

The (i)-(v) procedures were repeated several times. After each modification cycle, a weighted sample was taken for investigations. The samples, which were researched in detail, were marked as *CR-ZHP-1* (one modification cycle) and *CR-ZHP-7* (seven cycles). The *CR-ZHP-0* sample modified one time under room temperature similarly to [10] was also studied for a comparison.

2.2. Visualization of inorganic particles and polymer heterogeneities

Pretreatment of the ion-exchangers involved their grinding followed by ultrasonic treatment. TEM images were obtained by means of a *JEOL JEM 1230* transmission electron microscope (*Jeol*). In order to shade heterogeneities of the polymer, the samples were treated with a 0.001 M CuSO₄.

A *JEOL JSM 6700 F* scanning electron microscope (*Jeol*) was also used for ZHP visualization. Preliminarily an ultrathin layer of platinum was deposited onto the particles at 3 Pa using an *JEOL JFC-1600* Auto fine coater (*Jeol*).

2.3. Porosity measurements

Standard contact porosimetry (SCP) [35-38] was applied to investigation. Preliminary the samples were vacuumed at 353 K, weighted and put into a paper tablet. The tablet was placed between two ceramic standards, the set was impregnated with deionized water at 353 K. The contact between the investigated and standard samples was provided at 0.1 kPa. During drying at 293 K, the set was disassembled periodically, each its element was weighted. Based on the experimental results of mass loss, the pore size distributions as well as isotherms of water adsorption were plotted taking into consideration a known contribution of the paper.

Archimedes (picnometer) method [39] was also used to determine total porosity and particle density.

2.4. Functional properties

Total ion-exchange capacity of the materials towards Na⁺ (A) was determined by their treatment with a 0.1 M NaOH solution followed by washing with deionized water, regeneration and flame-photometric analysis of the effluent [10].

Electrical conductivity of H-forms of the ion-exchangers was measured at 298 K similarly to [40]. Preliminary additionally sorbed electrolyte was removed from the solid by multiple washing with deionized water. The sample was placed into a prismatic cell supplied by platinum electrodes (an area of each electrode was 2 cm², a distance between them was 1 cm). The cell with the ion-exchanger was filled with deionized water. The admittance spectra within the interval of 10⁻²-10⁶ Hz were obtained using an *Autolab* impedance system. The dc conductivity of the bed was determined from the wide plateau of real part of admittance similarly to [41].

2.5. Electrodeionization

The experimental set-up [7, 13] involved a three-compartment electrodialysis cell, 3 independent liquid lines, power supplier and measurement instrumentation. Geometric parameters of the space between the membranes (central compartment), where the ion-exchanger was placed, were as follows: an effective membrane area was 16 cm², a distance between the membranes was 1 cm, a height of the ion-exchanger bed was 16 cm. A top of the cell was opened to provide a possibility of bed compaction in order to avoid its fluidization.

The electrode compartments were separated from the centre chamber with homogeneous *Nafion 117* cation-exchange membranes (*DuPont*). A 1 M H₂SO₄ solution circulated through the anode compartment, the cathode camera was filled with a 1 M HCl solution. A volume of both catholyte and anolyte was 200 cm³.

Tap water containing 1.2 mmol dm^{-3} Ca^{2+} , 0.5 mmol dm^{-3} Mg^{2+} and also organics (mainly humates) was used for preparation of a Cd^{2+} -containing solution (0.5 mmol m^{-3} Cd^{2+}) after preliminary acidification down to pH 2.5. The solution passed through the central compartment according to “once through” scheme with a flow velocity of $60 \text{ cm}^3 \text{ min}^{-1}$. The process was performed at 8 V, probes (2 cm^3) from the cathode and central compartments were analyzed with an atomic absorption method using a *Pye Unicam SP9* spectrophotometer.

The EDI processes have been performed for 20 h, in the case of the *CR-ZHP-7* sample the process was repeated 5 times. After each experiment, the ion-exchanger was removed from the cell, washed with a 1 M H_2SO_4 solution and deionized water, further this ion exchanger was used again. Particle density of the samples was determined with Archimedes method after each series of EDI-regeneration. After the fifth experiment, the sample (marked as *CR-ZHP-7-ED*) was investigated using a SCP technique.

The *CR-ZHP-7* ion-exchanger (1 g) was also treated with a Cd^{2+} -containig solution of abovementioned composition (1 dm^{-3}), regenerated, further its particle density was determined. This procedure (blanc experiment) was repeated 5 times.

3. RESULTS AND DISCUSSION

3.1. ZHP precipitation inside ion exchange polymer

Zirconium ions forms polymerized hydroxocomplexes in aqueous media, such as $[\text{Zr}_4(\text{OH})_8(\text{H}_2\text{O})_{16}]^{8+}$ (where x is the integer), their composition strongly depends on the solution pH [42, 43]. During impregnation of the resin with a highly concentrated ZrOCl_2 solution, a part of species is sorbed according to ion exchange mechanism. The ion-exchanger contains also both cations (zirconium hydroxocomplexes as well as H^+) and anions (Cl^-), which are sorbed additionally.

Treatment of the impregnated resin with phosphoric acid causes formation of non-aggregated nanoparticles (10-15 nm) (Fig. 1a). Heterogeneities of the dry polymer (shaded with Cu^{2+}), from which the clusters are formed during swelling, are seen in Fig. 1b. Small aggregates of irregular shape (up to 25 nm) are also visible inside the polymer (see Fig. 1a). These particles can fill voids between gel fields. Large aggregates of micron size are formed in structure defects (Fig. 1c).

The sample, which was treated with phosphoric acid at low temperature, shows higher amount of non-aggregated nanoparticles in a comparison with *CR-ZHP-0* (compare Figs. 1a and 1d). The smallest ZHP particles are dissolved during precipitation in accordance with Ostwald-Freundlich equation [44]:

$$\ln \frac{C}{C_\infty} = \frac{\beta v_m \sigma \cos \varphi}{R T r} . \quad (1)$$

Here C is the compound concentration, C_∞ is the concentration of saturated solution, β is the shape factor of particles, v_m is the molar volume of the compounds, σ is the surface tension of the solvent, φ is the wetting angle, R is the gas constant, T is the temperature, r is the particle radius. In the case of hydrophylic compounds like ZHP, $\cos \varphi$ is assumed to be equal 1.

Since the C and C_∞ values for insoluble ZHP are extremely low, a size of the dissolved particles is affected mainly by temperature conditions. Decreasing in the temperature prevents dissolution of the smallest particles. In the case of higher temperature, dissolution of small particles and reprecipitation of larger formation occur. In other words, the control of temperature allows us to obtain ZHP particles in one or the other pores of the polymer matrix.

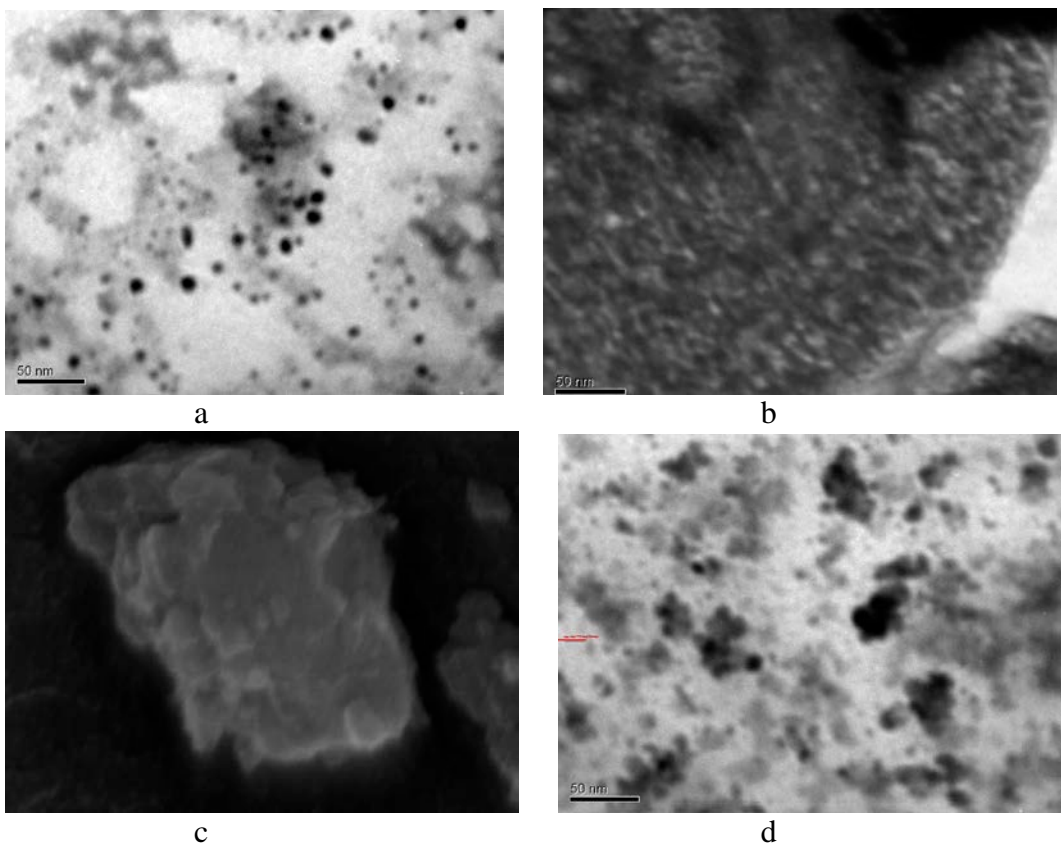


Fig. 1. Microphotographs of the *CR-ZHP-1* (a-c) and *CR-ZHP-0* samples. TEM images (a, b, d) show non-aggregated nanoparticles of ZHP and their small aggregates (a, d) as well as heterogeneities of the polymer (b). Large aggregates, which are located in structure defects are seen in SEM image (c). Decreasing in the temperature of ZHP deposition allows us to increase the fraction of single nanoparticles.

Impregnation of the resin with a ZrOCl_2 solution at elevated temperature leads to an increase of the modifier content in the polymer and results in a growth of ion exchange capacity per volume unit (A_v) of the composites (Fig. 2). This is evidently due to higher content of zirconium-containing species sorbed according to non-exchange mechanism. Inconsiderable growth of the ZHP content after the fifth modification cycle is probably due to formation of secondary porosity inside the polymer matrix. Small pores between the nanoparticles in the aggregates can be a barrier against additionally sorbed electrolyte, when the resin is treated with ZrOCl_2 or H_3PO_4 solutions.

Increasing in mass fraction (m) of incorporated ZHP causes an increment of ion exchange capacity. The $A_v - m$ plots show 2 regions: slow growth (due to considerable swelling of the composite [26, 28]) and rapid increase (due to decrease of swelling).

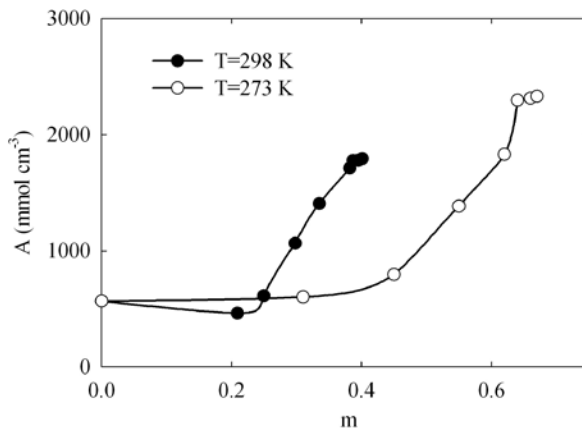


Fig. 2. Ion exchange capacity of the composites per volume unit as a function of mass fraction of ZHP. Legend shows temperature of the modifier precipitation. The curve for the samples obtained under room temperature was plotted according to data [10]. Increasing in temperature, at which the resin is impregnated with a $ZrOCl_2$ solution, allows us to amplify the content of the inorganic constituent in the polymer and also to improve ion exchange ability of the composites.

3.2. Porosity of the polymer constituent and isotherms of water adsorption

Since the conditions of thermal pre-treatment before the porosity measurements cannot provide removal of bonded water from ZHP surface, the results are related mainly to the polymer constituent.

Particle density of the ion-exchangers (ρ_p) was calculated as [39]:

$$\varepsilon = 1 - \frac{\rho_b}{\rho_p}, \quad (2)$$

where ε is the porosity, ρ_b is the bulk density. Insertion of ZHP predictably causes an increase of particle density (Table 1).

Table 1

Characteristics of ion-exchangers

Sample	Particle density, $kg\ m^{-3}$	A_m , $mmol\ g^{-1}$	Pore volume, $cm^3\ cm^{-3}$	A_{H_2O} , $mmol\ g^{-1*}$	n	P/P_s^{**}
CR	1750	4.51	0.92	2.41	30	<0.20
CR-ZHP-0	1960	1.44	0.69	0.39	6***	0.99
CR-ZHP-1	2060	1.93	0.79	0.75	13	0.94
CR-ZHP-7	2530	4.29	0.78	0.78	29	0.94
CR-ZHP-7-ED	2120	2.30	0.77	1.11	24	0.21

* Before sharp build-up of the isotherm.

** $A_{H_2O} = 0.7\ cm^3\ g^{-1}$.

*** $m = 0.28$ [26].

The exchange capacity per mass unit (A_m) of the composites is lower comparing with CR. It is evidently due to blockage of transport pores with the particles. As a result, functional groups are partially unavailable for ion exchange.

Isotherms of water adsorption (A_{H_2O}) for the pristine ion-exchanger are typical for the materials containing a wide spectrum of pores: long plateau at low P/P_s values attributed to micropores (here P is the pressure of water vapour, P_s

is the pressure of saturated vapour), semi-waves (mesopores) and extended vertical region at $P/P_s \rightarrow 1$ related to meso- and macropores (Fig. 3). At the same time, the isotherms for the modified ion-exchangers show mainly micropores. Meso- and macropores are less expressed in a comparison with the pristine resin.

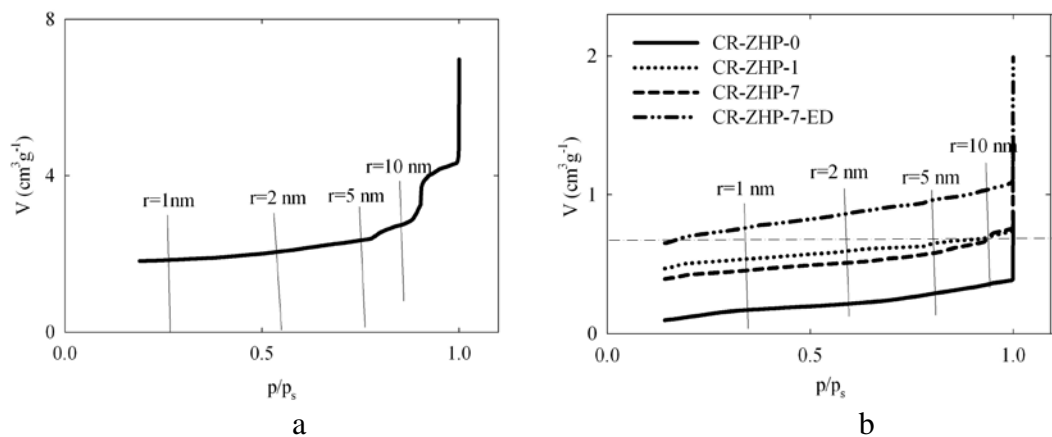


Fig. 3. Isotherms of water adsorption for the pristine resin (a) and composites (b). Insertion of ZHP into the polymer deteriorates water adsorption.

Horizontal branches of the isotherms are attributed to adsorbate monolayer. An amount of water molecules (n) in hydrate shells of counter-ions (H^+) of $-SO_3H$ groups was calculated as:

$$n = \frac{A_{H_2O}}{A_p V_{H_2O}} \quad (3)$$

for the pristine ion-exchanger and:

$$n = \frac{A_{H_2O}}{A_p V_{H_2O} (1-m)} \quad (4)$$

for the composites. Here V_{H_2O} is the molar volume of water, A_p is the exchange capacity of the pristine polymer. The highest n value has been found for the pristine ion-exchanger (see Table 1). In general, modification results in a reduction of this parameter. However, increase of ZHP content causes an increment of the n value (compare CR-ZHP-0 and CR-ZHP-7).

Let us consider thermodynamic aspects of swelling. Transport pores of the ion-exchangers contain high amount of counter-ions (H^+), which tend to solvation. It is possible to assume, that there is a solution of concentrated electrolyte inside transport pores, the “solution” is able to be diluted. This assumption is the closest to reality, when the ion-exchanger is in a contact with a weakly concentrated solution or deionized water. In this case, diffusion parts of intraporous double electric layers are overlapped in clusters. Thus, transport pores are filled with a “solution” completely. In macroscopic models, the tendency of the “solution” to be diluted is taken into consideration by a difference between osmotic pressures of liquids inside and outside granules (Gregor model [45]). It has been postulated, that the osmotic pressure inside ion-exchanger is higher, when the sample is equilibrated with a solvent or its vapour. A difference between the pressures is the swelling pressure, π . This value has been suggested for the ion-exchangers, which change their volume freely. According to the Gregor model, the π magnitude has not to be related to the swelling pressure of gel in a volume bounded with rigid walls.

When water content in the ion-exchanger increases, osmotic pressure decreases. At the same time, pressure from a side of the polymer net grows. These pressures become equal under equilibrium conditions.

The interrelation between the P/P_s value and swelling pressure, which is defined from the Gregor model, is written as [45]:

$$\pi v_{H_2O} = RT \ln \frac{P/P_s}{a_{H_2O}}. \quad (5)$$

Here a_{H_2O} is the activity of water in ion-exchanger, which is associated with free water. For instance, at $A_{H_2O} = 0.7 \text{ mmol g}^{-1}$, the P/P_s value decreases in the order: $CR\text{-ZHP-0} > CR\text{-ZHP-1} \geq CR\text{-ZHP-7} > CR$. This order can be caused by a decrease of swelling pressure or water activity.

3.3. Pore size distributions

Insertions of Figs. 4 illustrate integral pore size distributions, namely dependencies of pore volume (V) on logarithm of pore radius (r). Differential distributions are given in Fig. 4, An area of each peak corresponds to a volume of one or another type of pores.

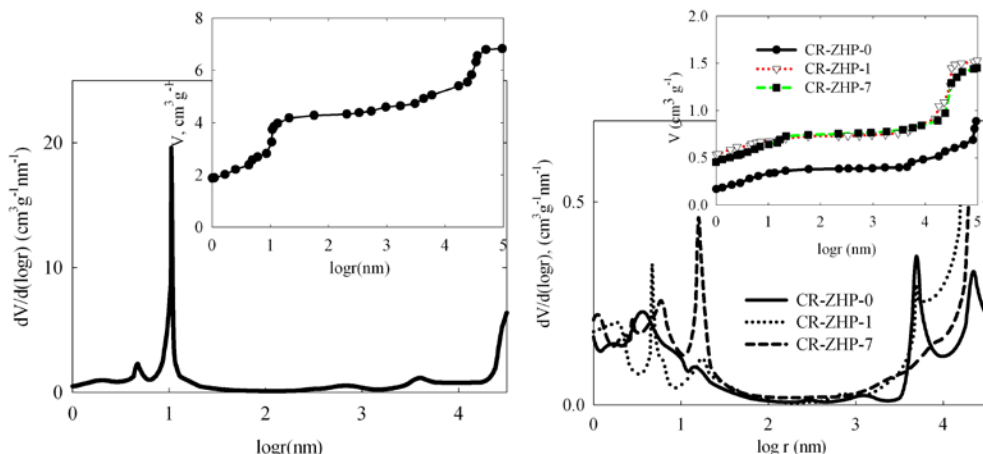


Fig. 4. Integral (insertions) and differential pore size distributions for the pristine resin (a) and composites (b). Modification results in transformation of porous structure of the polymer constituent.

Regarding the pristine ion-exchanger, several peaks are observed (Fig. 5a). The broad maximum at $\log r = 0.3$ (nm) evidently corresponds to channels, the narrower peak ($\log r = 0.7$ (nm)) is attributed to clusters, the most sharp maximum at $\log r = 0.7$ (nm) is caused by voids between gel fields. The maxima at $\log r = 2.8$ and 3.6 (nm) are due to structure defects. The peak at $\log r > 4$ (nm) is attributed to voids between the ion-exchanger grains, these pores will be outside our attention.

The pore size distributions for the $CR\text{-ZHP-0}$ sample demonstrates a shift of peaks, which are attributed to channels and clusters, towards lower $\log r$ values (to $\log r = 0.2$ and 0.5 (nm) respectively). A size of pores, which are free from functional groups, increases ($\log r = 1.1$ (nm) for voids between gel fields, $\log r = 3.1$ and 3.7 (nm) for structure defects).

Increase of fraction of non-aggregated nanoparticles ($CR\text{-ZHP-1}$) causes a shift of the peaks, which are related to transport pores and voids between gel

fields, towards a region of higher $\log r$ values. These peaks become narrower. The composite shows broader peaks of structure defects, but a size of these pores remains without changes.

Regarding the *CR-ZHP-7* sample, a size of channels decreases, clusters become larger in a comparison with *CR-ZHP-1*. Moreover, these peaks are split. No change of a size of voids between gel fields has been found, though their volume increases. At last, the peaks, which correspond to structure defects, become too broad and practically unexpressed.

Pores, a radius of which is less than 1.5 nm ($\log r = 0.17$ (nm)), contain only bonded water, larger pores contain both bonded and free water [30]. A volume of larger pores ($r > 1.5$ (nm)) reflects water activity in the ion-exchanger. Fig. 6 illustrates the volume of these pores for different ion-exchangers (for equilibrium state) as a function of P/P_s value at $A_{H_2O} = 0.7$ mmol g⁻¹.

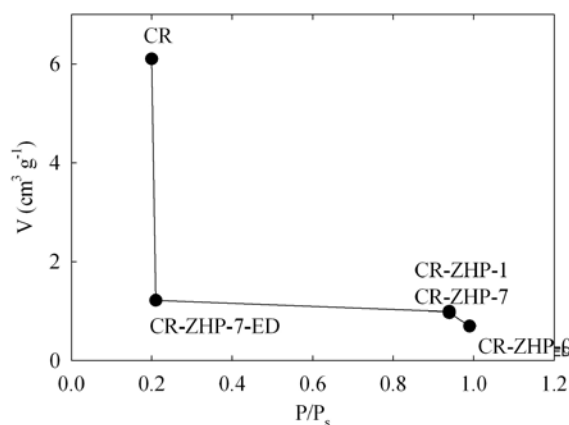


Fig. 5. Volume of pores, which contain free water (under equilibrium conditions) as a function of the P/P_s ratio, which corresponds to $A_{H_2O} = 0.7$ mmol g⁻¹. Modification decreases the content of free water.

In a comparison with the pristine resin, the composites are characterized by lower volume of pores containing free water. Thus, larger P/P_s values for the organic inorganic ion-exchanger can be due to lower a_{H_2O} magnitude and higher swelling pressure (see formula 5).

Among the *CR-ZHP-0*, *CR-ZHP-1* and *CR-ZHP-7* composites, no considerable change of the P/P_s ratio and volume of pores containing free water has been found. Thus, the swelling pressure for these samples is practically similar even under equilibrium conditions ($\pi_{V_{H_2O}} = -RT \ln a_{H_2O}$ [45]). However, a difference between the amounts of water molecules of counter-ions is sufficient (see Table 1). Moreover, a change of pore size is also observed (see Fig.4).

This is evidently due to various swelling pressure in different pores, which is caused by a presence of ZHP. Indeed, a change of amount of osmotically active species (counter-ions of hydrophosphate groups) in one or the other pores affects swelling pressure inside them. If the main amount of ZHP is localized in structure defects, they are able to squeeze the transport pores and pores between gel fields (transition from *CR* to *CR-ZHP-0*). Lower n value can be due to partial inaccessibility of transport pores for water adsorption and ion exchange (decrease

of ion exchange capacity per mass unit, see Table 1). As a result, the A_p magnitude, which is used for calculations, is overestimated.

Preferable deposition of ZHP inside clusters and voids between gel fields (transition from *CR-ZHP-0* to *CR-ZHP-1* and *CR-ZHP-7*) evidently causes higher swelling pressure inside these pores than that in structure defects. Changes of swelling pressure inside different pores are evidently compensated (similarity of the P/P_s ratios and free water content). A part of transport pores become available for water adsorption and ion exchange (increase on the A_m and n values).

3.4. Electrical conductivity

The impedance measurements were carried out for a packed bed. Thus, the resistance value, which is obtained by this manner, includes also the resistance of the grain boundaries. In owing to this, the conductivity is evidently less than those for “monoliths”. However, the data reflect a relative change of conductivity affected by the inorganic modifier.

Fig. 6 illustrates the dependence of ion-exchanger conductivity (κ) on concentration of free mobile charge (H^+), i.e. on ion-exchange capacity. In general, modification leads to the conductivity growth. The samples, in which ZHP was precipitated at low temperature, are characterized by higher conductivity, than those modified under room temperature.

In opposite to the composites based on the resin containing 8% DVB [26, 28], all materials demonstrate a build-up of conductivity with increasing of ZHP content (slow and rapid growth of the κ value). Extrapolation of the curve branches to the abscissa axis gives $A < 0$ (slow growth) and $A >> 0$ (rapid growth). A slow growth is evidently caused by transformation of porous structure of the polymer as well as by the modifier, which is characterized by slower ion transport than the flexible resin. Fast growth of the conductivity can be due to nanoparticles inside transport pores, since counter-ions of hydrophosphate groups are involved into ion transport. However, $A >> 0$ at $\kappa=0$, this indicates no contribution of nanoparticle aggregates to the conductivity, since these formations are located outside transport pores of the polymer.

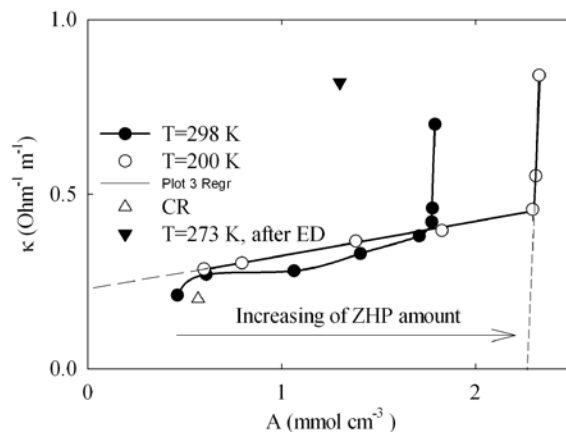


Fig. 6. Electrical conductivity of the ion-exchangers as a function of their ion exchange capacity. The curve for the samples obtained under room temperature was plotted according to data [10]. Legend shows temperature of the modifier precipitation.

3.5. Electrodeionization

Fig. 7 illustrates the amount of Cd^{2+} ions in the cathode compartment (n_c) as a function of time (τ). As seen, the rate of ion transport through the ion-exchanger bed and membrane decreases in the range $\text{CR-ZHP-7} > \text{CR} > \text{CR-ZHP-1} > \text{CR-ZHP-0}$. Among the composites, the order coincides to conductivity (see Fig. 6). The pristine resin shows higher rate of ion transport in a comparison with the composites containing low amount of the modifier. This is evidently due to inhibitory effect of ZHP, which squeeze transport pores of the polymer. Moreover, movement of species through clusters and channels can be complicated by additional interaction with functional groups of ZHP. The highest rate of ion transport, which is observed for CR-ZHP-7 , is probably due to high amount of Cd^{2+} species sorbed by non-aggregated nanoparticles.

In the case of the CR-ZHP-7 sample, the rate of ion transport was found to be constant. Thus, a flux of Cd^{2+} ions (N_c) calculated as $\frac{1}{A_e} \frac{dn_c}{d\tau}$ (where A_e is the effective area of the membranes) remains without changes within a wide range of time. No sufficient change of flux is observed from cycle to cycle of the EDI processes followed by chemical regeneration (Fig. 8). Residual concentration of Cd^{2+} species in the solution at the cell outlet was $1\text{-}2 \text{ mg dm}^{-3}$. Thus, the removal degree reached 96–98 %. Hardness ions are removed simultaneously, however, the relation of their summary molar concentration to the Cd^{2+} content was 7.4. In the case of initial solution, this ratio is 3.4.

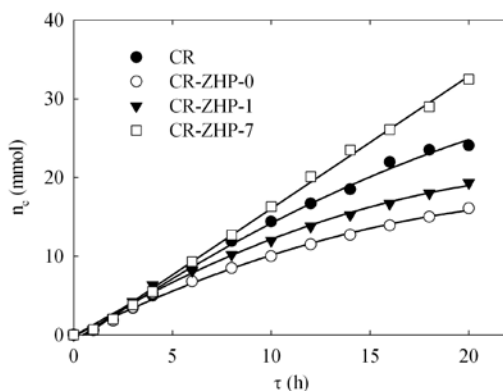


Fig. 7. Cd^{2+} amount in the catholyte as a function of time.

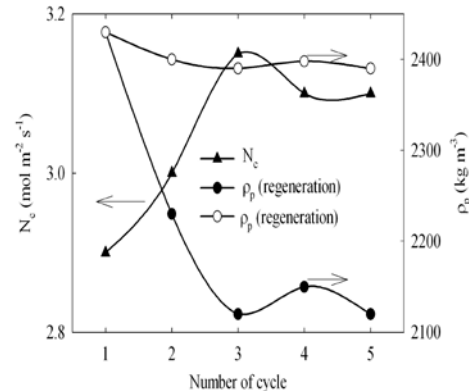


Fig. 8. Cd^{2+} flux for different cycles of EDI processes, which involve CR-ZHP-7 . The figure also illustrates particle density of this sample from cycle to cycle of EDI- chemical regeneration and ion exchange-chemical regeneration.

The particle density decreases from the first to third cycle of EDI-regeneration. This shows a diminishing of ZHP amount inside the ion-exchanger. Further a change of particle density remains within experimental error indicating constancy of the ion-exchanger composition. No considerable change of particle density was found for the composite after each cycle of ion exchange followed by regeneration. Thus, a decrease of the modifier content is affected by electric field.

3.6. Porous structure of ion-exchanger after ED process

Fig. 9 illustrates differential pore size distributions for the *CR-ZHP-7-ED* ion exchanger. In a comparison with *CR-ZHP-7*, the maximum related to channels is shifted towards higher r values (from $\log r=0.04$ (nm) to 0.15 (nm)) and becomes more irregular: the peak broadens up to $\log r=0.5$ (nm). Simultaneously, sizes of clusters and voids between gel fields decreases (from $\log r=0.77$ (nm) to 0.44 (nm)) and from $\log r=1.2$ to 1 (nm) respectively. The peaks, which are related to structure defects, become more expressed. In general, the pore size distribution looks similarly to that for the *CR-ZHP-7*, except the region of channels.

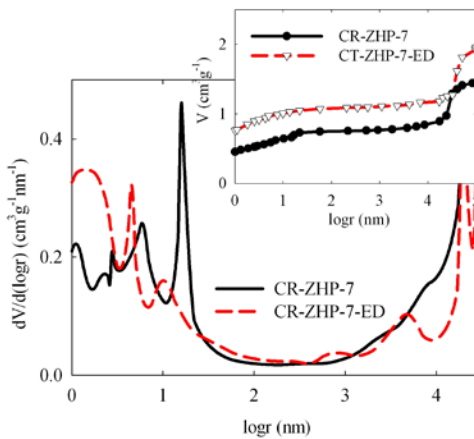


Fig.9. Integral (insertion) and differential pore size distributions for the composite before and after 5 cycles of EDI-chemical regeneration.

Slightly higher content of free water for *CR-ZHP-7-ED* (lower water activity) as well as much lower P/P_s ratio (see Fig. 5) indicates lower swelling pressure for this sample in a comparison with *CR-ZHP-7*. Higher amount of water molecules in hydrate shells of counter-ions (see Table 1) is due to shrinkage of small pores.

Thus, fragmentation of ZHP aggregates occurs during EDI processes, they partially leave the polymer phase, however, a part of them appears in widening of the smallest pores of the polymer constituent. As a result, no considerable change of electrical conductivity of the samples has been found (see Fig. 6, compare *CR-ZHP-7* and *CR-ZHP-7-ED*) despite a decrease of ZHP content. The nanoparticles can move through the polymer due to electrophoresis. Moreover, the particle movement can be affected by a convective flow of the solution inside pores.

4. Conclusions

Impregnation of ion exchange resin with a ZrOCl_2 solution under elevated temperature allows us to obtain high amount of ZHP due to precipitation from additionally sorbed electrolyte. At the same time, a decreasing in temperature, at which precipitation occurs, promotes formation of non-aggregated nanoparticles in transport pores of the ion exchange polymer.

Insertion of the inorganic constituent into the flexible resin leads to transformation of porous structure of the polymer, this is probably due to different swelling pressure in transport and non-transport pores. From a formal point of view, modification could be considered as an increasing of the content of cross-

linking agent, since the composites demonstrate more considerable swelling pressure and ion exchange capacity per volume unit in a comparison with the pristine resin. In opposite to cross-linking agent like DVB, ZHP enhances electrical conductivity of the resin. This is evidently due to participation of counter-ions of hydrophosphate groups in ion transport. Only nanoparticles in clusters contribute to the conductivity, the aggregates, which are located outside transport pores, behave as inert filler.

The composite with a maximal ZHP content provides a constancy of ion flux towards concentration compartment and high removal degree of Cd²⁺ ions during EDI process. Ca²⁺ and Mg²⁺ ions are removed simultaneously, however, they dominate in the effluent. For deeper deionization, particularly for the most complete removal of Cd²⁺ ions, reverse osmosis is recommended.

Partial release of ZHP from the ion-exchanger and redistribution of the particles inside the polymer occur during the first 40 h of the EDI process. However, no change of the composite conductivity have been found. This indicates destruction of aggregates and stability of nanoparticles in transport pores. Electrochemical method can be recommended for removal of aggregates from ion exchange material, such as organic-inorganic membranes.

Acknowledgements

The work was supported by projects within the framework of programs supported by the National Academy of Science of Ukraine “Fundamental problems of creation of new materials for chemical industry” (grant N 49/12).

References

- [1] H. Strathmann, Ion-exchange membrane separation processes, Membrane Science and Technology Series, V. 9, Elsevier, Amsterdam, 2004, p. 9.
- [2] L. Alvarado, A. Chen, *Electrochim. Acta* 132 (2014) 583–597.
- [3] Ö. Arar, Ü. Yüksel, N. Kabay, M. Yüksel, *Desalination* 342 (2014) 16–22.
- [4] Ö. Arar., Ü Yüksel, N. Kabay, M. Yüksel, *Desalination* 317 (2013) 48–54.
- [5] J. Wood, J. Gifford, J. Arba, M. Shaw, *Desalination* 250 (2010) 973–976.
- [6] P.B. Spoor, L. Grabovska, L. Koene, L.J.J. Janssen, W.R. ter Veen, *Chem. Eng. J.* 89 (2002) 193-202.
- [7] Yu.S. Dzyazko, V.N. Belyakov, *Desalination* 162 (2004) 179-189.
- [8] L.M. Rozhdestvenska, Yu.S. Dzyazko, V.N. Belyakov, *Desalination*, 198 (2006) 247-255.
- [9] H. X. Lu, J. Y. Wang, S. F. Bu, M. Q. Zhang, J. B. Zhang, *Adv. Mater. Res.* 183-185 (2011) 580-584.
- [10] Yu.S. Dzyazko, L.N. Ponomaryova, L.M. Rozhdestvenskaya, S.L. Vasiliuk, V.N. Belyakov, *Desalination* 342 (2014) 43–51.
- [11] G. Shang, G. Zhang, C. Gao, *Desalination* 353 (2014) 1–7.
- [12] H. Lu, Y. Wang, J. Wang, *J. Cleaner Prod.* 92 (2015) 257-266.
- [13] Yu. S. Dzyazko; S. L. Vasiliuk, L. M. Rozhdestvenskaya, V. N. Belyakov, N. V. Stefanyak, N. Kabay; M. Yulksel; O. Arar; U. Yulksel, *Chem.Eng.Commun.* 196 (2009) 22-38.
- [14] M.E.H. Bergmann, T. Iourtchouk, A. Rittel, H. Zuleeg, *Electrochim. Acta* 54 (2009) 2417.-2424.
- [15] L. Alvarado, A. Ramírez, I. Rodríguez-Torres, *Desalination* 249 (2009) 423-428.
- [16] L. Alvarado^a, I. R. Torres, A. Chen, *Separ. Purif. Technol.* 105 (2013) 55-62.

- [17] X. Feng, J.-S. Gao, Z.-C. Wu Journal of Zhejiang University SCIENCE A 9 (2008) 1283-1287.
- [18] Ö. Arar, Ü Yüksel, N. Kabay, M. Yüksel, Desalination, 277 (2011) 296-300.
- [19] A. Mahmoud, A.F.A. Hoadley, Water Research 46 (2012) 3364-3376.
- [20] Kyeong-Ho Yeon^a & Seung-Hyeon Moon, Separ. Sci. Technol. 38 (2003) 2347-2371.
- [21] F.-Z. Li, M. Zhang, X. Zhao, T. Hou, Li-Jun Liu, Nuclear Technol. 172 (2010) 71-76.
- [22] S. Gahlot, S. Sharma, V. Kulshrestha, Ind. Eng. Chem. Res., 54 (2015) 4664-4671.
- [23] H.-J. Lee, M.-K. Hong, S.-H. Moon, , Desalination 284 (2012) 221-227.
- [24] Q. Zhang, B. Pan, S. Zhang, J. Wang, W. Zhang, L. Lv, J. Nanoparticle Res., 13 (2011) 5355-5364.
- [25] S. Sarkar, E. Guibal, F. Quignard, A. K. SenGupta, J. Nanoparticle Res. 14 (2012) 715.
- [26] Dzyazko Yu.S., Ponomaryova L.N., Volkovich Yu.M., Sosenkin V.E., Belyakov V.N. Separ. Sci. Technol. 48 (2013) 2140-2149.
- [27] Q. Zhang, Q. Du, M. Hua, T. Jiao, F. Gao, B; Pan, Environ. Sci. Technol., 47 (2013) 6536-6544.
- [28] Yu. S Dzyazko, L. N. Ponomaryova, Yu. M. Volkovich, V.V. Trachevskii, A. V. Palchik, Micropor. Mesopor. Mater. 198 (2014) P. 55-62.
- [29] W.Y. Hsu, T.D. Gierke, J. Membr. Sci. 13 (1983) 307-326.
- [30] N. P. Berezina, N. A. Kononenko, O. A. Dyomina, N. P. Gnusin, Adv. Colloid. Interface Sci., 139 (2008) 3-28.
- [31] A. B. Yaroslavtsev, V. V. Nikonenko, Nanotechnologies in Russia, 4 (2009) 137-159.
- [32] B. Pan, Q. Zhang, W. Du, W. Zhang, B. Pan, Q. Zhang, Z. Xu, Q. Zhang, Water Res. 41 (2007) 3103-3111.
- [33] Yu. S. Dzyaz'ko, V.V. Trachevskii, L.M. Rozhdestvenskaya, S.L. Vasiliuk, V.N. Belyakov, Rus. J. Phys. Chem. A 87 (2013) 840-845.
- [34] F. B. Mainier, L. P. C. Monteiro, L. H. Fernandes, M. A. M. Oliveira, ARPN Journal of Science and Technology, 3 (2013) 176-180.
- [35] Yu. M. Volkovich, V. S. Bagotzky, V. E. Sosenkin, I.A. Blinov // Colloids Surf. A: Physicochem. Eng. Aspect. 187-188 (2001) 349-365.
- [36] Yu. M. Volkovich, V. E. Sosenkin, V. S. Bagotzky / J. Power Sources. 195 (2010) 5429-5441.
- [37] Yu. M. Volkovich, V. E. Sosenkin, Russ. Chem. Rev. 81 (2012) 936-959.
- [38] Yu. M. Volkovich, V.S. Bagotsky. in: Yu. M. Volkovich, A.N. Filippov, V.S. Bagotsky (Eds.), Porous materials and powders used in different fields of science and technology, Springer-Verlag, London, 2014, pp. 1-8,
- [39] A.D. Ward, S.W. Trimble, Environmental Hydrology, Boca Raton: CTC Press LLC, 2004, p. 74.
- [40] E. Heymann, J. O'Donnell, J. Colloid. Sci. 4 (1949) 395-404.
- [41] Yu.S. Dzyazko, V.M. Linkov, V.N. Belyakov, Electrical conductivity of a flexible resin loaded with Cr (III) ions, Desalination. 241 (2009) 57-67.
- [42] A. Singhal, L. M. Toth, J. S. Lin, K. Affholter, J. Am. Chem. Soc. 118 (1996) 11529-11534.
- [43] A. Clearfield, J. Mater. Res., 5 (1990) 161-162.

- [44] A.S. Myerson, R. Ginde, in: A.S. Myerson (Eds.), *Handbook of Industrial Crystallization*, Butterworth-Heinemann, Woburn, 2002, pp. 33-100.
- [45] F. Helfferich, *Ion Exchange*, Dover, New York, 1995, pp. 100-125.

Effect of Iron (Fe^{3+}) and Magnesium (Mg^{2+}) during biodegradation of organic matter by *Clostridium butyricum* in the leachate

M. Redzwan Tamat^a, M. Firdaus Othman^b, Y. Syafikah Razali^c, N.A. Serri^d, H. Azan Tajarudin^{e*}

^{a,b,c,d,e}School of Industrial Technology, Universiti Sains Malaysia, Malaysia

^eCluster of Solid Waste Management, Engineering Campus, Universiti Sains Malaysia, Malaysia

^aedztop91@gmail.com, ^bfirdauspcb@gmail.com, ^csyafikahyasm@yahoo.com,

^daziah_serri@usm.my, ^eazan@usm.my

Abstract

This research focuses on the relationship between Fe^{3+} and Mg^{2+} reduction with various sizes of inoculum. Three sizes of inoculum were applied such as 5% (v/v), 10% (v/v) and 15% (v/v) in the tube test by batch system. Antiseptic and sterilization technique were applied to avoid contamination, and anaerobic condition was archived by degassing using nitrogen gas into all of the tubes. The growth rate (h^{-1}) of *C. butyricum* also has influenced the size of inoculum and indirectly affected the reduction of Fe^{3+} and Mg^{2+} . The results showed that the smallest size of inoculum and growth rate (h^{-1}), gave the higher rate of reduction. The 5% (v/v) of inoculum size with 0.034 h^{-1} growth rate gave 96% reduction of Fe^{3+} and 38% reduction of Mg^{2+} . Meanwhile, for 10% (v/v) size of inoculum with 0.042 h^{-1} gave 86% reduction of Fe^{3+} and 26% of Mg^{2+} reduction. Besides that, 15% (v/v) size of inoculum with higher growth rate (0.065 h^{-1}) gave the lowest reduction of Fe^{3+} (26%) and Mg^{2+} (16%). As a conclusion, small inoculum size gives highest metal reduction.

Keywords: C.butyricum, Fe3+, growth rate, leachate, Mg2+

Introduction

Municipal solid waste (MSW) is an unwanted or useless solid waste produced in daily activity of a community in a given area [1]. While, leachate is a liquid that results from sanitary MSW landfill [2]. Leachate from landfill is characterized by high concentration of organic matter (biodegradable and non-biodegradable), ammonia nitrogen, heavy metals, and chlorinated organic and inorganic [3]. It is found that in most leachates also contain Fe^{3+} and Mg^{2+} . One of the objectives of this study is to reduce metals in a leachate which is contained Fe^{3+} and Mg^{2+} because metals is a containment.

From previous studies, it was found that there were several bacteria that can tolerate and favour growth in the presence of Mg^{2+} and Fe^{3+} . According to G. M. Gadd (2010), many metals is essential for life, for example Na, K, Cu, Zn, Co, CA, Mg, Mn and Fe [4]. From that perspective, sulfate reducing bacteria (SRB) are highly dependent to Mg^{2+} [5]. There are also bacteria that can grow anaerobically by using Fe^{3+} as an electron acceptor [6].

Fe^{3+} has diverse functions in bacterial cells, which influences cell composition, intermediary metabolism, secondary metabolism, enzyme activity and host cell interaction which can induce pathogenicity [7]. On the other hand, Mg^{2+} is essential for bacterial protoplasm synthesis, cell division and normal cell activity [8].

Methods

Leachate collection

Leachate sample was collected from the PBLS located in the northern region of Malaysia. This landfill is located in Byram Forest Reserve, Penang, Malaysia. The leachate was taken from the semi-aerobic pond, transported to the laboratory and stored within the temperature of 4°C in order to minimize the biological reaction.

Leachate characterization

Leachate sample was characterized for several properties like COD, BOD_5 , pH, TOC, Fe^{3+} and Mg^{2+} , nitrogen content, and phosphorus content. All the parameters were conducted thrice following Standard Method of Water and Wastewater [9].

Culture and inoculum

The bacteria used in this research was *C. butyricum* (NCIMB 7423) grown in the media containing 10 g/L of glucose; 10 g/L of yeast extract; 2.5 g/L of KH_2PO_4 ; 5 g/L of NH_4SO_4 ; and 0.05% (w/w) of resazurin. The culture was incubated in the oxygen-free environment at 37°C and pH of 6.5. The pH was adjusted by using sulfuric acid and sodium hydroxide. The size of inoculum used was 10% of the fermentation size and every subculture of the bacteria will take during 24 hours of the incubation time. Synthetic media which contain above described nutrient was used as an inoculum while leachate was used as a substrate in a fermentation.

Biodegradation

Biodegradation by these bacteria was performed in the 8ml working volume tube at 37°C and pH of 6.5. The optical density (O.D.) of the bacteria was carried out by using a spectrophotometer at 660 nm and converted to biomass by using cell dry weight method. Substrate used in this research was pre-treated leachate with the toxicity removed by using calcium carbonate treatment.

Fe^{3+} and Mg^{2+} analysis

Both ions were analysed by using inductively coupled plasma (ICP) and the experiments were conducted thrice according to Standard Method of Water and Wastewater (APHA, 2005). From the results of metal analysis, the following mass balance was constructed:

$$\text{MT} = \text{Ma} + (\text{Mbc} + \text{Mbs}) + \text{Mr}$$

MT stands for total metal in culture, whereas Ma is the cellular uptake of metal. Mbc represents metal bound by capsular polymer, Mbs is metal bound by soluble polymer and Mr represents free metal in solution.

Result and Discussion

Leachate Profile

Table 1: Leachate profile

No	Type	In leachate	Unit
1	pH	8.35 ± 0.5	-
2	Chemical Oxygen Demand (COD)	0.917 ± 0.5	g/L
3	Biochemical Oxygen Demand (BOD)	0.254 ± 0.5	g/L
4	Total Nitrogen (TN)	0.140 ± 0.5	g/L
5	Total Organic Carbon (TOC)	0.111 ± 0.5	g/L
6	Phosphorus	0.0036 ± 0.5	g/L
7	Magnesium, Mg ²⁺	82.45	ppm
8	Iron, Fe ³⁺	2.12	ppm

Table 1 shows the leachate profile used in the study, both Fe³⁺ and Mg²⁺ were detected in this sample. The pH measurement of the sample was at 8.35 ± 0.5, thus, indicated high alkalinity in the leachate properties. It was adjusted to pH 6.5 before the experiment was started. The rate of biodegradability was 0.3 (BOD/COD).

Relationship between growth of *C. butyricum* and Fe³⁺ reduction

The initial reading of Fe³⁺ in the leachate sample was 2.12 ppm detected by ICP-MS. However, *C. butyricum* cannot directly being induced to the leachate due to the toxicity. Therefore, a pre-treatment of the leachate has been done, which also reduce the concentration of the Fe³⁺ to 1.72 ppm and the value is taken as the initial leachate.

Figure 1: Relationship between growth of *C. butyricum* and Fe³⁺ reduction

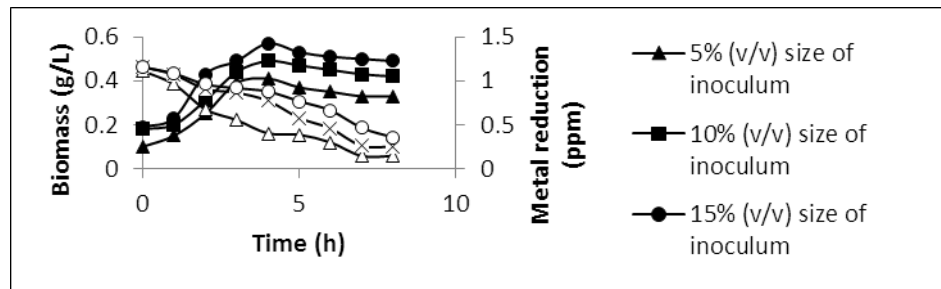


Table 2: Values of μ and amount of Fe³⁺ reduction

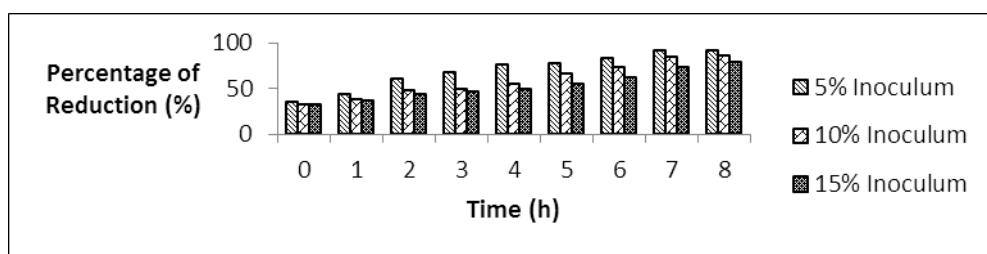
Size of inoculum (v/v)	μ (h ⁻¹)	Amount of Fe ³⁺ reduction (ppm)
5%	0.034	1.57
10%	0.042	1.47
15%	0.065	1.36

Fig 1 showed the relationship between the growth of *C. butyricum* and Fe³⁺ reduction by 5% (v/v), 10% (v/v) and 15% (v/v) size of inoculum. When the growth of bacteria increased, the ion reduction decreased. Lag phase occurred during the beginning of the experiments from 0 to 1 hour. At this phase, *C. butyricum* tried to adapt to the new environment so that the growth is slower. Then, the process continued to log phase up to 4 hours and underwent stationary

phase. *C.butyricum* growth increased rapidly at log phase due to the sufficient nutrients and minerals supplied for the bacteria to grow and the bacteria finally can adapt to the environment. Stationary phase occurred due to the depletion of nutrients and minerals, then the substrate started to become toxic to the bacteria. Bacterial specific growth rates, μ , were calculated during the phase of exponential growth under standard nutritional conditions. The values of μ for 5% (v/v), 10% (v/v) and 15% (v/v) size of inoculum were 0.034 h^{-1} , 0.042 h^{-1} and 0.065 h^{-1} , respectively as shown in Table 2. From Table 2, the ion was removed most efficiently at low specific growth rates, μ .

According to Fig 2, the percentage of removal of Fe^{3+} were 91.6%, 85.5% and 79.4% for the 5% (v/v), 10% (v/v) and 15% (v/v) sizes of inoculum, respectively. The highest percentage in the removal of Fe^{3+} was by using 5% (v/v) size of inoculum. It showed that only a small quantity of inoculum concentration was required to give an efficient result for the removal of Fe^{3+} .

Figure 2: Percentage of Fe^{3+} reduction



Relationship between growth of *C.butyricum* and Mg^{2+} reduction

The initial reading of Mg^{2+} being detected by ICP-MS was 82.45 ppm. After pre-treatment, Mg^{2+} was reduced to 19.61 ppm. Fig 3 shows that when the growth of *C.butyricum* increased, the Mg^{2+} decreased. While, Table 3 shows that low μ significantly reduce the ion even more. Thus, 5% (v/v) size of inoculum was effective in removing the ions from leachate which was 7.47 ppm compared to 10% (v/v) and 15% (v/v) sizes of inoculum which were 5.01 ppm and 3.19 ppm, respectively.

According to Fig 4, the reduction of Mg^{2+} was calculated by its percentage for the difference size of inoculum. It is observed that the reduction of Mg^{2+} in leachate for 5% (v/v), 10% (v/v) and 15% (v/v) size of inoculum was 38.1%, 25.6% and 16.3%, respectively. The percentage of Mg^{2+} removal was not very effective as it not achieve more than 50% removal efficiency compared to Fe^{3+} removal. Nevertheless, from Fig 4, it stated that the 5% (v/v) size of inoculum used in the fermentation was the best to reduce Mg^{2+} .

Figure 3: Relationship between growth of *C.butyricum* and Mg^{2+} reduction

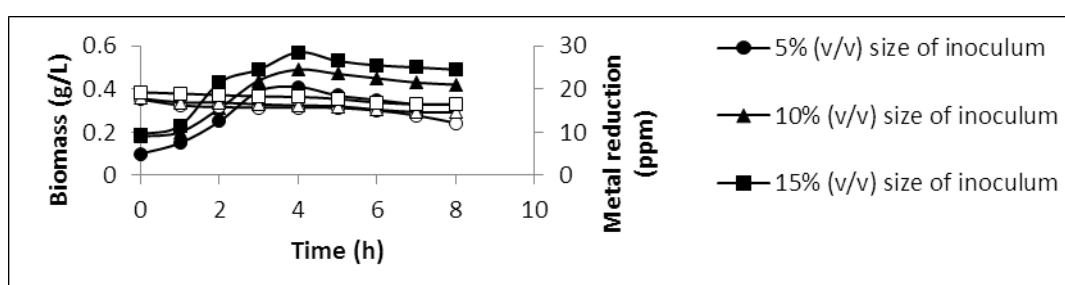
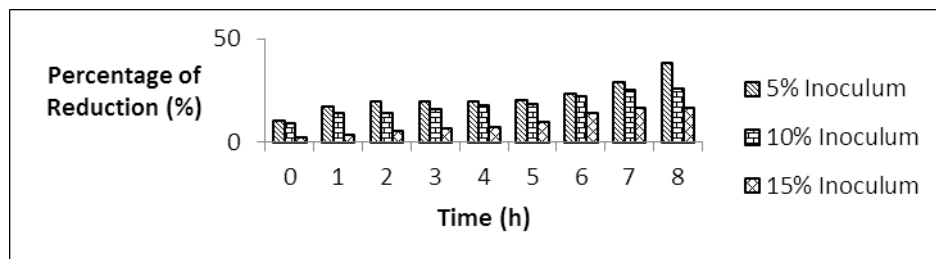


Table 3: μ and amount of Mg^{2+} reduction

Size of inoculum (v/v)	μ (h^{-1})	Amount of Mg^{2+} reduction (ppm)
5%	0.034	7.47
10%	0.042	5.01
15%	0.065	3.19

Figure 4: Percentage of Mg^{2+} reduction

Mass Balance

An estimation of the mass balance of metals for the fermentation in different concentration of inoculum was made using the total metal in leachate sample and the free metal in leachate sample after the fermentation.

$$MT = Ma + (Mbc + Mbs) + Mr$$

where, MT = total metal in culture; Ma = cellular uptake of metal

Mbc = metal bound by capsular polymer; Mbs = metal bound by soluble polymer
Mr = free metal in solution; Ma, Mbc and Mbs will be considered as 'X'.

Table 4: Mass balance of metals of Fe^{3+} and Mg^{2+}

Variable	Size of inoculum v/v	Metal removed, (Ma, Mbc, Mbs) ppm	Free metal in Solution (Mr) Ppm	Total metal in leachate (MT) ppm
Fe^{3+}	5%	1.58	0.14	1.72
	10%	1.47	0.25	
	15%	1.37	0.36	
Mg^{2+}	5%	7.48	12.13	19.61
	10%	5.02	14.59	
	15%	3.20	16.41	

Conclusion

Low growth rate cause the bacteria to be more stress due to the metals that contained in the leachate. In conjunction, the bacteria will produce extracellular polymeric substances (EPS) to protect them from metals. Directly, this situation causes higher production of EPS at low inoculum size compared to higher inoculum size. EPS which is negatively charged react with

Fe^{3+} and Mg^{2+} producing EPS-complex salt. This complex then precipitated leaving the cell unprotected which induces the cell to produce more EPS in order to protect them from metals until the concentration of metals in leachate becomes suitable for bacteria to survive.

Furthermore, low inoculum size indicates that less amount of cell being introduced into leachate which means that *C. butyricum* have plenty of nutrient and larger space in leachate to grow compared to high inoculum size. They need to replicate to produce new cell which needs nutrient. Fe^{3+} and Mg^{2+} was used by the cell resulting in lowering content of these metals in leachate. As a conclusion, low inoculum size give a high rate reduction of Fe^{3+} and Mg^{2+} in leachate.

Acknowledgement

The authors wish to thank the Research University Grant (1001/PTEKIND/811262) from Universiti Sains Malaysia and Fundamental Research Grant (203/PTEKIND/6711373) from the government of Malaysia for financial support of this project.

References

- [1] Adhikari, B., & Khanal, S. N. (2015). Qualitative Study of Landfill Leachate from Different Ages of Landfill Sites of Various Countries Including Nepal, 9(1), 23–36.
- [2] Umar, M., Aziz, H. A., & Yusoff, M. S. (2010). Variability of Parameters Involved in Leachate Pollution Index and Determination of LPI from Four Landfills in Malaysia, 2010.
- [3] Renou, S., Givaudan, J. G., Poulain, S., Dirassouyan, F., & Moulin, P. (2008). Landfill leachate treatment: Review and opportunity. Journal of Hazardous Materials, 150(3), 468–93.
- [4] Gadd, G. M. (2010). Metals, minerals and microbes: Geomicrobiology and bioremediation. *Microbiology*, 156(3),
- [5] Cao, J. Y., Zhang, G. J., Mao, Z. S., Fang, Z. H., Yang, C., & Han, B. L. (2009). Influence of Mg^{2+} on the growth and activity of sulfate reducing bacteria. *Hydrometallurgy*, 95(1-2), 127–134.
- [6] Nealson, K. H., & Myers, C. R. (1990). Iron reduction by bacteria: a potential role in the genesis of banded iron formations. *American Journal of Science*.
- [7] Messenger, A. J., & Barclay, R. (1983). Bacteria, iron and pathogenicity. *Biochemical Education*, 11(2), 54–63.
- [8] Webb, M. (1951). The influence of magnesium on cell division. IV. The specificity of magnesium. *Journal of General Microbiology*, 5(3), 480–484.
- [9] APHA, 2005. Standard Methods for the Examination of Water and Waste Water, twenty first ed. American Public Health Association, Washington, DC

The oxidation behavior of titanium aluminide at 850°C

Alexandra Banu¹, Elena Maria Anghel², Marcu Maria², Georgescu Luminita¹

*1. Politehnica University from Bucharest, Splaiul Independentei 313, ROMANIA
alexandrabanu14@yahoo.com*

*2. Institute of Physical Chemistry "Ilie Murgulescu", Splaiul Independentei 202, Bucharest,
ROMANIA*

Key words: titanium aluminide, oxidation, DSC analysis

Introduction

The study intends to evaluate the Differential scanning calorimetry (DSC) information, XRD and Raman analysis correlated with structural transformations that occur during heat treatment at temperatures of 850°C of α_2 titanium aluminide. The heat treatment consists from 100 hours of exposure at 850°C. At the end of experiments, the structure transformation and oxide coatings formation are evaluated by SEM/EDS microscopy and Raman spectroscopy.

Differential scanning calorimetry analysis highlights the influence of heating rate at different temperature levels on oxidation process.

The DSC curves of the TiAl based alloy for heating rate of 5 °C and 15 °C / min show that oxidation initiated at a few degrees below the 995 and 997 °C respectively. Identification of oxidation products was performed by X-ray diffraction and Raman spectroscopy analysis. The oxide layer formed on the surface of the heated specimen 5 and 10 °C / min. was peeled partially on the surface thereof. Therefore kinetic measurements made by Kissinger method using the peak temperature of the exothermic oxidation effects are strongly affected by the exfoliation. To determine the oxidation products and properties of oxide layers resulting from thermal oxidation have used different characterization techniques:morphology and elemental analysis of oxide films is performed with SEM and EDX. Identify types of oxides resulted after thermal oxidation was performed by Raman spectroscopy and X-ray (XRD).

Experimental details

Cast samples of titanium aluminide alloy were used in this study, having the chemical composition in Table 1. The samples for mechanical tests were made by Electrical Discharge machining because of material hardness.

Table 1 Chemical composition of tested material (at%)

Elem.	AlKα	TiKα	VKα	NbKα
% at.	30.48	63.09	1.93	4.5

The heat treatment consists from 100 hours of exposure at 850°C and were carried out in a Vulcan™ 3-130 Ney furnace. Prior the oxidation experiments, the crucibles holding the specimens were heated at 1000 °C until a constant weight was obtained. Three specimens for each type were oxidized in these conditions to probe reproducibility of the measurements. The oxidation weight-gain data were recorded by means of an analytical balance (accuracy ±0.1 mg).

At the end of experiments, the structure transformation and oxide coatings formation are evaluated by SEM/EDS microscopy with a microscope FEI Inspect F 50 high-resolution, field emission, equipped with energy dispersive spectroscopy (EDS) analysis and Raman spectroscopy by means of a LabRam HR spectrometer (Jobin-Yvon–Horiba) over 100-1200 cm⁻¹ range.

Prior to oxidation experiments was done a Differential scanning calorimetry (DSC) analysis of base material in order to rapid characterization of base material to oxidation at this temperature. This experiment was done using APS TG-DSC-DTA SETARAM LabSys Evo 1600, in air, at heating rates and cooling rates of 5, 10, 15 si 30°C/min., respectively up to 1050°C.

Results and discussions

Differential scanning calorimetry analysis highlights the influence of heating rate at different temperature levels on oxidation process. The DSC curves of the TiAl based alloy illustrated in Figure 1 for heating rate of 5 ° C and 15 ° C / min show that oxidation initiated at a few degrees below the 995 and 997 ° C respectively. Identification of oxidation products was performed by X-ray diffraction and Raman spectroscopy analysis. The oxide layer formed on the surface of the heated specimen 5 and 10 ° C / min. was peeled partially on the surface thereof. Therefore kinetic measurements made by Kissinger method (Figure 2) using the peak temperature of the exothermic oxidation effects are strongly affected by the exfoliation.

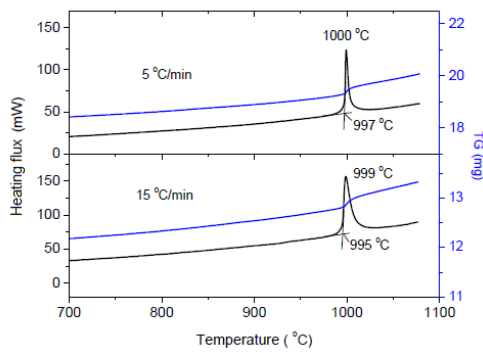


Figure 1 DSC curves for two heating rates 5°C and 15°C

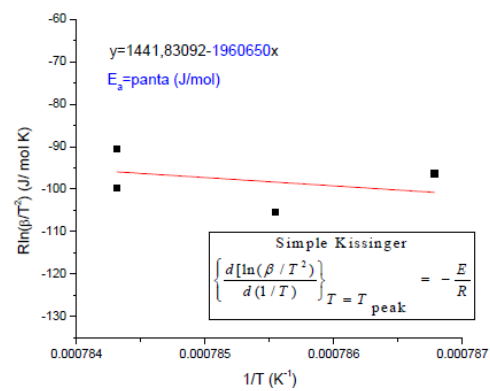


Figure 2 Kissinger dependence $R\ln(\beta T^{-2}) = f(T^{-1})$ where β is heating rate 5,10,15 and 30°C respectively

To determine the oxidation products and properties of oxide layers resulting from thermal oxidation at 850°C have used Raman and XRD Spectroscopy analysis. The obtained results are presented in figures 3.

After exposure at 850 °C for 100h, surface of the base alloy is covered with small oxide grains consisting in two types of morphologies, i.e. TiO₂ as rutile and Al₂O₃ (z1 and z2 in Fig. 3). Thickness of the thermally grown oxide (TGO) layer is estimated around 20-25 μm.

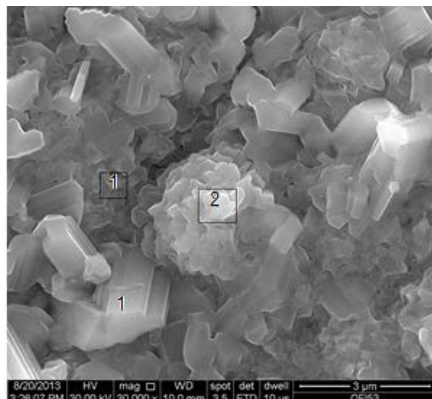


Figure 3 The ESM image of oxidized sample after 100hours at 850°C

X-ray diffraction (XRD) data were collected using a Rigaku Ultima IV diffractometer, with Cu K α radiation, operating at 40 kV and 30 mA equipped with Thin Films attachment for grazing incidence X-ray measurements, at an incidence angle $\omega=0.5^\circ$. The XRD data were recorded at room temperature at a rate of 5° (2θ)/min over a range of $10\text{--}70^\circ$. Rigaku's PDXL software package, connected to the ICDD database was used for the phase identification.

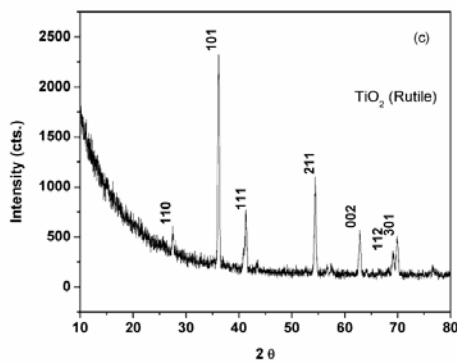


Figure 4 XRD curve spectra performed after 100 hours of oxidation at 850°C

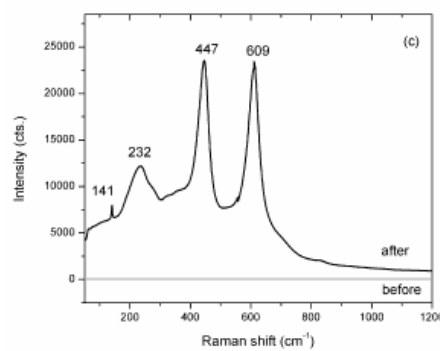


Figure 5 Raman spectra before and after heating al 850°C

The X-ray diffractogram and Raman spectrum [1] in Fig.4 and 5 confirmed that the mostly rutile polymorph of the TiO₂ is formation. The X-ray reflections at 43.47 and 62.85 (2θ) in Fig. 4 are assigned to NbO (DB card no 00-043-1290). According to the X-ray calculations, large rutile crystallites of 268 Å are formed on the surface of the α_2 . Also, literature data for the oxidized Ti₃Al alloys with various additions of Nb and V reported formation of predominant TiO₂ (rutile phase) and minor Al₂O₃ and NbO₂ [2,3,4, 5, 6,7]. The lower oxidation temperature used, the lower temperature Al₂O₃ phases, teta and/or delta, are formed [7].

The thickness of TGO formed during 100 hours of exposure at 850C explain the mass gain results at about 2.5mg cm^{-2} . The square of the mass gain increases linearly with the oxidation time figure 6, satisfying the parabolic kinetics law ($\Delta m^2=k_p t$), as early reported Taniguci et al. [8].

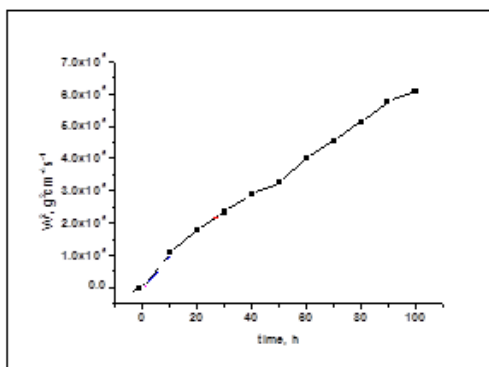


Figure 6 Mean mass gain of the alloy as a parabolic plot

Conclusion

The DSC analysis is useful technic for estimation of oxidation behaviour of titanium aluminide at temperature less 1000°C.

The oxidation of alfa titanium aluminide take place after parabolic low, because of mixt oxide titanium aluminium formation to the surface.

References

1. O. Frank, M. Zukalova, B. Laskova, J. Kurti, J. Koltai, L.Kavan L, Raman spectra of titanium dioxide (anatase, rutile) with identified oxygen isotopes (16, 17, 18). *Phys. Chem. Chem. Phys.* 14 (2012) 14567–14572.
2. C. Leyens, M. Peters, *Titanium and Titanium Alloys: Fundamentals and applications*, Wiley-VCH Verlag GmbH, Wenheim, 2003.
3. K. Kothari, R. Radhakrishnan, N.M.Wereley, Advances in gamma titanium aluminides and their manufacturing techniques, *Prog. Aerosp. Sci.* 55 (2012) 1–16.
4. G. Moskal, Thermal barriers coatings: characteristic of microstructure and properties, generation and directions of development of bonds, *JAMME* 37 (2013) 323-331.
5. L.C.H. Koo, J.W. Evans, K.Y. Song, T.H. Yu, High-temperature oxidation of $\text{Ti}_3\text{Al}-\text{Nb}$ alloys, *Oxid. Met.* 42 (1994) 529-544.
6. S. Djanarthany, J.-C. Viala, J. Bouix, An overview of monolithic titanium aluminides based on Ti_3Al and TiAl , *Mater. Chem. Phys.* 72 (2001) 301–319.
7. M. Zhu, M. Li, S. Duoi, Y. Zhou, Improvement on the Oxidation Resistance of a Ti_3Al Based Alloy by $\text{Cr}_{1-x}\text{Al}_x\text{N}$ ($0 < x < 0.47$) Coatings, *J. Mater. Sci. Technol.* 23 (2007) 373-378
8. P. Souza Santosa, H. Souza Santos, S.P. Toledo, Standard Transition Aluminas. Electron Microscopy Studies, *Materials Research* 3 (2000) 104-114.

Acknowledgments This research was supported by the National Authority for Scientific Research (PCCA Project 65/2012)

Oxygen isotopic comparisons of the microcrystalline silica; In the case of different chrysoprases in Turkey

Murat Hatipoğlu^{1,2} and Nurdane İlbeysi^{3,*}

¹Dokuz Eylül University, İMYO, İzmir Multidisciplinary Vocational School,
Gemmology and Jewellery Programme 35380 Buca-İzmir, Turkey

²Dokuz Eylül University, Graduate School of Applied and Science, Natural Building
Stone and Gemstone Programme 35370 Buca-İzmir, Turkey

³Akdeniz University, Faculty of Engineering, Department of Geological Engineering,
07058 Antalya, Turkey

* Corresponding author, ilbeyli@akdeniz.edu.tr

Abstract

The present geochemical study is focused on famous gem-quality chrysoprases deposits in terms of commercial quantities in the five different regions of Turkey (from west to east; Biga-Çanakkale, İkizce-Bilecik, Sivrihisar-Eskişehir, Oltu-Erzurum, Savur-Mardin). Chrysoprases in these regions are found in different geological zones. Therefore, the initial crystallization temperatures of the solutions responsible for genesis of the fine fibrous green cryptocrystalline silica are interesting and can be determined using a geochemical graphical modeling technique. Oxygen isotope analyses (SMOW) (using EA-IRMS) of the investigated chrysoprase materials of the five different mine deposits range between $\delta^{18}\text{O} = 21.3\text{\textperthousand}$ and $30.7\text{\textperthousand}$. In addition, the analyses of their water contents range between $\delta^{18}\text{O} = -8\text{\textperthousand}$ and 4\textperthousand . When the data are modeled graphically, the initial temperature of the formation of the investigated chrysoprases from Turkey can be determined as $\sim 125\text{ }^{\circ}\text{C}$ for those of the Biga (Çanakkale) deposit occurring in the cracked zone between schist and serpentinite, $\sim 83\text{ }^{\circ}\text{C}$ for those of the İkizce (Bilecik) deposit occurring in the crevices and large vacancies in dacite and andesite, $\sim 74\text{ }^{\circ}\text{C}$ for those of the Sivrihisar (Eskişehir) deposit occurring in the crevices and large vacancies in sandstone, $\sim 99\text{ }^{\circ}\text{C}$ for those of the Oltu (Erzurum) deposit occurring in the cracked zone between flysch and serpentinite, and $\sim 66\text{ }^{\circ}\text{C}$ for those of

the Savur (Mardin) deposit occurring in the crevices and large vacancies in sandstone. The chrysoprases from the cracked zone in serpentinites have higher degrees of temperature compared to those from the crevices in sandstones and volcanics in Turkey.

Key-words: Natural chrysoprase, oxygen isotope analyses (SMOW), initial microcrystallization temperatures, geochemical graphical modelling technique, Turkey.

1. Introduction

The application of oxygen isotope geochemistry to mineralogy provides a much needed foundation for radiogenic isotope and initial crystallization temperature approaches of silica minerals. Since oxygen isotope fractionations at low and moderate temperatures can be determined, there is a demand for high analytical precision in order to recognize and interpret small variations in isotopic ratios (IAEA, 2004; Bindeman, 2008).

Chrysoprase is cryptocrystalline, which means that it is composed of crystals so fine that they cannot be seen as distinct particles under normal magnification, and consists mainly of fibrous radial quartz (optical length-fast chalcedony). Chrysoprase, chrysophrase or chrysoprasus is a gemstone variety of chalcedony. Its color is normally apple-green but varies to deep green (Frondel, 1978; Miehe *et al.*, 1984; Rossman, 1994; Back & Mandarino, 2008). The origin of its name is Greek for “gold leek” (Mitchell, 1979). Cut and polished chrysoprases have been used since ancient times and are found as architectural objects (artifacts). Chrysoprase has been identified in ancient Egyptian artifacts (Lucas, 1989). In addition, chrysoprase was used as a decorative stone during the European Middle Ages. Only two economical locations of chrysoprase

are currently known in Europe. Both of them are in SE Poland, namely the Szklary and Wiry mines (Sachanbinski *et al.*, 2001). Today, worldwide commercial deposits of gem-quality chrysoprase are mainly located in Australia (Nagase *et al.*, 1997; Befi, 2009), Poland (Sachanbinski *et al.*, 2001; Skrzypek *et al.*, 2003, 2004), Kazakhstan (Sachanbinski *et al.*, 2001; Witkowski & Zabinski, 2004), Brazil (Komov *et al.*, 1994), Tanzania (Witkowski & Zabinski, 2004; Shigley *et al.*, 2009; Graetsch, 2011), and Turkey (Hatipoğlu *et al.*, 2011; Ayvacıklı *et al.*, 2012).

Chrysoprase occurs on almost all continents, but an understanding of its material genesis has proved to be problematic regarding geochemistry. The most important discussed factors are the temperature and origin of the solutions responsible for formation of chrysoprase. To reveal these factors, oxygen isotope has been used in this study. Giuliani *et al.* (2000) used $\delta^{18}\text{O}$ values to understand the actions of hydrothermal fluids in which emeralds crystallized. They noted that $\delta^{18}\text{O}$ values of solutions could be ruled by (i) the composition of the rocks, (ii) the fluid-rock interactions, and (iii) the temperature of the fluid.

When the various geological formation conditions in Turkey are considered, it is highly probable that there exist many chrysoprase-bearing localities as mining fields, in terms of commercial quantity, are found in about five different regions of Turkey: Biga (Çanakkale), İkizce (Bilecik), Sivrihisar (Eskişehir), Oltu (Erzurum), and Savur (Mardin). These locations and their typical chrysoprase samples are shown in Fig. 1.

The paper aims to compare and contrast the initial formation temperatures using the geochemical graphical modeling technique according to the oxygen isotopic data (SMOW) of these chrysoprases. This paper is also going to be a first study to compare the isotopic data from the chrysoprases of different regions in Turkey.

2. Materials and methods

The investigated chrysoprase samples with various green hues were collected from the five different geologically occurring deposits in Turkey: from west to east, Biga (Çanakkale), İkizce (Bilecik), Sivrihisar (Eskişehir), Oltu (Erzurum), and Savur (Mardin).

Some basic gemmological characterization tests were carried out on the all investigated chrysoprase samples (Table 1). Firstly, the average specific gravity (SG) values were measured using an electronic balance scale (measurement sensitivity of 0.001 g) with an SG kit, based on the formula [SG = W(air) / W(air) - W(water)]. Secondly, the optical character, optical sign, and refractive indexes were determined by the “spot” method, using an Eickhorst SR/XS standard refractometer device with an optical contact liquid of 1.79 RI and a quartz lamp with a wavelength of 589 nm. Thirdly, ultraviolet (UV) photo-luminescence reactions of Biga chrysoprases were observed using a System Eickhorst UV 240 shortwave (255 nm) and longwave (366 nm) 4W UV lamp. Finally, cleavage, hardness, and luster features were observed by eye. All gemmological data were obtained in the Dokuz Eylül Gemmological Test Laboratory (DGL), İzmir (Turkey).

Polarizing microscope images of thin sections of the investigated chrysoprases were obtained using an Olympus BX41 binocular polarizing microscope with a high-intensity 6V, 30W halogen light source combined with U-CPA and U-OPA optical systems after thin sections of the samples had been mounted on glass lamellae. The investigation was performed in the Optical Mineralogy Laboratory of the Department of Geology at Dokuz Eylül University, Turkey.

The base silica-building components of the investigated chrysoprases were detected from X-ray powder diffraction patterns made using a Cubi-XRD device with a Cu tube and a graphic monochromotor. The d-spacing [\AA°] diffraction matchings using the comparative matching technique are based on the positions of peaks with relative intensities [$\%(\text{I}/\text{I}_0) \geq 2$], 2-theta values below 70° , and a tolerance range of ± 0.01 . The FWHM values were calculated using the Broker AXS diffract plus software. The samples were analyzed with Cu radiation and a 0.3 mm collimator at atmospheric pressure for 10 min each in the range between 5 and 70° 2-theta in the material research laboratory of the Western Anatolian Cement Factory in Izmir (Fig. 2).

Chemical analyses of the investigated chrysoprase samples utilized XRF for major oxides, ICP-AES for trace elements, and WST-SIM to determine ignition losses. These analyses were performed under contract by the accredited ALS Chemex Laboratory in Canada.

Studies of stable oxygen isotopes of the investigated chrysoprase samples were made using Elemental-Analysis-Isotope-Ratio Mass Spectrometry (EA-IRMS) in the MAM-Laboratory of TÜBİTAK (Gebze-Turkey). A CO₂-laser ablation preparation technique was applied for oxygen isotope analyses. After this, the obtained CO₂ was contributed to a mass spectrometer, and the oxygen stable isotope ratio ($\delta^{18}\text{O}$) was measured (with precision of $\pm 0.05 \text{ ‰}$). Values are quoted relative to SMOW with precision of $\pm 0.35 \text{ ‰}$.

3. Results and discussion

First of all, we characterize the five different chrysoprases from Turkey, defining their constitutive silica building phases using several destructive and non-destructive

analytical techniques. Especially when the gemmological features as well as the other verifying results (Table 1) of the investigated chrysoprase samples are considered, it can be stated that the chrysoprases from Turkey (Fig. 1) have a typical microcrystalline structure with pores (called chalcedonic-quartz) (Miehe *et al.*, 1984; Rossman, 1994; Shigley *et al.*, 2009; Graetsch, 2011; Hatipoğlu *et al.*, 2011). Polarizing microscopic examination reveals that the investigated chrysoprases consist of a fibrous silica matrix and, in some of them, centrally located inclusions of crystalline silica. The identification of the silica matrix was also confirmed by X-ray powder diffraction data using the comparative matching technique. The X-ray diffraction patterns (Fig. 2) of the chrysoprase samples of the five different regions in Turkey show typical microcrystalline length-fast quartz (chalcedonic quartz) peaks.

Table 2 shows the chemical bulk contents of the chrysoprases belonging to the investigated five different regions. Thus, it can be stated that the chemical bulk contents are characteristic for every chrysoprase deposit and certainly reflect the origin of the solutions responsible for the formation of these chrysoprases. These bulk contents are similar when compared and contrasted to chrysoprase samples from Poland, Kazakhstan, Australia, and Tanzania (Sachanbinski *et al.*, 2001; Skrzypek *et al.*, 2003, 2004).

Even though measuring O-18 values in silicate minerals is difficult and hazardous due to the difficulty in breaking Si-O-Si bonds, stable oxygen isotope values were safely obtained from the five different chrysoprase samples. It is seen that the oxygen isotope analyses (SMOW) of the chrysoprase materials in the five different mine deposits range between $\delta^{18}\text{O} = 21.3\text{\textperthousand}$ and $30.7\text{\textperthousand}$. In addition, the analyses of their water contents range between $\delta^{18}\text{O} = -8\text{\textperthousand}$ and 4\textperthousand .

When the data are modeled in a graphic (Fig. 3), the initial temperature of the formation of the investigated chrysoprases from Turkey can be determined, from lower to higher temperatures, as ~66 °C for those of the Savur (Mardin) deposit occurring in the crevices and large vacancies in sandstone, ~74 °C for those of the Sivrihisar (Eskişehir) deposit occurring in the crevices and large vacancies in sandstone, ~83 °C for those of the İkizce (Bilecik) deposit occurring in the crevices and large vacancies in dacite and andesite as ~99 °C for those of the Oltu (Erzurum) deposit occurring in the cracked zone between flysch and serpentinite, and ~125 °C for those of the Biga (Çanakkale) deposit occurring in the cracked zone between schist and serpentinite.

As can be seen from Fig. 3, the $\delta^{18}\text{O}_{(\text{SMOW})}$ values are not related to the geological positions of the chrysoprases analyzed. On the other hand, the chrysoprases from the cracked zone in serpentinites have higher degrees of temperature than do those from the crevices in sandstones and volcanics. This might be related to the origin of water or to the water to rock ratio (Skrzypek *et al.*, 2003).

The chrysoprases from Turkey also have high $\delta^{18}\text{O}$. Skrzypek et al. (2003) also observed high oxygen isotope ratios from the Wiry and Szklary mines. They noted that these high values were due to the precipitation of mixed solutions of meteoric at pneumo-hydrothermal conditions.

In addition, similar values were obtained by Kolodny and Epstein (1976), who studied deep-sea sediments.

Skrzypek and his colleagues (2003) have the following temperatures of crystallization of chrysoprase. Under oxygen isotope equilibrium with $\delta^{18}\text{O}$ of water, a range from -8 to 4‰ has been calculated: from 5–55 °C to 40–115 °C (Szklary); from 10–60 °C to 40–110 °C (Wiry); from 20–75 °C to 25–85 °C (Marlborough Creek), and

from 30–95 °C (Sarykul Boldy). Summing up, the estimated isotope temperature of the crystallization of chrysoprases ranges from 5 to 132 °C (Skrzypek *et al.*, 2003, 2004).

As a result, some important worldwide gem-quality chrysoprase samples, such as those from Poland, Kazakhstan, and Australia, probably precipitated from warm solutions at similar conditions.

4. Conclusions

Measurements of initial microcrystallization temperatures using the geochemical graphical modeling technique are simplifier when they compare and contrast with data from studies using existing methodologies.

Stable oxygen isotope data were obtained from five different chrysoprase samples in Turkey. It is seen that the oxygen isotope analyses (SMOW) of the chrysoprase materials ranges between $\delta^{18}\text{O} = 21.3\text{\textperthousand}$ and $30.7\text{\textperthousand}$. Accordingly, initial microcrystallization temperatures measured using the geochemical graphical modeling technique are found to be ~66 °C (the lowest value) for those of the Savur (Mardin) deposit occurring in the crevices and large vacancies in sandstone and ~125 °C (the highest) for those of the Biga (Çanakkale) deposit occurring in the cracked zone between schist and serpentinite. The others have interval values among them. Thus, we state that these chrysoprases do not have a syngenetic origin temperature during the coagulation of microcrystalline silica from silicic-acid (H_4SO_4). These differences are probably caused by the mixture of meteoric and magma genetic waters in the subsequent hydrothermal stages of the alteration and dissolving of the surrounding rocks.

TABLES

Table 1. Some essential gemmological measurements of the investigated natural chrysoprases.

Basic gemmological measurements	Chrysoprases from Turkey				
	Biga (Çanakkale)	İkizce (Bilecik)	Sivrihisar (Eskişehir)	Oltu (Erzurum)	Savur (Mardin)
Specific Gravity (SG)	2.56 gr/cm ³	2.58 gr/cm ³	2.54 gr/cm ³	2.59 gr/cm ³	2.52 gr/cm ³
Optical Character	Anisotropic, Uniaxial (+)	Anisotropic, Uniaxial (+)	Anisotropic, Uniaxial (+)	Anisotropic, Uniaxial (+)	Anisotropic, Uniaxial (+)
Refractive Index (RI)	N _ω =1.54	N _ω =1.54	N _ω =1.54	N _ω =1.54	N _ω =1.54
Luminescence against UV excitation	None	None	None	None	None
Cleavage	None	None	None	None	None
Hardness	6.75	6.50	6.75	6.75	6.75
Luster	Vitreous	Vitreous	Vitreous	Vitreous	Vitreous

Table 2. Chemical bulk analyses of the investigated natural chrysoprases in the mining deposits in terms of commercial quantities in about five different regions of Turkey.

Oxides	Instrument (XRF)	Chrysoprase				
		Detection limits	Biga (Çanakkale)	İkizce (Bilecik)	Sivrihisar (Eskişehir)	Oltu (Erzurum)
SiO₂	0.01 %	95.50	90.11	91.19	93.03	92.02
TiO₂	0.01 %	0.02	<0.01	<0.01	0.04	<0.01
Al₂O₃	0.01 %	0.99	0.76	1.03	0.78	1.21
Fe₂O_{3t}	0.01 %	1.98	3.43	1.27	2.23	1.56
NiO	0.01 %	1.04	0.56	1.34	0.72	0.67
MnO	0.01 %	0.03	<0.01	<0.01	0.02	0.01
MgO	0.01 %	0.12	0.70	0.14	0.62	0.11
CaO	0.01 %	0.06	0.08	0.02	0.87	0.04
Na₂O	0.01 %	0.13	0.01	1.08	0.05	1.01
K₂O	0.01 %	0.18	0.02	0.38	0.23	1.56
P₂O₅	0.001 %	0.013	0.007	0.002	0.024	0.006
Cr₂O₃	0.01 %	0.15	0.34	0.07	0.34	0.08
SrO	0.01 %	0.01	0.02	0.05	0.02	0.08
BaO	0.01 %	0.01	<0.01	<0.01	0.01	<0.01
LOI	0.01 %	0.64	2.92	1.76	0.79	1.98
Total	0.01 %	100.87	98.96	98.33	99.77	100.34

Table 3. $\delta^{18}\text{O}_{(\text{SMOW})}$ values and geological surrounding rocks of the investigated natural chrysoprases in the mining deposits in terms of commercial quantities in about five different regions of Turkey as well as $\delta^{18}\text{O}_{(\text{SMOW})}$ value of waters which present during formation of the chrysoprases. As a result, initial temperatures of formation obtained from Fig. 3.

Gem-Chrysoprase deposits in Turkey	$\delta^{18}\text{O}_{(\text{SMOW})}$ of Chrysoprase	$\delta^{18}\text{O}_{(\text{SMOW})}$ of Water	Initial Temperature of Formation	Geological Surrounding Rocks
Biga (Çanakkale)	21.3‰	4‰	~125°C	Contact zone between schist and serpentinite
İkizce (Bilecik)	27.1‰	1‰	~83°C	Crevises and large vacancies in dacite and andesite
Sivrihisar (Eskişehir)	29.4‰	-6‰	~74°C	Crevises and large vacancies in sandstone
Oltu (Erzurum)	23.9‰	2‰	~99°C	Cracked zone between flysch and serpentinite
Savur (Mardin)	30.7‰	-8‰	~66°C	Crevises and large vacancies in sandstone

FIGURES

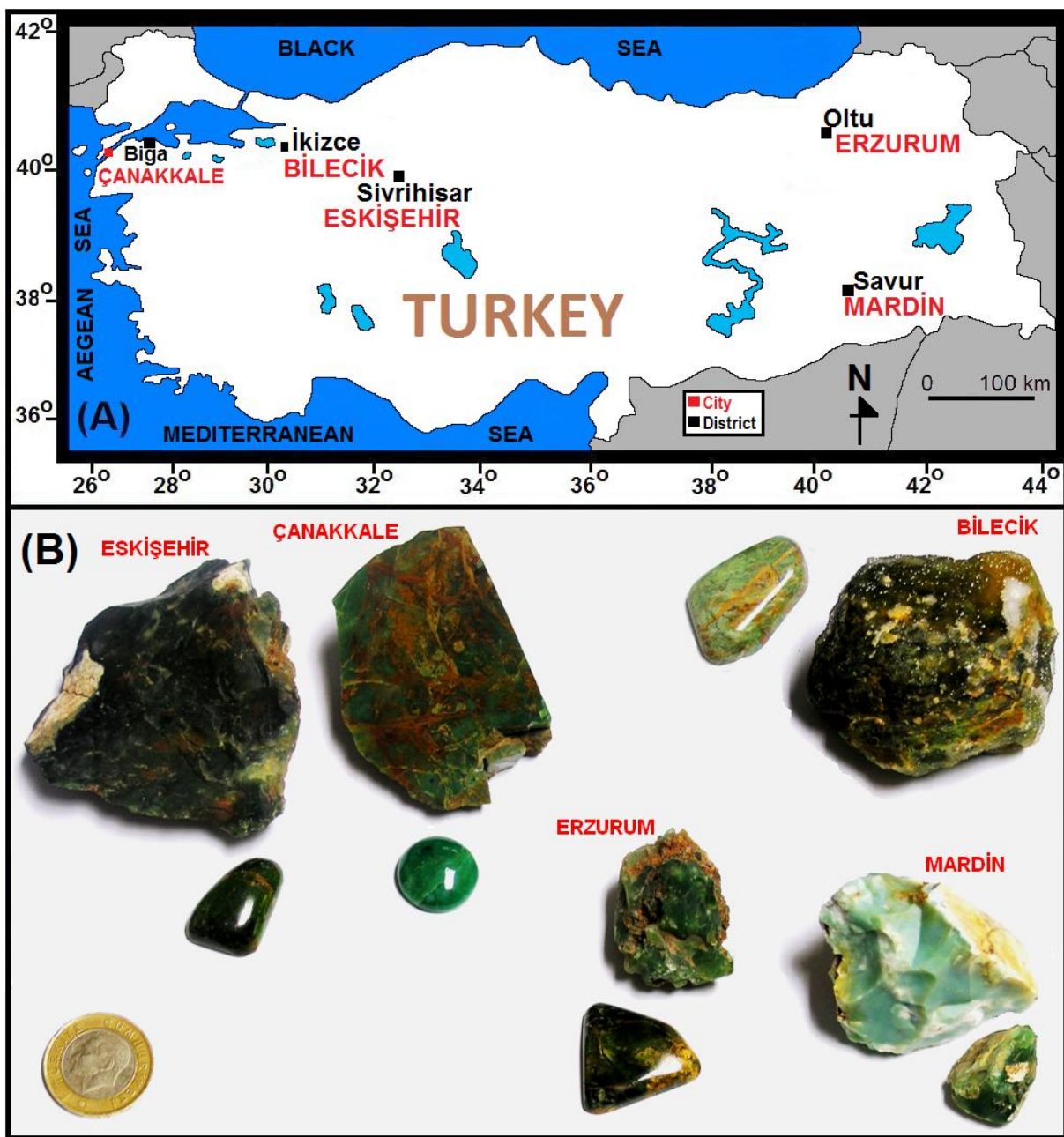


Fig. 1. The mining deposits in terms of commercial quantities in about five different regions of Turkey, such as Biga (Çanakkale), İkizce (Bilecik), Sivrihisar (Eskişehir), Oltu (Erzurum), and Savur (Mardin) **(A)**. Some chrysoprase rough and polished samples obtained from these localities **(B)**.

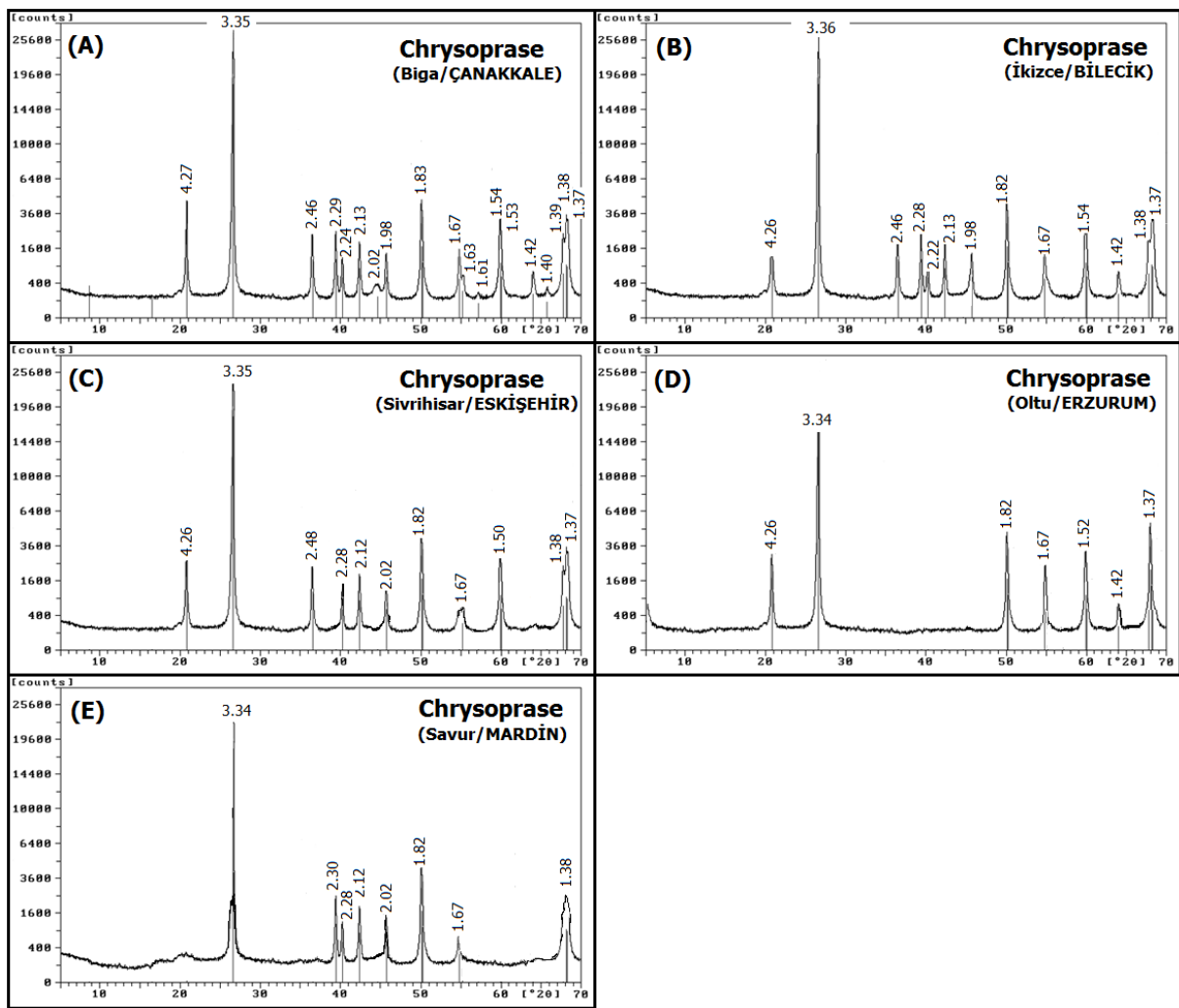


Fig. 2. The XRD patterns of the investigated chrysoprases. The positions of peaks with d-spacings [Å] and relative intensities [%(I/I_0)] $\geq 0.2\%$ are labelled for 2-theta values below 70 degrees.

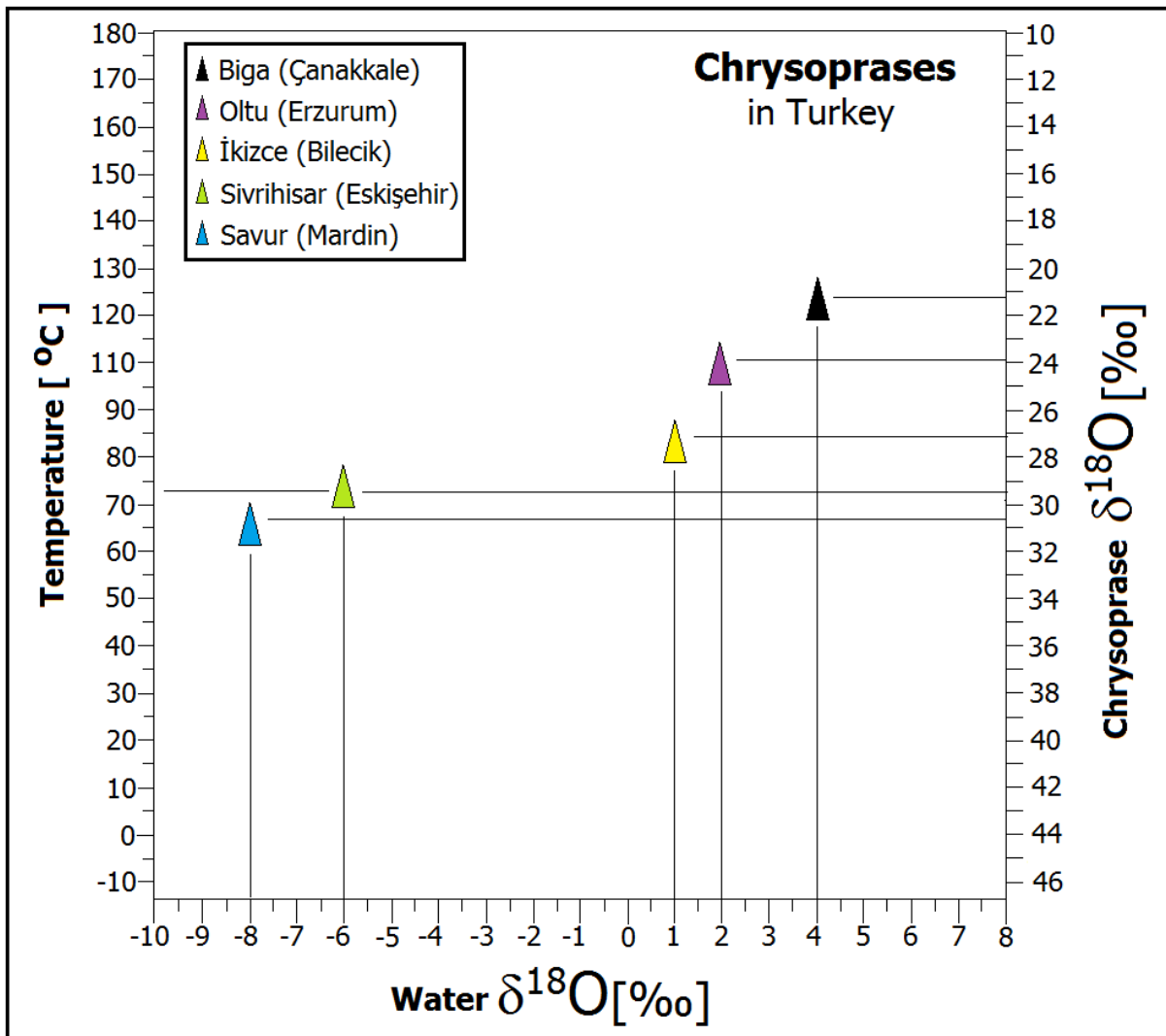


Fig. 3. A geochemical modelled diagram showing the initial temperatures of the formations obtained from $\delta^{18}\text{O}_{\text{(SMOW)}}$ values of the investigated natural chrysoprases versus $\delta^{18}\text{O}_{\text{(SMOW)}}$ values of waters which present during formation of the chrysoprases (Kita et al., 1985; IAEA, 2004).

Authors Index

Aboarik, H.	77	Khorshid, F.	72, 77
Abojassim, A. A.	61	Mallick, B.	66
Al-Aomar, R.	11	Maniadaki, K. G.	42
AlAttas, S. G.	72	Marcu, M.	106
Anghel, E. M.	106	Mastorakis, N. E.	34
Antonidakis, E. N.	42	Melcher, J.	23
Banu, A.	106	Mishra, P. C.	66
Behera, S.	66	Mpirouraki, A. E.	42
Belyakov, V. N.	85	Noor, S. O.	72
Blagikh, E.	81	Othman, M. F.	100
Bora, R. S.	77	Papafilippaki, A. K.	42
Boteanu, N. N.	16, 34	Ponomaryova, L. N.	85
Brîndușa, C. C.	34	Rabah, S. O.	77
Bulenbayev, M.	81	Ravigan, F.	16
Bulucea, Ca. A.	34	Razali, Y. S.	100
Bulucea, Co. A.	34	Rigakis, I. I.	42
Carvalho, J.	48	Rios, R.	48
Doitsidis, L. D.	42	Sabir, J. S.	77
Dzyazko, Y. S.	85	Sarantopoulos, I. V.	42
Elsourojy, Y. A.	72	Savizky, R.	81
Fouskitakis, G. N.	42	Serri, N. A.	100
Galvão, F.	48	Shakieva, T.	81
Georgescu, L.	106	Sosenkin, V. E.	85
Glodeanu, M.	34	Tajarudin, H. A.	100
Gofită, E.	34	Tamat, M. R.	100
Hajrah, N. H.	77	Tawfik, N.	72
Hassan, A. B.	61	Tiwari, T. N.	66
Hatipoğlu, M.	110	Tounsi, S.	54
Hussain, M.	11	Tussupbaev, N.	81
Iacob, M.	16	Varikou, K. N.	42
İlbeyli, N.	110	Velazco, S. J. E.	48
Jaffat, H. S.	61	Volfkovich, Y. M.	85
Jeles, A. C.	34	Yemelyanova, V.	81
Karmazínová, M.	23	Zhakenovich, A. Y.	81